DOE/ER/12933-3
DOE/ID-10499
September 1996

FILM BOILING ON SPHERES IN SINGLE- AND TWO-PHASE FLOWS

C. Liu and T. G. Theofanous

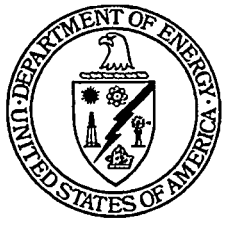

Department of Energy

Advanced
Reactor
Severe
Accident
Program

DOE/ER-12933-3
DOE/ID-10499
September 1996

FILM BOILING ON SPHERES IN SINGLE- AND TWO-PHASE FLOWS

C. Liu and T.G.Theofanous

Center for Risk Studies and Safety
Departments of Chemical and Mechanical Engineering
University of California, Santa Barbara
Santa Barbara, CA 93106

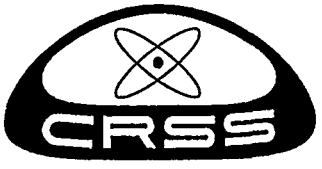

Prepared for the
U. S. Department of Energy
Idaho Operations Office
Under ANL Subcontract No. 962762402

DISCLAIMER

Portions of this document may be illegible in electronic image products. Images are produced from the best available original document.

ABSTRACT

Film boiling on spheres in single- and two-phase flows was studied experimentally and theoretically with an emphasis on establishing the film boiling heat transfer closure law, which is useful in the analysis of nuclear reactor core melt accidents.

Systematic experimentation of film boiling on spheres in single-phase water flows was carried out to investigate the effects of liquid subcooling (from 0 to 40 °C), liquid velocity (from 0 to 2 m/s), sphere superheat (from 200 to 900 °C), sphere diameter (from 6 to 19 mm), and sphere material (stainless steel and brass) on film boiling heat transfer. Based on the experimental data a general film boiling heat transfer correlation is developed. Utilizing a two-phase laminar boundary-layer model for the unseparated front film region and a turbulent eddy model for the separated rear region, a theoretical model was developed to predict the film boiling heat transfer in all single-phase regimes.

The film boiling from a sphere in two-phase flows was investigated both in upward two-phase flows (with void fraction from 0.2 to 0.65, water velocity from 0.6 to 3.2 m/s, and steam velocity from 3.0 to 9.0 m/s) and in downward two-phase flows (with void fraction from 0.7 to 0.95, water velocity from 1.9 to 6.5 m/s, and steam velocity from 1.1 to 9.0 m/s). The saturated single-phase heat transfer correlation was found to be applicable to the two-phase film boiling data by making use of the actual water velocity (water phase velocity), and an adjustment factor of $(1-\alpha)^{1/4}$ (with α being the void fraction) for downward flow case only. Slight adjustments of the Reynolds number exponents in the correlation provided an even better interpretation of the two-phase data.

Preliminary experiments were also conducted to address the influences of multi-sphere structure on the film boiling heat transfer in single- and two-phase flows.

TABLE OF CONTENTS

NOMENCLATURE

Ar	Archimedes number, $g(\rho_l - \rho_v)d^3/(\rho_v \upsilon_v^2)$
C_p	specific heat, [J/(kg °C)]
d, D	diameter of sphere or cylinder, [m]
d'	dimensionless diameter, $d/[\sigma/g/(\rho_l - \rho_v)]^{1/2}$
Fr	Froude number, $U_l^2/(gd)$
g	gravitational constant, [kg m/sec^2]
Gr	Grashof number, $g\beta_l(T_{sat} - T_l)d^3/\upsilon_l^2$
h	heat transfer coefficient, $q/\Delta T$
h_{fg}	latent heat of vaporization, [J/kg]
h'_{fg}	latent heat plus sensible heat, $h_{fg} + 0.5C_{pv}\Delta T_{sup}$
K	density ratio, ρ_l/ρ_v
k	thermal conductivity, [W/(m °C)]
l'	capillary length, $[\sigma/g/(\rho_l - \rho_v)]^{1/2}$
Nu	average Nusselt number, hd/k
Pr	Prandtl number
q	average surface heat flux, [W/m^2]
R	radius; or dimensionless ratio, $[(\mu\rho)_v/(\mu\rho)_l]^{1/2}$
Re_l	Reynolds number of liquid phase, $U_l d/\upsilon_l$
Sc	dimensionless subcooling, $(C_{pl}\Delta T_{sub})/(h_{fg}\mathrm{Pr}_l)$
Sc'	dimensionless subcooling, $(C_{pl}\Delta T_{sub})/(h'_{fg}\mathrm{Pr}_l)$
Sp	dimensionless superheat, $(C_{pv}\Delta T_{sup})/(h_{fg}\mathrm{Pr}_v)$
Sp'	dimensionless superheat, $(C_{pv}\Delta T_{sup})/(h'_{fg}\mathrm{Pr}_v)$
T	temperature, [°C]
U	velocity, phase velocity
V	superficial velocity

Greek symbols

α	thermal diffusivity, $k/(\rho C_p)$; or void fraction
ΔT_{sub}	liquid subcooling, $T_{sat} - T_l$
ΔT_{sup}	average superheat of solid or solid wall, $T_w - T_{sat}$
ϵ	radiation emissivity
λ_c	critical wavelength, $2\pi l'$
μ	viscosity, [kg/(m sec)]
υ	kinematic viscosity, [m^2/sec]
ρ	density, [kg/m^3]

σ	surface tension of vapor-liquid interface, [N/m]
σ_B	Stefan-Boltzman constant, 5.67×10^{-8} [W/(m^{2}K^4)]

Subscripts

c	film boiling without radiation
f, F	forced convection film boiling
l	liquid, or water
nc	natural convection (non film boiling)
p	pool film boiling
r	radiation
s	saturated value, or steam
sat	saturated
sub	subcooled
t	total heat flux
two	two-phase
v	vapor, or steam
w	wall of sphere/cylinder, or water

ACKNOWLEDGEMENTS

This work was supported in the main part by Grant No. DE-FG02-90ER12933 under DOE's Nuclear Engineering Education Research Grant Program. The work was completed under, and results utilized, in the ROAAM program carried out for the US DOE's Advanced Reactor Severe Accident Program (ARSAP), administered by ANL subcontract No. 23572401 to UCSB. The authors are grateful for the support and cooperation of the program managers, Mr. W. Pasedag (DOE, Headquarters) and Mr. S. Sorrell (DOE, Idaho Operations Office).

1 INTRODUCTION AND OVERVIEW

Film boiling is a major heat transfer mechanism that occurs when large temperature differences exist between a liquid and a hot surface. It has applications in cryogenic systems, metallurgic industries, and other areas where heating, cooling, and quenching of high temperature surfaces are encountered.

In recent years, film boiling has become an important concern in the nuclear reactor safety analyses. During postulated core melt accidents (CMAs), the core/fuel may melt, fall into water, and fragment into spheres or sphere-like particles. The subsequent fuel-coolant interaction may result in spontaneous evaporation — a destructive steam explosion. One of the important concerns in the analysis of fuel-coolant interaction (premixing) is the heat transfer between the fuel particles and the water/steam two-phase flow in all the flow regimes, which cover from natural convection (pool film boiling) to forced convection, from saturated to highly subcooled, and from single-phase flow to two-phase flow.

Recently, Theofanous (1987), Amarasooriya (1991) and Yuen (1994) have developed a three-fluid model for general systems in a wide range of flow regimes. Such models have been found useful for establishing upper limits on the energy of large-scale steam explosions. In the absence of experimental data and appropriate film boiling correlations, the initial computations were based on single-phase film boiling correlation and extrapolations of two-phase formulations. The situations are the same for other fuel-coolant analysis codes. Thus, there is a need for a complete closure law — the heat transfer correlation for film boiling on spheres in a wide range of single- and two-phase flow regimes.

Regarding previous work on film boiling from spheres, it can be concluded that: For two-phase Flows: No experiment or analysis for sphere film boiling in two-phase flows can be located. For Single-Phase Flows: (1) All the meaningful single-phase film boiling heat transfer data were obtained through short cool-down transients (by passing a preheated sphere through a liquid tank). Although the short cool-down transient technique is good enough for pool or low speed forced convection film boiling experiments, it is not adequate for high velocity forced convection film boiling, because the transient is too short. For example, with sphere speed at 2.0 m/s and pool length 0.5 m, the film boiling cool-down transient is only about 0.25 second! Within such a short time, the entrance thermal response may affect the accuracy of the experimental data. (2) The accuracy of the single-phase data may be very poor as a result of the large heat loss from the support-tube, since the sphere-support-tube diameter to sphere diameter ratios of the previous experimental work are about 0.12 to 0.3. (3) For each single-phase film boiling regime,

the basic form of heat transfer correlation has been well developed, but there are some uncertainties in the correlation constants, as shown in Table 2.5. (4) There is no general correlation or complete theoretical analysis for film boiling on spheres which covers all the single-phase flow regimes. There is no theoretical model for the heat transfer in the separated rear region of the sphere.

The main purpose of this work is to establish the experimental data base and to derive the heat transfer correlation (closure law) for film boiling on spheres. The emphasis is on very high temperature film boiling (pure film boiling with the sphere temperature higher than the quenching point) in all the flow regimes, which cover from natural convection (pool film boiling) to forced convection, from saturated to highly subcooled, and from single-phase flow to two-phase flow. Besides this, theoretical analysis is carried out to understand the fundamentals of film boiling and to formulate better heat transfer correlations.

A versatile two-phase flow loop/mixer has been built to provide a variety of steady state single- and two-phase flow to obtain reliable, high quality, and complete experiment data. A radio frequency induction heating technique was investigated and applied to heat metallic spheres directly inside the test section to maintain a steady state film boiling. With these setups, the film boiling heat transfer data can be obtained either by transient mode runs or by steady-state mode runs. An X-ray radiograph technique was applied to measure the void fraction of two-phase flow in the test section. Another unique feature of the present experiment approach is that it provides a convenient way to observe clearly the film boiling process, since the sphere is held still during the run. After the induction power is turned off, the induction coil could be moved away to allow the whole film boiling cool-down transient to be observed. With test spheres directly supported by small sheathed thermocouples (thermocouple O.D. vs test sphere O.D. being: 0.25 mm/6.35 mm; 0.5/9.35; and 0.81/12.7), the heat loss from the support is significantly minimized and is relatively small.

Systematic experimentation of film boiling on sphere in single-phase water flow has been carried out (Chapter 4) to investigate and check the effects of liquid subcooling (from 0 to 40 °C), liquid velocity (from 0 to 2 m/s), sphere superheat (from 200 to 900 °C), sphere diameter (from 6 to 19 mm), and sphere material (stainless steel and brass) on film boiling heat transfer. The single-phase experiment results are presented, discussed, and correlated in saturated pool, saturated forced convection, subcooled pool, and subcooled forced convection film boiling regimes, respectively; and then a general film boiling heat transfer correlation is developed (Chapter 6).

A theoretical analysis of film boiling from a sphere in single-phase flows was conducted (Chapter 5). With the two-phase laminar boundary layer model (an integral method modified from Shigechi, Ito and Nishikawa's (1983) model) for the un-separated front film region and the turbulent eddy model (based on Theofanous, Houze and Brumfield's (1987) model) for the separated rear region, the combined theoretical model can predict the film boiling heat transfer in all regimes.

The film boiling from a sphere in two-phase flows has been investigated (Chapter 7) both in an upward two-phase flow (with void fraction from 0.2 to 0.65, water phase velocity from 0.6 to 3.2 m/s, and steam phase velocity from 3.0 to 9.0 m/s) and in a downward two-phase flow (with void fraction from 0.7 to 0.95, water phase velocity from 1.9 to 6.5 m/s, and steam phase velocity from 1.1 to 9.0 m/s). The void fractions were measured by an X-ray radiography. The calculated void fraction of downward two-phase flow, which is based on the acceleration due to the gravity and steam drag, agrees well with the X-ray measurements. The saturated single-phase heat transfer correlation is found to be applicable to the two-phase film boiling data by making use of the actual water velocity (water phase velocity), and an adjustment factor of $(1-\alpha)^{1/4}$ for downward flow case only. Slight adjustments of the Reynolds number exponents in the correlation provide an even better interpretation of the two-phase data. The power dependency on the Reynolds number should decrease to 0.2 in the upward two-phase case and increase to 0.75 in the downward two-phase case to correlate better the film boiling heat transfer data respectively.

The film boiling from a multi-sphere group has also been investigated (Chapter 8) through a five-sphere array with four spheres placed in the front of the test sphere. The experiments indicate that: (1) the presence of boiling spheres in the front of the test sphere decreases the film boiling heat transfer in the upward two-phase flow and increases the heat transfer in downward two-phase flow; and (2) in a saturated single-phase upward flow, the presence of boiling spheres in the front of the test sphere increases the heat transfer in pool film boiling regime and decreases the heat transfer in forced convection film boiling regime. These trends are consistent with the expectation using the single-sphere correlation and the theoretical interpretation in conjunction with the flow field changes due to the presence of the four spheres ahead of the test sphere.

2 A REVIEW ON FILM BOILING FROM SPHERES AND HORIZONTAL CYLINDERS IN SINGLE-PHASE FLOWS

2.1 Film Boiling and Radiation Effect

Boiling is the evaporation process that occurs at the interface of a liquid and a hot solid or another hot liquid. This process is associated with mass and heat transfer from the hot surface to the liquid through the vapor film. According to the temperature difference across the interface and the configuration of the vapor film around the interface, boiling is usually classified into three sub-groups: nucleate, transition and film boiling.

In film boiling, a complete vapor film is formed at the interface which prevents the liquid directly contacting with the hot solid (or liquid) surface. Film boiling only exists when the temperature difference across the interface is large enough to sustain it (usually over 100 °C – 700 °C depending on subcooling, surface condition and liquid flow velocity). In film boiling, the heat transfer mechanism is mainly by heat conduction and radiation across the vapor film. The low conductivity of the vapor film through which the heat must be transported characterizes the low value of heat transfer coefficient. The radiation heat transfer contributes higher and higher percentage in the total heat flux when the temperature difference becomes bigger and bigger.

According to the geometry of the interface, film boiling can be categorized into: film boiling on plane surfaces (vertical, horizontal upward, horizontal downward, inclined and curved), on cylinders, and on spheres. Actually, the film boiling on sphere and on cylinder are quite similar to each other, both in vapor film configurations and in the ways that the heat transfer data are correlated. Here, the review and discussion are limited only on the film boiling from cylinders and spheres.

On the configuration of the vapor film on spheres and cylinders, several papers are relevant, such as Walfort (1969), Stevens and Witte (1971), Aziz and Hewitt (1986), Zvirin, Hewitt, and Kenning (1990), and Dix and Orozco (1990). According to these observations, the conclusions about the vapor film configuration on the front part of the sphere or cylinder (with $\theta < \pi/2$) are consistent: a complete vapor film either smooth or wavy is covered on the front of the sphere/cylinder. But, on the other hand, the descriptions of the film configuration on the rear part are quite diverse. There are two reasons for this diversity. Firstly, the shape of the rear vapor film itself depends on the liquid condition: the velocity of flow and the degree of subcooling. Secondly, the back film configurations are also significantly affected by the sphere supports, which are at the rear side. For most

of the previous experimental observations, the support effects were not avoided and even not discussed.

Regarding the influences of the sphere/cylinder itself on the film boiling, some experimental investigations [such as Bromley (1950) and Dhir (1978)] indicate that, if only the convective heat transfer is considered, the materials, the properties and the surface conditions do not affect the film boiling heat transfer significantly. However, the thermal conductivity of the sphere may affect the temperature distribution inside the sphere, and the radiation heat transfer (emissivity of the surface) strongly depends on the material and the surface condition of the spheres/cylinders. Moreover, the materials, properties, and surface conditions of the sphere significantly affect the quenching (or transition) point and the heat transfer during the transition boiling. In conclusion, for film boiling, the sphere itself only affects the radiation heat transfer but not the convective heat transfer.

On the other hand, in regard to the effects from the liquid, many quantities and conditions should be considered. Firstly, the properties of the liquid should be considered. Such properties are densities, heat conductivities and viscosities of the liquid phase and the vapor phase, saturation temperature at certain system pressure, latent heat of evaporation and surface tension at the liquid vapor interface. Secondly, the liquid temperature and the system pressure must be specified, which determines the subcooling of the liquid. According to this, the film boiling is classified into: saturated and subcooled film boiling. In the case of saturated film boiling, most of the heat that is transferred through the interface becomes the heat source for evaporation, and the produced vapor does not (or hardly) condense. So, the front vapor film is thick and wavy; the film on back of the sphere becomes thicker and thicker and eventually develops into a stable (or unstable) vapor dome; there is a two-phase wake behind the sphere. In contrast, in the case of subcooled film boiling, most of the heat transferred to the interface is convected away into the liquid and only part of the heat becomes the heat source for net evaporation. The bubbles that separated from the vapor film condense very quickly and vanish after a short path in the liquid. Finally, according to the liquid flow velocity, the film boiling can be divided into two regimes: pool (or natural free convection) and forced convection film boiling. Experimental investigations indicate that as long as the square root of the Froude number is smaller than $\sim$1.5, the velocity of the liquid does not affect the film boiling heat transfer rate, and this serves as the criterion to distinguish the pool and forced convection film boiling.

There are many aspects of film boiling; a complete review on the film boiling from spheres/cylinders is not intended here. Since our purpose is to get new data by using new

techniques and to develop a general correlation for film boiling on spheres in single- and two-phase flows, the review will emphasize existing film boiling analyses, correlations, experimental techniques and experimental results. The review is divided into four sections according to the flow velocity and liquid subcooling, which are saturated pool, subcooled pool, saturated forced convection and subcooled forced convection film boiling.

Before the detailed review on the film boiling which only takes account to the convective heat transfer (with the radiative heat transfer contribution being subtracted away), let us look how the radiation heat transfer is considered first.

Since radiation from the sphere/tube is largely absorbed in a small thickness of the liquid, it serves to produce more vapor that goes into the vapor film. This means that with the existence of radiation the convective contribution of film boiling heat transfer will be affected, and the heat transfer contributions of the convection and radiation can not be simply added together.

Bromley (1950) did an analysis for the case of pool film boiling and obtained an equation

$$h = h_c(h_c/h)^{1/3} + h_r \tag{2.1}$$

He also indicated that, as long as h_r is smaller than h_c, the simple equation

$$h = h_c + 0.75h_r \tag{2.2}$$

gives a good approximation to Eq. (2.1) within an accuracy of 5%. If h_r is very large (h_r/h_c ranges up to 10.0) the following equation was suggested

$$h = h_c + h_r\{0.75 + 0.25/(2.62h_c/h_r + 1)\} \tag{2.3}$$

Bromley, Leroy and Robbers (1953) did a similar analysis for the case of forced convection film boiling by assuming that all heat transfer above the separation point θ_s is by radiation , and they obtained an expression

$$h = h_c + h_r\{1 - \theta_s/(4\pi)\} \tag{2.4}$$

At high velocities, θ_s equals $\pi/2$, so

$$h = h_c + (7/8)h_r = h_c + 0.88h_r \tag{2.5}$$

In all the above cases, h_r is given by

$$h_r = \epsilon\sigma[T_w^4 - T_s^4]/\Delta T_{sup} \tag{2.6}$$

Since then, Eq. (2.2) and (2.5) are usually used in literature when radiation is concerned. However, recently, Sakurai, Shiotsu and Hata (1990) did a rigorous numerical solution for pool film boiling with subcooling. By comparing the results with and without radiation, they suggested that the radiation effect can be considered in the following way

$$h = h_c + Jh_r \tag{2.7}$$

$$J = F + (1 - F)/(1 + 1.4h_c/h_r) \tag{2.8}$$

$$F = [1 - 0.25\exp(-0.13Sp)]\exp(-0.64R^{0.6}\mathrm{Pr}_l^{0.65}Sp^{-0.73}Sc^{1.1}) \tag{2.9}$$

The J factors for pool and forced convection film boiling (with the heat transfer coefficient h being estimated by our general correlation, see chapter 6) are plotted in Fig. 2.1 and Fig. 2.2 respectively; they show a big difference between the two ways of calculating the radiation factors, especially when the sphere superheat is low and liquid subcooling is large. The ratios of total heat transfer coefficients obtained by using Eq. (2.5) and Eq. (2.7) are given in Fig. 2.3 and Fig. 2.4 for pool and forced convection film boiling cases respectively. In the case of pool film boiling, the maximum difference is about 16% which occurs at the condition of 80 °C liquid subcooling and 1300 °C wall superheat. In the case of forced convection film boiling, the maximum difference is about 11% at the condition of 80 °C liquid subcooling and 2200 °C wall superheat. These comparisons indicate that the complicated Sakurai's radiation factor dose not differ greatly from the simple Bromley's factor of 7/8, and the Bromley's factor may still be used in a practical sense.

2.2 Saturated Pool Film Boiling

2.2.1 1/4 Power Law

Bromley (1950) is the first work to study the pool film boiling at saturated condition systematically. It showed that heat transfer coefficients are independent of the tube materials except for the radiation contribution. By an analysis that is similar to the Nusselt's analysis for condensation, Bromley obtained:

$$\mathrm{Nu} = C[\mathrm{Ar}/Sp']^{1/4} \tag{2.10}$$

Where the Archimides number Ar is given as: $\mathrm{Ar} = g(\rho_l - \rho_v)d^3/(\rho_v\upsilon_v^2)$. He argued that, in general, the constant C is function of $Sp' = [(\Delta T_{sup}C_{pv})/(h'_{fg}\mathrm{Pr}_v)]$. According to the stable pool film boiling experiments that were conducted with electrical heated graphite

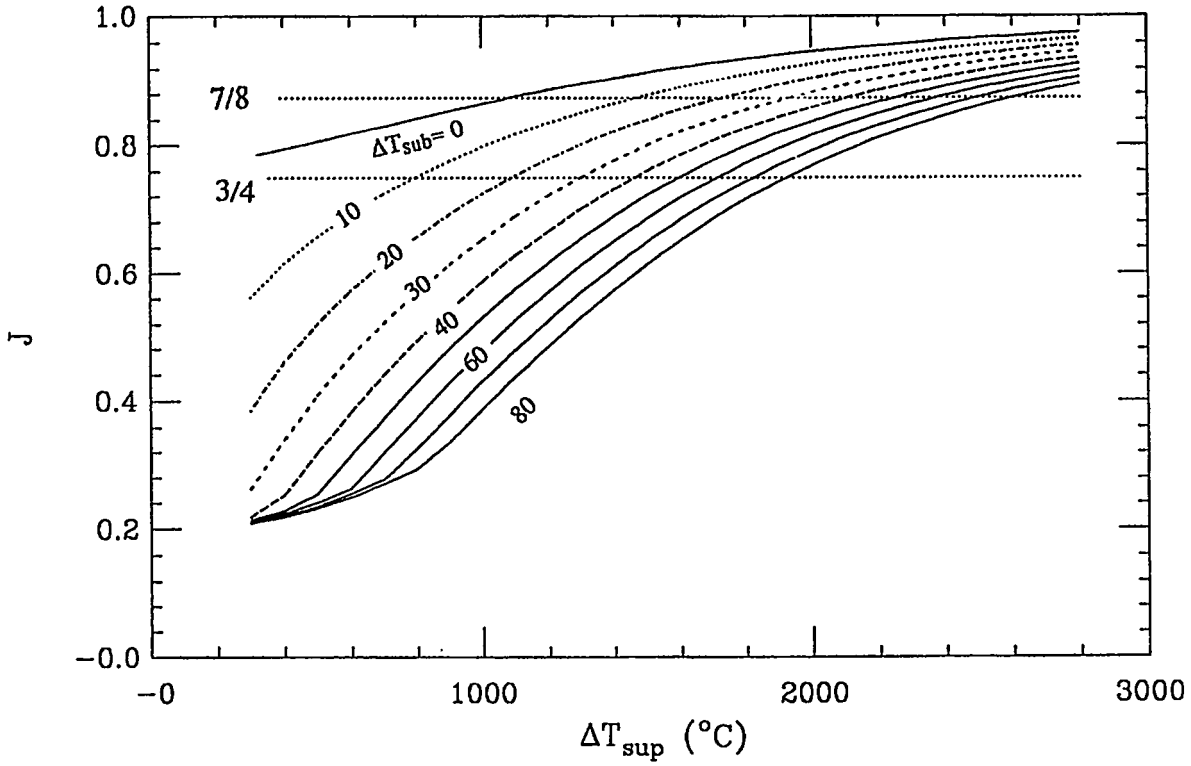

Fig. 2.1. Radiation J factor in the case of pool film boiling.

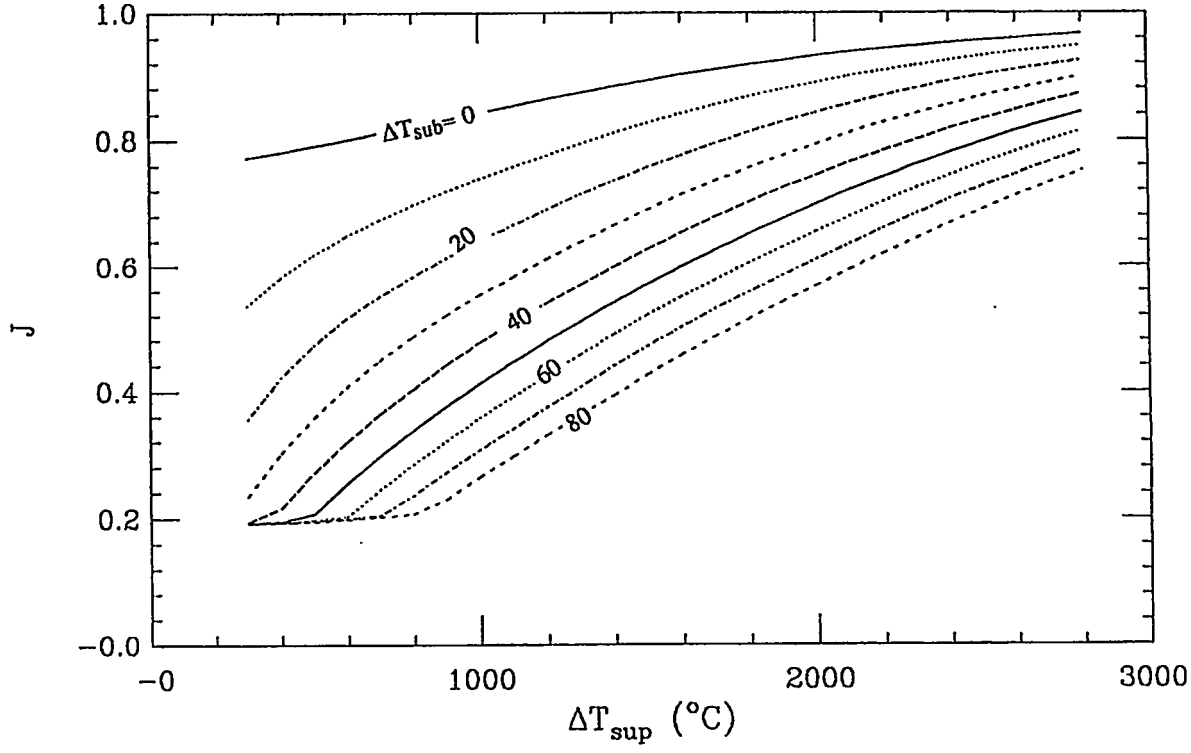

Fig. 2.2. Radiation J factor in the case of forced convection film boiling.

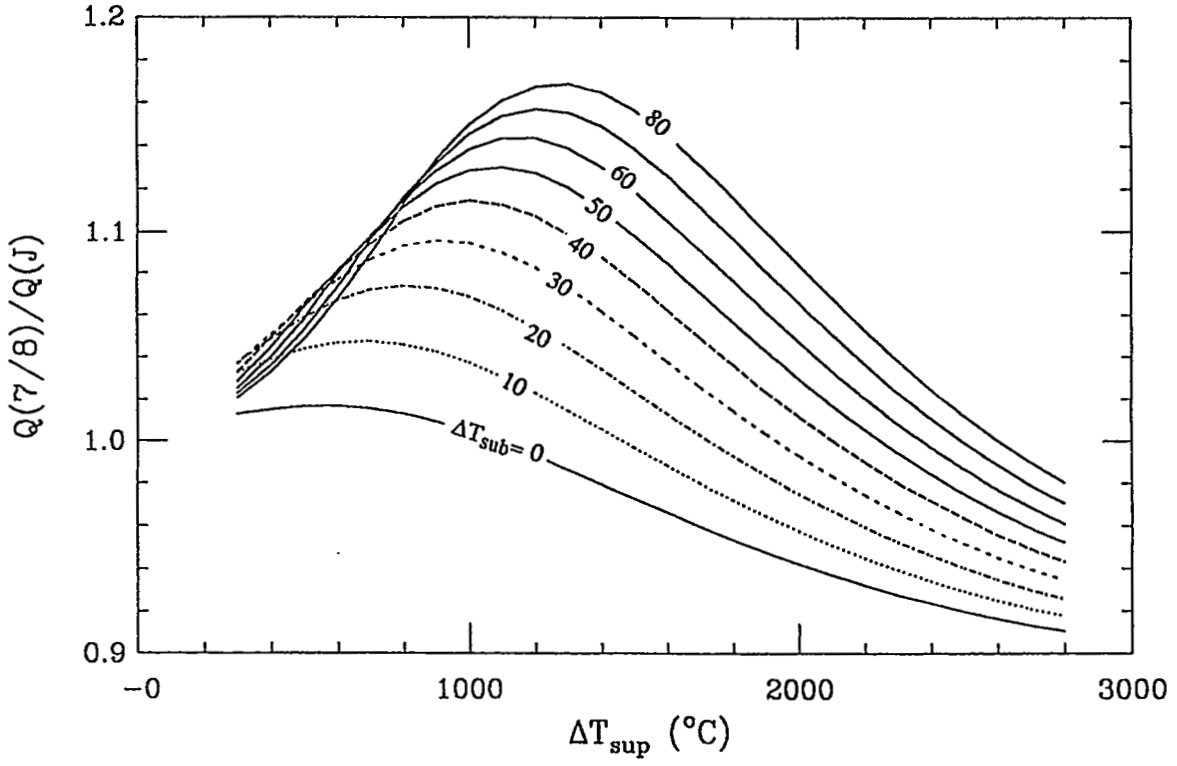

Fig. 2.3. The ratio of heat transfer coefficients obtained by Eq. (2.5) and Eq. (2.7) in pool film boiling.

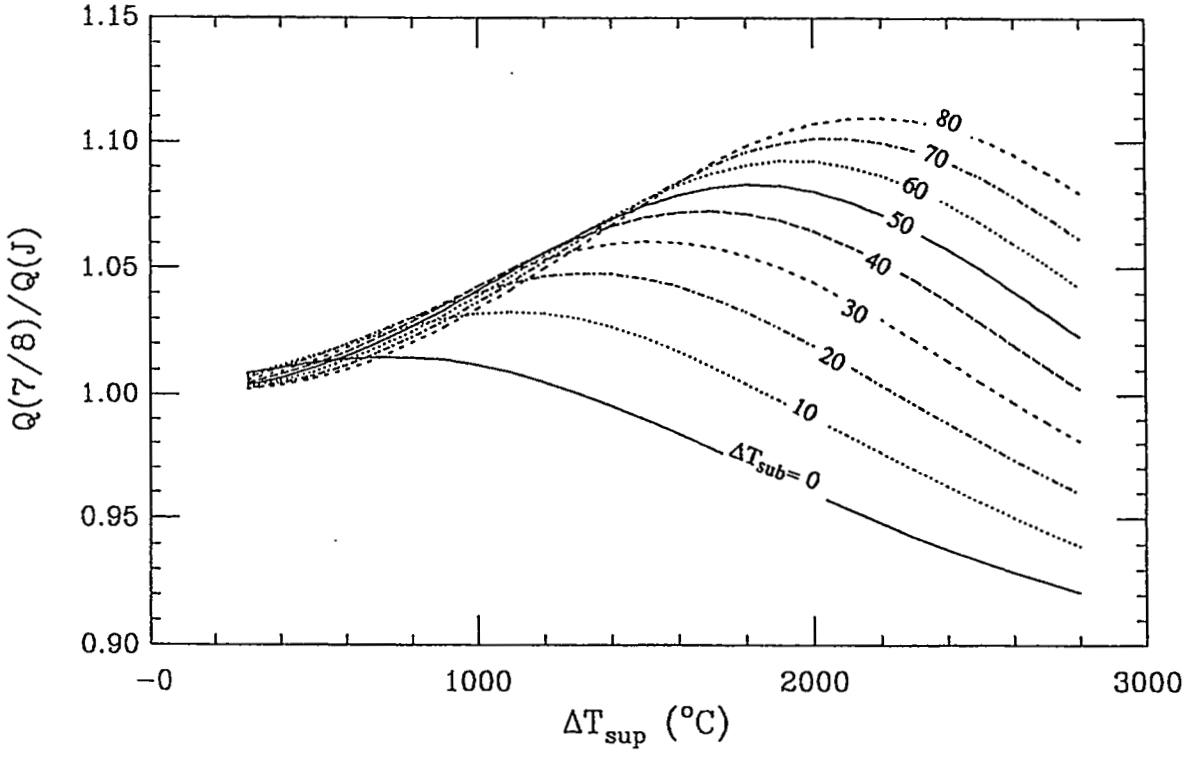

Fig. 2.4. The ratio of heat transfer coefficients obtained by Eq. (2.5) and Eq. (2.7) in forced film boiling.

tubes ($D = 9.8-16.2$ mm) and with 7 different fluids (water, soap solution, liquid nitrogen, n-pentane, benzene, carbon tetrachloride and ethyl alcohol) at atmosphere pressure, he concluded that the constant C does not vary significantly and suggested that a constant $C = 0.62$ could be used to correlate all of his data. Thus it gives,

$$\mathrm{Nu} = 0.62[\mathrm{Ar}/Sp']^{1/4} \tag{2.11}$$

Ten years later, Berenson (1961) applied the Taylor-Helmhotz Hydrodynamic Instability concept to his analysis of pool film boiling from a large horizontal surface, and he reached a correlation,

$$\mathrm{Nu}_{\lambda c} = h\lambda_c/k_v = 0.672[\mathrm{Ar}_{\lambda c}/Sp']^{1/4} \tag{2.12}$$

which is similar to that of Bromley's correlation for horizontal cylinder besides the substitution of critical wave length $\lambda_c = 2\pi l'$ for the tube diameter in Nu and Ar number.

In 1963, Frederking and Clark, applied a laminar analysis which is similar to that used by Bromley to the pool film boiling from a sphere and got a similar correlation:

$$\mathrm{Nu} = 0.586[\mathrm{Ar}/Sp]^{1/4} \tag{2.13}$$

Dhir and Purohit (1978) did an experiment with 19 and 25.4 mm spheres of steel, copper, and silver in water. They found that the properties of the sphere do not affect the heat transfer coefficient provided a stable film exists, which agrees with Bromley's (1950) argument. When they correlated their pool film boiling data at saturated condition, they got:

$$\mathrm{Nu} = 0.8[\mathrm{Ar}/\mathrm{Sp}]^{1/4} \tag{2.14}$$

The constant is higher than that in Eq. (2.13), however it is not clear which is right because of the following two reasons. First, because their support tube is 3 mm in diameter, the heat loss from the support could contribute large portion in the total heat transfer. Second, their experiment was operated at the "minimum film boiling temperature" state, the boiling may be partially in the transition boiling regime. So their experimental data may over estimated the film boiling heat transfer from sphere, and the correlation constant C = 0.8 may be too high for pool film boiling.

In addition to the above literature, there are also some others that obtained or applied the 1/4 power law for pool film boiling at both saturated and subcooled conditions, such as Farahat and Nasr (1975), Farahat and Halfawy (1975), Farahat (1978), Klimenko (1980),

Michiyoshi, Takahashi and Kikuchi (1988), Tso, Low and Ng (1990), Sakurai, Shiotsu, and Hata (1990a,b). Especially, when the diameter effect on the heat transfer is concerned, the base of the correlation is usually the 1/4 power law, this will be discussed later.

2.2.2 1/3 Power Law

Through research which concerns the pool film boiling from spheres (usually, D > 20 mm) in cryogenic liquids or in some organic liquids which have small capillary length l', the correlations with 1/3 power law were developed.

The first work may be attributed to Frederking and Clark (1963). They obtained a 1/4 power law from their theoretical analysis, however, the 1/3 power law emerged from the fact that the pool film boiling heat transfer coefficients obtained from their experiments were independent of the diameter of the test sphere over their range of geometry. So they applied the 1/3 power law to correlate their data in the form of

$$\mathrm{Nu} = 0.14[\mathrm{Ar}/Sp']^{1/3} \tag{2.15}$$

Merte and Clark (1964) did an experiment by cooling-down a sphere (D = 25.4 mm) in liquid nitrogen under different gravity conditions ($0.0 < a/g < 1.0$). Their data were correlated by:

$$\mathrm{Nu} = 0.15[\mathrm{Ar}/Sp' \cdot (a/g)]^{1/3} \tag{2.16}$$

They argued that the power increasing from Bromley's 1/4 to 1/3 is due to the transition from laminar to turbulent flow, and the transition appears to occur at a Rayleigh number of about 5×10^7.

In the researching of oscillation effect on the pool film boiling heat transfer, Rhea and Nevins (1969) conducted an experiment with 25.4, 19.0 and 12.7 mm diameter spheres in liquid nitrogen, and Schmidt and Witte (1972) did an experiment with 19 mm diameter sphere in Freon-11. Both of them used the same correlation

$$\mathrm{Nu} = 0.14[\mathrm{Ar}/Sp' \cdot \{a/g + x^2 f^2/(dg)\}]^{1/3} \tag{2.17}$$

where x and f are the amplitude and frequency of the oscillation respectively.

There are also some other literature that apply 1/3 power law to saturated pool film boiling. Such as, Frederking, Chapman, and Wang (1965), Barron and Gorgolis (1977), Farahat and Nasr (1978), Kliimenko (1980), Grigoriev, Klimenko and Shelepen (1982).

It seems that with big diameter sphere or in cryogenic liquids, 1/3 power law should be used to correlate the pool film boiling heat transfer data if $d/l' > 10$.

2.2.3 The Diameter Effect

Banchero, Barker, and Boll (1955) found that Bromley's equation did not correlate well with their data over a wide range of diameters. They modified Bromley's correlation to the form of

$$\mathrm{Nu} = A(1/d + C)d^{1/4}[\mathrm{Ar}/Sp']^{1/4} \tag{2.18}$$

where A and C are constants determined from experiment: A is given as about 0.045 (in)(ft)$^{-1/4}$, presumably for a variety of liquids, whereas C is 9.5, 36.5 and 84.0 (in)$^{-1}$ for n-pentance, oxygen, and water, respectively, at atmospheric pressure. This correlation does not allow the heat transfer coefficient to approach zero as the diameter approaches infinity. The disadvantage of this correlation is that the constant C depends on the kind of boiling liquid.

In 1962, Bareen and Westwater made another contribution to the understanding of the diameter effect on the pool film boiling heat transfer on cylinders. By introducing the Berenson's (or critical) wave length λ_c, they correlated all available pool film boiling heat transfer data on horizontal tubes by means of an empirical equation:

$$\mathrm{Nu} = (0.59 + 0.069\lambda_c/d)(d/\lambda_c)^{1/4}[\mathrm{Ar}/Sp']^{1/4} \tag{2.19}$$

Baumeister and Hamill (1967) developed a theoretical model for pool film boiling from small diameter wires. Following the trend of the experiment data, they suggested an equation

$$\mathrm{Nu} = 0.373\left[\left(\frac{d}{l'}\right)\left(1 + \frac{9}{\sqrt{6}}\frac{l'}{d} + \frac{8}{3\sqrt{6}}\left(\frac{l'}{d}\right)^3\right)\right]^{1/4}\left(\frac{\mathrm{Ar}}{Sp'}\right)^{1/4} \tag{2.20}$$

Hendick and Baumeister (1969) following the same idea developed a theoretical model for film boiling from spheres. They characterized the size of the vapor dome by the critical wave length λ_c and applied the principle of a maximum rate of entropy production. The correlation is given as

$$\mathrm{Nu} = 2 + \frac{1}{4}\left[-\frac{2}{3}\frac{\mathrm{Ar}}{Sp'}G(B_o)\right]^{1/4} + \left[0.177\left(\frac{\mathrm{Ar}}{Sp'}\sqrt{B_o}\right)^{1/4} + csc(\theta^*(B_o))\right](1 + cos(\theta^*(B_o))) \tag{2.21}$$

Where $B_o = (d/l')^2$ and $\theta^*(B_o)$, $G(B_o)$ are functions of B_o given in graphical form. This correlation was verified by experimental data with small spheres ranging from 0.397 to 12.7 mm in diameter by Hendick and Baumeister (1970).

Irving and Westwater (1986) and Westwater, Hwalek and Irving (1986), in their research on the limitation for obtaining boiling curves by the quenching method, indicated that when $d/\lambda_c > 7.8$, the heat transfer coefficient will not depend on the diameter of the sphere.

Grigoriew, Klimenko and Shelepen (1982) combined the 1/4 power law and 1/3 power law to account for the diameter effect and the turbulent effect. They use 1/4 power law for laminar film boiling when diameter is small and 1/3 power law for turbulent film boiling when diameter is large.

$$\mathrm{Nu} = 0.7\mathrm{Ar}^{1/4}\mathrm{Pr}_v^{1/3} f_1(K), \qquad \mathrm{Ar} < 3 \times 10^7 \tag{2.22a}$$

$$f_1(K) = \begin{cases} 1.0 & K \le 1.4 \\ 0.92K^{1/4} & K > 1.4 \end{cases}$$

$$\mathrm{Nu} = 0.165\mathrm{Ar}^{1/3}\mathrm{Pr}_v^{1/3} f_2(K), \qquad \mathrm{Ar} \ge 3 \times 10^7 \tag{2.22b}$$

$$f_2(K) = \begin{cases} 1.0 & K \le 1.6 \\ 0.85K^{1/3} & K > 1.6 \end{cases}$$

where $K = h_{fg}/(C_{pv}\Delta T_{sup})$. This correlation, was claimed, fits well with the data from 11 research groups which include 5 liquids and different size spheres with the diameter ranging from 0.25 to 96 mm.

Sakurai, Shiotsu and et al. (1990a, 1990b, 1992) introduced an empirical diameter-correction factor $K(d')$ to account for the diameter influence in their correlation.

$$\mathrm{Nu}/(1 + 2/\mathrm{Nu}) = K(d')(\mathrm{Ar}/Sp')^{1/4} M_c^{1/4} \tag{2.23}$$

$$\begin{aligned} K(d') &= 0.44d'^{-1/4}, && \text{for } d' < 0.14 \\ K(d') &= 0.75/(1 + 0.28d'), && \text{for } 0.14 < d' < 1.25 \\ K(d') &= 2.1d'/(1 + 3.0d'), && \text{for } 1.25 < d' < 6.6 \\ K(d') &= 0.415d'^{1/4}, && \text{for } d' > 6.6 \end{aligned}$$

where $M_c(p_{sys}, \Delta T_{sup}, \Delta T_{sub})$ is a function of liquid and steam properties at given p_{sys}, ΔT_{sup}, ΔT_{sub}, which will be given later when the pool film boiling at subcooled condition is concerned. The correlation was verified by their pool film boiling steady-state experiment

with cylinders of diameter ranging from 0.3 to 6.0 mm, in 7 different liquids and at system pressures ranged from 1 to 5 bar.

It is interesting to compare the above correlations. The six correlations were plotted in terms of $\mathrm{Nu}_{l'}/(\mathrm{Ar}_{l'}/Sp')^{1/4}$ and l'/d in Fig. 2.5 at a condition of 1.0 bar system pressure and 600 °C sphere superheat. The nondimensional group for the y coordinate is independent of diameter, and it could be expressed as

$$\frac{\mathrm{Nu}_{l'}}{(\mathrm{Ar}_{l'}/Sp')^{1/4}} = \frac{\mathrm{Nu}_d}{[(\mathrm{Ar}_d/Sp')\,(d/l')]^{1/4}} = h\left\{\frac{h'_{fg}gk_v\rho_v(\rho_l-\rho_v)}{l'\mu_v\Delta T_{sup}}\right\}^{-1/4}$$

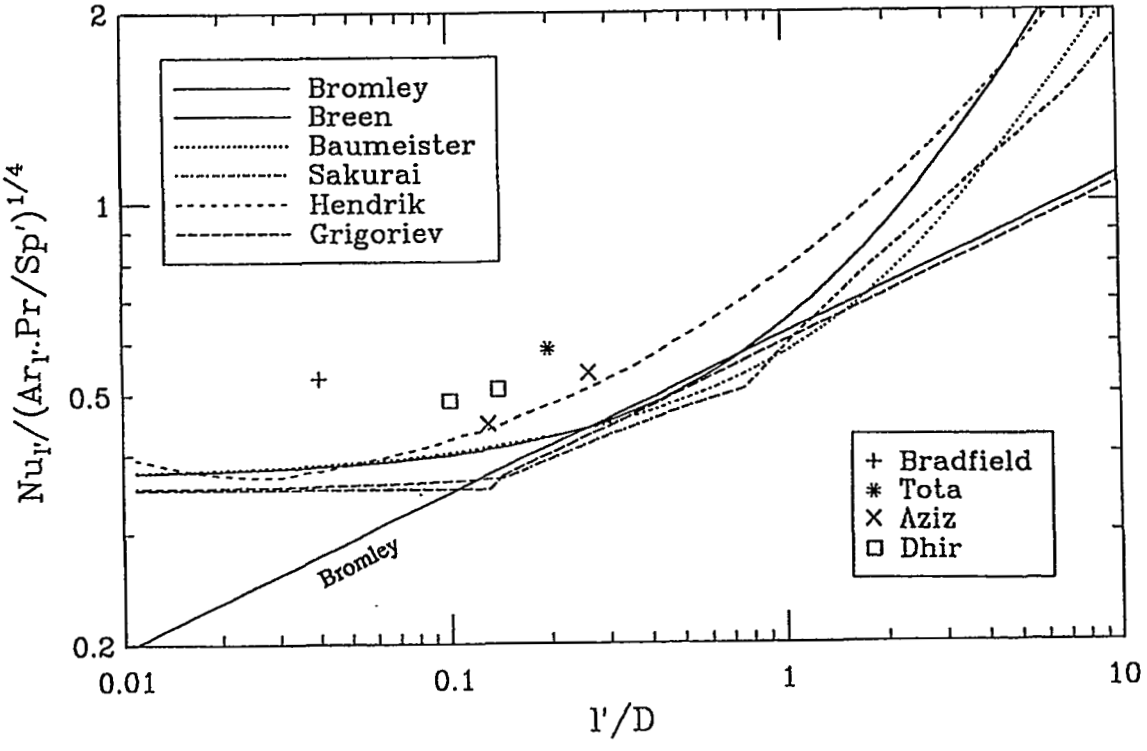

Fig. 2.5. Comparison of pool film boiling correlations for saturated condition. Comparison of experimental data with the correlations.

The comparison shows that in the l'/d range of 0.2 to 1.0, all the correlations are well agreed in a band less than 10% except Hendricks's correlation which is about 20% higher than others. Bromley's correlation is applicable in this range, but out of this range, Bromley's under predicted the pool film boiling heat transfer. For big diameter case, all correlations tend to depart from Bromley's at the l'/d value of about 0.15 and then keep at a constant level in a band of about 13%. On the other hand for small diameter, all

correlations start to deviate from Bromley's at the l'/d value of about 2.0 except the Grigoriev's correlation. In the l'/d range of 2.0 to 10.0, the Hendricks's and Breen's correlation are about 30% higher than Baumeister's and Sakurai's. Under other system pressure and superheat conditions, the comparisons is little bit different, but not significantly.

2.2.4 Experiments of Pool Film Boiling From Sphere in Water

Besides Dhir (1978), as mentioned above, there are also several other saturated pool film boiling experiment (conducted with cool-down transient of sphere in water) could be found in the literature. Bradfield (1967) obtained film boiling cool-down transient curves by 59 mm diameter pure copper sphere in water at temperatures of 95, 53 and 27 °C and at atmospheric pressure. Marschall and Farrar (1975) obtained the heat transfer coefficient by a partially submerged inconel sphere of 18.75 mm in diameter. Toda and Mori (1982) did an experiment with a 12.7 mm stainless steel sphere. Aziz , Hewitt and Kenning (1986) studied the film boiling on stainless steel spheres of 10 and 20 mm in diameter.

Some of the experimental results are given in Table 2.1 in terms of the 1/4 power law $C - 1/4$ and $C_{l'} = \mathrm{Nu}_{l'}/(\mathrm{Ar}_{l'}/Sp')^{1/4}$. The latter are plotted in Fig. 2.5. It is clear that the experimental data are about 10–20% higher than the correlations except that Aziz's data are on the line of Hendricks's. There may be two reasons for this: firstly, in the experiments the water was not completely at saturated condition, and secondly, the heat losses from the sphere support have not been concerned or correctly counted.

2.3 Subcooled Pool Film Boiling

2.3.1 The Addition Law

The earliest work on the subcooled pool film boiling may go back to 1960's. Tachibana and Fukui (1961) experimentally and theoretically studied the pool film boiling from fine nichrome wires with diameters of 0.5 and 0.8 mm in water, alcohol and carbon tetrachloride over a subcooling range of 0.0 to 45 °C at atmospheric pressure, but no correlation was generated.

Hamill and Baumeister (1967) did a theoretical analysis of film boiling from a horizontal plate with subcooling and radiation. The analysis is based on the postulation that the rate of entropy production is maximized. The general solution enables the total heat transfer coefficient to be calculated by addition of the saturated pool film boiling coefficient h_{sat}, radiation heat transfer coefficient h_r, and the subcooled turbulent convective heat transfer contribution term, which is given by

Table 2.1. Experiments of Saturated Pool Film Boiling				
Reference	d(mm)/(d/l')	T_w(°C)	$C_{1/4}$	$C_{l'}$
Bradfield(1967)	59.7/23.0	600.0	1.13	0.53
Dhir (1978)	25.4/9.77	210.0	0.86	0.49
Dhir (1978)	19.0/7.31	209.0	0.86	0.51
Toda (1982)	12.7/4.88	320.0	0.88	0.59
Aziz (1986)	20.0/7.69	510.0	0.91	0.45
Aziz (1986)	10.0/3.80	475.0	0.88	0.54

$C_{1/4} = \mathrm{Nu}/[\mathrm{Ar}/Sp']^{1/4}$; $\qquad C_{l'} = \mathrm{Nu}_{l'}/[\mathrm{Ar}_{l'}/Sp']^{1/4}$

$$h_t = h_{sat} + 0.88h_r + 0.12h_{nc}\Delta T_{sub}/\Delta T_{sup} \tag{2.24}$$

where $h_{nc} = q_{nc}/\Delta T_{sub}$ is the turbulent free-convection heat transfer coefficient for subcooled liquid, and $h_r = \epsilon\sigma(T_w^4 - T_s^4)/\Delta T_{sup}$ is the radiation heat transfer coefficient.

Bradfield (1967) experimentally studied the effect of subcooling on pool film boiling from a pure copper sphere (59 mm in diameter) and obtained the film boiling cool-down transient heat flux curves in water at temperatures of 95, 53 and 27 °C at atmospheric pressure. The study shows a strong effect of the subcooling.

Siviour and Ede (1970) investigated the subcooled pool film boiling from horizontal tubes of diameter 3.2 and 6.4 mm in water with 0–80 °C liquid subcooling. They correlated their experimental data by the addition law:

$$\mathrm{Nu}_t = \mathrm{Nu}_{sat} + J\,\mathrm{Nu}_r + \mathrm{Nu}_{nc}(Sc/Sp)(\mu_l/\mu_v) \tag{2.25}$$

$$\mathrm{Nu}_{sat} = 0.613[\mathrm{Ar}/Sp]^{1/4},\ \ \mathrm{Nu}_{nc} = 0.59[\mathrm{GrPr}_l]^{1/4}\,\mathrm{Pr}_l^{1/4}$$

where J is 0.78, $\mathrm{Nu}_r = h_r d/k_v$, and $\mathrm{Nu}_{nc} = h_{nc}d/k_l$.

Farahat, Eggen and Armstrong (1972,1974,1975) studied the pool film boiling from spheres (with diameters of 25.4, 19.0, and 12.7 mm) in subcooled sodium and water.

Following the analysis of Hamill and Baumeister (1967), They correlated their data by

$$\mathrm{Nu}_t = \mathrm{Nu}_{sat} + 0.88\mathrm{Nu}_r + K\mathrm{Nu}_{nc}(Sc/Sp)(\mu_l/\mu_v) \tag{2.26}$$

$$\mathrm{Nu}_{nc} = 0.75[\mathrm{GrPr}^n]^{1/4},$$
$$K = 11.9(\Delta T_{sub})^{-0.7}, \qquad \text{for d = 25.4 mm}$$
$$K = 18.8(\Delta T_{sub})^{-0.65}, \qquad \text{for d = 19-13 mm}$$

where Nu_{sat} is calculated by Hendricks and Baumeister (1969)'s correlation, $n = 1$ is for nonmetallic fluids and $n = 2$ is for metallic liquids. The K is a function of liquid subcooling and the diameter of the sphere.

Dhir and Purohit (1978) also applied the addition law to correlate their subcooled film boiling data that were obtained by cool-down transient of 19 and 25.4 mm diameter spheres of steel, copper and silver in water at atmospheric pressure. The correlation is given by

$$\mathrm{Nu}_t = \mathrm{Nu}_{sat} + C_r\mathrm{Nu}_r + \mathrm{Nu}_{nc}(Sc/Sp)(\mu_l/\mu_v) \tag{2.27}$$

where

$$\mathrm{Nu}_{sat} = 0.8[\mathrm{Ar}/Sp]^{1/4}, \quad \mathrm{Nu}_{nc} = 0.9[\mathrm{GrPr}_l]^{1/4}$$

2.3.2 Ratio Law

Shih and El-Wakil (1981) carried out an analysis for pool film boiling from a sphere by using an integral method. Based on their theoretical analysis, they obtained:

$$\mathrm{Nu}/\mathrm{Nu}_{sat} = 1 + 13.91[Sc\mathrm{Ar}/\mathrm{Gr}]0.39 \tag{2.28}$$

They emphasized that: for subcooled film boiling it is the ratio, not the difference between the subcooled and the saturated film boiling Nusselt numbers, that is significant. They also claimed that their experiment with stainless steel spheres of 3.2, 4.8 and 6.4 mm in diameter in Freon-11 and Freon-113 with 0–20 °C subcooling supports this correlation.

Michiyoshi, Takahashi and Kikuchi (1988) obtained an universal correlation for subcooled pool film boiling from vertical plate, horizontal plate and sphere by an analysis with integral method (see Appendix A),

$$\mathrm{Nu} = K(\mathrm{Ar}/Sp')^{1/4}M_c^{1/4} \tag{2.29}$$

where

$$
\begin{aligned}
M_c &= E^3/[1+E/(Sp'\mathrm{Pr}_l)]/(R\mathrm{Pr}_l Sp')^2 \\
E &= (A+CB^{1/2})^{1/3}+(A-CB^{1/2})^{1/3}+(1/3)Sc^* \\
A &= (1/27)Sc^{*3}+(1/3)R^2 Sp'\mathrm{Pr}_l Sc^*+(1/4)R^2 Sp'^2\mathrm{Pr}_l^2 \\
B &= (-4/27)Sc^{*2}+(2/3)Sp'\mathrm{Pr}_l Sc^*-(32/27)Sp'\mathrm{Pr}_l R^2 \\
&\quad +(1/4)Sp'^2\,\mathrm{Pr}_l^2+(2/27)Sc^{*3}/R^2 \\
C &= (1/2)R^2 Sp'\mathrm{Pr}_l, Sc^* = C_{pl}\Delta T_{sub}/h'_{fg}
\end{aligned}
$$

where $K = 0.696$ for sphere, $K = 0.610$ for horizontal cylinder, and $K = 0.793$ for vertical plate. Comparing this correlation with their own data in water and potassium and others data from literature, they concluded that: the correlation is suitable for characterizing pool film boiling in various nonmetallic liquids especially for water.

Later in 1990, Tso, Low and Ng presented a detailed derivation of this correlation for sphere case, which is given Appendix A. They also compared their experimental data which were obtained by cool-down transient of copper spheres (20 and 25 mm in diameter) in Freon-12 over a subcooling range of 0 to 70 °C. Their data are clearly (about 50%) higher than the theoretical correlation.

Sakurai, Shiotsu and Hata (1990a) carried out a rigorous solution to a theoretical pool film boiling model which including the radiation contribution for the case of horizontal cylinder. Their study indicated that the rigorous solution is in good agreement with the simple analytical solution which is the same as that obtained by Michiyoshi (1988).

Sakurai etc. (1990b) conducted a systematic experiment with electrical heated platinum cylinders in various liquids, including water, ethanol, isopropanol, Freon-113, Freon-11, Liquid nitrogen and liquid argon. The experiment was carried out in a wide range of system pressure, liquid subcooling, surface superheat and cylinder diameter. Based on their experiment, they modified their analytical solution by introducing a diameter depending empirical function $K(d')$ on the right hand side of the correlation and a factor $(1+2/\mathrm{Nu})^{-1}$ on the left hand side, which is only effective when Nu is very small. Their correlation is given as

$$\mathrm{Nu}/(1+2/\mathrm{Nu}) = K(d')(\mathrm{Ar}/\mathrm{Sp}')^{1/4} M_c^{1/4} \tag{2.30}$$

where

$$
\begin{aligned}
K(d') &= 0.44d'^{-1/4}, && \text{for } d' < 0.14 \\
K(d') &= 0.75/(1+0.28d'), && \text{for } 0.14 < d' < 1.25 \\
K(d') &= 2.1d'/(1+3.0d'), && \text{for } 1.25 < d' < 6.6 \\
K(d') &= 0.415d'^{1/4}, && \text{for } d' > 6.6
\end{aligned}
$$

Several other theoretical studies on subcooled pool film boiling from tubes, such as Nishkawa, Ito and Kuroki (1972), Nishkawa and Ito (1966), Srinivasan and Rao (1984), Nakayama and Koyama (1986a,1986b) could also be located.

2.3.3 Comparison of the Correlations

The correlations mentioned above are compared in Fig. 2.6 at a condition of 1 bar system pressure, 660 °C sphere superheat and 9.53 mm in diameter. The prediction of Shih's correlation is far above the others. Michiyoshi's, Sakurai's and Dhir's correlations give fairly consistent prediction except in the low subcooling case in which Dhir's is about 15% higher than the other two. Farahat's line is higher than the others. The Siviour's correlation is lower than others when the subcooling is large. It is clear that both correlations in ratio form and addition form show a common trend: Nu increasing with the liquid subcooling approximately linearly. This suggests us that, with the same Nu_{sat} number at saturated condition and with a proper constant for calculating the Nu_{nc} (the natural convective Nusselt number for liquid side), a correlation in addition form (as the one used by Dhir) should give the same prediction as the one in ratio form (as the one used by Michiyoshi) in a special condition. According to this thought, the following correlation in addition law may be constructed to match Michiyoshi's correlation for 1 bar pressure condition.

$$\mathrm{Nu} = \mathrm{Nu}_{sat} + \mathrm{Nu}_{nc}(Sc/Sp)(\mu_l/\mu_v) \tag{2.31}$$

$$\mathrm{Nu}_{sat} = 0.67[\mathrm{Ar}/Sp']^{1/4}, \qquad \mathrm{Nu}_{nc} = 1.45[\mathrm{GrPr}_l]^{1/4}$$

The two correlations are compared at five sphere temperatures in Fig. 2.7. It shows that for the sphere temperature higher than 500 °C, the simple correlation in addition form given by Eq. (2.31) agrees well with the correlation in ratio form given by Eq. (2.29). However, for the sphere temperature lower than 500 °C, the correlation in addition form tends to give higher predictions than the correlation in ratio form.

Moreover, the two correlations are also compared at system pressures of 1, 10 and 50 bars in Fig. 2.8. It is clear that the increase in pressure has much more effect on the correlation in ratio form than in addition form. Since the correlation in ratio form has been verified by experiment at high pressure, as claimed by Sakurai (1990b), the correlation in addition form with a fixed constant is only valid at certain pressure (for this case, it is atmospheric pressure).

From the above comparisons, it can be concluded that the correlation in ratio form given by Eq. (2.29) or (2.30) are likely valid for various of liquids and a wide range of liquid

subcooling, surface superheat and system pressure, while the correlation in addition form is only valid in certain conditions.

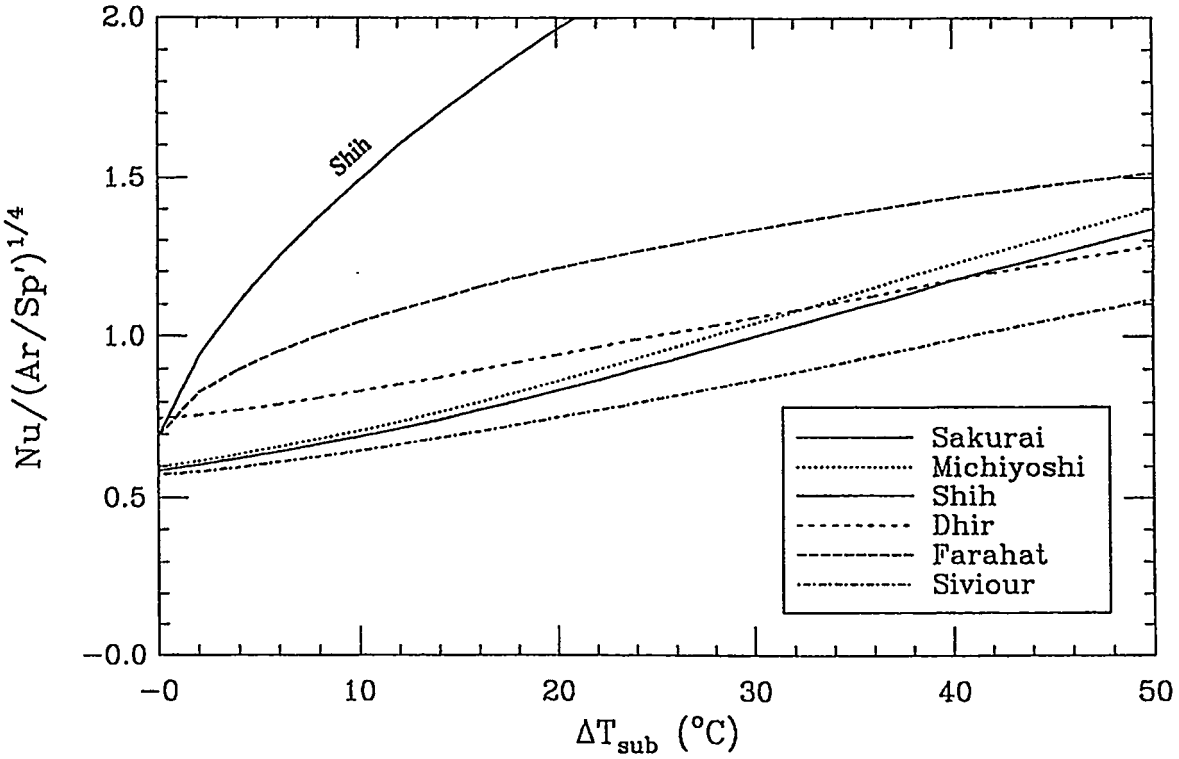

Fig. 2.6. Comparison of pool film boiling correlations at subcooled condition (with superheat of 660 °C at 1 bar pressure).

2.4 Saturated Forced Convection Film Boiling

2.4.1 Mode 1 Correlation

Bromley, Leroy and Robbers (1953) conducted a forced convection film boiling experiment with electrically heated graphite tubes (d = 9.8 – 16.2 mm) in saturated benzene, ethyl alcohol, n-hexane and carbon tetrachloride at atmospheric pressure. The flow velocity ranged from 0 to 4.0 m/sec. They also carried out an analysis which is based on Bernoulli's theorem and a consideration of the viscous drag to the vapor. From the analysis they obtained two dimensionless groups and correlated them according to their experimental data in a linear form

$$h\left[\frac{d^2\Delta T_{sup}\mu_v}{U^2k_v^3\rho_v\rho_l h'_{fg}}\right]^{1/4} = 0.88\left[\frac{gd(\rho_l-\rho_v)}{4U^2\rho_l}+\frac{3d\mu_v h^2}{Uk_v^2\rho_l}\left(\frac{\pi}{\theta'}\right)^2\right]^{1/4} \tag{2.32}$$

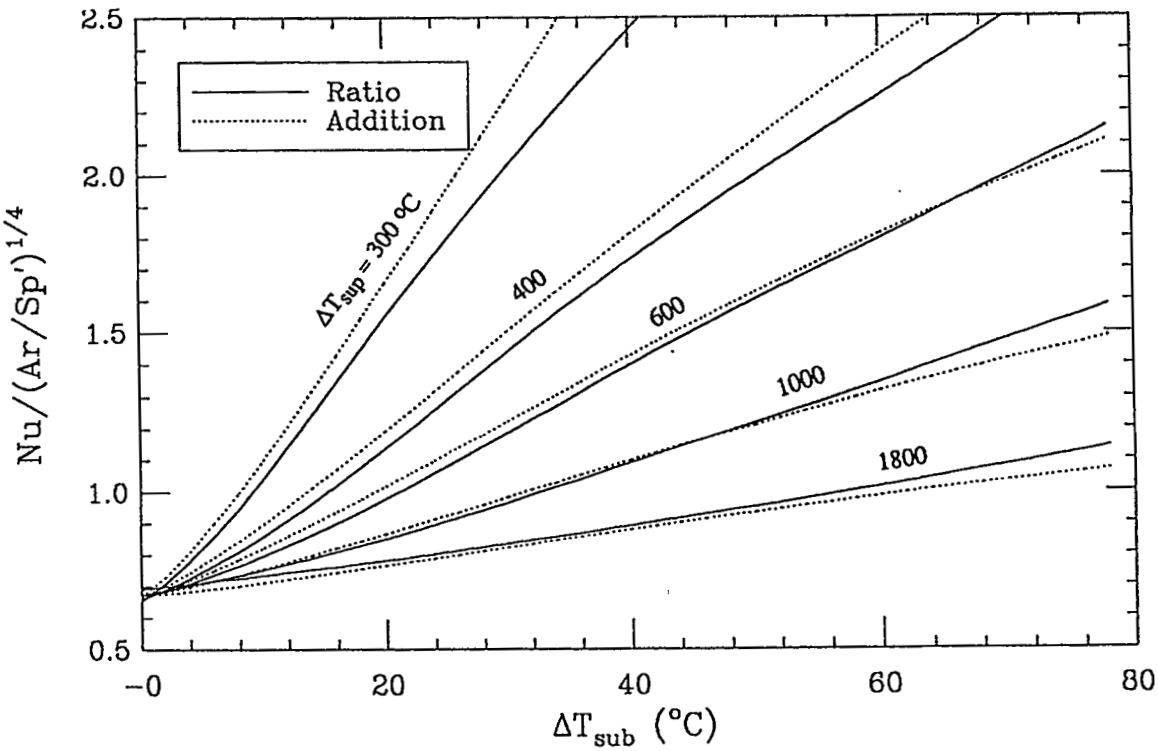

Fig. 2.7. Comparison of pool film boiling correlations in addition and ratio laws, at five different sphere superheats and 1 bar pressure.

At very low flow regime ($Fr^{1/2} < 1.0$), this equation reduces to Eq. (2.11) that is the correlation for pool film boiling. At high flow regime ($Fr^{1/2} > 2.0$) the equation becomes

$$Nu = 2.70 Re_l^{1/2} \{(v_l/v_v)/Sp'\}^{1/2} \tag{2.33}$$

Cess and Sparrow (1961) did an analysis on film boiling from a horizontal flat plate. According to their analysis, at conditions of $(\mu\rho)_v/(\mu\rho)_l$ less than 0.1 and large Re, the following equation could be obtained

$$Nu = 1.0 Re_l^{1/2} \{(v_l/v_v)/Sp'\}^{1/2} \tag{2.34}$$

which is the same correlation as that of Bromley's Eq. (2.33) except that the constant is smaller.

Witte (1968) did a simple analysis for film boiling on sphere with a given average vapor velocity $U = 3/4 U_m sin\theta$, which is the velocity of the potential flow. The theoretical result is

$$Nu = 0.698 Re_l^{1/2} \{(v_l/v_v)/Sp'\}^{1/2} \tag{2.35}$$

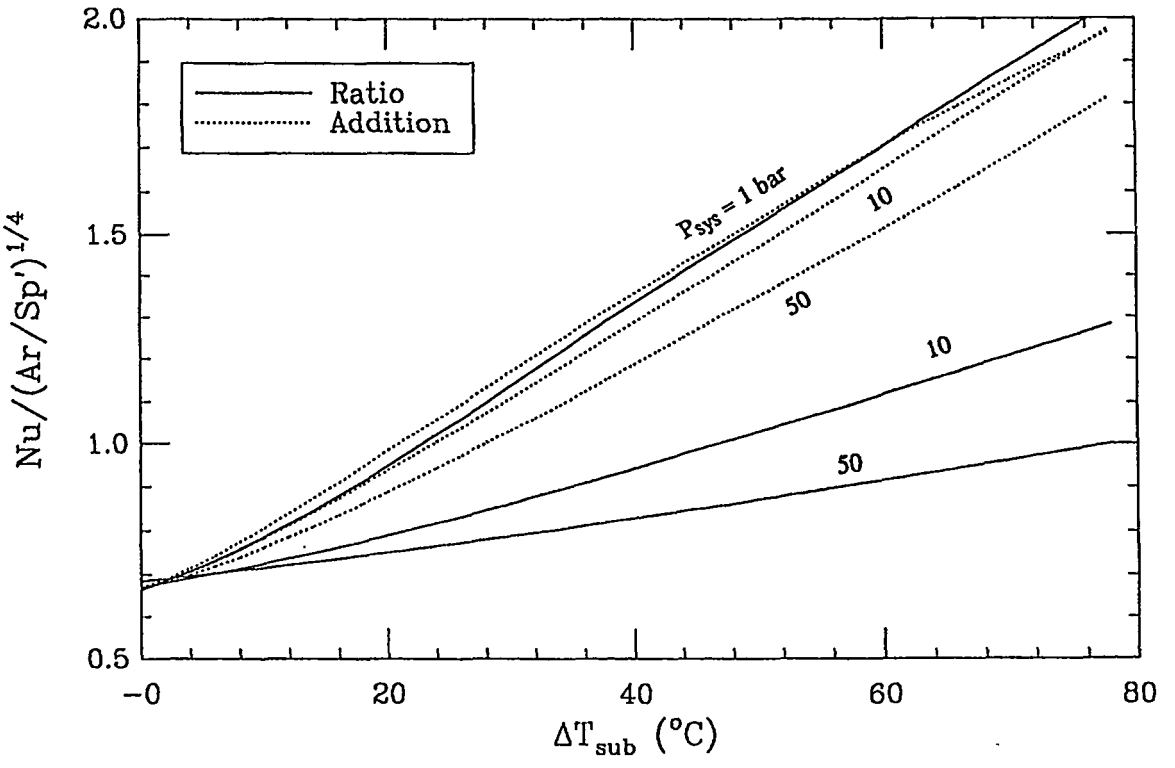

Fig. 2.8. Pressure effect on pool film boiling correlations.

Based on the ratio of his theoretical constants for sphere and tube and the Bromley's experimental correlation for tube given by Eq. (2.33), he suggested that a constant of 2.98 should be used for the saturated film boiling on spheres.

Nakayama and Koyama (1986) carried out an analysis for forced convection film boiling on a vertical plate and reached the same result as that of Cess and Sparrow (1961).

2.4.2 Mode 2 Correlation

Kobayasi (1965, 1966), following the analysis used by Bromley (1953), did an analysis for forced convection film boiling on sphere and reached two dimensionless groups

$$\Lambda = \frac{4}{3}\left\{\frac{\mu_v^2}{\mu_l^2}\frac{\rho_l}{\rho_v}Sp\right\}^{1/2}\frac{\mathrm{Nu}_c^2}{\mathrm{Re}_l}$$

$$\Psi = 16\frac{\mathrm{Nu}_c^2}{\mathrm{Re}_l}\frac{\mu_v}{\mu_l}\frac{1}{(1-cos\theta')^2} + \frac{4}{9}\frac{1}{\mathrm{Re}_l^2}\frac{gd^3}{v_l^2}$$

when $\mathrm{Fr}^{1/2} > 1.5$, $\Psi \to 0$, and $\Lambda \to 0.2066$, so the Nusselt number may be expressed as

$$\mathrm{Nu} = 0.393\,\mathrm{Re}_l^{1/2}(\mu_l/\mu_v)[R^4K/Sp]^{1/4} \tag{2.36}$$

where

$$K = \rho_l/\rho_v, \qquad R = [(\mu\rho)_v/(\mu\rho)_l]^{1/2}$$

Wilson (1979) did a theoretical study of film boiling on a sphere in forced convection. For the case of small subcooling, he obtained equation for local Nusselt number

$$\mathrm{Nu}(\theta) = C(\theta)\mathrm{Re}_l^{1/2}(\mu_l/\mu_v)[R^4K/Sp]^{1/4} \tag{2.37}$$

Epstein and Hauser (1980) applied similarity boundary theory and the perturbation method to model the forced convection film boiling in the stagnation region of a sphere or cylinder. They obtained a explicit solution for the film thickness. By consider two extremes of slight subcooling and large subcooling, they reached a theoretical Nusselt number for saturated film boiling in forced convection

$$\mathrm{Nu} = 0.553\mathrm{Re}_l^{1/2}(\mu_l/\mu_v)[R^4K/Sp]^{1/4} \tag{2.38}$$

However, by comparing with the experimental data from Bromley (1953), Motte (1957) and Dhir (1978) in both small subcooling and high subcooling cases, they suggest a factor 2.04 should be applied to their theoretical equation to predict the film boiling heat transfer. This is definitely too high for the case of saturated film boiling, as shown later, and it is obvious even from the Fig. 2 in Epstein and Hauser (1980).

Ito, Nishikawa and Shigechi (1981) theoretically studied the saturated forced convection film boiling from a cylinder by means of integral method with two-phase boundary layer. Their numerical solution indicated that for $\mathrm{Fr}^{1/2} > 2.0$

$$\mathrm{Nu} = 0.46\mathrm{Re}_l^{1/2}(\mu_l/\mu_v)[R^4K/Sp]^{1/4} \tag{2.39}$$

The constant is slightly different for different fluids, with 0.46 for water, 0.48 for ethanol and 0.51 for hexane.

Liu, Shiotsu and Sakurai (1992) carried out an approximate analytical solution for saturated film boiling from a horizontal cylinder. They reached a solution in the form of

$$\mathrm{Nu} = C\ \mathrm{In(Fr)}[\mathrm{Ar}/Sp]^{1/4} \tag{2.40}$$

where C is a constant which depends on the assumption of boundary condition, In(Fr) is a function of Fr number. Based on their experiment with water and Freon-113 at system pressures from 1 to 5 bar, they obtained a correlation

$$\mathrm{Nu}/(1 + 2/\mathrm{Nu}) = H(\mathrm{Fr}, d')K(d')[\mathrm{Ar}/Sp'M_c]^{1/4} \tag{2.41}$$

$$H(\mathrm{Fr}, d') = (1 + 0.68\mathrm{Fr}^{2.5/4})^{1/2.5} + 0.45 tanh\{0.04(d' - 1.3)\mathrm{Fr}\}$$

for the case of forced convection, $H(\mathrm{Fr}, d') = 0.75\ \mathrm{Fr}^{1/4}$ and $H \cdot K(4.0) = 0.554\mathrm{Fr}^{1/4}$. Thus, for forced convection with $d' = 4.0$ ($d = 10$ mm), it gives approximately

$$\mathrm{Nu} = 0.554\mathrm{Re}_l^{1/2}(\mu_l/\mu_v)[R^4 K/Sp]^{1/4} \tag{2.42}$$

In addition to the studies mentioned above, there are several other papers that are related with the experimental study of saturated forced convection film boiling such as Dhir and Purohit (1978), Aziz, Hewitt and Kenning (1986), Zvirin, Hewitt and Kenning (1990), and Dix and Orozco (1990). All the experiments were done by pass a preheated sphere through a still water pool. In aspect of analysis, Witte and Orozco (1984) did a theoretical study on the effect of vapor velocity profile shape on saturated and subcooled flow film boiling from sphere and cylinder. Their study indicated: a comparison of the analysis to available experimental data shows that heat transfer results based on a quadratic vapor velocity profile compare much better with experiments than those based on linear profile; the heat transfer results for linear and quadratic vapor velocity profiles become virtually identical as subcooling increases.

2.4.3 Comparison and Comments

In order to compare the two kinds of correlations, the mode 1 correlation can be rewritten as

$$\begin{aligned}\mathrm{Nu} &= C_1\mathrm{Re}_l^{1/2}(\mu_l/\mu_v)[R^4 K/Sp']^{1/4}[KSp']^{-1/4} \\ &= C_1\mathrm{Re}_l^{1/2}(\mu_l/\mu_v)[R^4/Sp'^2]^{1/4}\end{aligned} \tag{2.43}$$

Besides using Sp' instead of Sp, the mode 1 correlation has an extra term $[KSp']^{-1/4}$ in comparison with the mode 2 correlation (such as given by Eq. (2.42). Because the powers on the Re_l are the same in both kinds of correlation, the velocity dependencies are the same in both cases, however, the dependencies on temperature are different. The constant C_1 is about 2.7 while the constant C_2 used in the second mode correlations is about 0.5.

Now the question is: which mode is better in taking account of the surface superheat and other effects, such as system pressure and different liquids? Since the mode 2 correlations come out from more rigorous analyses than mode 1 and the mode 2 correlation used by Liu, et al (1990) was claimed to be verified by various liquids at pressures range from 1 to 5 bar, the mode 2 correlation is likely to be the better one. This is also confirmed by our experimental data, as shown later.

2.5 Subcooled Forced Convection Film Boiling

2.5.1 Theoretical Analysis

Motte and Bromley (1957) did an analysis for subcooled forced convection film boiling by arguing that

$$q = q_v + q_l \tag{2.44}$$

where q is the total film boiling heat flux, q_v the net heat flux that flow into the vapor layer and q_l is the heat flux that flow into the liquid stream. From the Bromley's correlation Eq. (2.32), they obtained the q_v. They suggested that q_l may be evaluated in three different ways according to the turbulence intensity of flow system. By a universal expression they give a correlation in the form of

$$h\left(\frac{d\Delta T_{sup}}{Uk_v\rho_v h'_{fg}}\right)^{1/2} - \frac{7.29}{h}\left(\frac{Uk_v\rho_v h'_{fg}}{d\Delta T_{sup}}\right)^{1/2} = K\Delta T_{sub}C_{pl}\rho_l\left(\frac{(\alpha+\alpha_t)}{\Delta T_{sup}k_v\rho_v h'_{fg}}\right)^{1/2} \tag{2.45}$$

where α_t is the turbulent eddy diffusivity for heat. This correlation has been used by Chou and Witte (1992) to compare their analysis with experimental data.

Cess and Sparrow (1961b), following their analysis for saturated film boiling in Cess and Sparrow (1961a), carried out a boundary-layer analysis for forced convection film boiling on a flat plate in subcooled liquid. For the case of high subcooling, their explicit expression can be rearranged in the form of average Nusselt number.

$$\mathrm{Nu}_x = (2/\sqrt{\pi})\mathrm{Re}_{l,x}^{1/2}\mathrm{Pr}_l^{1/2}(\mu_l/\mu_v)(Sc/Sp) \tag{2.46}$$

Wilson (1979) did a theoretical study of film boiling on a sphere in forced convection. He assumed that the liquid velocity field, including the liquid boundary-layer, could be given by a potential flow distribution. Then the integral method was used to the vapor boundary-layer. By applying Pohlausen-type integral technique, an ordinary differential equation of the film thickness was obtained. For low subcooling and high subcooling cases, the differential equation can be integrated analytically. In the case of low subcooling the result is given in the form of Eq. (2.37). In the case of large subcooling, the solution can be expressed in the form of local Nusselt number

$$\mathrm{Nu}(\theta) = C(\theta)\mathrm{Re}_l^{1/2}\mathrm{Pr}_l^{1/2}(\mu_l/\mu_v)(Sc/Sp) \tag{2.47}$$

As mentioned early, Epstein and Hauser (1980) did an analysis of forced convection film boiling in the stagnation region of a sphere or cylinder and obtained an explicit

solution of the film thickness. By considering the two extremes of slightly subcooling and large subcooling, they obtained two simple expressions. The Nusselt number for the saturated case is given in Eq. (2.38), and for the large subcooling case is given as

$$\mathrm{Nu} = 0.977\mathrm{Re}_l^{1/2}\mathrm{Pr}_l^{1/2}(\mu_l/\mu_v)(Sc/Sp) \tag{2.48}$$

Then they simply combined them for all subcooling cases in the following way

$$\mathrm{Nu} = \{\mathrm{Nu}_{sat}^4 + \mathrm{Nu}_{sub}^4\}^{1/4} \tag{2.49}$$

By comparing with the experimental data from Bromley (1953), Motte (1957) and Dhir (1978) in both small subcooling and high subcooling cases, they suggested that a factor 2.04 should be applied to the theoretical equation Eq. (2.49) to predict the film boiling heat transfer.

Fodemski and Hall (1982) in their analysis of forced convection film boiling in subcooled liquid applied the *ordinary* forced convection correlation

$$\mathrm{Nu}_{fc}(\theta) = \frac{q_{fc}(\theta)}{\Delta T_{sub}}\frac{d}{k_l} = C(\theta)(\mathrm{Re}_l\mathrm{Pr}_l)^{1/2} \tag{2.50}$$

to calculate the heat flow into the liquid stream. In the case of large subcooling, the film boiling heat flux q will approximately equal the convective heat flux q_{fc}. Eq. (2.49) can be rearranged into the form of Eq. (2.47).

Shigechi and Ito (1983) extended Ito et al (1981)'s study for saturated film boiling to subcooled case. The integral method was applied to both liquid boundary-layer and vapor film layer to get differential equations. The numerical solution given by the Fig. 6 in their report shows that, for Fr > 0.5 and large subcooling $Sc > 0.05$, the following expression holds for all the three liquids: water, ethanol and hexane.

$$\mathrm{Nu} = 1.15\mathrm{Re}_l^{1/2}\mathrm{Pr}_l^{1/2}(\mu_l/\mu_v)(Sc/Sp) \tag{2.51}$$

All the above theoretical analyses except Motte et al (1957) reached the same expression except the constant, as given by Eq. (2.51), for large subcooled forced convection film boiling, and this may also be interpreted as

$$\mathrm{Nu}_{fc} = \frac{q_{fc}}{\Delta T_{sub}}\frac{d}{k_l} = C(\mathrm{Re}_l\mathrm{Pr}_l)^{1/2} \tag{2.52}$$

So, it can be concluded that at large subcooling cases, $q_c \approx q_{fc}$, and Eq. (2.51) is the best formula for correlating the subcooled forced convection film boiling heat transfer data, as we know right now.

Since all the studies mentioned above have laminar assumption in the analysis, the 1/2 power on Reynolds number and Prandtl number may only be correct in laminar flow film boiling. If the flow around the sphere is turbulent the power should be higher than 1/2 as in the case of conventional forced convection.

Additional theoretical work can be found in Fodemski (1985, 1992), Hsiao, Witte and Cox (1975), Orozco, Stellman and Poulikakos (1987), and Walsh (1979).

2.5.2 Experimental Studies

Motte and Bromley (1957) conducted a film boiling experiment with electrically heated graphite tube in subcooled ethyl alcohol, benzene, carbon tetrachoride, and hexane. The diameters of the test tube were 9.8, 12.6 and 16.2 mm; the flow velocity ranged from 1.0 to 4.0 m/s; the liquid subcooling was from 0. to 40 °C, and the system pressure was at atmospheric pressure. They also studied the turbulence effect by putting screens in the upstream of the test section, and they found that this can cause approximately 30% increase in one of their dimensionless group, which is given by the left hand side of Eq. (2.45).

Shigechi and Ito (1983) cited the forced convection film boiling data from Nishikawa et al (1978). The experiment was carried out with 16 mm diameter cylinder in water at 5, 10, and 15 °C subcooling and at atmospheric pressure.

For subcooled forced convection film boiling *on cylinders*, those are the only two experiments that could be located. On the other hand, there are lots of experiments for film boiling on sphere in subcooled liquids, some of them are summarized in Table 2.2.

All the experiments were conducted at atmospheric pressure. Most of the experiments were done by a cool-down transient through a still water pool in a very short time interval, except Jacobson and Shair's (1970) and Orozco and Witte's (1986) (will be discussed latter). The maximum sphere traveling length is given in the table by L. The sphere traveling time in the liquid can be calculated from L/U which is much less than 0.5 s for most of the high speed cases. In such a short time, the thermal response of the sphere and the entrance effect will limit the accuracy of the experimental data. This implies that the accuracy of all the large velocity data obtained from above experiments are questionable.

Table 2.2. Film Boiling Experiments with Spheres

Reference	D (mm)/ L (m)	Material	Liquid	Subcooling (°C)	Velocity (m/sec)
Walford 1969	6.35/0.3	nickel	water	5–60	0.50–1.80
Jacobson 1970	12.7	steel	water	50–80	0.04–0.27
Stevence 1971	19.0/0.9	copper	water	40–76	2.90-6.00
Stevence 1973	25.4/0.9	silver	water	23-76	1.52
Dhir 1978	19.0/0.8	s. steel	water	0-50	0.02-0.45
Aziz 1986	20.0/0.2	copper	water	0-20	0.01-1.80
Orozco 1986	38.1	copper	Freon-11	9-19	1.60-2.32
Dix 1990	38.4/3.0	copper	Freon-113	0-20	0.50-1.90
Zvirin 1990	16, 32/1.5	copper	water	0-40	1.60-2.40

On the other hand, with low speed (lower than 0.5 m/s) the obtained data may be reasonably correct, but they are not in the forced convection regime. Dhir and Purohit's (1978) experiment is an example of a such case. They suggested a correlation

$$\mathrm{Nu} = \mathrm{Nu}_{p,s} + 0.8\mathrm{Re}_l^{1/2}\{1 + (\mu_l/\mu_v)(Sc/Sp)\} \tag{2.53}$$

which is only valid in the regime of $0.046 < \mathrm{Fr}^{1/2} < 1.03$ ($1200 < \mathrm{Re}_l < 19000$). Where $\mathrm{Nu}_{p,s} = 0.8\,(\mathrm{Ar}/Sp)^{1/4}$ is the Nusselt number at saturated pool film condition.

Jacobson and Shair (1970) conducted an experiment with continually heating the test sphere by induction. The sphere was supported by the liquid flow with a Lavit disk in the front of the sphere. The temperature of the sphere was determined with a Pyro microptical pyrometer. Although the experimental techniques are quite interesting, the test flow velocity is too low to be interesting.

Orozco and Witte (1986) heated their test sphere by circulating Dowtherm G through a passage in a hemisphere sphere. Although this technique avoids the short transient problem, it may be difficult to account for the heat loss at the back side of the sphere. From their experiment, a correlation was suggested in the form of

$$\mathrm{Nu} = 18.73(\rho_v/\rho_l)[\mathrm{Re}_l Sc\mathrm{Pr}_l^2]^{5/8} Sp'^{-3/2} \tag{2.54}$$

Dix and Orozco (1990) carried out a study on local heat transfer distribution on a sphere surface. They concluded that in the stable pool film boiling, the heat flux were relatively uniform as a function of angular position along the surface of the sphere. In

forced convection film boiling, significant heat flux were recorded in the vapor wake region of the sphere; and these heat flux varied from 0.3 to 1.5 times of the heat flux at the front stagnation region. The heat flux in rear wake region were most noticeably affected by detachment of the vapor wake because of the subcooling. But the authors did not pay attention to and discuss the effects of the big support tube both on the observation and on local heat transfer result in the rear part of the sphere.

2.5.3 Comments and Conclusion

There are no good experiments for film boiling on sphere in subcooled forced convection regime (with high Fr number) because the cool-down transient technique used by most of the experiments is not suitable for high speed test.

The equations in the form of $\mathrm{Nu} = C\mathrm{Re}_l^{1/2}\mathrm{Pr}_l^{1/2}(\mu_l/\mu_v)(Sc/Sp)$ are likely to be the best way to correlate large subcooled film boiling in forced convection regime. But the 1/2 power on Re and Pr may not be good for turbulent flow film boiling. How to combine the saturated and large subcooled correlations to express the small subcooled film boiling is a very practical issue and it is addressed in this work.

2.6 Summary of the Previous Studies and the Goals of the Present Work

In conclusion, regarding the previous work on film boiling from spheres, the experimental studies are summarized in Table 2.3 and the theoretical studies are summarized in Table 2.4. According to the experimental and theoretical studies, the best heat transfer correlations for film boiling on spheres in single-phase flows are listed in Table 2.5.

Regarding previous work on film boiling from spheres, it can be concluded that: For two-phase Flows: No experiment or analysis for sphere film boiling in two-phase flows can be located. For Single-Phase Flows: (1) All the meaningful single-phase film boiling heat transfer data were obtained through short cool-down transients (by passing a preheated sphere through a liquid tank). Although the short cool-down transient technique is good enough for pool or low speed forced convection film boiling experiments, it is not adequate for high velocity forced convection film boiling, because the transient is too short. For example, with sphere speed at 2.0 m/s and pool length 0.5 m, the film boiling cool-down transient is only about 0.25 second! Within such a short time, the entrance thermal response may affect the accuracy of the experimental data. (2) The accuracy of the single-phase data may be very poor as a result of the large heat loss from the support-tube, since the sphere-support-tube diameter to sphere diameter ratios of the previous experimental work are about 0.12 to 0.3. (3) For each single-phase film boiling regime,

the basic form of heat transfer correlation has been well developed, but there are some uncertainties in the correlation constants, as shown in Table 2.5. (4) There is no general correlation or complete theoretical analysis for film boiling on spheres which covers all the single-phase flow regimes. There is no theoretical model for the heat transfer in the separated rear region of the sphere.

The main purpose of this work is to establish the experimental data base and to derive the heat transfer correlation (closure law) for film boiling on spheres. The emphasis is on very high temperature film boiling (pure film boiling with the sphere temperature higher than the quenching point) in all the flow regimes, which cover from natural convection (pool film boiling) to forced convection, from saturated to highly subcooled, and from single-phase flow to two-phase flow. Besides this, theoretical analysis is carried out to understand the fundamentals of film boiling and to formulate better heat transfer correlations. The key techniques and scopes of the present experimental work are listed in Table 2.3 and the basic models used in the present theoretical analysis are shown in Table 2.4.

The goals of the present study are:

- Build a robust and flexible experimental system for sphere film boiling experiment in both single- and two- phase flows.
- Obtain high quality single-phase film boiling heat transfer data, clarify the uncertainties and construct a general correlation.
- Develop a theoretical model to predict the film boiling heat transfer in single-phase flows with an emphasis on the modeling of the separated rear region.
- Establish data base for sphere film boiling in two-phase flows and formulate heat transfer correlations.
- Study the influence of multi-sphere array structure on the sphere film boiling heat transfer in single- and two- phase flows.

In the following chapters each individual aspect of these goals will be presented in detail respectively.

Table 2.3. Experimental Studies of Film Boiling On Spheres

	Previous Studies		Present Work
Single - Phase	Saturated Pool	Bradfield (1967) Dhir (1978) Toda (1982) Aziz (1986) Farahat (1972) Shih (1981) Stick a pre-heated sphere into a liquid Tank	• Induction heating • Testing in a flow loop • Whole transient cooldown from 900 C to quench • Steady state mode operation • Sphere directly supported by thermocouples (less heat loss) • Experimental Ranges: Velocity: 0 -- 2.3 m/s; Re < 2.10^5 Fr < 80 Subcooling: 0 -- 40 C Superheat: 900 C to quench Diameter: 6 -- 19 mm Sphere material: stainless steel or brass
	Subcooled Pool		
	Saturated Forced Convection	Walford (1969) Stevence (1971) Dhir (1978) Aziz (1986) Pass a pre-heated sphere through a liquid tank	
	Subccooled Forced Convection	Jacobson(1969) Induction Heating Orozco(1986) Internal Convective Heating	
Two-Phase	Bubbly Two - Phase	None	• Two-phase mixer • X-ray radiography for void fraction measurement • Experimental Ranges: Upward two-phsae flow: Water Velocity: 0.6 -- 3.2 m/s Steam Velocity: 3.0 -- 9.0 m/s Void Fraction: 0.2 -- 0.65 Downward two-phase flow: Water Velocity: 1.9 -- 6.5 m/s Steam Velocity: 1.1 -- 9.0 m/s Void Fraction: 0.7 -- 0.95
	Mist-Jet Two - Phase	None	

Table 2.4. Theoretical Studies Of Film Boiling on Spheres In Single- Phase Flows

	Previous Studies			Present Work
	Reference	Subcooling	Method	
Pool	Frederking (1963)	Saturated	Laminar Boundary Layer, Integal Method	Two-Phase Laminar Boundary Layers Model Integal Method
	Hendick (1969) Shih (1981) Dhir (1978) Michiyoshi (1988)	Subcooled		
Forced Convection	Kobayasi (1965)	Saturated	Bernoulli's Theorem	*Unseparated Region:* Two-Phase Laminar Boundary Layers Model *Separated Region:* Turbulent Eddy Model Integal Method
	Witte (1968)	Subcooled	Uniform Film Vapor Velocity	
	Wilson (1979)	Subcooled	Similarity	
	Epstein (1980)	Subcooled	Stagnation Point Perturbation	
	Whitte (1984)	Subcooled	Velocity Distribution Effect	

Table 2.5. Heat Transfer Correlations for Film Boiling on Spheres in Single-Phase Flows

Regime	Basic Correlation	Constant	References
Saturated Pool	$\mathrm{Nu} = C(\mathrm{Ar}/Sp')^{1/4}$	0.62 0.586 0.8 $C(d)$	T: Bromley (1950) S: Frederking (1963) S: Dhir (1978) T: Bareen (1962)
Subcooled Pool	$\mathrm{Nu} = C(\mathrm{Ar}/Sp')^{1/4} M_c^{1/4}$	0.696 0.696 $K(d)$	S: Michiyoshi (1988) S: Tso (1990) T: Sakurai (1990)
Saturated Forced Convection	$\mathrm{Nu} = C\,\mathrm{Re}_l^{1/2} \mu_l/\mu_v (KR^4/SP')^{1/4}$	0.393 0.553 0.46	S: Kobayasi (1966) S: Epstein (1980) T: Ito (1981)
Subcooled Forced Convection	$\mathrm{Nu} = C\,\mathrm{Re}_l^{1/2}\,\mathrm{Pr}_l^{1/2} (\mu_l/\mu_v)(Sc/Sp)$	0.977/2.0 1.15 1.13	S: Epstein (1980) T: Shigechi (1983) P: Cess (1961b)
S – Sphere; T – Cylinder; P – Plate; $\mathrm{Ar} = g(\rho_l - \rho_v)d^3/(\rho_v \upsilon_v^2)$; M_c is given by Eq. (2.29)			

3 EXPERIMENTAL APPROACHES AND TECHNIQUES

In order to get film boiling heat transfer data in well defined flow conditions (either two-phase or single-phase), the flow inside the test section must reach a steady state before the heat transfer data are collected. This requires an adequate and well-controlled heat supply to sustain a high temperature (over ~1000 °C) film boiling in a steady-state flow. This is a very significant experimental challenge, since all the conventional heating techniques do not work in this case. For instance, the conventional internal electrical heating cannot work at such a high temperature; the surface heating by electric current is not possible for spherical geometry; and the internal convective heating (circulating hot liquid into a passage inside the test sphere) is impossible in high temperature cases. Moreover, all these techniques require either insulated wires for electric power supply or channels for heating fluid and they unavoidably cause large amounts of heat loss and disturbance on the flow field. After extensive experimentation with various alternatives, the radio frequency induction heating method was selected for our experiment. Eventually, it became possible to heat the sphere and to sustain film boiling at a temperature over 1000 °C in any desired flow conditions. Besides the cool-down transient technique, the heat flux can also be obtained through a steady state operation based on the induction power coupling calibration.

Other major difficulties are the generation and characterization of the two-phase flows in various two-phase flow regimes. A well designed two-phase mixer was used to generate the two-phase flows. An X-ray radiography was applied to measure the void fraction in the test section for two-phase runs.

3.1 Flow Loop

The flow loop is schematically illustrated in Fig. 3.1. The water loop is built up with copper tube of 38 mm (1.5 in.) I.D. The steam loop is built up with copper tube of 25.4 mm (1.0 in.) I.D. The arrangement of the mixer/test-section assembly is reversible so that they can be connected to the "top separator" or to the "water tank," to generate upward flow and downward flow respectively. The up-flow geometry is necessary for single-phase flow and low void fraction bubbly two-phase flow, while the down-flow geometry is more suitable for high void fraction two-phase flow. However, for very high liquid velocity two-phase flows, either upward or downward geometry could be used.

Water is recirculated with a pump and thermostatically maintained to a fixed temperature. The steam is supplied from lab lines, filtered, metered and used in a once-through

fashion, i.e., vented into the atmosphere or to a condenser after separation. All loop components are externally insulated except the test section.

All flow measurements are made with venturis. The pressure differences given by the venturis are read both by mercury U-tubes and by Validyne pressure transducers which are interfaced with a PC computer through a data acquisition system. Venturis of different sizes can be easily switched into the loop for different ranges of flow rate. The water flow rate measurement is calibrated by volumetric method, providing a measurement accuracy of about $\pm 4\%$. The steam flow rate measurement is calibrated and checked by calorimetric method, which confirms a measurement accuracy of about $\pm 5\%$.

In the present arrangement, the loop system is designed to be operated at atmospheric pressure. However, with modifications of the water tank and test section, the whole loop can be operated at system pressure of 10 bar. The maximum water flow rate is 50 GPM, which provides superficial water flow velocity of 2 m/s in the test section. The peak steam supply rate is 12 gram/s, which gives an equivalent superficial steam velocity of 20 m/s in the test section.

3.2 Two-Phase Mixer

The two-phase mixer is schematically illustrated in Fig. 3.2. The tube needles are made of brass. On each tube needle assembly, there are a total of 69 tubes on a square grid of 3.81 mm center to center. Three tube-needle assemblies are used in the experiment. The sizes of the tubes and the ratios of tube-hole opening area to base area of these assemblies are as follows:

No. 1 tube-needle assembly:	1.37 mm I.D.;	1.83 mm O.D;	10.2% ,
No. 2 tube-needle assembly:	1.80 mm I.D.;	2.41 mm O.D.;	17.5% ,
No. 3 tube-needle assembly:	2.31 mm I.D.;	2.77 mm O.D.;	28.9% .

With opening and closing the valves, the loop can supply either water or steam into each of two chambers in the mixer. The mixing is achieved by injecting or flowing one phase of the flow into another through the tube needles.

To generate an upward bubbly two-phase flow, the steam is supplied to the needle chamber and introduced into the water flow through the tube needles. On the other hand, to generate high void fraction droplet or jet flow, the water drop or jet is introduced into the steam flow through the tube-needles, and the downward flow arrangement is preferred. To generate a high speed mist/jet flow, either of the above arrangements may be used.

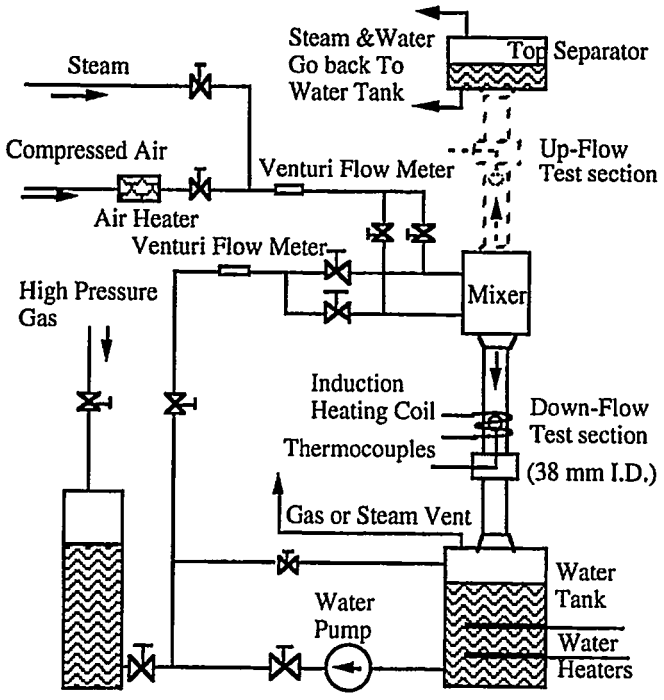

Fig. 3.1. Schematic of the flow loop.

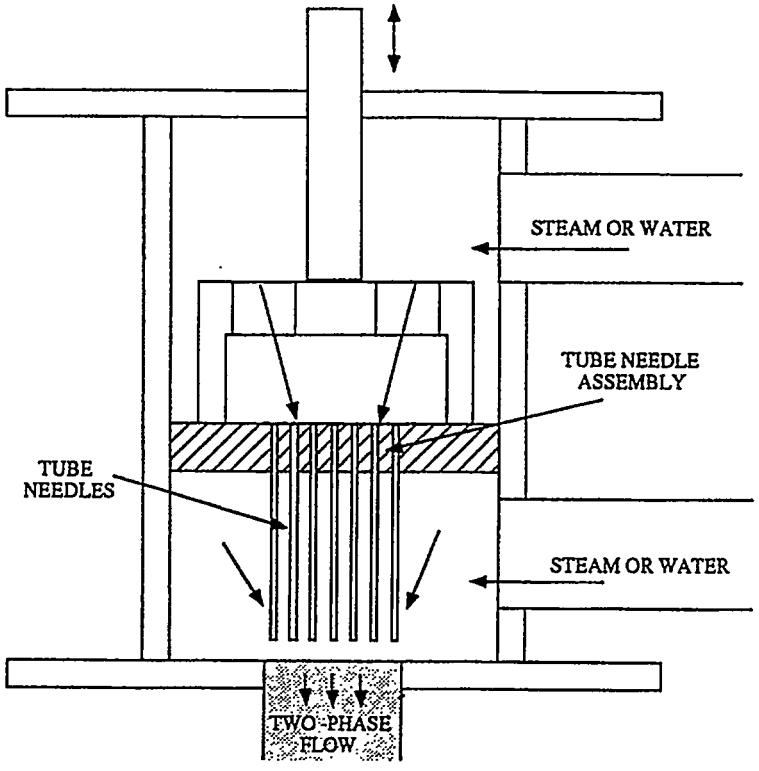

Fig. 3.2. Schematic illustration of the two-phase mixer. The tubes (69 total) are on a square grid of 3.81 mm center to center.

3.3 Test Section and Test Spheres

The test section, as shown in Fig. 3.1, consists of two pieces of Pyrex tube and a middle flange which serves as the sphere support. The circular test section is 38 mm in diameter and 330 mm in length. The induction copper-tube coil is tightly wound on the outer side of the test section (which is 47 mm O.D.) and hooked up to a RF induction power supply.

The test sphere is supported from the middle flange, as shown in Fig. 3.3, with its distance from the entrance of the test section usually being 170 mm (or 4.3 pipe diameters). Stainless steel and brass balls/spheres of 6.35, 9.53, 12.7, 19.1 mm O.D are used in the experiments. The spheres are drilled, as shown in Fig. 3.4, to accept thermocouples (stainless steel sheathed, K type) at three positions: the forward stagnation point, the center, and the rear stagnation point — these are referred to as positions 1, 2 and 3, respectively. The three thermocouple assembly is used to show the temperature distribution inside the sphere. Since the Biot number is about 0.3 at subcooled forced convection case and is much aller at saturated condition, the lump capacity mode is assumed for simplicity. So, in all the runs for heat transfer data only one thermocouple was installed in the test sphere with its tip located on the center line and 1/4 diameter from the front stagnation. The temperature measured from this thermocouple is treated as the average temperature of the sphere. The sphere is directly supported by these sheathed thermocouples (in some tests only one is used to minimize the heat loss from the thermocouples). Approximately 15 mm from the sphere, as shown in Fig. 3.3, the thermocouple stems are reinforced by a stainless steel tube of 1.53 mm O.D., which is fixed to the end of a steel duct-beam. At the other end of the duct-beam, four strain gauges are installed on the surface inside the duct to measure the force/drag on the sphere. The duct keeps the strain gauges away from water and steam and also serves as a passage for the thermocouples to pass through. The sphere itself and the thermocouple sheaths provide an adequate shielding from the RF electromagnetic field to allow undisturbed thermocouple signals, even with the induction heating power on.

The reason for supporting the sphere directly by thermocouple is to minimize the heat loss from the support. In our experiments, 0.25 mm O.D. sheathed thermocouples are used for 6.35 mm O.D. spheres; 0.5 mm sheathed thermocouples for 9.53 mm spheres; and 0.81 mm sheathed thermocouples for 12.7 and 19.1 mm spheres. With these selections, the thermocouple to sphere diameter-ratios are less than 0.06 (the corresponding area-ratios are less than 1%). In contrast, Dhir and Purohit's (1978) diameter-ratios are about 0.15; Aziz, Hewitt and Kenning's (1986) ratios are 0.3 and 0.15; Dix and Orozco's (1990) ratio is 0.25. Thus, the heat loss from the supports is significantly minimized in our experiments.

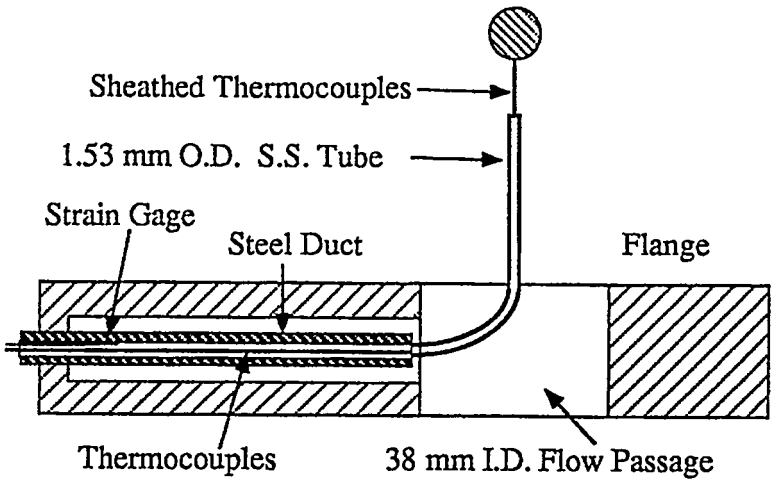

Fig. 3.3. Schematic illustration of the test sphere support flange.

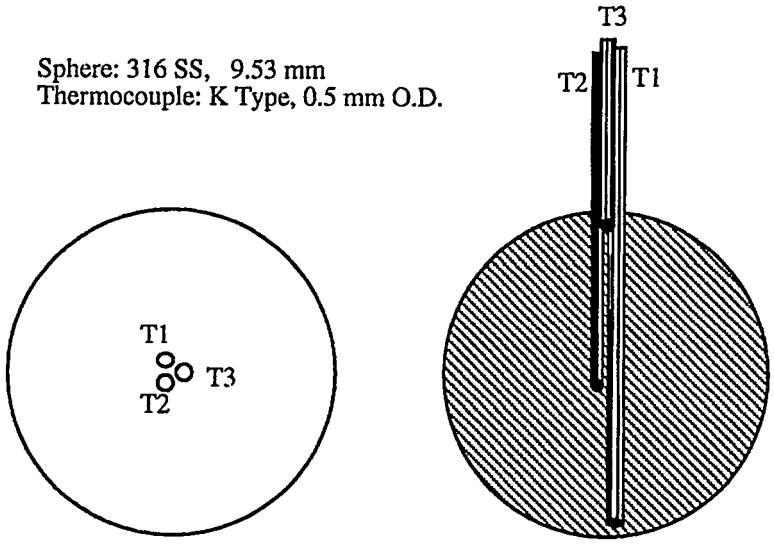

Fig. 3.4. Schematic of the instrumented test sphere.

Our experiment also indicates that, in the case 9.53 mm O.D. sphere, using three 0.5 mm O.D. thermocouples instead of only one will cause about a 20% increase in the film boiling heat transfer with all the other conditions being the same. Actually, the mechanism of this increasing is quite complicated because the adding of two more thermocouples not only triples the heat transfer surface but also helps to drain more water to the surface on the back of the sphere. This means the increase of heat loss is more than twice. This will be discussed at some depth later on.

The arrangement of the test-section/support-flange assembly is also reversible such that the sphere support tube can be located either down-stream of the sphere (as shown in Fig. 3.1), which is more suitable for heat transfer tests, or up-stream of the sphere, which is more suitable for film configuration observation (because the disturbance of the support to the vapor film on the rear part of the sphere can be avoided). The distance of the test sphere to the entrance of the test section can be adjusted by changing the lengths of the two Pyrex tubes if necessary.

3.4 Induction Heating and Power Calibration

The test section (47 mm O.D.) is wound by 10 turns of 4.5 mm O.D. copper tube coil with the test sphere located at the center of it, as shown in Fig. 3.1. The coil is hooked up to an RF induction power supply unit (RFC 3160) which is able to supply a peak of 20 kW induction power at frequency of 250–800 kHz.

The induction power coupling (the heating power obtained by the sphere) not only depends on the relative position of the sphere to the coil but also depends on the physical properties of the sphere and the medium inside the coil. The more ferric the metallic material, the better the coupling. The electromagnetic properties of the sphere may change with temperature and thus the power coupling is also temperature dependent. The medium inside and around the coil influences the intensity of the electromagnetic field, so it also affects the power coupling. If the operating condition of the induction power supply and the medium inside/around the sphere are fixed, the power coupling then only depends on the induction power level (monitored by the plate current) and the sphere temperature.

The main mode of operation, in our experiments, is to follow the transient cool-down of the test sphere from a well established steady-state. The instantaneous heat fluxes can be deduced from the energy balance on the sphere and the quantitative knowledge of induction power coupling is not needed in this case. In this manner, from a single cool-down transient with the sphere temperatures transients and the information of the heat

capacity of the sphere, we can obtain a large number of data pairs, heat fluxes at respective sphere temperatures, between the initial and the final (just before quenching) states.

Besides the transient mode operation, it is also interesting to obtain data at steady-state (without the cool-down transient), which is uniquely possible in the present experimental set-up. In particular, this experimental technique may be used to enhance the robustness of the data base generated by the transient mode runs. However, this method requires the information of the power coupled to the sphere during the steady-state run, which is referred to as induction power calibration, and we discovered that it is not as straightforward as we initially anticipated. Specifically, in the early stages of the work, we didn't know how the presence of water as the medium in the test-section would affect the power coupling, and how we would tackle and quantify the influence of water. After lots of experimentation, eventually, we found out that compared with the case with air as medium, the presence of pure water (distilled or deionized) as medium in the test section decreases the power coupling; and the electric conductivity of the water affects the power coupling significantly. More interesting and useful discovery was that the influence of the electric conductivity of water on the power coupling diminished essentially when the conductivity is over ~200 micromho, and beyond this point the power coupling is the same as that with air as the medium. This means that the power calibration obtained in air could be used to determine the power coupling when water or steam is present in the test section during the steady-state mode operation, as long as the water electrical conductivity is higher than 200 micromho. This will be demonstrated later.

The power calibration in air was carried out as follows. With the test sphere in its usual position in the test section, the power was turned on and maintained at a given level until the sphere reached a temperature of ~1000 °C, at which the power was triggered off. This process was repeated at various power levels indicated by the "plate current" of the induction power supply (the plate current is also read by the PC computer). A typical temperature transient is shown in Fig. 3.5. From these temperature data, which were recorded on the PC computer at sampling rate of 10 Hz, the power coupled to the sphere could be obtained as a function of the sphere temperature as shown in Fig. 3.6 (actually it shows the normalized power with respect to the sphere surface area). This involves getting the temperature gradient (carried out with a "local" sliding curve-fit to 5 consecutive readings) and using the energy balance equation,

$$q = \frac{m_s C_p(T_w)}{\pi D^2} \frac{dT_w}{dt} + h(T_w - T_a) + \epsilon\sigma(T_w^4 - T_a^4) \tag{3.1}$$

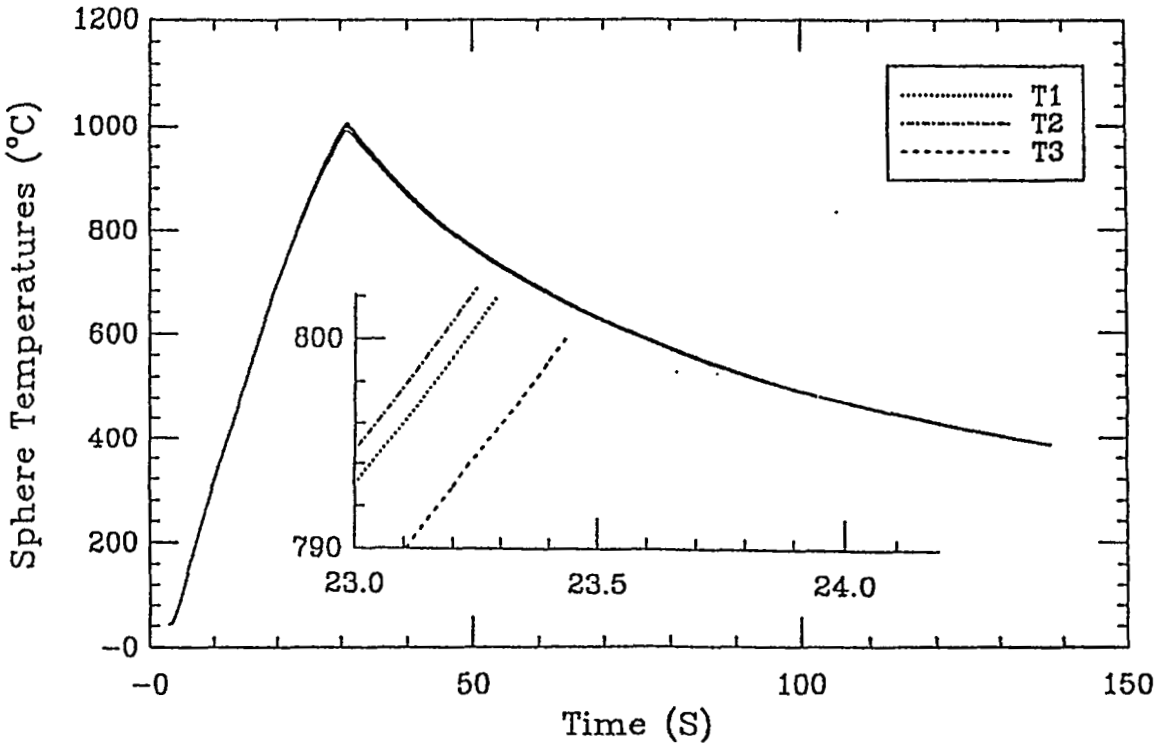

Fig. 3.5. A typical temperature transient during a calibration run in air. The insert shows a magnified portion.

In this equation, the heat capacity of the sphere material (stainless steel or brass) as a function of temperature is from Touloukian and Buyco (1970). The heat transfer coefficient, which accounts for the natural convection heat loss from the sphere to the air, was estimated by the correlation from Yuge (1960). The corrected or the true power obtained from Eq. (3.1) is also shown in Fig. 3.6. The emissivity of radiation can be obtained by matching the corrected power to zero for the whole cool-down period; thus obtained emissivities for new and "aged" stainless steel spheres are 0.5 and 0.8 respectively. From these results, a composite of calibration curves could be assembled as shown in Fig. 3.7. So, for a given power setting (plate current) and sphere temperature, the coupling power could be determined.

3.5 X-Ray Radiography for Void Fraction Measurement

X-ray radiograph is a photographic record produced by the passage of X-rays through an object onto a film. In our application, the X-rays produced by an X-ray tube pass through the test tube and then expose the film behind it, as illustrated in Fig. 3.8. Since the water has a much higher attenuation factor than the air and steam, the attenuation of the X-rays and thus the lightness of image on the film depends on the water fraction (or void

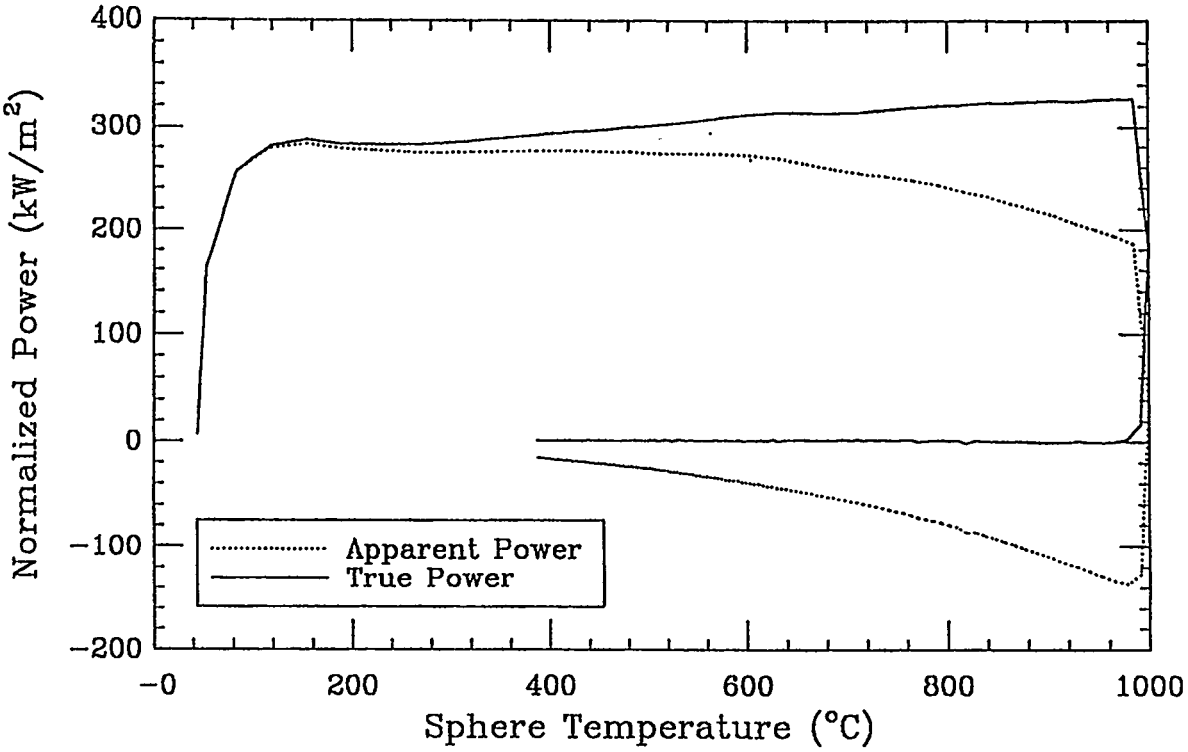

Fig. 3.6. The reduction of data in Fig. 3.5, as described in the text.

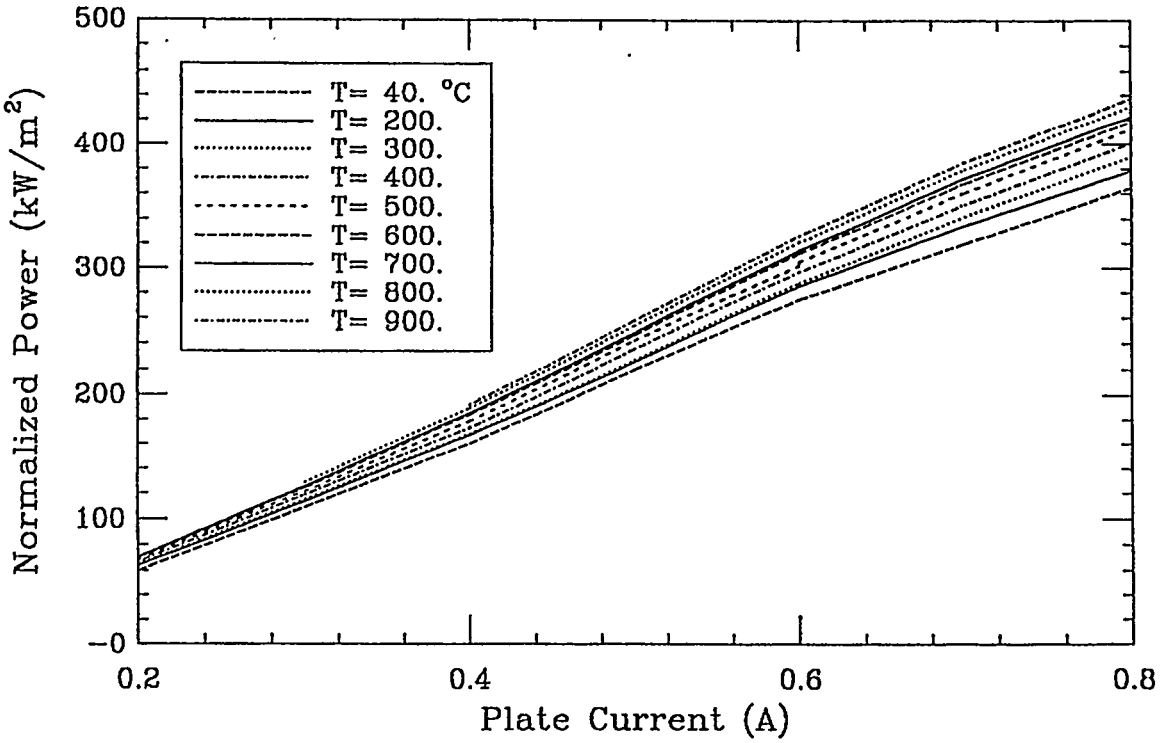

Fig. 3.7. Calibration (in air) of the power delivered to the sphere with its temperature as the parameter.

fraction) inside the test tube. So from the analysis of the lightness of the X-ray radiograph, the average void fraction inside the test tube can be determined.

To obtain a quantitative measurement of void fraction, another glass tube called a calibration tube, which is the same as the test tube was set beside the test tube. A calibration piece, as shown in Fig. 3.10, was set inside the calibration tube. The calibration piece, which is made from a stepped aluminum piece with empty holes inside, provides various voids inside the calibration tube, as illustrated in Fig. 3.9.

Two typical X-ray radiographs obtained from downward and upward two-phase flows are shown in Figs. 3.11 (a) and (b) respectively. By comparing the lightness near the center line of the test tube with the lightness of the holes in the calibration piece on the same film, the average void fraction in the test tube could be obtained. Radio graphing the calibration tube and the test tube on the same film by the same exposure not only avoids the error caused by the intensity differences of different X-ray exposures, but also eliminates the errors from the film development processing.

Another nice aspect of this radiograph technique is that with selected film (Kodak Industrix AA film), optimized X-ray generator voltage, and optimized distance from X-ray tube to target, the lightness of the X-ray radiograph is almost linear to the void fraction inside the tube, as indicated by Fig. 3.12. This allows us easily to extrapolate the void fraction that falls between two adjacent samples provided by the calibration piece.

The radiograph can be made either "off line" (without boiling sphere in the test tube) to determine the void fraction of coming two-phase flow at certain flow conditions, or "on line" (with boiling sphere in the test tube) to have an overall radiograph of the sphere film boiling in a two-phase flow. The results will be presented and discussed in Chapter 7.

3.6 Experiment Procedures and Data Reduction

For all the experiments, the film boiling is established by the following procedures: depleting the water from the test section, heating up the sphere to a temperature over the quenching point, turning on the water flow and then adjusting the power level to let the film boiling stabilized at a certain flow condition with a desired sphere temperature.

In a transient mode operation, after the flow reaches steady state and the sphere temperature stabilizes, the induction power is triggered off and the temperature transients are recorded by the PC computer at a sampling rate of 10 Hz. A typical temperature transient is shown in Fig. 3.13. The total heat flux is obtained from

$$q_t = -\frac{m_s C_p(T_w)}{\pi D^2}\frac{dT_w}{dt} \tag{3.2}$$

which is also illustrated in Fig. 3.13.

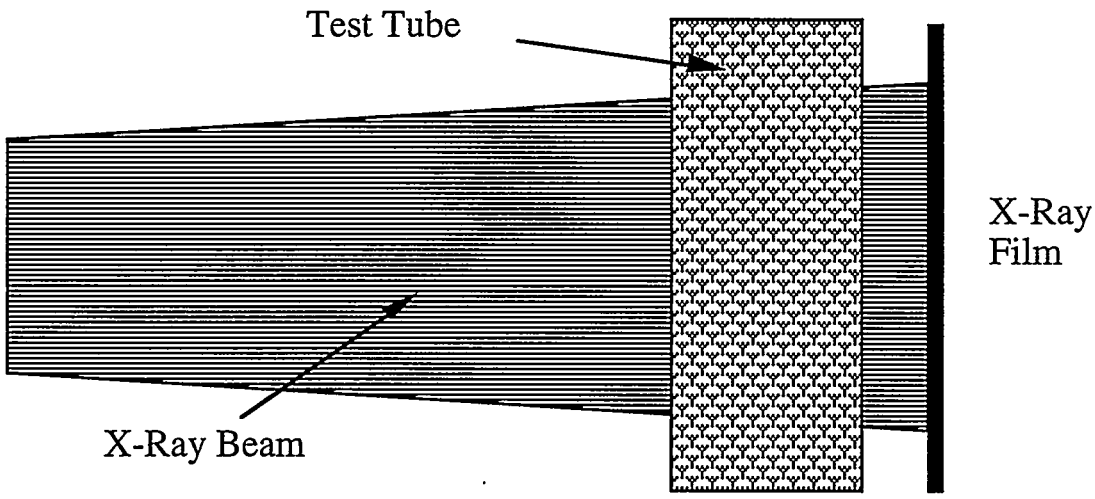

Fig. 3.8. Schematic diagram showing the fundamentals of a X-ray radiograph void fraction measurement technique.

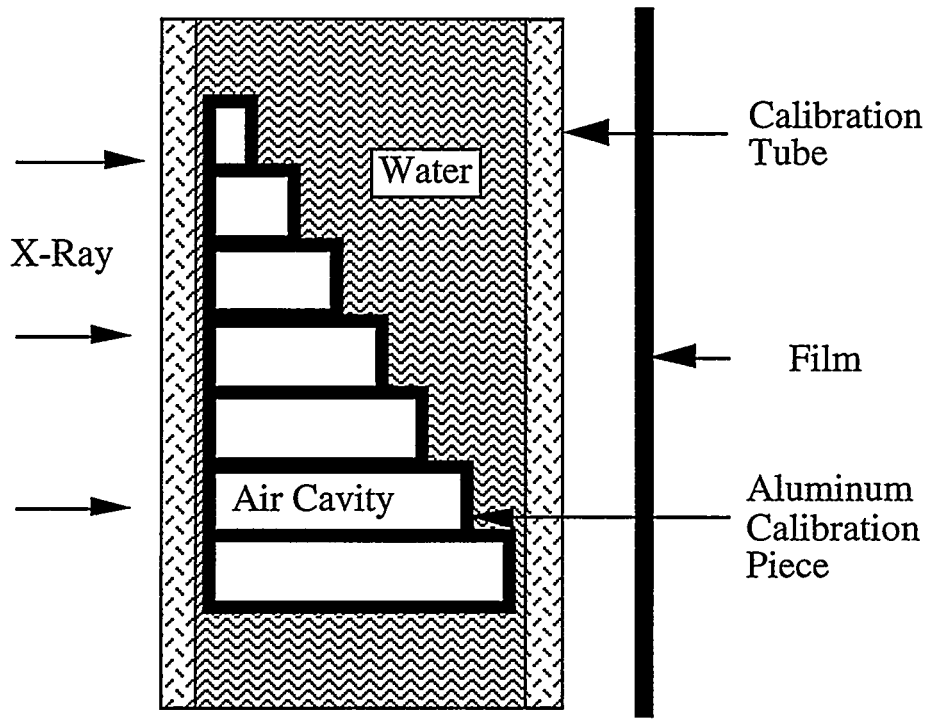

Fig. 3.9. Schematic illustration of void made by the caliberatiion piece in the caliberation tube.

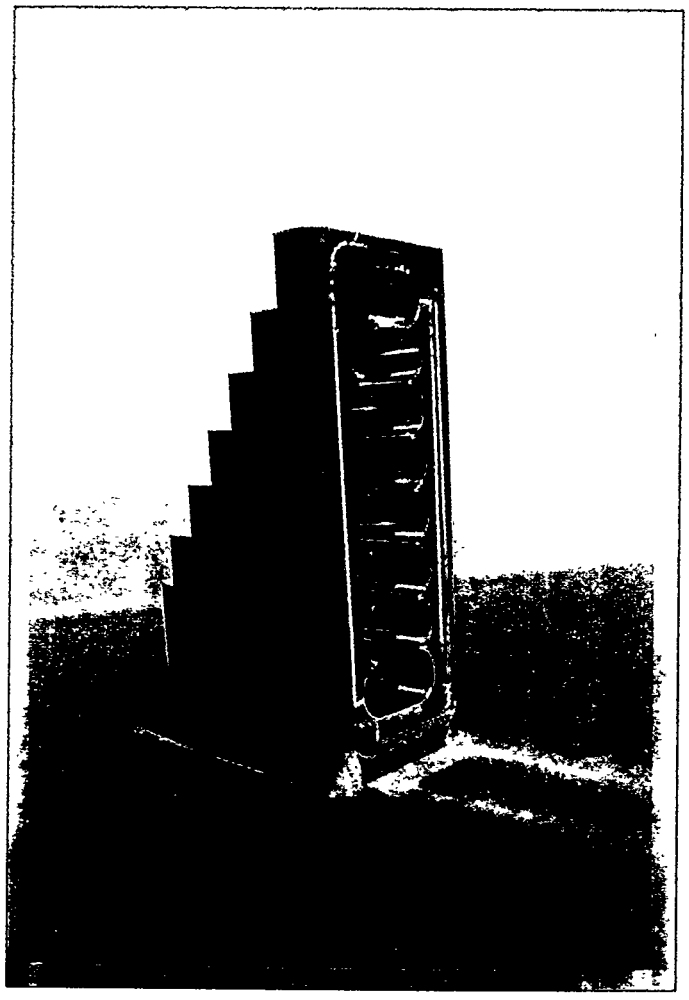

Fig. 3.10. A photograph of the void fraction caliberation piece.

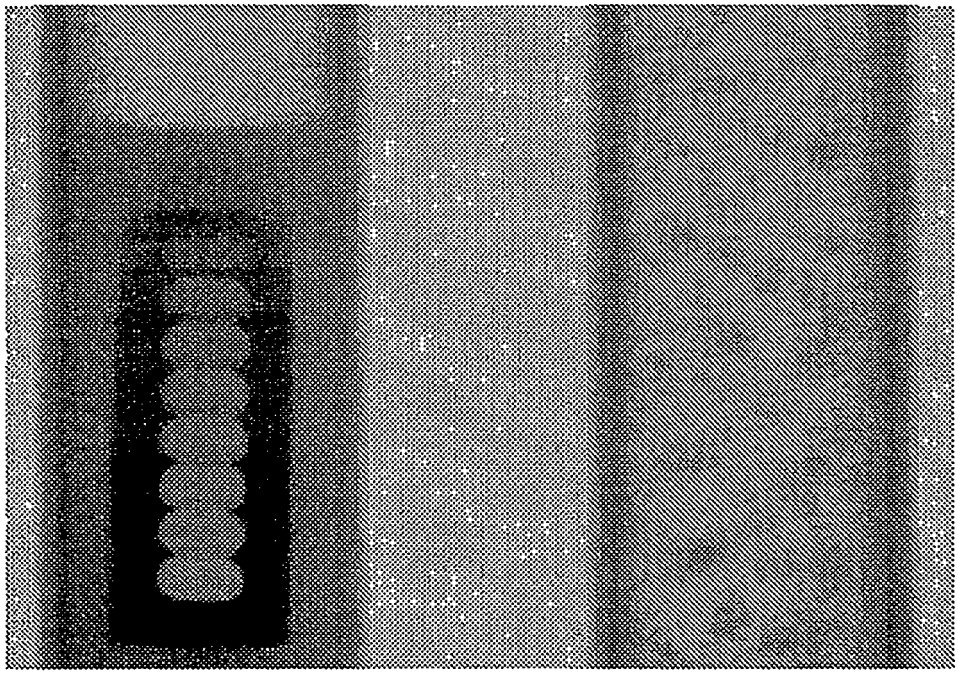

(a)

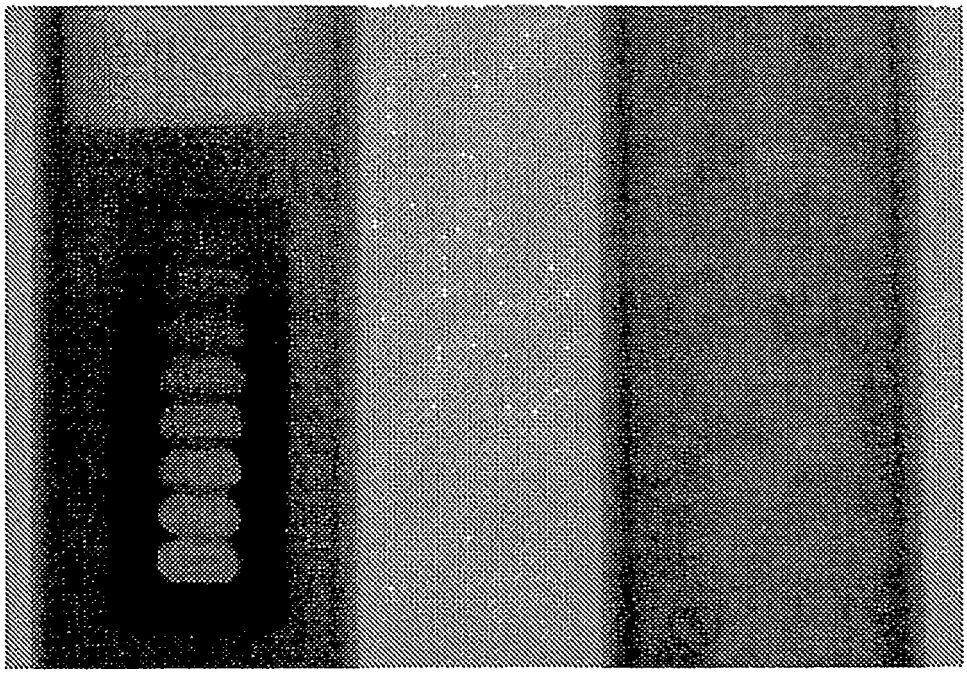

(b)

Fig. 3.11. X-ray radiographs obtained with (a) downward two-phase flow and (b) upward two phase flow.

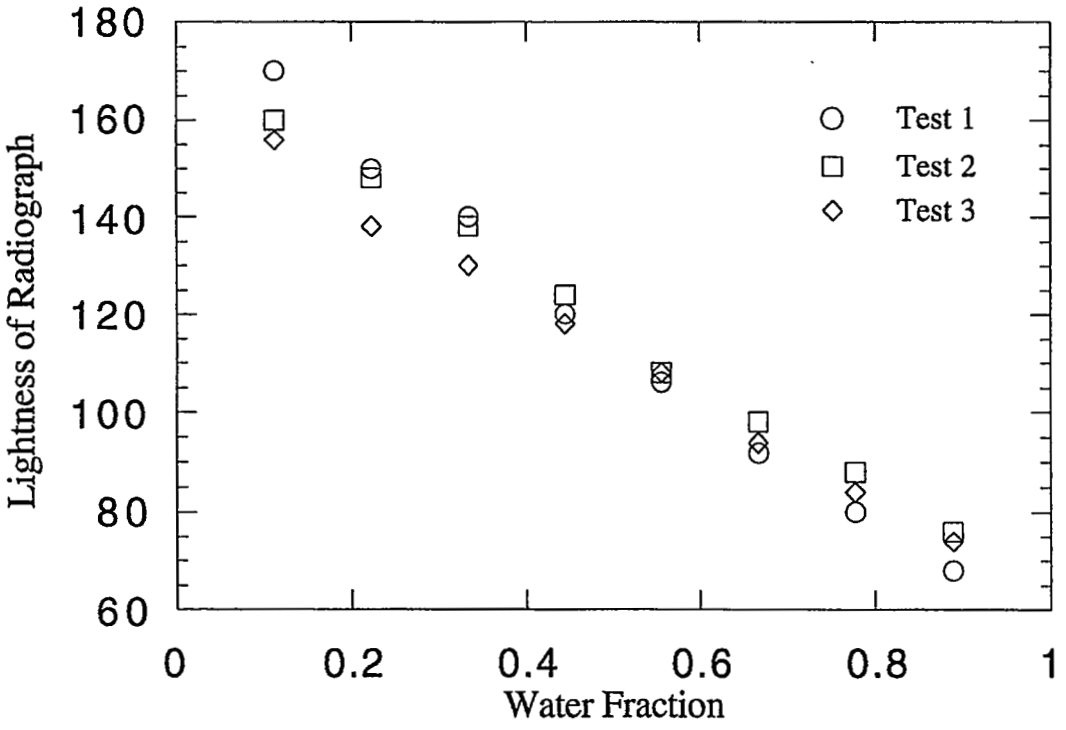

Fig. 3.12. The correspondent radiograph lightness of the void generated by the caliberation piece.

In a steady-state mode operation, the power level is adjusted from one to another (either increase, decrease, or randomly). A each level, the temperature (or film boiling) is allowed to stabilize, as shown in Fig. 3.14. The total heat flux (including both convective and radiative contribution) at each steady state, as shown by the plateau in Fig. 3.14, can be obtained from the respective plate currents and the sphere average temperature in conjunction with the power calibration that is shown in Fig. 3.7.

As usually treated in the literature, the total heat flux is split into convective and radiative contributions. The radiation from the sphere is to be largely absorbed in a thin layer of the liquid and hence will help to produce vapor and thus affect the convective contribution, so a radiation-factor J is usually used when radiation contribution is subtracted out from the total heat flux. Thus the convective heat flux is given by

$$q_c = q_t - J q_r \tag{3.3}$$

where $q_r = \epsilon\sigma[T_w^4 - T_s^4]$ and $J = 7/8$ which comes from Bromley, Leroy and Robbers (1953), as discussed in Section 2.1. The emissivity of radiation is obtained experimentally by matching the transient cool down of the sphere in still air with the radiation and natural

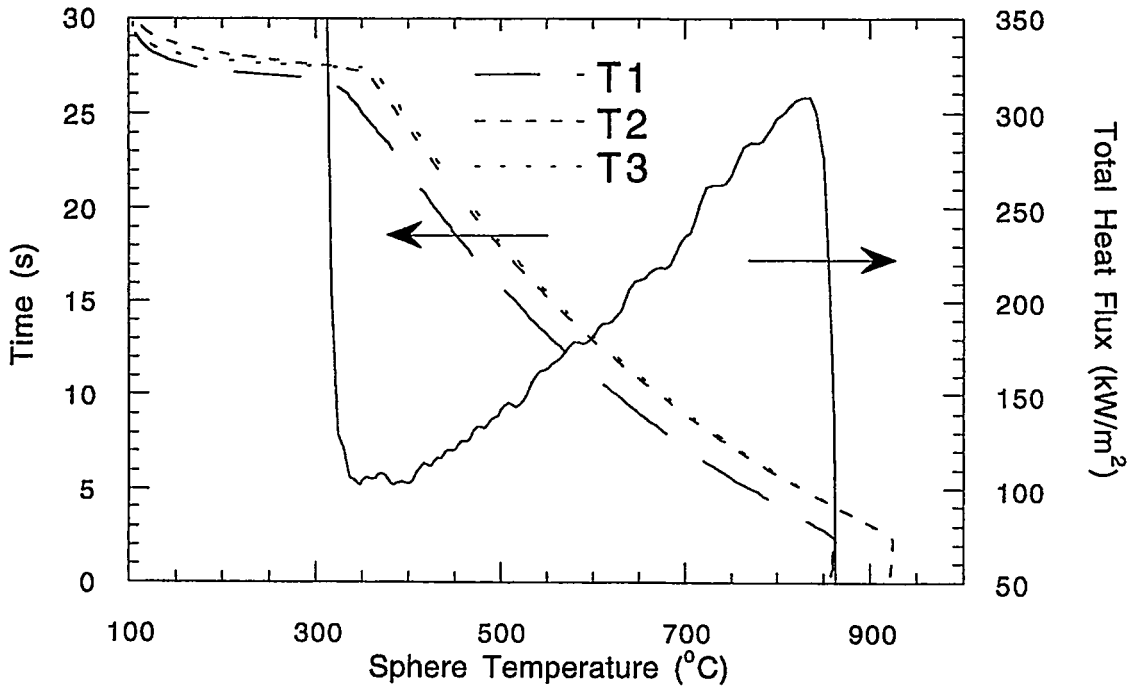

Fig. 3.13. Measured sphere temperature transients and implied heat flux transient, in a transient mode run.

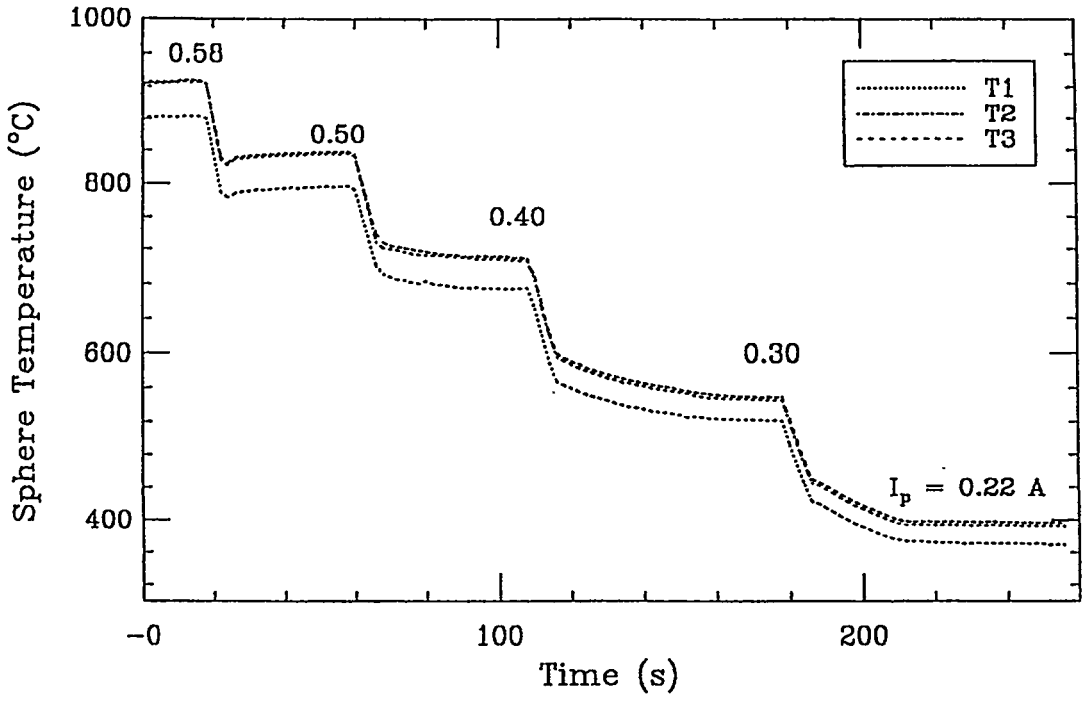

Fig. 3.14. Temperatures recorded in a run made in the steady-state mode operation. Each plateau provides a steady-state measurement.

convection heat loses; see Liu and Theofanous (1992). Thus obtained emissivity for new and "aged" stainless steel sphere are about 0.5 and 0.8 respectively.

Based on the convective heat flux, all the data were reduced to heat transfer coefficients, usually presented in terms of Nusselt numbers. All the properties are evaluated at the film temperatures, which are $(T_w + T_s)/2$ and $(T_s + T_l)/2$ for vapor and liquid respectively.

3.7 A Consideration for the Non-Uniform Temperature Distribution within the Sphere

As it is known, during the film boiling cool-down transient, neither the heat flux nor the temperature are uniform on the surface of the sphere or within the sphere. For instance, at the front stagnation point, the heat flux is higher and the temperature is lower than any other part of the surface; the center temperature is higher than the temperatures on the surface. However, in most cases the maximum temperature difference within the sphere is much smaller compared to the average sphere superheat, especially when the superheat is high and thermal conductivity of the sphere is large. For example, for a transient cool-down of a stainless steel sphere (which has a very low thermal conductivity) in a saturated single-phase film boiling, the temperature differences between the front stagnation point and the center are only about 50 °C, which is less than 10% of the superheat. In the case of a brass sphere, the difference is about 10 times smaller than this. So in both the above cases, the temperature distribution inside the sphere and on the surface can be assumed to be uniform and the temperature measured at any location within the sphere could be used as the characteristic sphere temperature.

Based on the discussion above and the concern to avoid too much heat loss from more thermocouples, in most of our single-phase experiments for obtaining the heat transfer data, only one thermocouple was used to support and measure the temperature of the sphere. The tip of the thermocouple is located on the center line and 1/4 diameter from the front stagnation point.

But this isothermal assumption is not good in some extreme cases when the liquid-phase velocity is high and the subcooling is large, especially when the sphere thermal conductivity is low (as in the case of stainless steel). According to our rough analysis for the cool-down transient of stainless steel spheres in a single-phase forced convection with velocity of 2 m/s and 30 °C subcooling, the temperature difference between the surface and the center could be about 20% of the sphere average superheat. This is also confirmed by our experimental measurement with three thermocouples. However even in these

cases, the temperature at 1/4 diameter from the front stagnation point can also be regarded as the sphere average temperature because the temperature at the front stagnation point is very low and all the back half of the sphere remained at relative high temperatures, which are equal or even higher than the temperature of the center of the sphere.

4 FILM BOILING IN SINGLE-PHASE FLOWS

Experiments on film boiling from spheres in single-phase water flows have been conducted systematically to observe the vapor film configurations and to investigate and check the effects of water flow velocity, water subcooling, sphere superheat, sphere diameter, and sphere material on the film boiling heat transfer. The ranges of the experimental parameters are:

- Water Velocity : 0.0–2.3 m/s; $\mathrm{Re} \leq 2 \cdot 10^5$; $\mathrm{Fr} \leq 80$
- Water Subcooling: 0.0–40.0 °C
- Sphere Superheat: 900 °C – Quench
- Sphere Diameter: 6.0–19.0 mm

The average liquid (water) velocity at the equator of the test sphere is used as the characteristic velocity U_l in the single phase data reduction. Thus defined velocities are 6 and 11% higher than the average velocity based on the test tube cross section for 9.53 and 12.7 mm diameter spheres respectively. Due to the parabolic velocity profile inside the test tube, thus defined velocity is also more appropriate in representing the local velocity at the front stagnation point of the sphere.

The flow in the test section was arranged upward. Stainless steel spheres with outer diameter of 6.35, 9.53, 12.7 and 19.1 mm and brass spheres with outer diameter of 9.53 and 12.7 mm were used in the experiments. In order to minimize the heat loss, in most of the tests, only one sheathed thermocouple was installed in the sphere with its tip located at 1/4 diameter from the front stagnation point. The experiments were conducted with distilled water, deionized water and tap water. Also, tests were made with the sphere at different stages of oxidation: essentially metallic, slightly oxidized but still mostly metallic in appearance, well oxidized (dark, but smooth), and heavily oxidized and corroded. In each case, the emissivity was measured by the power-calibration procedure described in Chapter 3 and was found to gradually progress from $0.5-0.6$ to $0.8-0.9$ through these four stages of oxidation. Most of the data were obtained from transient cool-down operations; however, steady-state operations were also carried out to obtain the heat transfer data at saturated conditions.

In this chapter, the observations of vapor film configurations and heat transfer results of film boiling on a 12.7 mm diameter stainless steel sphere are presented first. Then, the heat transfer data are presented in several different ways according to the correlations

discussed in Chapter 2 and the fitness of these correlations is discussed; the diameter and material effects are checked and correlated. Finally, the results obtained by steady state mode operation are presented and compared.

4.1 Observations of Film Configurations of Film Boiling

One of the unique features of the present experimental approach is that it provides a convenient way to observe the film boiling process clearly, because the sphere is held still during the test. In the cool-down transient mode operation, after the induction power is triggered off, the induction coil can be moved away so the whole film boiling cool-down transient can be observed.

In order to get rid of the support wire's influence on the rear part of the film, in the runs for observation purpose, the sphere can be held by a small sheathed thermocouple from the front stagnation point. In this way, our experiment provided very unique and realistic observations of the film boiling on the sphere. The observations were videotaped for runs at wide ranges of flow velocity (0 to 2 m/s), liquid subcooling (0 to 40 °C), sphere superheat (200 to 900 °C) and diameter of the spheres (6.35, 9.53, 12.7, and 19.0 mm). Normal camera pictures were also taken at a shutter speed of 1/2000 second in all typical flow conditions. Typical pictures that were taken from the film boiling on a stainless steel sphere (12.7 mm in diameter) supported with one sheathed thermocouple (0.81 mm O.D.) are shown and discussed as follows.

Pool film boiling in saturated water: As shown in Fig. 4.1, the test spheres were supported from the up-stream (front stagnation point) in the first three cases (a,b,c), and were held from the down-stream (rear stagnation point) in the last three cases (d,e,f) . The whole vapor surface is quite wavy and the induced free convection is turbulent, especially when the sphere temperature is high, as shown in Fig. 4.1 (a) and (d). However, as the sphere temperature decreases, the vapor surface at the front part of the sphere tends to be smoother, especially when the diameter is small, as shown in Fig. 4.1 (c) and (e). On the rear part of the sphere, there is always a periodic generation and detachment of vapor dome, which makes a two-phase wake behind the sphere.

Pool film boiling in subcooled water: As shown in Fig. 4.2, for subcooled pool film boiling, the vapor film is smooth on the front part of the sphere. There is a small vapor dome at the back of the sphere. Small bubbles periodically detach from the top of the dome. The frequency of the bubble detachment depends on the sphere temperature and the subcooling of the water. When the sphere temperature is high, the detachment frequency

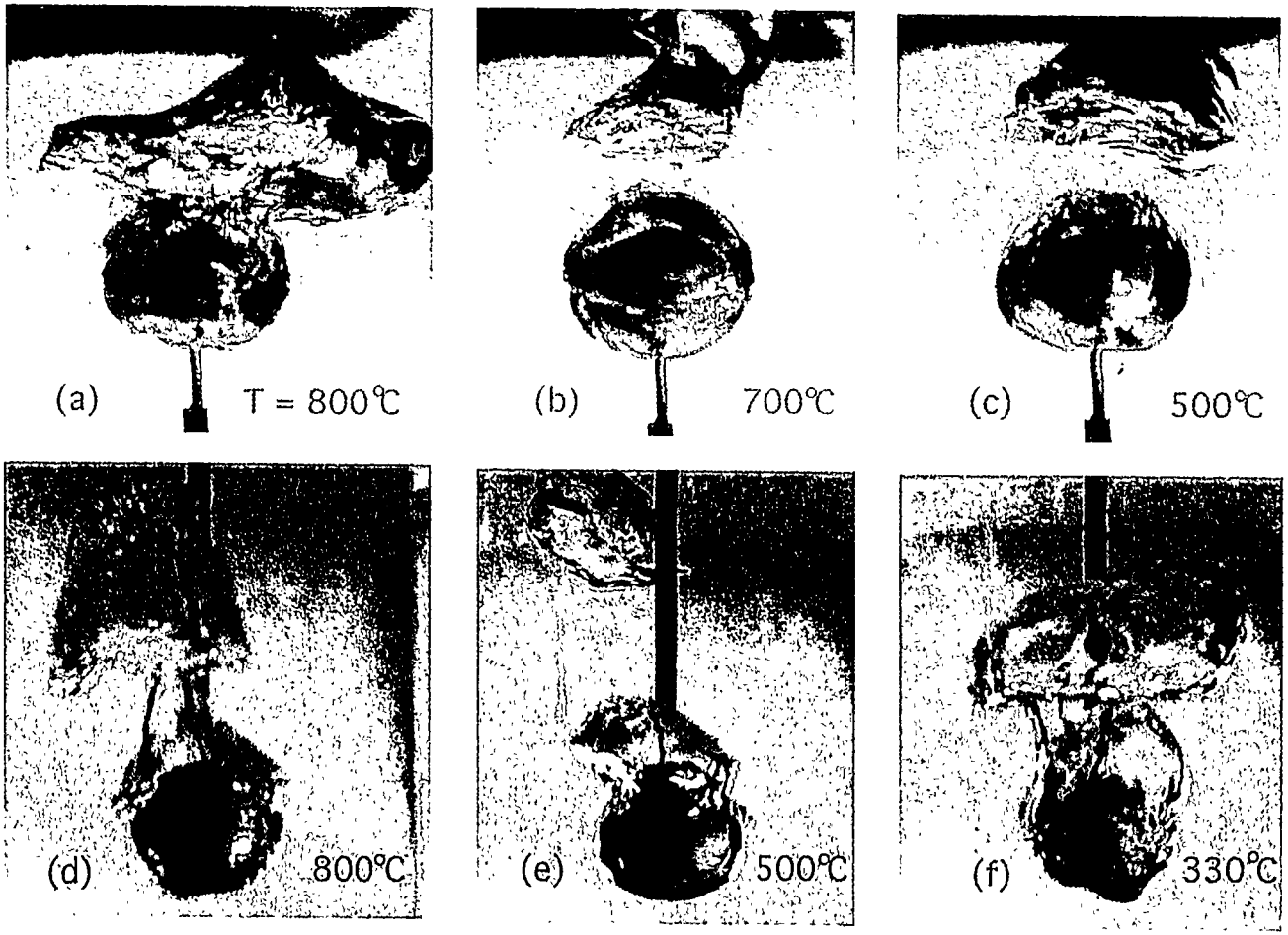

Fig. 4.1 Pool film boiling in saturated water

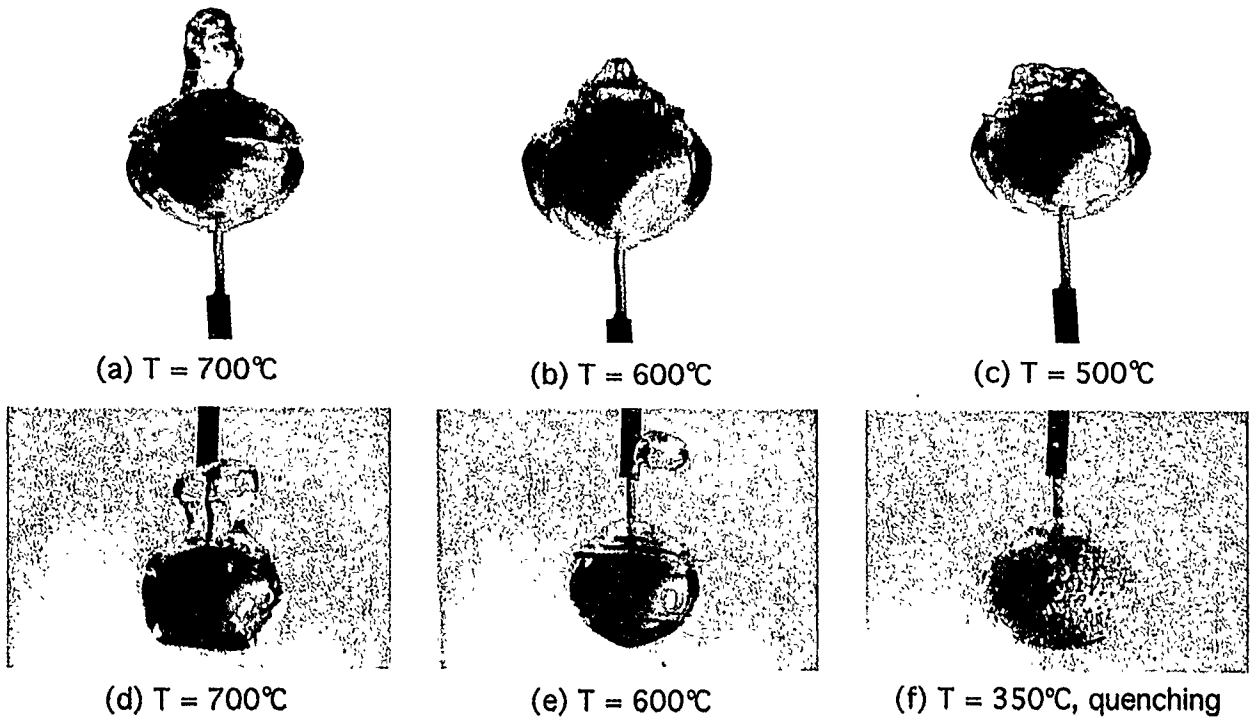

Fig. 4.2 Pool Film Boiling in 10 °C subcooled water

is fast. When the sphere temperature is low, the detachment frequency is low or even zero (with no vapor escaping). Figure 4.2 (f) was taken during the quenching.

Forced convection film boiling in saturated water flow: In forced convection saturated film boiling, as shown in Fig. 4.3 (a,b,c), a large and long "perfect" vapor wake can be seen regardless of what the sphere temperature is. The higher the sphere temperature and the faster the flow, the longer is the vapor wake, which may be as long as 10 times the sphere diameter. Big vapor slugs always periodically detach from the tail of the wake. Generally, the film on the front part of the sphere is quite wavy, as in the case of saturated pool film boiling. It is very interesting that a little bit of water subcooling (just about 0.5 °C) can destroy the "perfection" of the wake behind the sphere, especially when the sphere temperature is low. In this case, the tail of the wake is torn apart and some water is dripped and bounces on the back surface of the sphere in the wake, as shown in Fig. 4.3 (d) and (e). This also happens when the sphere is supported from the up-stream and it is worse when the support is at the rear stagnation point. This may be part of the reason why only one degree subcooling could cause about 30–40% increase in the overall film boiling heat transfer from a sphere that is supported from the rear stagnation point.

Forced convection film boiling in subcooled water flow: In this regime, the vapor wake at the back of the sphere disappears and a wavy vapor film is formed on the back of the sphere, as shown in Fig. 4.4. The film on the front part of the sphere is always smooth, as in the case of subcooled pool film boiling. In the case of moderate water velocity, as shown in Fig. 4.4 (a, b, d and e), there is almost no vapor escaping from the vapor film and the surface of the back film is very wavy in the equator region. When the water velocity becomes large, the occasional escape of vapor bubbles from the vapor film near the upper-equator region can be observed, but the bubbles disappear in the subcooled liquid quickly.

In the subcooled cases, either from up-stream or from down-stream, the support (the thermocouple) makes no difference on the observation. However in the saturated cases, there are some differences between the film configurations that were obtained by up-stream support and by down-stream support, although the differences are not very significant. The best way of supporting is up-stream, if the observation is the only concern.

The observed phenomena for typical film boiling regimes are summarily sketched in Fig. 4.5. In general, for saturated film boiling, the front vapor film is wavy and on the back of the sphere there is large vapor wake in forced convection and a periodic detachment of vapor dome in natural convection. For subcooled film boiling, the front film is always

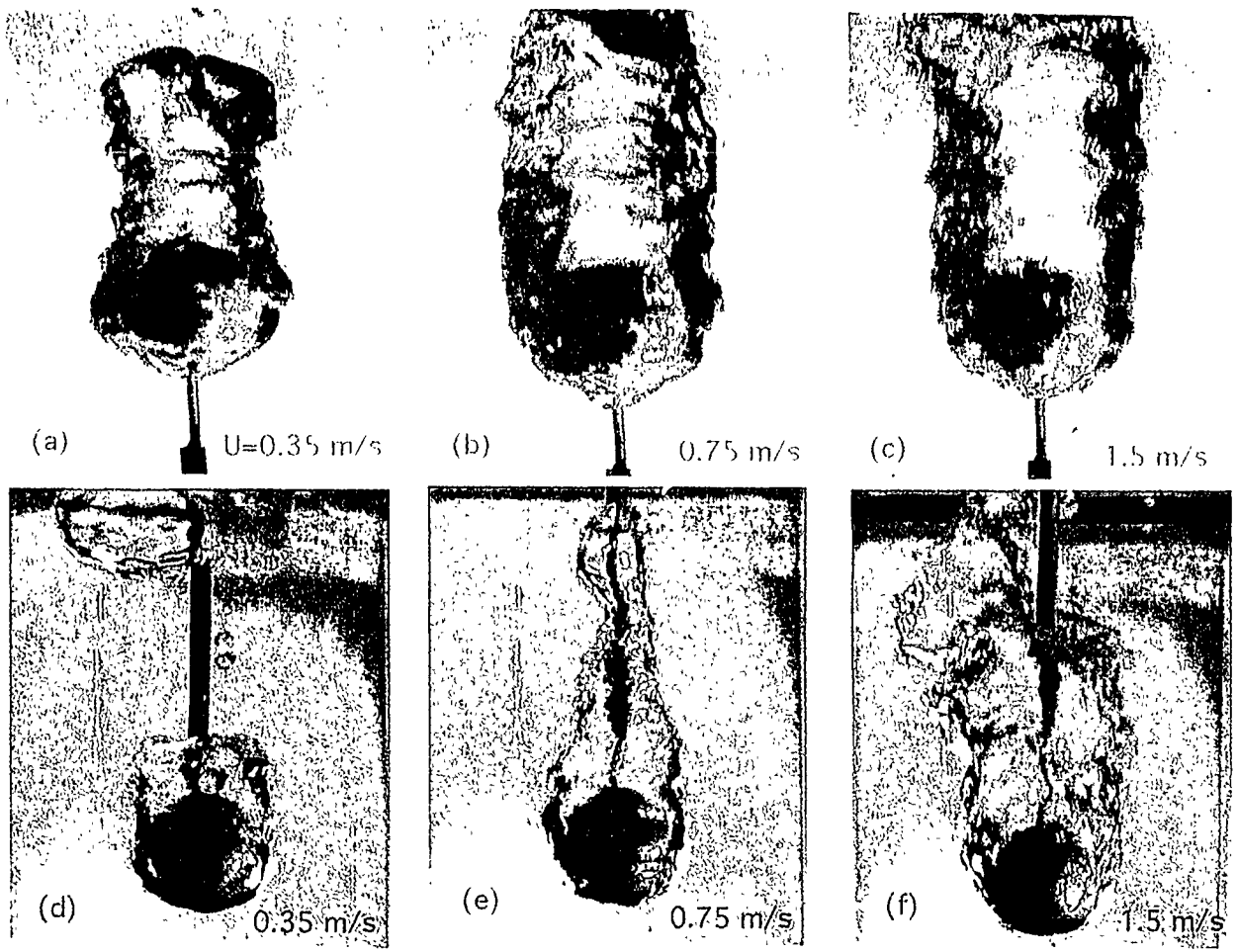

Fig. 4.3 Forced convection film boiling in upward saturated water flow

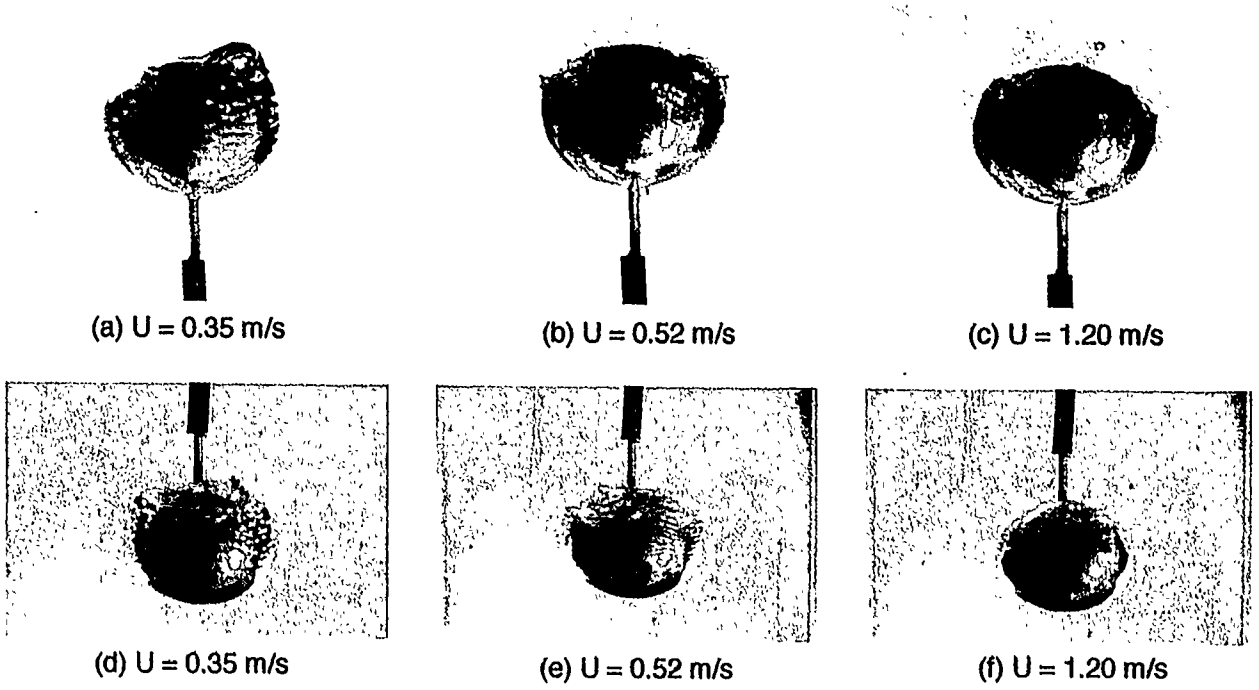

Fig. 4.4 Forced convection film boiling in upward 10 °C subcooled water flow

smooth, the back film is wavy and very few or no vapor bubbles can be observed in the water.

Most of the above observations are new and could provide good bases for theoretical analysis in helping us to understand the mechanism of film boiling in different film boiling regimes.

4.2 Film Boiling in Saturated Conditions

The total heat flux of one typical series of transient mode runs (with 316 stainless steel spheres of 12.7 mm in diameter) are shown in Fig. 4.6. The influences of temperature and flow velocity on the total heat flux are very clear. The quench temperatures are about 250 °C for pool film boiling and increase gradually with the water flow velocity in the forced convection regime. More data are tabled in Appendix C.

The same data are plotted in terms of Nu vs Re in Fig. 4.7, where $\mathrm{Nu} = q_c D/(\Delta T_{sup}/k_v)$, $q_c = q_t - q_r$, $\mathrm{Re} = UD/\upsilon_l$, and the k_v is evaluated at the film temperature $(T_s + 0.5\Delta T_{sup})$. It is obvious that: (1) the Nu is nearly independent of Re, when Re is less than 20000 ($\mathrm{Fr}^{1/2} = 1.5$, pool film boiling regime); (2) Nu increases with Re, when Re is larger than 20000 (forced convection film boiling regime). With constant flow rates, the Nu decreases significantly when the sphere temperature increases.

Pool Film Boiling Interpretation

Basically, there are two ways to correlate the heat transfer data for pool film boiling in saturated liquid, which are regarded (by us) as 1/4-power law and 1/3-power law:

$$\text{1/4-Power Law}: \quad \mathrm{Nu} = C_{sat,N}\{\mathrm{Ar}/Sp'\}^{1/4} \tag{4.1}$$

$$\text{1/3-Power Law}: \quad \mathrm{Nu} = C_{sat,N}\{\mathrm{Ar}/Sp'\}^{1/3} \tag{4.2}$$

The data are plotted in terms of the 1/4-power law in Fig. 4.8. For $\mathrm{Fr}^{1/2} < 1.5$, the heat transfer characteristic $\mathrm{Nu}/(\mathrm{Ar}/Sp')^{1/4}$ ranges from 0.59 to 0.70, which approximates the Bromley's (1961) experimental constant of 0.62, Frederking and Clark's (1963) theoretical constant 0.586, and Dhir's (1978) experimental constant 0.8. In Fig. 4.9, the data are presented in the form of the 1/3-power law; the heat transfer characteristic $\mathrm{Nu}/(\mathrm{Ar}/\mathrm{Sp}')^{1/3}$ is about 0.15, which is exactly the same as that of Merte and Clark (1964). The data are also plotted in the form of Michiyoshi's (1988) correlation in Fig. 4.10. The $\mathrm{Nu}/(M_c\mathrm{Ar}/Sp')^{1/4}$ ranges from 0.65 to 0.75, which is in agreement with the theoretical value of 0.696 from Michiyoshi et al. (1988) analysis.

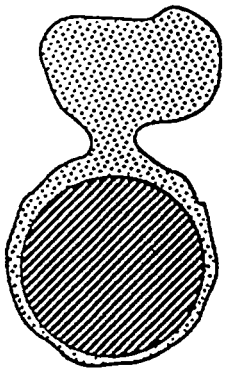

Saturated Pool Film Boiling

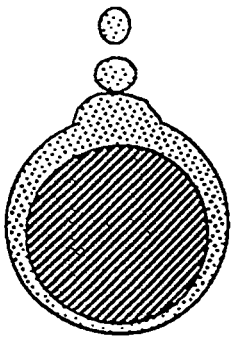

Subcooled Pool Film Boiling

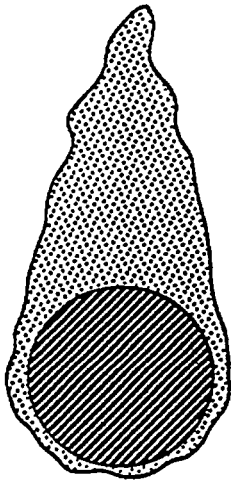

completely saturated

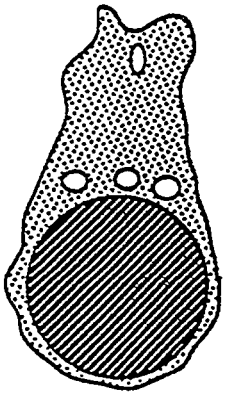

~0.5 C subcooling

Saturated Film Boiling in Forced Convection

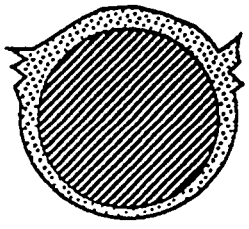

at moderate velocity

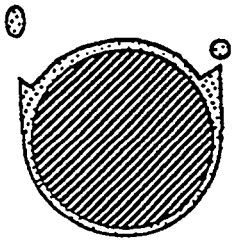

at high velocity

Subcooled Film Boiling in Forced Convection

Fig. 4.5. Sketches of typical film boiling configurations.

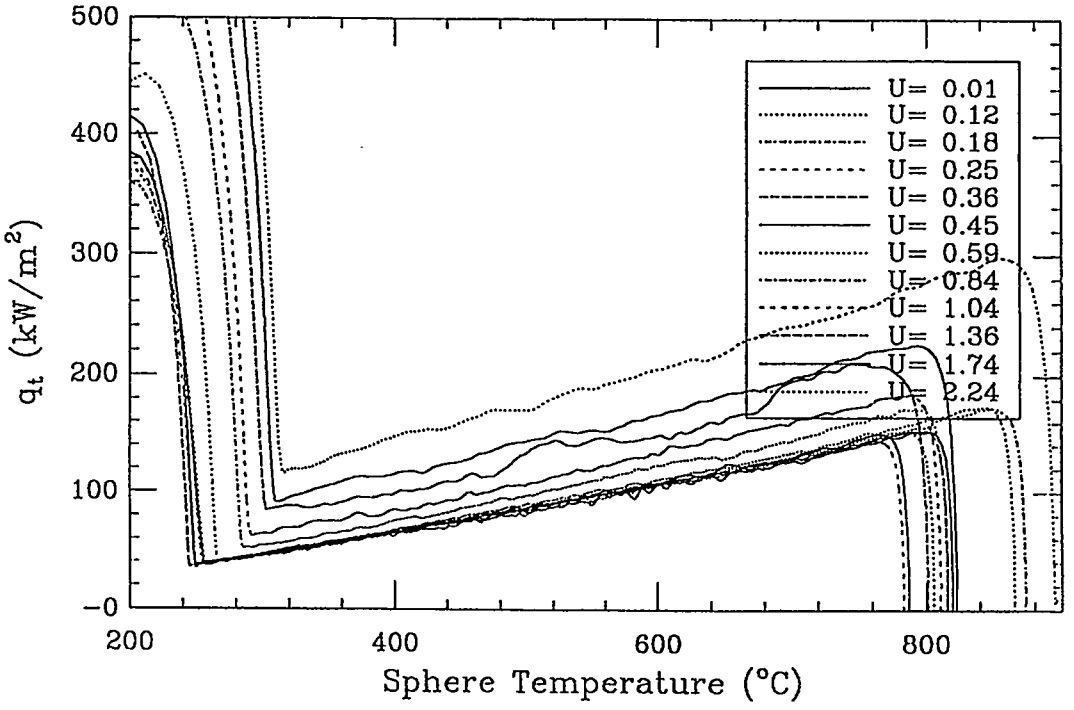

Fig. 4.6. Total heat flux transients from a typical series of transient mode runs in saturated experiment.

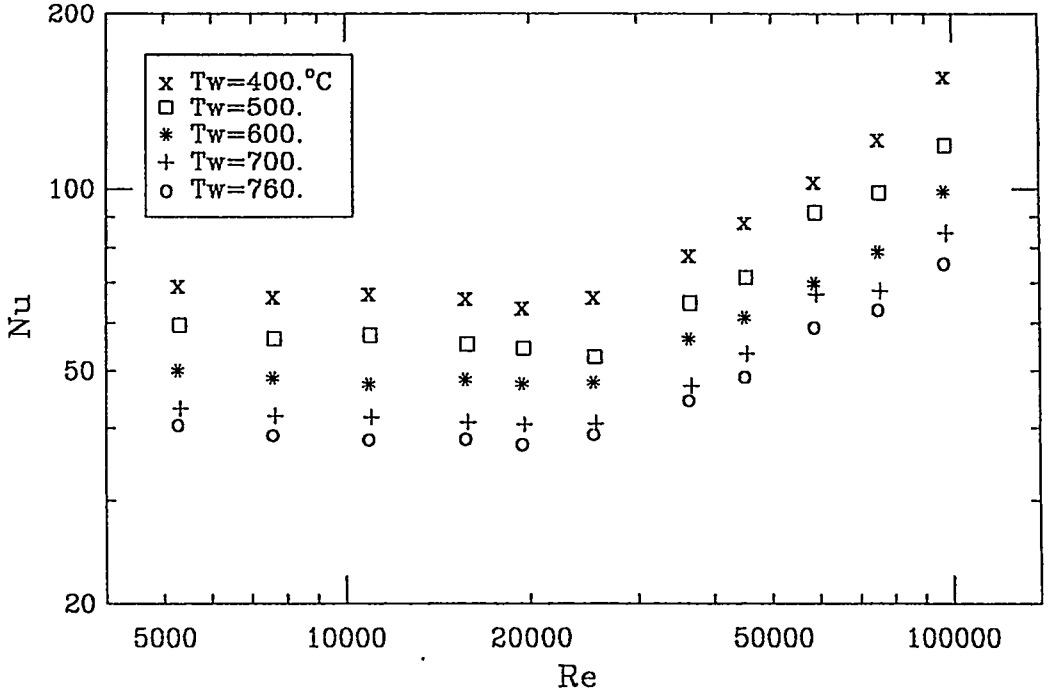

Fig. 4.7. Saturated film boiling data plotted in the form of Nu vs Re.

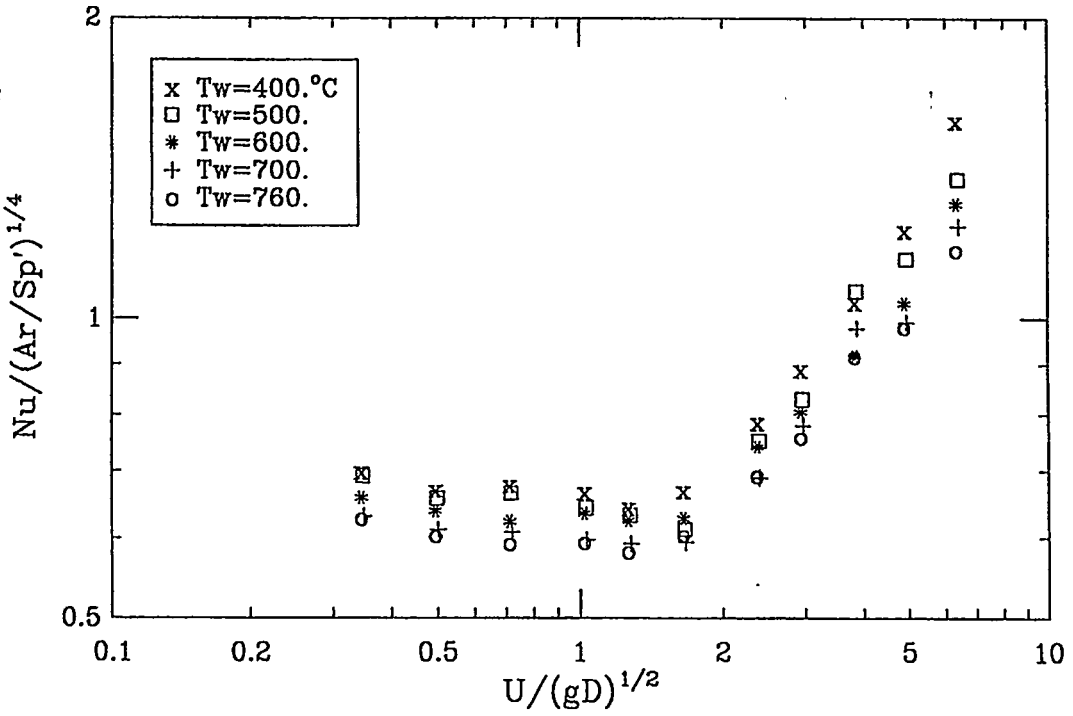

Fig. 4.8. Saturated film boiling data plotted in the form of 1/4 power law.

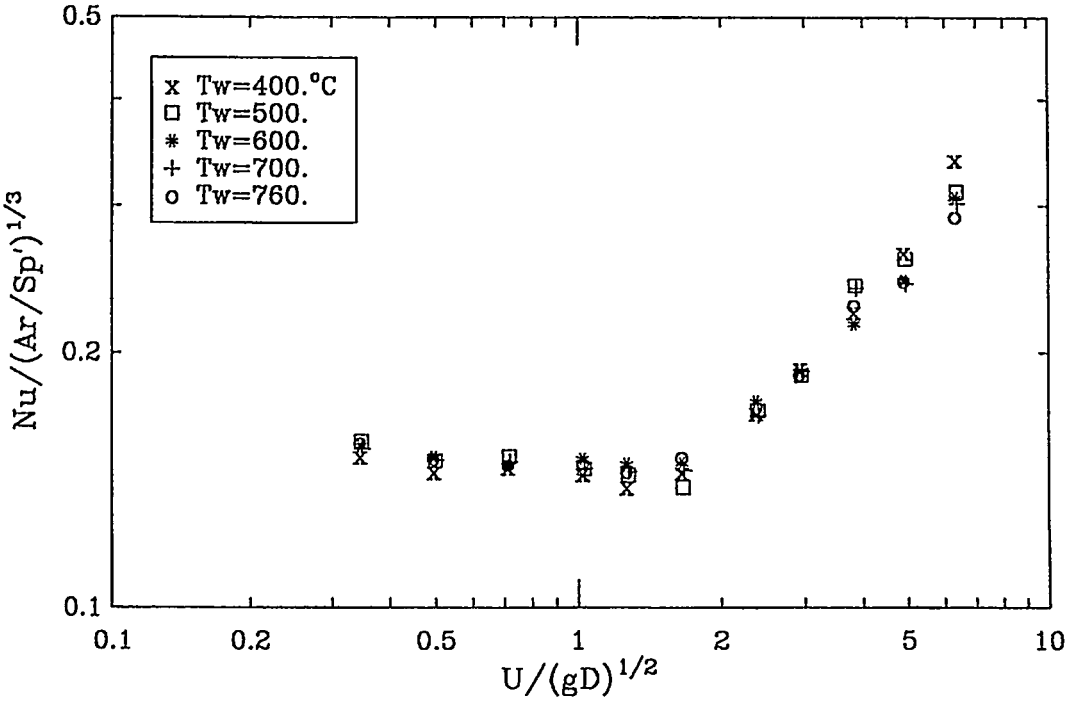

Fig. 4.9. Saturated film boiling data plotted in the form of 1/3 power law.

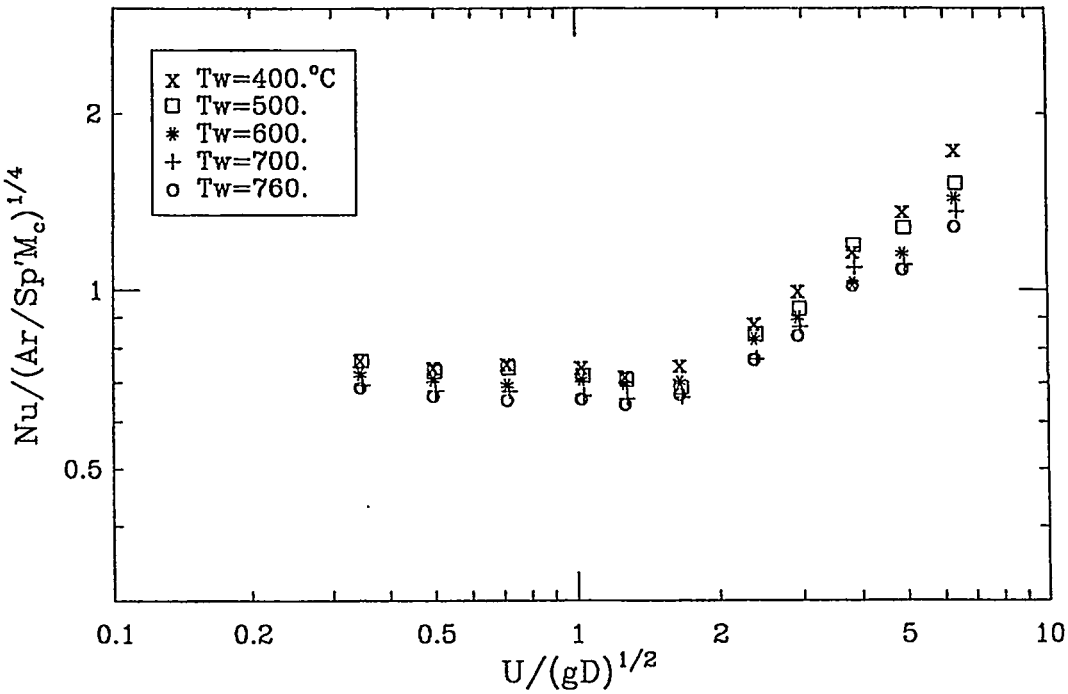

Fig. 4.10. Saturated film boiling data plotted in the form of Eq. (2.29).

The $Fr^{1/2}$ ranges from 0 to 1.5 for pool film boiling, which is in agreement with that found by Bromley et al. (1961) for cylinders. In general, all the three correlations could be used to express the saturated pool film boiling Nusselt number even without changing the constant, but the 1/3-power law correlation is better for taking account of the sphere temperature effect. However, for general purposes, the Michiyoshi's formula (which is in 1/4-power law) is preferred since it also covers subcooled conditions, correlates system pressure effects and is better for small diameter spheres.

Forced Convection Film Boiling In Saturated Water Flow

As mentioned in our literature review, there are two kinds of correlations:

$$\text{Mode 1: Nu} = C_{sat,F1}\text{Re}_l^{1/2}(\mu_l/\mu_v)[R^4/Sp'^2]^{1/4} \tag{4.3}$$

$$\text{Mode 2: Nu} = C_{sat,F2}\text{Re}_l^{1/2}(\mu_l/\mu_v)[R^4K/Sp']^{1/4} \tag{4.4}$$

where $\text{Re}_l = \text{Re} = UD/\upsilon_l$. The mode 1 correlation was first obtained by Bromley (1961) and the mode 2 correlation may be derived from Kobayasi's (1965) or Wilson's (1979) analyses, the latter is presented in Appendix B.

Figure 4.11 shows the data plotted in the form of mode 1 correlation; the $C_{sat,F1} = \mathrm{Nu}/\{\mathrm{Re}_l^{1/2}(\mu_l/\mu_v)[R^4/Sp'^2]^{1/4}\}$ changes significantly with the sphere temperature and ranges from 2.0 to 3.2. In terms of mode 1 correlation, the value obtained from Bromley's (1961) experiment for cylinder is 2.7. On the other hand, in terms of mode 2 correlation, the data are plotted in Fig. 4.12. It is obvious that the $C_{sat,F2} = \mathrm{Nu}/\{\mathrm{Re}_l^{1/2}(\mu_l/\mu_v)[R^4K/Sp]^{1/4}\}$ depends much less on the sphere temperature and is about 0.5 in the forced convection regimes, which can be compared with the theoretical constants 0.393 of Kobayasi (1965,1966), 0.553 of Epstein and Hauser (1980), 0.46 of Nishikawa et al. (1981), and the experimental constant of 0.554 from Liu, Shiotsu and Sakurai's (1992) cylinder experimental correlation. In addition, Figs. 4.11 and 4.12 also indicate that forced convection film boiling starts from $\mathrm{Fr}^{1/2}$ of 2.0, which also agrees with that found by Bromley (1953).

It is obvious that the mode 2 correlation is better than mode 1, as it was indicated in our literature review in Chapter 2, and the constant is 0.5 based on our experiment. Therefore, mode 2 correlation is recommended for forced convection film boiling in saturated water flows.

The Sensitive Effect of Little Liquid Subcooling

In saturated film boiling experiments, the liquid is usually regarded as being saturated. But in reality, the liquid may not be 100% saturated because of the heat loss, and this may affect the interpretation of the results. Therefore, experimental assessment of the effect of a little subcooling on the film boiling heat transfer is very useful.

The experimental data obtained at conditions of 0.0, 1.0 and 2.0 °C subcooling are shown in Fig. 4.13 in terms of mode 2 correlation. It is obvious that only one or two degrees subcooling can have a significant effect on the film boiling heat transfer, especially in the forced convection regime. It also implies that the so claimed saturated condition by Aziz (1986) may have about one degree of subcooling.

4.3 Film Boiling in Subcooled Conditions

Figure 4.14 shows the total heat flux of one typical series of transient mode runs of film boiling on a 12.7 mm stainless steel sphere in 80 °C tap water. The influences of temperature and flow velocity on the total heat flux could be easily identified. The quench temperature is about 300 °C in still water and increases slowly with the water velocity when the velocity is small ($0 < U < 0.5$ m/s), and increases quickly when the velocity is high. The quench temperatures are much higher than those obtained at saturated conditions. More data are tabled in Appendix D.

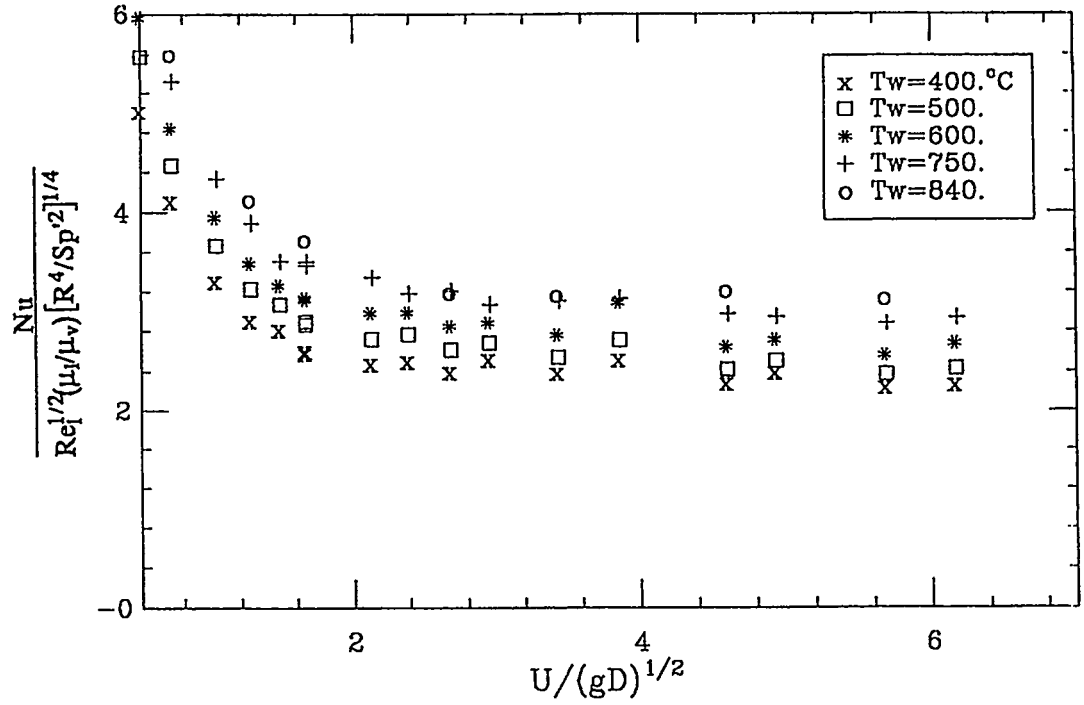

Fig. 4.11. Saturated film boiling data plotted in the form of mode 1 forced convection film boiling correlation.

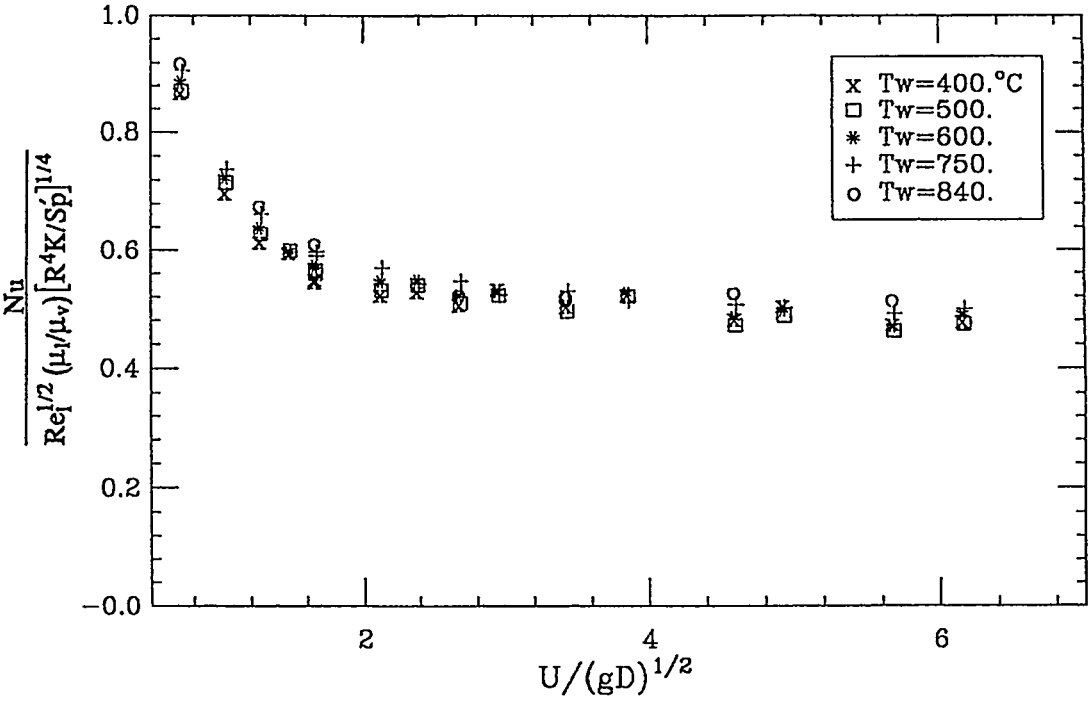

Fig. 4.12. Saturated film boiling data are plotted in the form of mode 2 forced convection film boiling correlation.

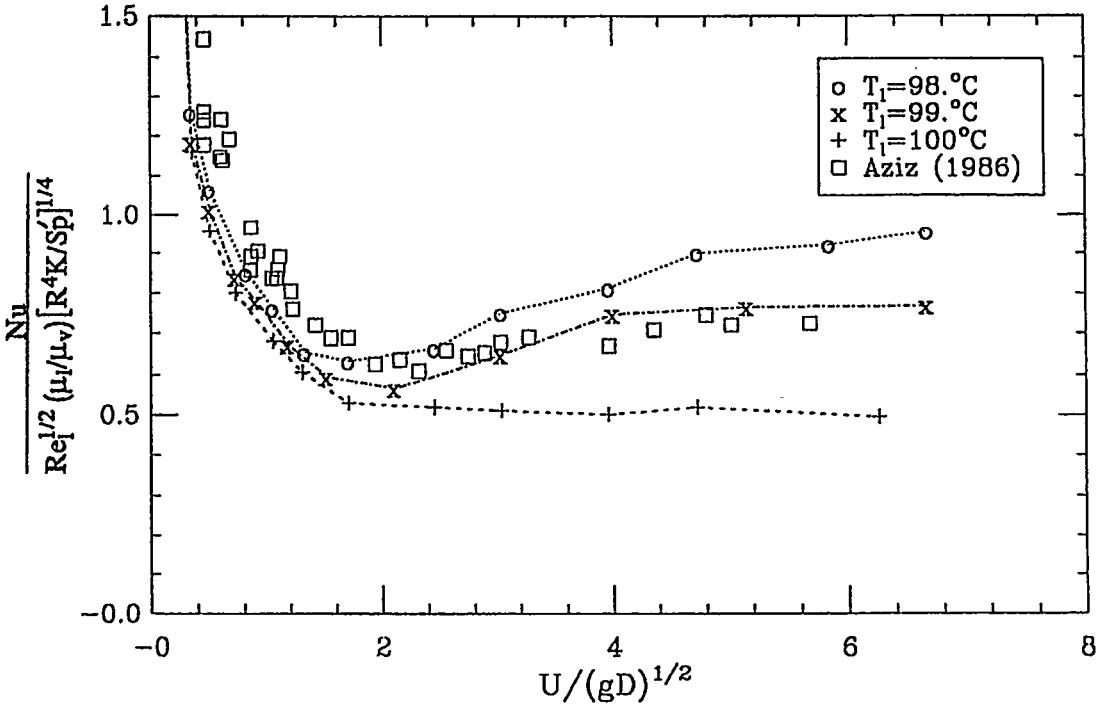

Fig. 4.13. The effect of little liquid subcooling on the film boiling heat transfer.

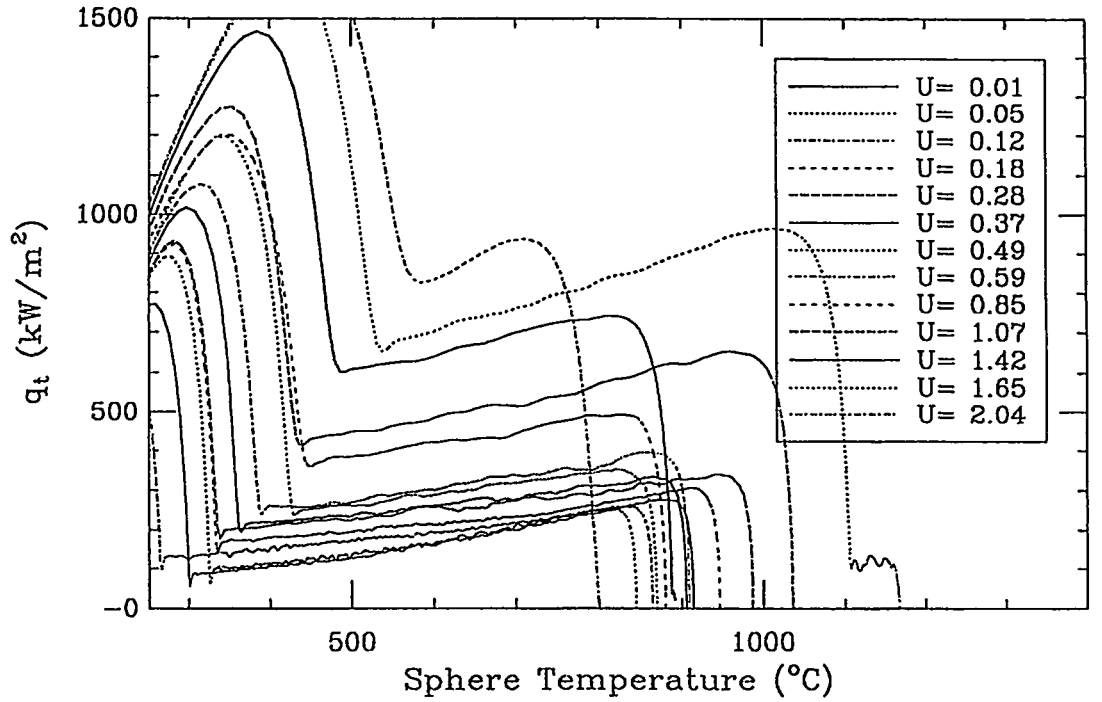

Fig. 4.14. The total heat flux transients from a typical series of transient mode runs in 20 °C subcooled water.

The experimental Nusselt numbers obtained in 10 and 20 °C subcooling conditions are shown in Figs. 4.15 and 4.16 respectively. Unlike the case in a saturated condition, the Nu always increases with the Re, first slowly and then quickly when Re is greater than 10000, especially when the subcooling is high. As in the case of the saturated condition, the Nusselt number decreases significantly when the sphere temperature increases.

Pool Film Boiling in Subcooled Water

For pool film boiling in subcooled liquid, correlations in addition law [such as Farahat (1972), Siviour (1970) and Dhir (1978)] and correlations in ratio law [such as Michiyoshi (1988) and Sakurai (1990b)] are usually used to correlate the heat transfer data, as indicated in Chapter 2. Thus, our experimental data are compared with these correlations, as shown in Fig. 4.17, at a condition of sphere temperature 760 °C; the experimental data is about 8% higher than Michiyoshi's correlation and about 14% higher than Sakurai's ratio correlation for cylinders. Compared with Dhir's correlation, our data is a little lower for low subcooling and a little higher for large subcooling.

The experimental data, including all the data with sphere temperatures from 900 °C to quench, are plotted in form of Michiyoshi's correlation in Fig. 4.18, and it shows agreement within a ±15% band. The Michyoshi's correlation is given as

$$\mathrm{Nu} = 0.696(\mathrm{Ar}/Sp')^{1/4} M_c^{1/4} \tag{4.5}$$

where

$$M_c = E^3/[1 + E/(Sp'\mathrm{Pr}_l)]/(R\mathrm{Pr}_l Sp')^2$$
$$E = (A + CB^{1/2})^{1/3} + (A - CB^{1/2})^{1/3} + (1/3)Sc^*$$
$$A = (1/27)Sc^{*3} + (1/3)R^2 Sp'\mathrm{Pr}_l Sc^* + (1/4)R^2 Sp'^2 \mathrm{Pr}_l^2$$
$$B = (-4/27)Sc^{*2} + (2/3)\mathrm{Sp'Pr}_l Sc^* - (32/27)Sp'\mathrm{Pr}_l R^2 + (1/4)Sp'^2\mathrm{Pr}_l^2 + (2/27)Sc^{*3}/R^2$$
$$C = (1/2)R^2 Sp'\mathrm{Pr}_l, Sc^* = C_{pl}\Delta T_{sub}/h'_{fg}$$

Forced Convection Film Boiling in Subcooled Water Flows

To give a sense of how the water subcooling and water velocity affect the film boiling heat transfer, the ratios of experimental Nusselt number over the corresponding saturated pool film boiling Nusselt number are plotted in Fig. 4.19. In general, the subcooling has a stronger effect than the flow velocity; the velocity influence is enhanced when the subcooling is large.

For highly subcooled forced convection film boiling, as mentioned in Chapter 2, several analyses suggested the same correlation in the form of

$$\mathrm{Nu} = C_{sub,F}\mathrm{Re}_l^{1/2}\mathrm{Pr}_l^{1/2}(\mu_l/\mu_v)(Sc'/Sp') \tag{4.6}$$

This expression is not suitable for saturated or small subcooled cases. So in order to correlate all the forced convection film boiling by one equation, the following expression may be suggested

$$\mathrm{Nu} = \mathrm{Nu}_s + C'_{sub,F}\mathrm{Re}_l^n\mathrm{Pr}_l^{1/2}(\mu_l/\mu_v)(Sc'/Sp') \tag{4.7}$$

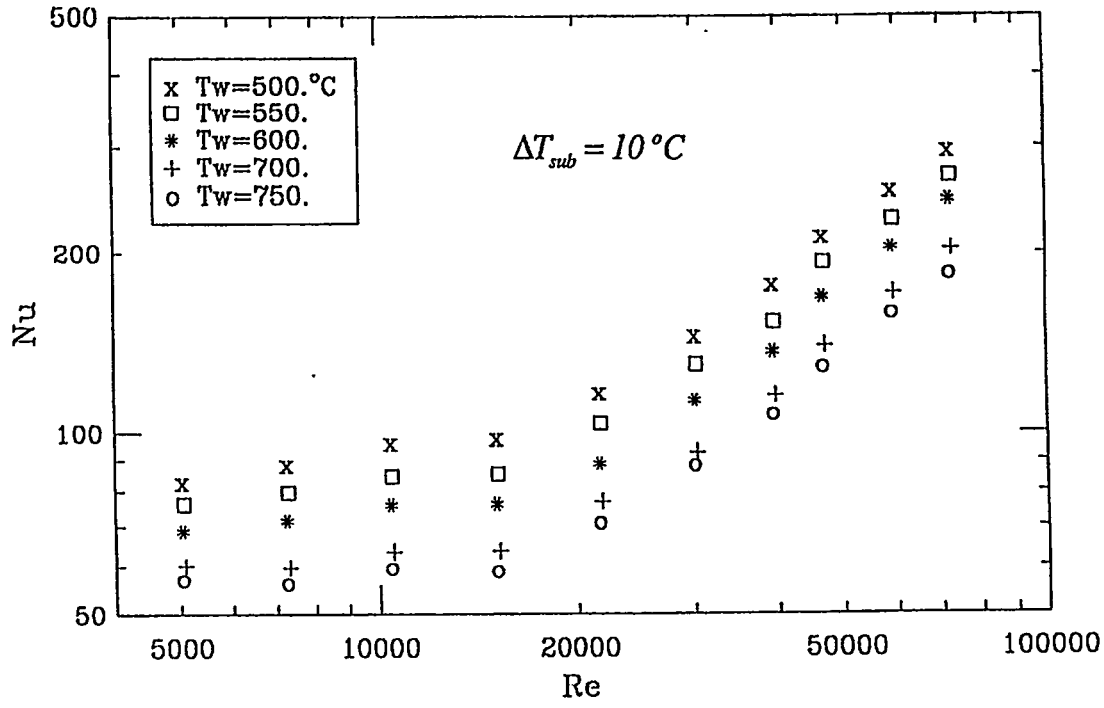

Fig. 4.15. Subcooled film boiling data plotted in the form of Nu vs Re.

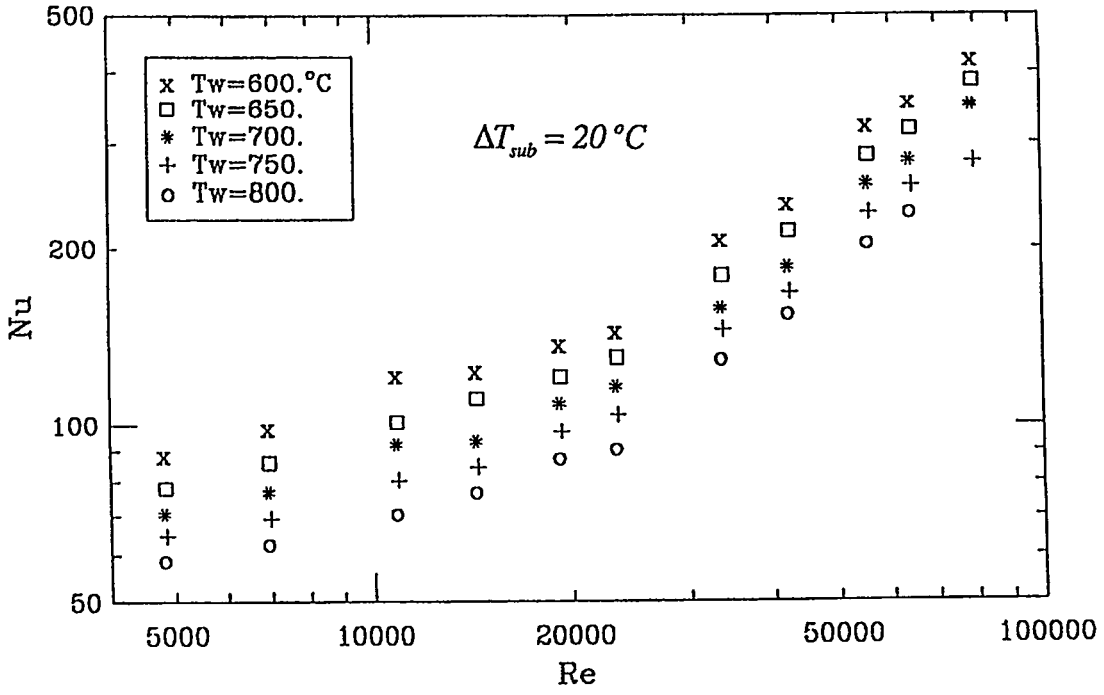

Fig. 4.16. Subcooled film boiling data plotted in the form of Nu vs Re.

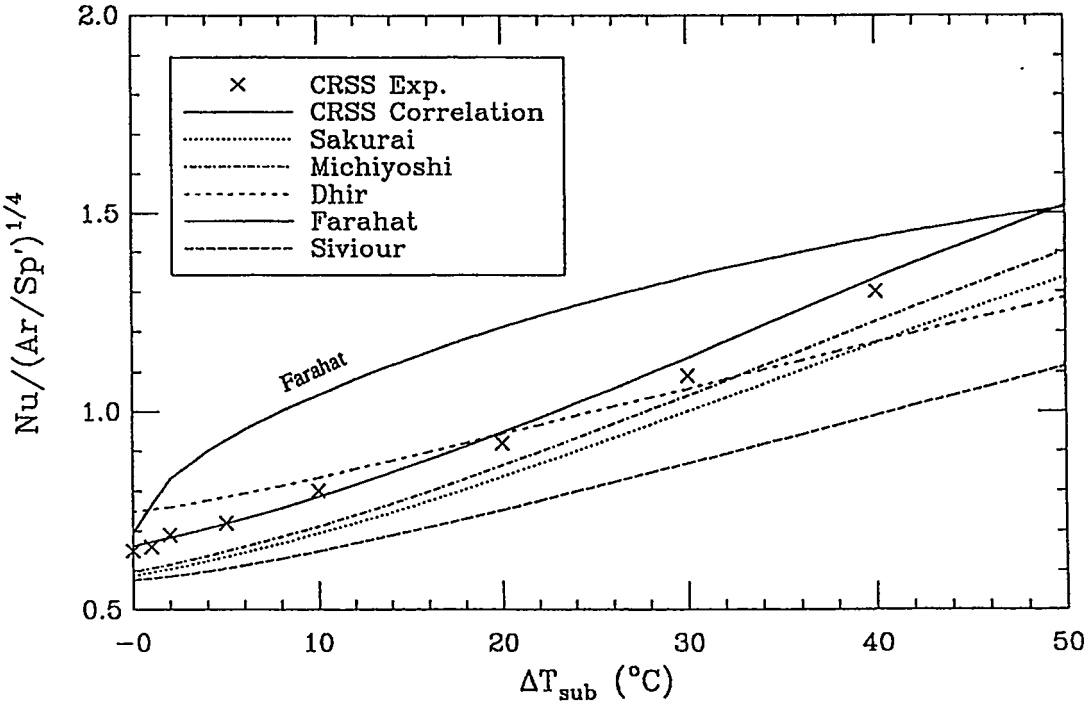

Fig. 4.17. A comparison of subcooled film boiling data with the correlations, at sphere superheat of 660 °C and 1 bar pressure.

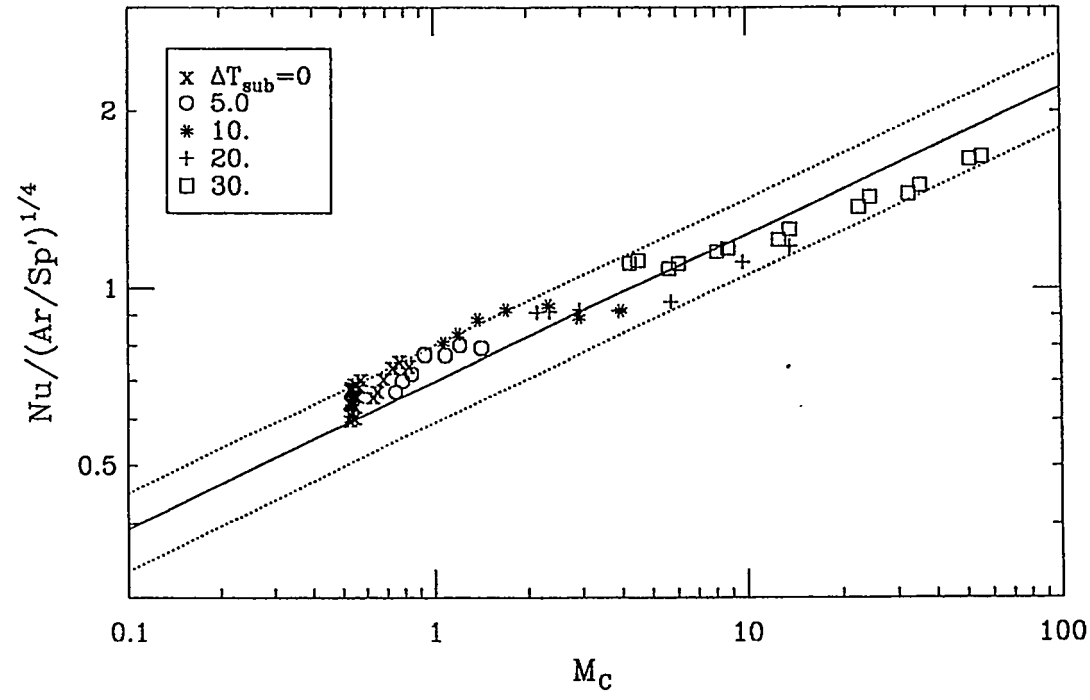

Fig. 4.18. Subcooled film boiling data correlated in the form of Eq. (2.29).

where the Nu_s is the corresponding Nusselt number for saturated forced convection film boiling, given by $Nu_s = 0.5Re_l^{1/2}(\mu_l/\mu_v)[R^4K/Sp']^{1/4}$. Physically, Eq. (4.7) may be interpreted as: the total heat flux equals the heat that is required to sustain the vapor film plus the heat that convected into the liquid stream. The Constant $C'_{sub,F}$ and the power n on Re_l should be determined by experimental data.

In terms of Eq. (4.6), the experimental data obtained at 20 °C subcooling are plotted in Fig. 4.20. The sphere superheat influence is well correlated and the heat transfer characteristic $C_{sub,F} = Nu/\{Re_l^{1/2}Pr_l^{1/2}(\mu_l/\mu_v)(Sc/Sp)\}$ varies from 1.5 to 2.0, in contrast with the theoretical constant of 0.977 from Epstein and Hauser's (1980) analysis and the suggested (by them) constant of 2.04.

According to our highly subcooled forced convection film boiling experimental data, we found that the best constants for Eq. (4.7) are $C'_{sub,F} = 0.072$ and $n = 0.77$ in order to correlate well with the data. Thus, Eq. (4.7) becomes

$$Nu = Nu_s + 0.072Re_l^{0.77}Pr_l^{1/2}(\mu_l/\mu_v)(Sc'/Sp') \tag{4.8}$$

The reason for our empirical power n being greater than 1/2 is due to the turbulence effect. The fact that turbulence increases the power on the Reynolds number is also shown in Wang and Peng's (1992) study of film boiling on a horizontal flat plate in forced convection, where the power n is 0.8.

In the form of Eq. (4.8), the data are plotted in Fig. 4.21; the sphere superheat effect is still well correlated. More data obtained at various subcooling conditions are shown in Fig. 4.22. For $Fr^{1/2}$ greater than 2.0, the $C'_{sub,F} = (Nu\text{-}Nu_s)/Re_l^{0.77}Pr_l^{1/2}(\mu_l/\mu_v)(Sc/Sp)$ is about 0.072.

4.4 Diameter Effect on Film Boiling

Four different sizes of spheres (6.35, 9.53, 12.7 and 19.1 mm O.D.) were used in our experiment to check the effect of sphere diameter on the film boiling heat transfer. The diameter effects on correlation Eq. (4.4) for saturated forced convection film boiling and the effects on correlation Eq. (4.8) for subcooled forced convection film boiling are shown in Figs. 4.23 and 4.24 respectively. The results indicate that in our diameter range from 0.635 to 19.1 mm, the diameter effects on forced convection film boiling correlations are not distinguishable.

The same conclusion was obtained for pool film boiling if Eq. (4.5) is used to correlate the data. However, according to several previous studies on pool film boiling, as indicated in the literature review in Chapter 2, this correlation does not work well for very small and very large diameter spheres. Sakurai et al. (1990b), based on their systematic experimental data obtained from film boiling on cylinders, modified their analytical solution (which is the same as Michiyoshi's correlation Eq. (4.5), by introducing a diameter-effect correction-factor $K(d')$ on the right hand side of the equation and a factor $(1 + 2/Nu)^{-1}$ on the left hand side to correlate their small wire/cylinder film boiling data well. Since the film boilings on spheres and on cylinders are quite similar, it is reasonable to assume that the Sakurai's diameter-effect correction- factor for cylinders should also apply to the case of spheres. Comparing our data with Sakurai's correlation, we found our experimental data

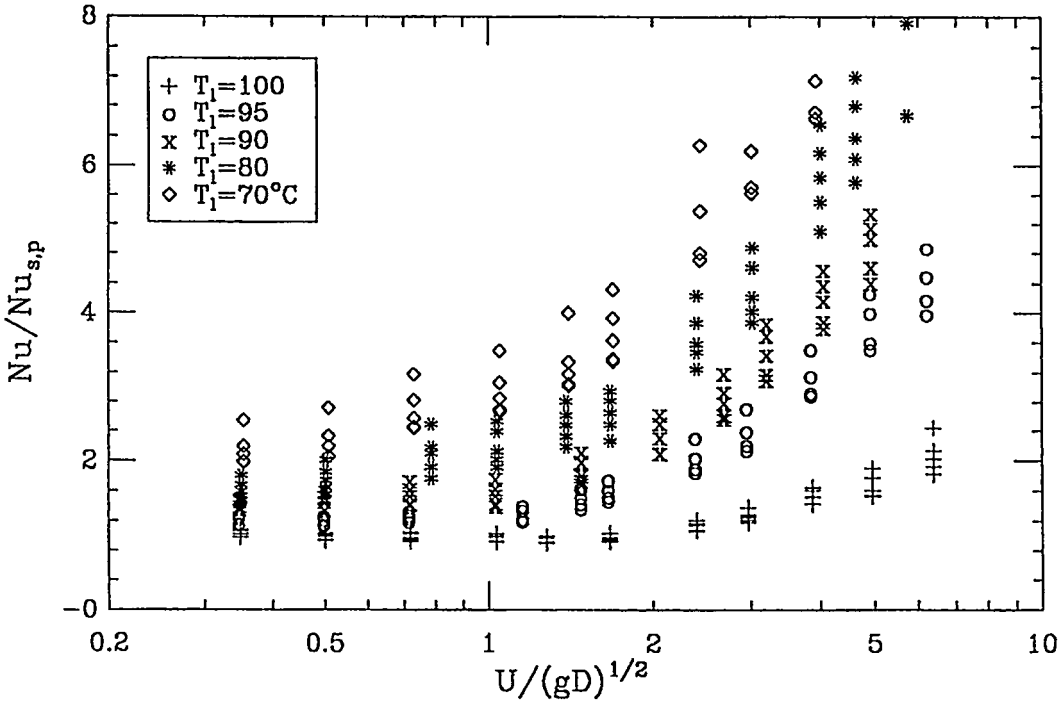

Fig. 4.19. The enhancement of liquid subcooling and velocity on the film boiling heat transfer.

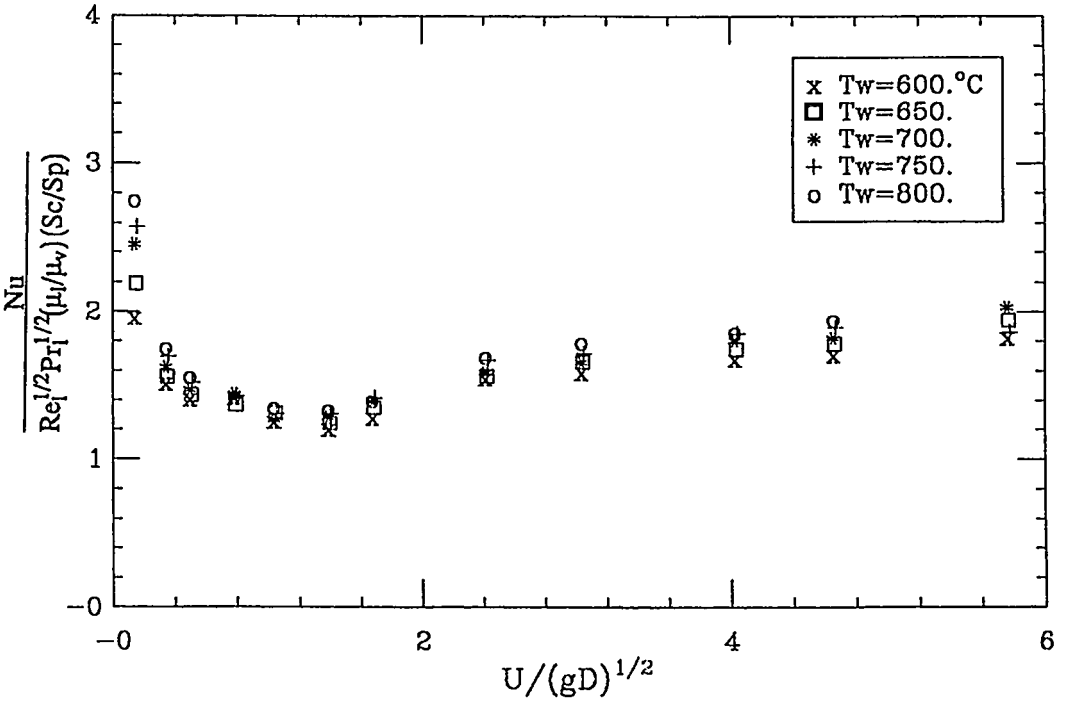

Fig. 4.20. Subcooled film boiling data plotted in the form of Eq. (4.6).

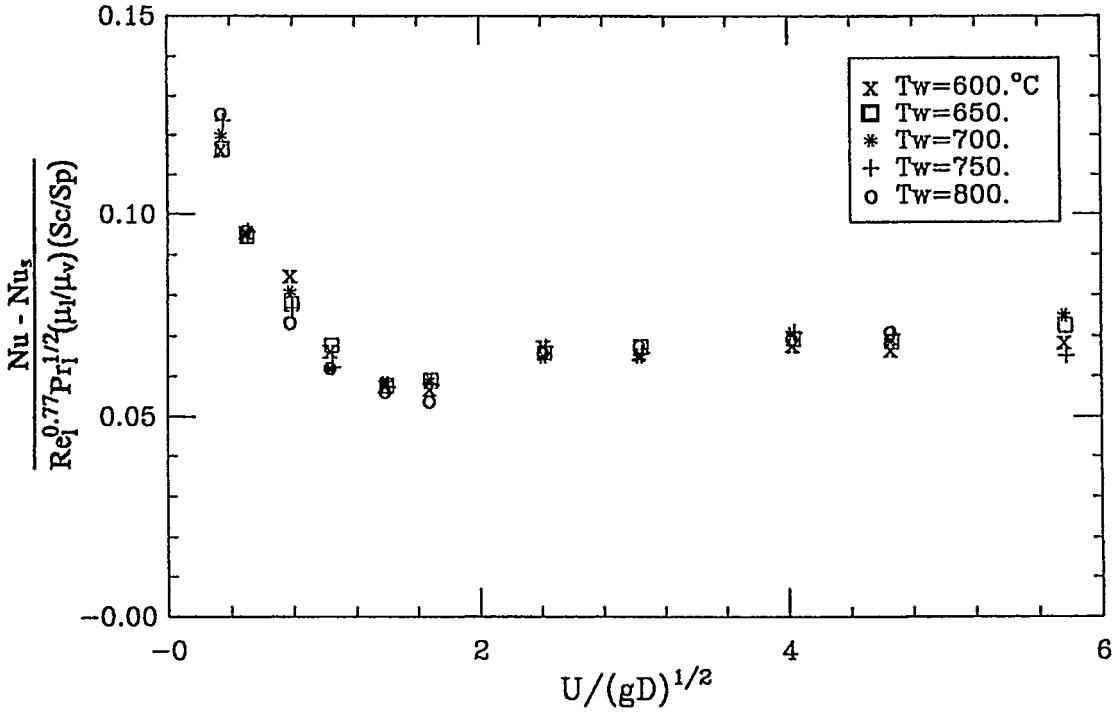

Fig. 4.21. Subcooled film boiling data plotted in the form of Eq. (4.7).

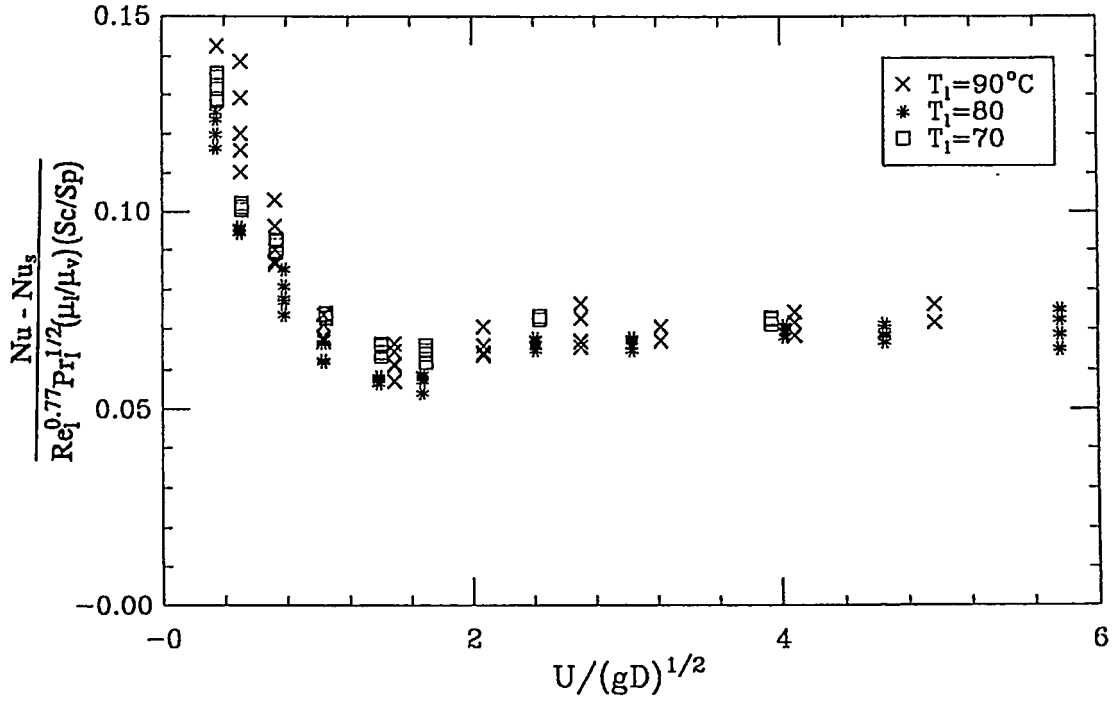

Fig. 4.22. More subcooled data plotted in the form of Eq. (4.7).

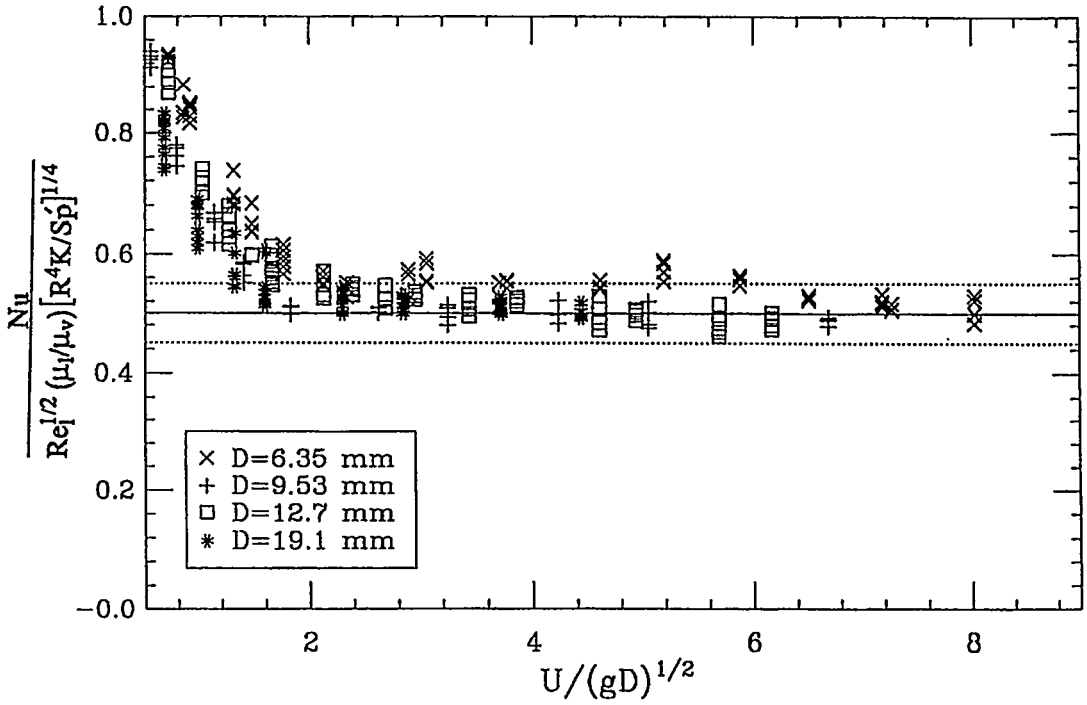

Fig. 4.23. Data obtained from different sizes of sphere at saturated condition, plotted in terms of saturated forced convection correlation.

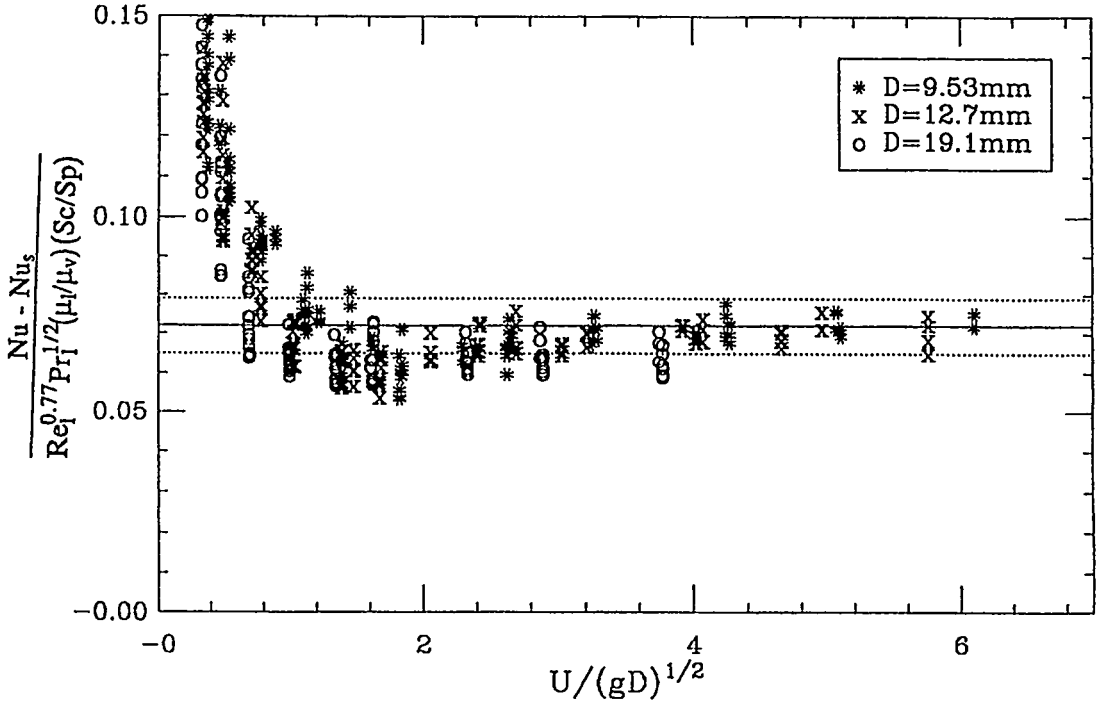

Fig. 4.24. Data obtained from different sizes of sphere at subcooled conditions, plotted in terms of subcooled forced convection correlation.

are about 10% to 14% higher than their correlation. In addition, according to Michiyoshi's et al (1988) theoretical analysis, the Nusselt number for spheres is 14% higher than that for horizontal cylinders. Therefore a factor of 1.14 is applied to Sakurai's et al (1990b) correlation to correlate our sphere pool film boiling experimental data, and the agreement turned out to be very good within a ±15% band, as shown in Fig. 4.25. The complete correlation for pool film boiling at both saturated and subcooled conditions is given as

$$\mathrm{Nu}/(1+2/\mathrm{Nu}) = K_c(d')(\mathrm{Ar}/Sp')^{1/4}M_c^{1/4} \tag{4.9}$$

where M_c is the same as that in Eq. (4.5) and $K_c(d')$ is calculated by

$$\begin{aligned}
&K_c(d') = 0.5d'^{-1/4}, && \text{for } d' < 0.14\\
&K_c(d') = 0.86/(1+0.28d'), && \text{for } 0.14 < d' < 1.25\\
&Kc(d') = 2.4d'/(1+3.0d'), && \text{for } 1.25 < d' < 6.6\\
&Kc(d') = 0.47d'^{1/4}, && \text{for } d' > 6.6
\end{aligned}$$

4.5 Material and Water Effects on Film Boiling

Our experiments were conducted with distilled water, deionized water, tap water, and deionized water with salt additions. The experiment shows that the kind of water used has no effect on the heat transfer data obtained from the transient mode operation, and it only affects the speed of sphere surface oxidation.

For the cool-down transient experimental technique, one concern is that the nonuniformity of temperature distribution in the stainless steel sphere may affect the accuracy of the film boiling heat transfer data. This was investigated and checked by doing the transient experiment with brass spheres of diameters 9.53 and 12.7 mm, which have a thermal conductivity that is 10 times higher than stainless steel. The total film boiling heat flux obtained with a brass sphere in saturated water is shown in Fig. 4.26; it is very close to that obtained with a stainless steel sphere, and the only difference is that the brass sphere has a little lower quench temperature than the stainless steel sphere, especially when the water velocity is high.

The ratios of experimental Nusselt numbers (obtained with brass) over the predicted Nusselt numbers from Eq. (4.9) for pool film boiling are shown in Fig. 4.27, which shows excellent agreement when $\mathrm{Fr}^{1/2}$ is smaller than 1. For forced convection, the ratios of experimental Nusselt numbers over the predicted Nusselt numbers from Eq. (4.4) are shown in Fig. 4.28, which also shows good agreement when $\mathrm{Fr}^{1/2}$ is greater than 2. This indicates that the film boiling heat transfer does not depend on the sphere material. It also implies that the nonuniformity of temperature distribution in the stainless steel sphere does not affect the accuracy of film boiling heat transfer data significantly.

4.6 Steady-State Mode Operation Results

Steady-state mode operations have been conducted with stainless-steel spheres in waters with different water electrical conductivities. The ratios of experimental data over the predicted values from Eq. (4.4) which is obtained from transient mode experiment are shown in Fig. 4.29. If we assume that the film boiling heat transfer in the transient state and steady state are the same, these data are seen to confirm the applicability of the power calibration (in air) to an all-water flow system, provided the electrical conductivity is adequately large (over 200 micromho).

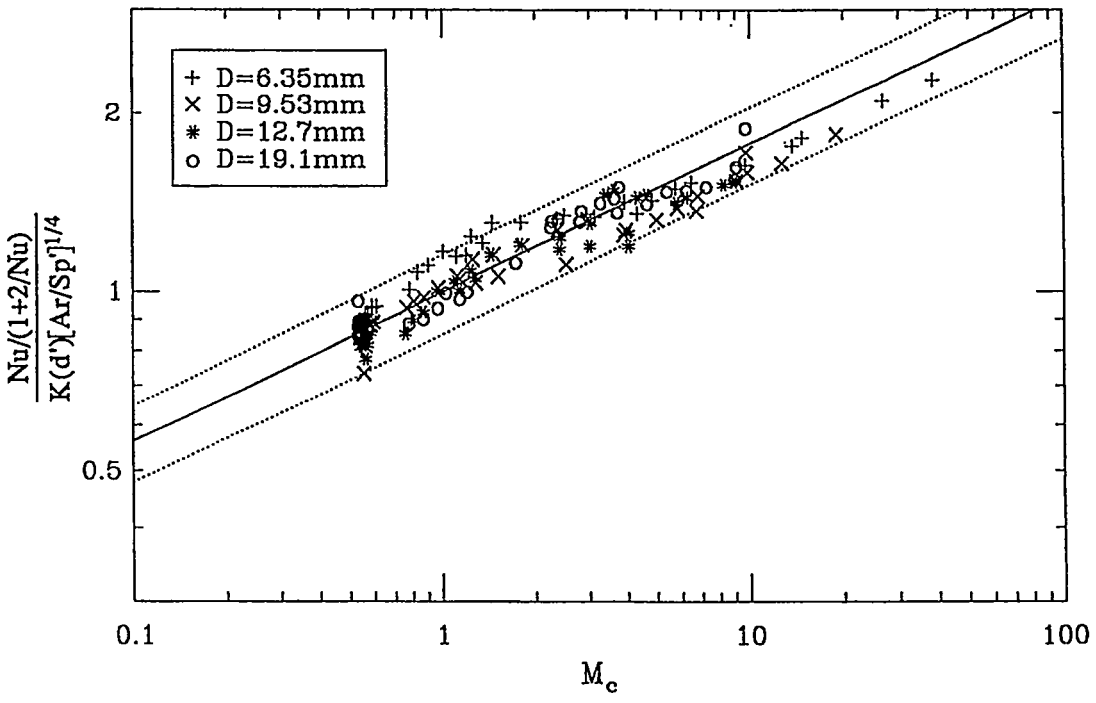

Fig. 4.25. Data obtained from different sizes of sphere at subcooled pool film boiling conditions (from 0.0 to 40 °C).

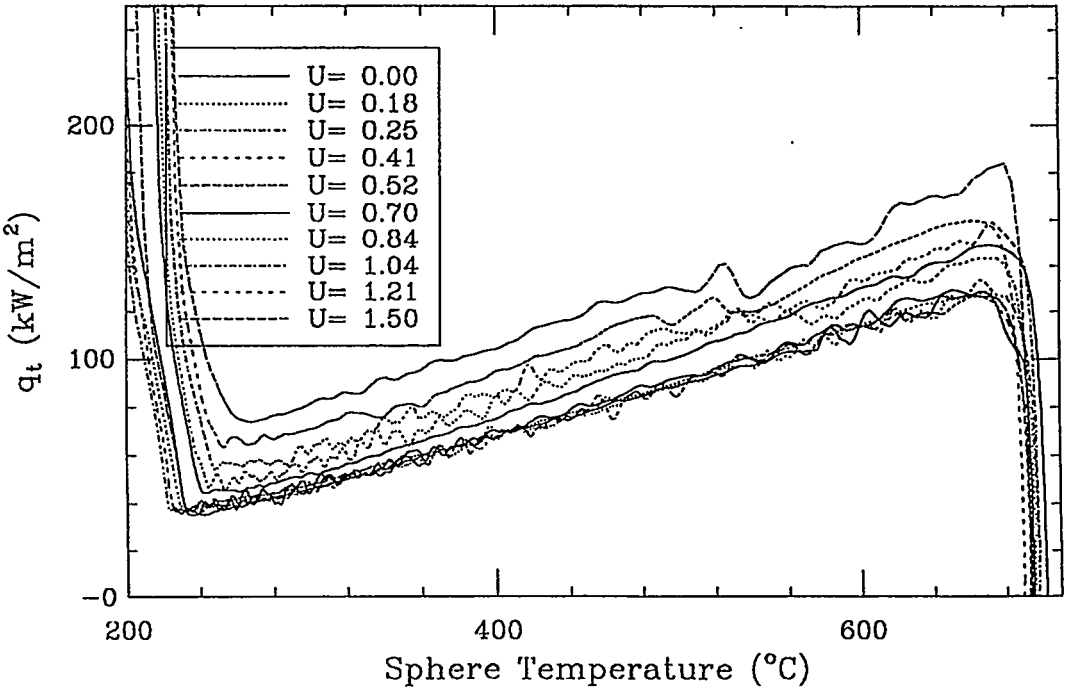

Fig. 4.26. Total heat flux transients from a typical series of transient mode runs in the saturated condition with a brass sphere.

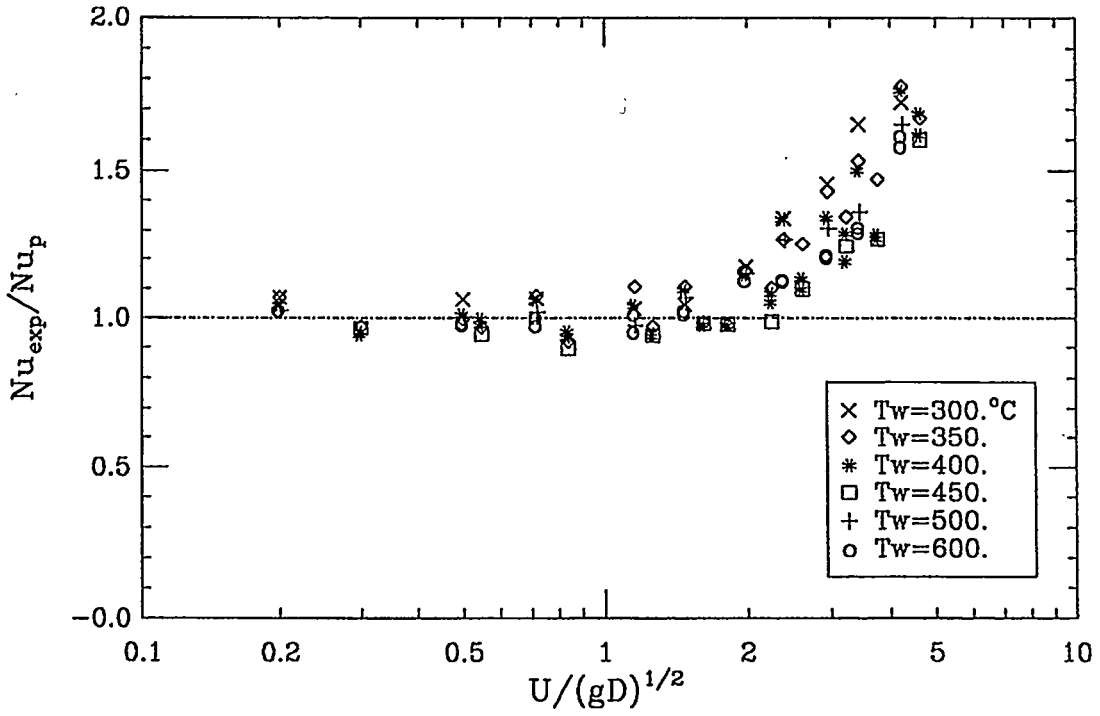

Fig. 4.27. Data obtained from brass sphere are compared with pool film boiling correlation.

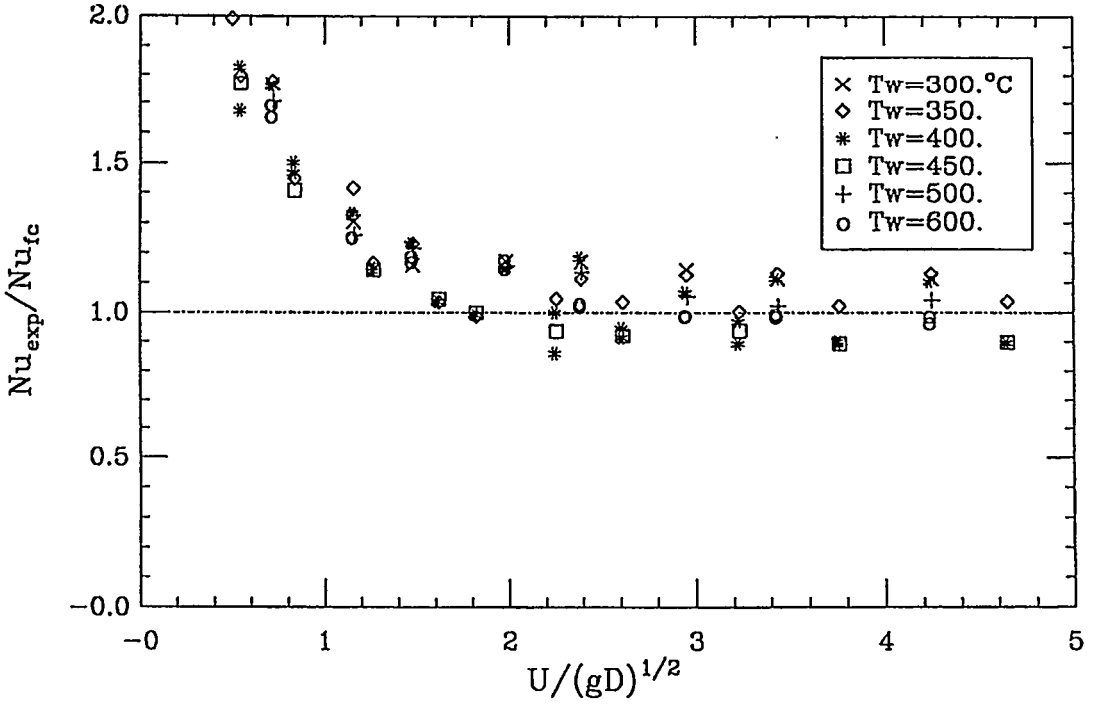

Fig. 4.28. Data obtained from brass sphere are compared with forced convection film boiling correlation.

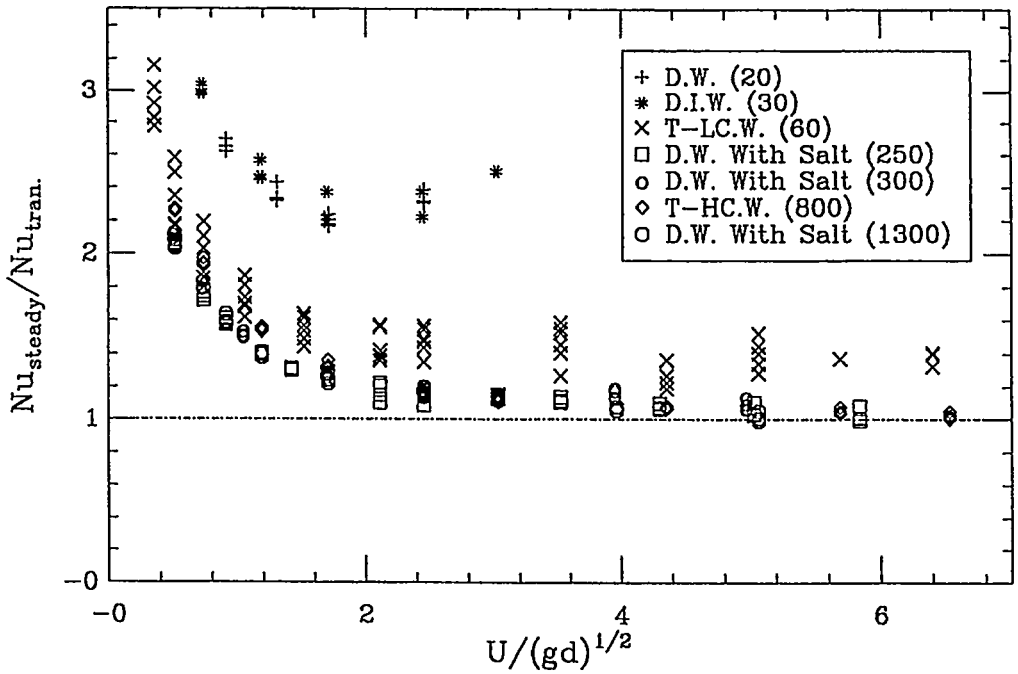

Fig. 4.29. The effect of water electrical conductivity (shown in parenthesis in micromho) on the power coupling to the sphere. D.W. is for distilled water; D.I.W is for deionized water; T-LC.W. and T-HC.W. are for low conductivity and high conductivity tap water respectively.

5 A THEORETICAL ANALYSIS OF FILM BOILING IN SINGLE-PHASE FLOWS

5.1 Introduction to the Theoretical Analysis

As the literature review in Chapter 2 indicates, from theoretical aspect, film boiling on spheres has been studied extensively. However, there is still no theoretical film boiling model that, by itself, covers all the single-phase film boiling regimes for spheres (from natural to forced convection and from completely saturated to highly subcooled conditions). Frederking and Clark's (1963) analysis, which is similar to Nusselt's analysis for condensation on a vertical wall, is only for *saturated natural convection*. Witte's (1968) simple analysis, which uses the potential velocity around the sphere as the vapor velocity, is only for *saturated forced convection*. Kobayasi (1965), following the Bromley's (1953) analysis, is only for *saturated* cases. Epstein's (1980) model, which applies similarity boundary layer theory and perturbation method to the front stagnation point of the sphere, is only for *forced convection*, either saturated or highly subcooled. Michiyoshi (1988) and Tso (1990) obtained a close form analytical solution for *natural free convection* film boiling on a sphere.

For film boiling on cylinders, there are also many pieces-wise analyses. For example, Bromley (1953) carried out an analysis for *saturated* cases based on Bernoulli's theorem and a consideration of viscous drag to the vapor. Motte and Bromley (1957) also did an analysis for *subcooled forced convection* film boiling from an energy partition and turbulent point of view. Liu, Shiotu and Sakurai (1992) did an analysis for *saturated forced convection* by means of an integral method with a single-phase boundary layer. Shigechi, Ito and Nishikawa's (1983) analytical model, which is based on an integral method with a two-phase laminar boundary-layer theory, covers all the single-phase film boiling regimes, although it must be solved numerically.

In this chapter, an analysis which is similar to that of Shigechi, Ito and Nishikawa (1983) is carried out for a sphere in all the film boiling regimes. There are two major differences between our model and Shigechi's. First, the boundaries around the sphere are axial symmetric instead of two-dimensional as for cylinders. Secondly, the potential flow over a sphere is different from that over a cylinder. Additionally in our model, the film properties and the effective latent heat of evaporation are used instead of the properties at the saturation point.

Shigechi, Ito and Nishikawa's analysis treats the separated rear region with an arbitrary film thickness function. This is fine for the saturated case since the heat transfer in

this region is very small compared with that in the unseparated front region. However, with this arbitrary thickness function for the rear separated region, the overall heat transfer becomes arbitrary for subcooled cases because the rear region also contributes a significant amount in heat transfer. In this work, a turbulent eddy model [Theofanous et al (1976)] is applied to calculate the heat transfer in the separated rear region for the subcooled forced convection cases, which agree with the experimental data very well.

5.2 Physical Model and Fundamental Equations

Consider film boiling from a sphere with a uniform surface temperature T_w, which is placed in a stream of liquid flowing upward with a uniform velocity U_∞, as shown in Fig. 5.1. The gravitational force is opposite to the coming flow direction. The liquid is subcooled by ΔT_{sub} below the saturation temperature T_s corresponding to the system pressure. The following assumptions are made.

(1) The vapor film and the liquid (water) flow adjacent to the vapor-liquid interface are regarded as boundary-layers. This is a two-phase boundary-layer.

(2) The flows in the vapor and liquid boundary-layer are steady laminar flow and the flow outside the liquid boundary-layer is a potential flow.

(3) Physical properties are constant and are evaluated at the film temperatures. The density of vapor is negligible compared with that of liquid when the vapor momentum equation is concerned.

(4) The inertia terms in the momentum equation and the convection terms in the energy equation for vapor film layer are neglected for simplicity. The effects of convective terms are compensated by using an effective latent heat of vaporization h'_{fg} at the interface.

$$h'_{fg} = h_{fg} + 0.5 C_{pv} \Delta T_{sup}$$

(5) The vapor-liquid interface is smooth and the pressure difference due to surface tension is small and not considered.

(6) Radiation heat transfer is not considered.

Under the above assumptions, the fundamental equations for the vapor layer are as follows

Continuity equation:

$$\frac{1}{r}\frac{\partial u_v}{\partial \theta} + \frac{\partial v_v}{\partial y} + \frac{u_v}{r} cot\theta = 0 \tag{5.1}$$

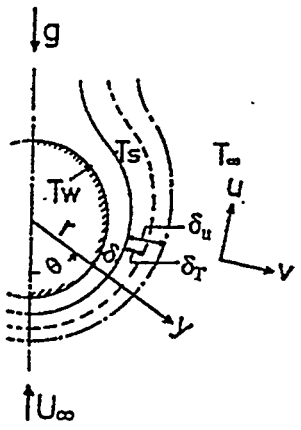

Fig. 5.1 Physical model and coordinate system.

Momentum equation:

$$0 = -g\rho_v sin\theta - \frac{1}{r}\frac{\partial p_v}{\partial \theta} + \mu_v \frac{\partial^2 u_v}{\partial y^2} \tag{5.2}$$

Energy equation:

$$0 = k_v \frac{\partial^2 T_v}{\partial y^2} \tag{5.3}$$

For the potential flow outside the liquid boundary-layer, the pressure is given by

$$p_l = p_0 + g\rho_l r cos\theta + \frac{1}{2}\rho_l U_\infty - \frac{1}{2}\rho_l \left(\frac{3}{2}U_\infty sin\theta\right)^2$$

Thus the pressure gradient is

$$-\frac{1}{r}\frac{\partial p_l}{\partial \theta} = \rho_l \left(g sin\theta + \frac{9}{8}\frac{U_\infty^2}{r} sin2\theta\right)$$

Neglecting the pressure difference due to curvature of the vapor-liquid interface, using the assumption that the pressure in the vapor layer equals the pressure in the liquid layer, which is assumed to be the pressure of potential flow around the sphere, substituting the above equation into the vapor layer momentum Eq. (5.2) and taking account of the third assumption, the following equation is obtained

$$\frac{\mu_v}{\rho_v}\frac{\partial^2 u_v}{\partial y^2} + g\frac{\rho_l}{\rho_v} sin\theta + \frac{9}{8}\frac{\rho_l}{\rho_v}\frac{U_\infty^2}{r} sin2\theta = 0 \tag{5.4}$$

For the liquid boundary-layer, the three governing equations are as follows:

Continuity equation:

$$\frac{1}{r}\frac{\partial u_l}{\partial \theta} + \frac{\partial v_l}{\partial y} + \frac{u_l}{r}cot\theta = 0 \tag{5.5}$$

Momentum equation:

$$\frac{u_l}{r}\frac{\partial u_l}{\partial \theta} + v_l\frac{\partial u_l}{\partial y} = g\beta_1(T_l - T_\infty)sin\theta + \frac{9}{8}\frac{U_\infty^2}{r}sin2\theta + \frac{\mu_l}{\rho_l}\frac{\partial^2 u_l}{\partial y^2} \tag{5.6}$$

Energy equation:

$$\frac{u_l}{r}\frac{\partial T_l}{\partial \theta} + v_l\frac{\partial T_l}{\partial y} = \frac{k_l}{c_{pl}\rho_l}\frac{\partial^2 T_l}{\partial y^2} \tag{5.7}$$

The boundary conditions and the compatibility conditions at the vapor-liquid interface are

$y = 0$:

$$u_v = v_v = 0 \tag{5.8}$$

$$T_v = T_w \tag{5.9}$$

$y = \delta$:

$$u_v = u_l = u_\delta \tag{5.10}$$

$$\mu_v\left(\frac{\partial \mu_v}{\partial y}\right)_\delta = \mu_l\left(\frac{\partial u_l}{\partial y}\right)_\delta \tag{5.11}$$

$$\rho_v\left(v_v - \frac{u_v}{r}\frac{d\delta}{d\theta}\right)_\delta = \rho_l\left(v_l - \frac{u_l}{r}\frac{d\delta}{d\theta}\right)_\delta \tag{5.12}$$

$$T_v = T_l = T_s \tag{5.13}$$

$$-k_v\left(\frac{\partial T_v}{\partial y}\right)_\delta = -\dot{m}h'_{fg} - k_l\left(\frac{\partial T_l}{\partial y}\right)_\delta \tag{5.14}$$

$y = \delta + \delta_u$:

$$u_l = u_{l,\delta_u} = \frac{3}{2}U_\infty sin\theta \tag{5.15}$$

$$\left(\frac{\partial u_l}{\partial y}\right)_{\delta_u} = 0 \tag{5.16}$$

$y = \delta + \delta_T$:

$$T_l = T_\infty \tag{5.17}$$

$$\left(\frac{\partial T_l}{\partial y}\right)_{\delta_T} = 0 \tag{5.18}$$

The $\dot{m}$ in Eq. (5.14) is given by

$$-\dot{m} = \rho_v \left(\frac{1}{r}\frac{d}{d\theta}\int_0^\delta u_v dy + \frac{cot\theta}{r}\int_0^\delta u_v dy\right) \tag{5.19}$$

Before transforming these equations into dimensionless forms, integrating Eq. (5.1) with respect to y from 0 to δ and substituting the result into Eq. (5.19), we have

$$-\dot{m} = \rho_v \left(\frac{1}{r}\frac{d}{d\theta}\int_0^\delta u_v dy + \frac{cot\theta}{r}\int_0^\delta u_v dy\right) = -\rho_v \left(v_v - \frac{u_v}{r}\frac{d\delta}{d\theta}\right)_\delta \tag{5.20}$$

Integrating the vapor layer energy equation, Eq. (5.3), with the boundary conditions, Eqs. (5.9) and (5.13), we obtain a linear temperature distribution. Substituting it into Eq. (5.14) and applying Eq. (5.19), we have

$$h'_{fg}\rho_v \left(\frac{1}{r}\frac{d}{d\theta}\int_0^\delta u_v dy + \frac{cot\theta}{r}\int_o^\delta u_v dy\right) = k_v \frac{T_w - T_s}{\delta} + k_l \left(\frac{\partial T_l}{\partial y}\right)_\delta \tag{5.21}$$

$$h'_{fg}\rho_v \left(v_v - \frac{u_v}{r}\frac{d\delta}{d\theta}\right)_\delta = -k_v \frac{T_w - T_s}{\delta} - k_l \left(\frac{\partial T_l}{\partial y}\right)_\delta \tag{5.22}$$

We define the dimensionless variables and parameters as follows:

$$l^* = \left(\frac{\mu_v^2 r}{\rho_v^2 g}\right)^{1/4}; \quad u^* = (\Delta g r)^{1/2}; \quad v^* = \left(\frac{\mu_v^2 g}{\rho_v^2 r}\right)^{1/4} \tag{5.23}$$

$$Y = y/l^*; \quad \Delta = \delta/l^*; \quad \Delta_u = \delta_u/l^*; \quad \Delta_r = \delta_r/l^* \tag{5.24}$$

$$U_v = u_v/u^*; \quad U_l = u_l/u^*; \quad V_v = v_v/v^*; \quad V_l = v_l/v^* \tag{5.25}$$

$$F = U_\infty^2/gr = 2\mathrm{Fr} \tag{5.26}$$

$$K = \rho_l/\rho_v \tag{5.27}$$

$$R = (\rho_v \mu_v/\rho_l \mu_l)^{1/2} \tag{5.28}$$

$$\Theta = c_{pl}(T_l - T_\infty)/\mathrm{Pr}_l h'_{fg} \tag{5.29}$$

$$Sc = c_{pl}(T_s - T_\infty)/\mathrm{Pr}_l h'_{fg} \tag{5.30}$$

$$Sp = c_{pv}(T_w - T_s)/\mathrm{Pr}_v h'_{fg} \tag{5.31}$$

$$B_l = \beta_l h'_{fg}/c_{pl} \tag{5.32}$$

The dimensionless governing equations and boundary conditions now become as follows:

For the vapor film:

$$\frac{\partial U_v}{\partial \theta} + \frac{\partial V_v}{\partial Y} + U_v cot\theta = 0 \tag{5.33}$$

$$\frac{\partial^2 U_v}{\partial Y^2} + K\left(1 + \frac{9}{4}Fcos\theta\right) sin\theta = 0 \tag{5.34}$$

$$\frac{d}{d\theta}\int_0^{\Delta} U_v dY + cot\theta \int_0^{\Delta} U_v dY = \frac{Sp'}{\Delta} + \frac{1}{R^2 K}\left(\frac{\partial \Theta}{\partial Y}\right)_{\Delta} \tag{5.35}$$

For the liquid boundary layer:

$$\frac{\partial U_l}{\partial \theta} + \frac{\partial V_l}{\partial Y} + U_l cot\theta = 0 \tag{5.36}$$

$$U_l\frac{\partial U_l}{\partial \theta} + V_l\frac{\partial U_l}{\partial Y} = \mathrm{Pr}_l B_l \Theta sin\theta + \left(\frac{1}{RK}\right)^2 \frac{\partial^2 U_l}{\partial Y^2} + \frac{9}{8}Fsin2\theta \tag{5.37}$$

$$U_l\frac{\partial \Theta}{\partial \theta} + V_l\frac{\partial \Theta}{\partial Y} = \frac{1}{\mathrm{Pr}_l}\left(\frac{1}{RK}\right)^2 \frac{\partial^2 \Theta}{\partial Y^2} \tag{5.38}$$

The boundary conditions:

At $Y = 0$:

$$U_v = V_v = 0 \tag{5.39}$$

At $Y = \Delta$:

$$U_v = U_l = U_{\Delta} \tag{5.40}$$

$$\left(\frac{\partial U_v}{\partial Y}\right)_{\Delta} = \frac{1}{R^2 K}\left(\frac{\partial U_l}{\partial Y}\right)_{\Delta} \tag{5.41}$$

$$\left(V_v - U_v\frac{d\Delta}{d\theta}\right)_{\Delta} = K\left(V_l - U_l\frac{d\Delta}{d\theta}\right)_{\Delta} \tag{5.42}$$

$$\Theta_{\Delta} = Sc' \tag{5.43}$$

$$\left(V_v - U_v\frac{d\Delta}{d\theta}\right)_{\Delta} = -\frac{Sp'}{\Delta} - \frac{1}{R^2 K}\left(\frac{\partial \Theta}{\partial Y}\right)_{\Delta} \tag{5.44}$$

At $Y = \Delta + \Delta_u$:

$$U_l = U_{l,\Delta_u} = (3/2)F^{1/2} sin\theta \tag{5.45}$$

$$\left(\frac{\partial U_l}{\partial Y}\right)_{\Delta_u} = 0 \tag{5.46}$$

At $Y = \Delta + \Delta_T$:

$$\Theta_{\Delta_T} = 0 \tag{5.47}$$

$$\left(\frac{\partial \Theta}{\partial Y}\right)_{\Delta_T} = 0 \tag{5.48}$$

5.3 Method of Solution

Integrating Eq. (5.34) twice with respect to Y and determining the integral constant by boundary condition Eqs. (5.39) and (5.40), we have a vapor layer velocity distribution function

$$U_v = \left\{\frac{U_\Delta}{\Delta} + \frac{K\Delta}{2}\left(1 + \frac{9}{4}F\cos\theta\right)\sin\theta\right\}Y - \left\{\frac{K}{2}\left(1 + \frac{9}{4}F\cos\theta\right)\sin\theta\right\}Y^2 \tag{5.49}$$

As an approximation, we assume quadratic functions of Y for the radial distributions of tangential velocity U_l and temperature Θ in the liquid boundary layer and determine the constants of these functions by Eqs. (5.40), (5.45) and (5.46) for U_l, and by Eqs. (5.43), (5.47) and (5.48) for Θ. So the velocity and temperature distributions in the liquid layer are

$$U_l = U_\Delta + \left(\frac{3}{2}F^{1/2}\sin\theta - U_\Delta\right)\left[2\left(\frac{\xi}{\Delta_u}\right) - \left(\frac{\xi}{\Delta_u}\right)^2\right] \tag{5.50}$$

$$\Theta = Sc'\left[1 - \left(\frac{\xi}{\Delta_T}\right)\right]^2 \tag{5.51}$$

where

$$\xi = Y - \Delta = (y - \delta)/u^* \tag{5.52}$$

Integrating Eqs. (5.36) and (5.37) from Δ to $\Delta + \Delta_u$ with respect to Y we have

$$\frac{d}{d\theta}\int_\Delta^{\Delta+\Delta_u} U_l dY - U_{l,\Delta_u}\frac{d(\Delta+\Delta_u)}{d\theta} + U_{l,\Delta}\frac{d\Delta}{d\theta} + \cot\theta\int_\Delta^{\Delta+\Delta_u} U_l dY + V_{l,\Delta_u} - V_{l,\Delta} = 0 \tag{5.53}$$

$$\frac{d}{d\theta}\int_\Delta^{\Delta+\Delta_u} U_l^2 dY - U_{l,\Delta_u}^2\frac{d(\Delta+\Delta_u)}{d\theta} + U_{l,\Delta}^2\frac{d\Delta}{d\theta} + (V_l U_l)_{\Delta_u} - (V_l U_l)_\Delta = \mathrm{Pr}_l B_l \sin\theta\int_\Delta^{\Delta+\Delta_u}\Theta dY - \left(\frac{1}{RK}\right)^2\left(\frac{\partial U_l}{\partial Y}\right)_\Delta + \frac{9}{8}F\Delta_u\sin 2\theta \tag{5.54}$$

Eliminating V_{l,Δ_u} between the above two equations and transforming the integral variable Y to ξ, we get

$$\frac{d}{d\theta}\int_0^{\Delta_u} U_l^2 d\xi - U_{l,\Delta_u}\frac{d}{d\theta}\int_0^{\Delta_u} U_l d\xi + (U_{l,\Delta} - U_{l,\Delta_u})\left\{\frac{Sp'}{K\Delta} + \left(\frac{1}{RK}\right)^2\left(\frac{\partial\Theta}{\partial\xi}\right)_0\right\} = \mathrm{Pr}_l B_l \sin\theta \int_0^{\Delta_u}\Theta d\xi - \left(\frac{1}{RK}\right)^2\left(\frac{\partial U_l}{\partial\xi}\right)_0 + \frac{9}{8}F\Delta_u \sin 2\theta + U_{l,\Delta_u}\cot\theta\int_0^{\Delta_u} U_l d\xi \tag{5.55}$$

Integration of Eq. (5.38) from Δ to $\Delta+\Delta_T$ with respect to Y and applying Eq. (5.36) yields

$$\frac{d}{d\theta}\int_{\Delta}^{\Delta+\Delta_T} U_l\Theta dY - Sc'\left(V_{l,\Delta} - U_{l,\Delta}\frac{d\Delta}{d\theta}\right) + \cot\theta\int_{\Delta}^{\Delta+\Delta_T} U_l\Theta dY = -\frac{1}{\mathrm{Pr}_l}\left(\frac{1}{RK}\right)^2\left(\frac{\partial\Theta}{\partial Y}\right)_{\Delta} \tag{5.56}$$

Applying Eq. (5.44) and transforming the integration variable Y to ξ, we obtain

$$\frac{d}{d\theta}\int_0^{\Delta_T} U_l\Theta d\xi + \frac{Sc'Sp'}{K\Delta} + \cot\theta\int_0^{\Delta_T} U_l\Theta d\xi + \left(Sc' + \frac{1}{\mathrm{Pr}_l}\right)\left(\frac{1}{RK}\right)^2\left(\frac{\partial\Theta}{\partial\xi}\right)_0 = 0 \tag{5.57}$$

Substitution of Eqs. (5.49) and (5.50) into Eq. (5.41) yields a relationship between Δ_u and Δ as follows:

$$\Delta_u = \frac{4}{R^2K}\frac{(3/2)F^{1/2}\sin\theta - U_\Delta}{2U_\Delta - K\Delta^2(1+(9/4)F\cos\theta)\sin\theta}\Delta \tag{5.58}$$

Substituting Eq. (5.49) for U_v, Eq. (5.50) for U_l, and Eq. (5.51) for Θ into Eqs. (5.35), (5.55) and (5.57) and eliminating Δ_u by Eq. (5.58), the final differential equations for Δ, Δ_T and U_Δ are

$$F_{11}\frac{d\Delta}{d\theta} + F_{12}\frac{dU_\Delta}{d\theta} = F_{1c} \tag{5.59}$$

$$F_{21}\frac{d\Delta}{d\theta} + F_{22}\frac{dU_\Delta}{d\theta} = F_{2c} \tag{5.60}$$

$$F_{31}\frac{d\Delta}{d\theta} + F_{32}\frac{dU_\Delta}{d\theta} + F_{33}\frac{d\Delta_T}{d\theta} = F_{3c} \tag{5.61}$$

where F_{11}, F_{12},$F_{1c}\ldots F_{3c}$ are functions of the variables Δ, U_Δ, Δ_T and θ, and of the parameters B_l, Fr, K, Pr_l, R, Sc' and Sp'. The algebraic expressions of these functions for

the case of $\Delta_u > \Delta_T$ are as follows:

$$F_{11} = \frac{U_\Delta \Delta}{2} + \frac{K\Delta^3}{4}\left(1 + \frac{9}{4}F\cos\theta\right)\sin\theta; \quad F_{12} = \frac{\Delta^2}{2}$$

$$F_{1c} = Sp' - \frac{2Sc'}{R^2K}\frac{\Delta}{\Delta_T} - \frac{K\Delta^4}{12}\left(\cos\theta + \frac{9}{4}F\cos 2\theta\right)$$
$$- \left\{\frac{\Delta^2}{2}U_\Delta + \frac{K\Delta^4}{12}\left(1 + \frac{9}{4}F\cos\theta\right)\sin\theta\right\}\cot\theta$$

$$F_{21} = G_u G_{F\Delta}; \quad F_{22} = \Delta_u\left(\frac{2}{5}U_\Delta - \frac{1}{10}F^{1/2}\sin\theta\right) - 2G_u\left(\frac{2\Delta}{R^2K} + \Delta_u\right)$$

$$F_{2c} = \mathrm{Pr}_l B_l \frac{Sc'\Delta_T}{3}\sin\theta - \Delta_u\left\{\frac{2}{5}U_\Delta F^{1/2}\cos\theta - \frac{27}{40}F\sin 2\theta\right\}$$
$$+ \left(\frac{3}{2}F^{1/2}\sin\theta - U_\Delta\right)\left\{\frac{Sp'}{K\Delta} - 2\left(\frac{1}{\Delta_u} + \frac{Sc'}{\Delta_T}\right)\left(\frac{1}{RK}\right)^2\right\} - G_u G_{FC}$$
$$+ \frac{3}{2}F^{1/2}\sin\theta\Delta_u\left(\frac{U_\Delta}{3} + F^{1/2}\sin\theta\right)\cot\theta$$

$$F_{31} = G_T G_{F\Delta}; \quad F_{32} = \frac{\Delta_T}{3} - \frac{1}{6}\left(\frac{\Delta_T^2}{\Delta_u} - \frac{\Delta_T^3}{5\Delta_u^2}\right) - 2G_T\left(\frac{2\Delta}{R^2K} + \Delta_u\right)$$

$$F_{33} = \frac{U_\Delta}{3} + \frac{1}{6}\left\{\frac{3}{2}F^{1/2}\sin\theta - U_\Delta\right\}\left\{2\frac{\Delta_T}{\Delta_u} - \frac{3}{5}\left(\frac{\Delta_T}{\Delta_u}\right)^2\right\}$$

$$F_{3c} = \frac{2}{\Delta_T}\left(Sc' + \frac{1}{\mathrm{Pr}_l}\right)\left(\frac{1}{RK}\right)^2 - \frac{Sp'}{K\Delta} - \frac{1}{4}\left(\frac{\Delta_T^2}{\Delta_u} - \frac{\Delta_T^3}{5\Delta_u^2}\right)F^{1/2}\cos\theta - G_T G_{FC}$$
$$- \left\{\frac{U_\Delta \Delta_T}{3} + \frac{1}{6}\left(\frac{3}{2}F^{1/2}\sin\theta - U_\Delta\right)\left(\frac{\Delta_T^2}{\Delta_u} - \frac{\Delta_T^3}{5\Delta_u^2}\right)\right\}\cot\theta$$

$$G_{F\Delta} = \frac{4}{R^2K}\left\{\frac{3}{2}F^{1/2}\sin\theta - U_\Delta\right\} + 2K\Delta\Delta_u\left(1 + \frac{9}{4}F\cos\theta\right)\sin\theta$$

$$G_{FC} = \frac{6\Delta}{R^2K}F^{1/2}\cos\theta + K\Delta^2\Delta_u\left(\cos\theta + \frac{9}{4}F\cos 2\theta\right)$$

$$G_u = \frac{2U_\Delta^2 - U_\Delta F^{1/2}\sin\theta - 3F\sin^2\theta}{10[2U_\Delta - \Delta^2 K(1 + (9/4)F\cos\theta)\sin\theta]}$$

$$G_T = \frac{\{(3/2)F^{1/2}\sin\theta - U_\Delta\}\{(2/5)(\Delta_T/\Delta_u)^3 - (\Delta_T/\Delta_u)^2\}}{6[2U_\Delta - \Delta^2 K(1 + (9/4)F\cos\theta)\sin\theta]} \tag{5.62}$$

For the case of $\Delta_u < \Delta_T$, which occurs in subcooled natural convection conditions, the functions that are different from those of the case of $\Delta_u > \Delta_T$ are given as follows:

$$F_{2c} = \mathrm{Pr}_l B_l \frac{Sc'\Delta_T}{3} sin\theta\left[1 - \left(1 - \frac{\Delta_u}{\Delta_T}\right)^3\right] - \Delta_u\left\{\frac{2}{5}U_\Delta F^{1/2}cos\theta - \frac{27}{40}Fsin2\theta\right\}$$

$$+\left(\frac{3}{2}F^{1/2}sin\theta - U_\Delta\right)\left\{\frac{Sp'}{K\Delta} - 2\left(\frac{1}{\Delta_u}+\frac{Sc'}{\Delta_T}\right)\left(\frac{1}{RK}\right)^2\right\} - G_u G_{FC}$$

$$+\frac{3}{2}F^{1/2}sin\theta\Delta_u\left(\frac{U_\Delta}{3}+F^{1/2}sin\theta\right)cot\theta$$

$$F_{31} + G_T G_{F\Delta}; \quad F_{32} = \frac{\Delta_T}{3} - G'_T - 2G_T\left(\frac{2\Delta}{R^2K}+\Delta_u\right)$$

$$F_{33} = \frac{U_\Delta}{3} + \left\{\frac{3}{2}F^{1/2}sin\theta - U_\Delta\right\}\left\{\frac{1}{3}\left(1-\frac{\Delta_u}{\Delta_T}\right)^3 + \frac{\Delta_u}{\Delta_T} - \frac{7}{6}\left(\frac{\Delta_u}{\Delta_T}\right)^2 + \frac{2}{5}\left(\frac{\Delta_u}{\Delta_T}\right)^3\right\}$$

$$F_{3c} = \frac{2}{\Delta_T}\left(Sc' + \frac{1}{\mathrm{Pr}_l}\right)\left(\frac{1}{RK}\right)^2 - \frac{Sp'}{K\Delta} - \frac{3}{2}F^{1/2}cos\theta G'_T - G_T G_{FC}$$

$$-\left\{\frac{U_\Delta\Delta_T}{3} + \left(\frac{3}{2}F^{1/2}sin\theta - U_\Delta\right)G'_T\right\}cot\theta$$

$$G'_T = \frac{\Delta_T}{3}\left(1-\frac{\Delta_u}{\Delta_T}\right)^3 + \Delta_u\left[\frac{2}{3} - \frac{5}{6}\frac{\Delta_u}{\Delta_T} + \frac{3}{10}\left(\frac{\Delta_u}{\Delta_T}\right)^2\right]$$

$$G_T = \frac{\{(3/2)F^{1/2}sin\theta - U_\Delta\}\{(1/3)(\Delta_u/\Delta_T - 1) - 0.1(\Delta_u/\Delta_T)^2\}}{[2U_\Delta - \Delta^2 K(1+(9/4)Fcos\theta)sin\theta]} \tag{5.63}$$

Since the Prandtl number of water is always larger than 1.0, we may assume that the Δ_u is always larger than or equal to Δ_T at the front stagnation point. Our model shows that this is true. So the functions for the case of $\Delta_u > \Delta_T$ are always used at the front stagnation point. These functions are then continually used as long as $\Delta_u > \Delta_T$, as in the cases of subcooled forced convection. However, for the subcooled natural convection, Δ_T is equal to or almost equal to Δ_u in the front and rear stagnation regions, but larger than Δ_u when away from the stagnation points. In the computation, as long as $\Delta_u < \Delta_T$, the functions given by Eq. (5.63) are used.

Because of the singularity at the stagnation point $\theta = 0$, a forward-integration of Eqs. (5.59) to (5.61) cannot be directly performed. To overcome this difficulty, we assume that $\Delta = A_0 + A_2\theta^2$, $U_\Delta = B_1\theta$ and $\Delta_T = C_0 + C_2\theta^2$ in the region from $\theta = 0$ to 0.05 rad. Substituting them into Eqs. (5.59), (5.60) and (5.61) and solving the resulting equations for A_0, A_2, B_1, C_0 and C_2 by the Newton method, the starting values of Δ, U_Δ and Δ_T are determined. Then starting from $\theta = 0.05$ rad, Eqs. (5.59), (5.60) and (5.61) are forward integrated by means of Fourth-Order-Runge-Kutta method with a step interval of 0.001 rad.

The numerical integration can be performed up to the rear stagnation point without any problem as long as Fr $< 2/9$. However, when Fr $> 2/9$, the integration blow up at

a certain angle between $\theta = \pi/2$ and $\theta = \pi$, depending on the Fr; we call it separation. After the separation, the numerical integration based on the model given above can not be performed further. To account for the heat transfer in the region after separation, as a preliminary model, it is assumed that a film with a uniform equivalence thickness Δ_e is covered all over the separated rear part of the sphere. The heat transfer in that region is merely the heat conduction through the film. According to our experimental observations and heat transfer data, it is also assumed that $\Delta_e = \Delta_s$, where Δ_s is the dimensionless vapor film thickness at the separation point. The effect of the equivalent film thickness on the overall heat transfer will be discussed latter. This is just a preliminary model for the heat transfer in the separated rear region, later a better turbulent heat transfer model based on Theofanous et al.'s (1976) model will be used to calculate the heat transfer in this region.

After solving the Eqs. (5.59), (5.60) and (5.61), the heat transfer characteristics are calculated as follows:

Local heat transfer coefficient in terms of Δ,

$$h_\theta = \frac{q_\theta}{\Delta T_{sup}} = \frac{k_v}{\delta} = \left(\frac{2g}{\nu_v^2 d}\right)^{1/4} \frac{k_v}{\Delta} \tag{5.64}$$

Average heat transfer coefficient in terms of Δ_{av},

$$h = \frac{q}{\Delta T_{sup}} = \frac{k_v}{\delta_{av}} = \left(\frac{2g}{\nu_v^2 d}\right)^{1/4} \frac{k_v}{\Delta_{av}} \tag{5.65}$$

Average Nusselt number in terms of Δ_{av},

$$\frac{\mathrm{Nu}}{\mathrm{Re}_l^{1/2}} \left(\frac{\mu_v}{\mu_l}\right) = \left(\frac{2R^4}{\mathrm{Fr}}\right)^{1/4} \frac{1}{\Delta_{av}} \tag{5.66}$$

where Δ_{av} is defined by

$$\frac{1}{\Delta_{av}} = \frac{1}{\pi d^2} \int_0^\pi \frac{\pi d}{\Delta} \sin\theta \frac{d}{2} d\theta = 0.5 \int_0^\pi \frac{\sin\theta}{\Delta} d\theta \tag{5.67}$$

5.4 Results and Discussion

The numerical calculation was carried out for water at atmospheric pressure. The superheat ΔT_{sup}, subcooling ΔT_{sub} and Fr number were given first. Then the density ratio K, $\rho\mu$ ratio R, Prandtl number of liquid Pr_l, buoyant force parameter B_L, dimensionless

superheat Sp′, and dimensionless subcooling Sc′ were evaluated at film temperatures of $T_{f,v} = (T_w + T_s)/2$ and $T_{f,l} = (T_l + T_s)/2$. The ranges of Fr , Δ_{sup} and Δ_{sub} are:

Fr = 0.01–500; Δ_{sup} = 300–2000 °C; Δ_{sub} = 0–80 °C

The corresponding values for K, R, Pr_l and B_L are 2300–6200, 0.004–0.0055, 1.76–3.0 and 0.46–0.86 respectively. The corresponding ranges of Sp′ and Sc′ are 0.25–1.2 and 0–0.023 respectively.

Separation Point, Vapor Film and Liquid Boundary-Layer Thickness

As mentioned earlier, the vapor film boundary layer separates if Fr is larger than 2/9. This critical Froude number is larger than the 1/8 that was obtained by Shigechi, Ito and Nishikawa (1983) for a cylinder. The separation points of the numerical integration, i.e. the angles at which the integration breaks down, are shown in Fig. 5.2. When Fr > 2/9, the separation angles can be expressed exactly by

$$\theta_s = \cos^{-1}\left(\frac{2}{9\mathrm{Fr}}\right) \tag{5.68}$$

for both saturated and subcooled conditions. This is also different from that obtained by Shigechi et al. (1983) for a cylinder, which was $\theta_s = \cos^{-1}(1/8\,\mathrm{Fr})$.

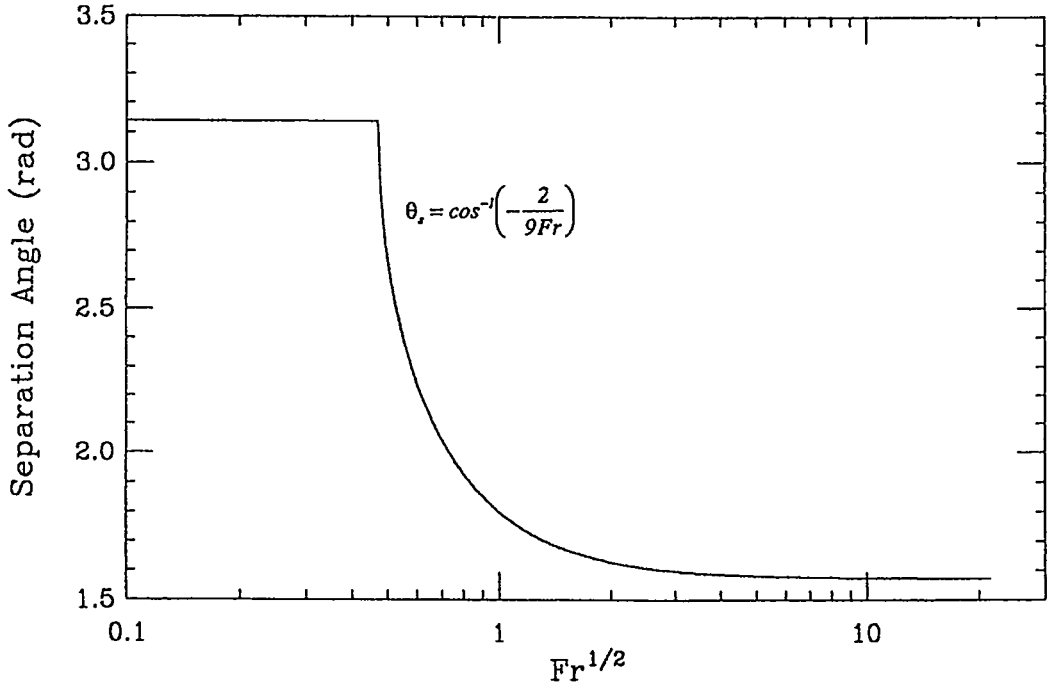

Fig. 5.2. The dependence of the separation angle θ_s of the theoretical model on the Froude number Fr.

No liquid layer separation (i.e. numerical integration breaking down) was found prior to the separation of vapor layer, although the liquid momentum boundary layer thickness Δ_u is much larger than the vapor layer thickness Δ for highly subcooled forced convection conditions. In these cases, the liquid-vapor interface velocity is almost equal to the velocity of the potential flow and the liquid momentum boundary layer is almost a layer with uniform velocity. For this case, the thickness Δ_u is not important in the calculation. To verify this argument, another numerical integration scheme based on the assumption that $U_\Delta = 1.5\,F^{1/2}\sin\theta$ was developed for the cases whenever $\Delta_u/\Delta > 5$. It shows that the vapor film thickness, hence the heat transfer, was not affected significantly by this modification.

The angular distributions of the reciprocal of the dimensionless vapor film thickness 1/D, which is proportional to the local heat transfer coefficient, are shown in Figs. 5.3 and 5.4 for saturated and subcooled cases respectively. In these figures, the slopes of the curve are discontinuous at the separation point for the cases of Fr = 1.0, 3.0 and 30.0. Fig. 5.3 shows that, for saturated forced convection cases, there is significant variation in heat transfer in the front part of the sphere and most of the heat transfer is contributed from this regime. In contrast, for subcooled forced convection, Fig. 5.4 shows that there is less variation in the front part of the sphere (except in the vicinity of the front stagnation point), and the rear part of the sphere is as equally important as the front part in transfer heat.

For saturated film boiling, the angular variation of the ratio Δ_u/Δ is shown in Fig. 5.5. It shows that, in the front part of the sphere, this ratio essentially only depends on the superheat ΔT_{sup} and is independent of the angle θ. But, for the rear part of the sphere, this ratio decreases as the angle θ increases in the case of natural free convection film boiling (Fr < 0.01).

For subcooled conditions, the ratios of Δ_u/Δ and Δ_T/Δ are shown against the angle in Figs. 5.6 and 5.7 respectively. Fig. 5.6 indicates that, unlike the saturated case, the ratio Δ_u/Δ becomes more Froude number dependent when it is highly subcooled. Fig. 5.7 shows that, except in the vicinity of the front stagnation point, the ratio Δ_T/Δ decreases with the angle for all flow conditions. Comparing Fig. 5.6 with Fig. 5.7, it is obvious that Δ_T/Δ_u is always smaller than or equal to one.

Heat Transfer Results at Saturated Conditions

The variation of $(\mathrm{Nu}/\mathrm{Re}_l^{1/2})(\mu_v/\mu_l)$ against the Froude number Fr and superheat ΔT_{sup} is shown in Fig. 5.8. The variation of $C_{sat,F1} = (\mathrm{Nu}/\mathrm{Re}_l^{1/2})(\mu_v/\mu_l)(\mathrm{Sp}'^2/R^4)^{1/4}$, (the heat transfer characteristic of mode 1 forced convection saturated film boiling correlation), is shown in Fig. 5.9 with the superheat as the parameter. It is obvious that both of these two heat transfer characteristics are superheat dependent. As mentioned in the previous chapters, the best way to correlate the saturated film boiling heat transfer is by

$$C_{sat,N} = \frac{\mathrm{Nu}}{\mathrm{Re}_l^{1/2}}\frac{\mu_v}{\mu_l}\left(\frac{\mathrm{FrSp}'}{R^4K}\right)^{1/4} = \mathrm{Nu}\left(\frac{\mathrm{Sp}'}{\mathrm{Ar}}\right)^{1/4} \tag{5.69}$$

$$C_{sat,F} = \frac{\mathrm{Nu}}{\mathrm{Re}_l^{1/2}}\frac{\mu_v}{\mu_l}\left(\frac{\mathrm{Sp}'}{R^4K}\right)^{1/4} \tag{5.70}$$

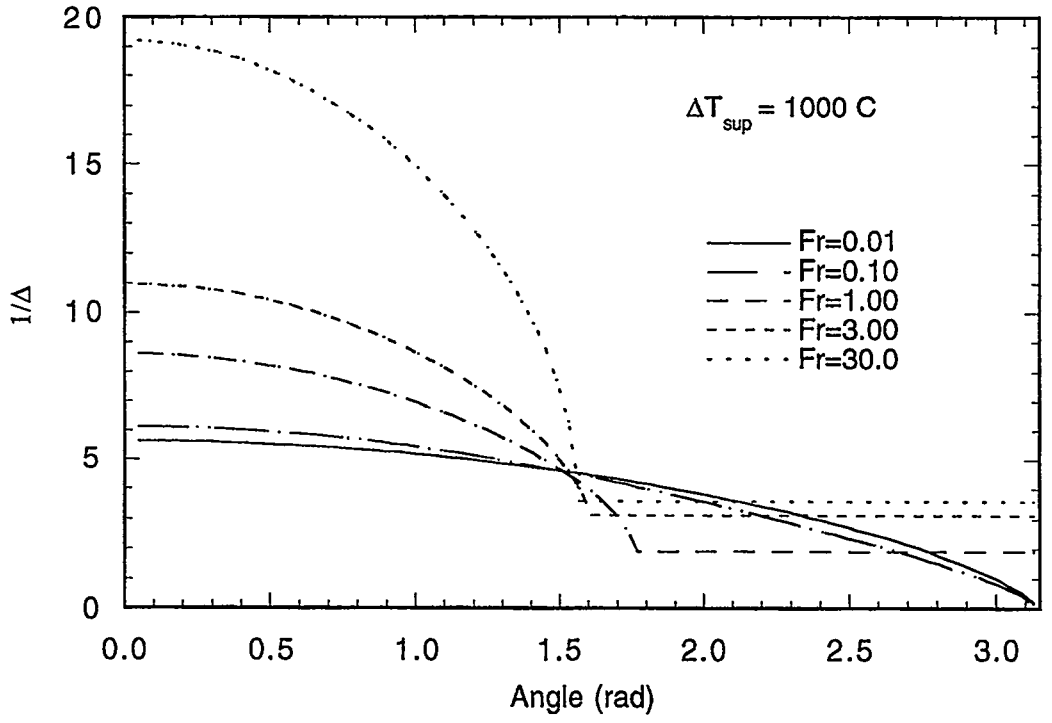

Fig. 5.3. Angular distribution of the dimensionless local heat transfer coefficients for saturated film boiling with $\Delta T_{sup} = 1000$ °C.

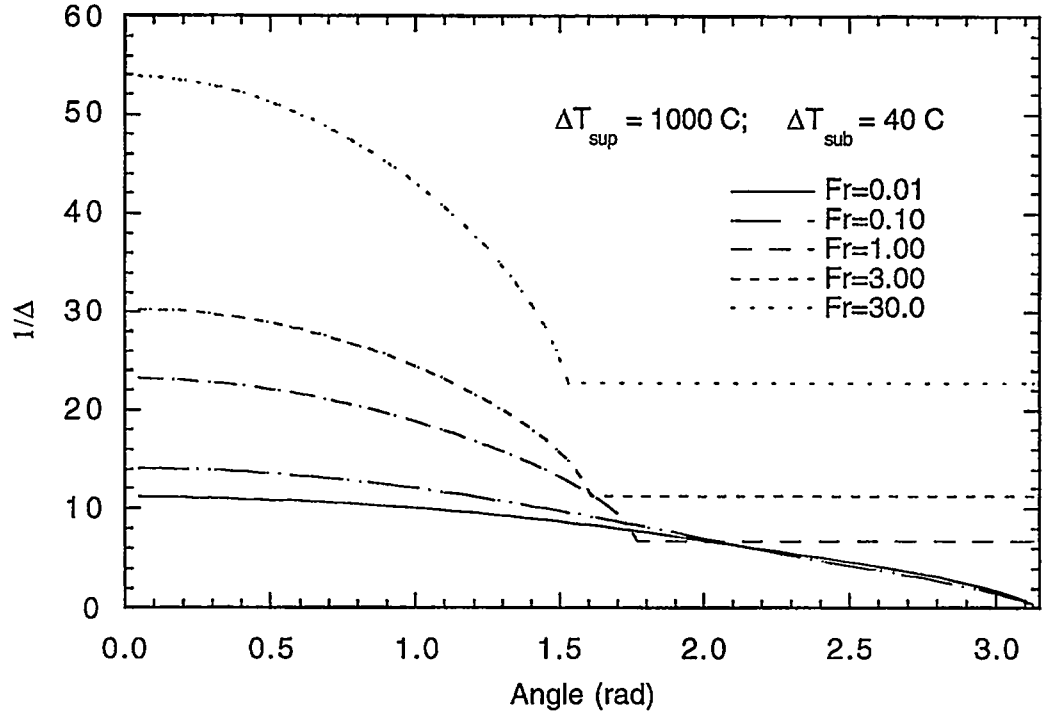

Fig. 5.4. Angular distribution of the dimensionless local heat transfer coefficients at sub-cooled condition.

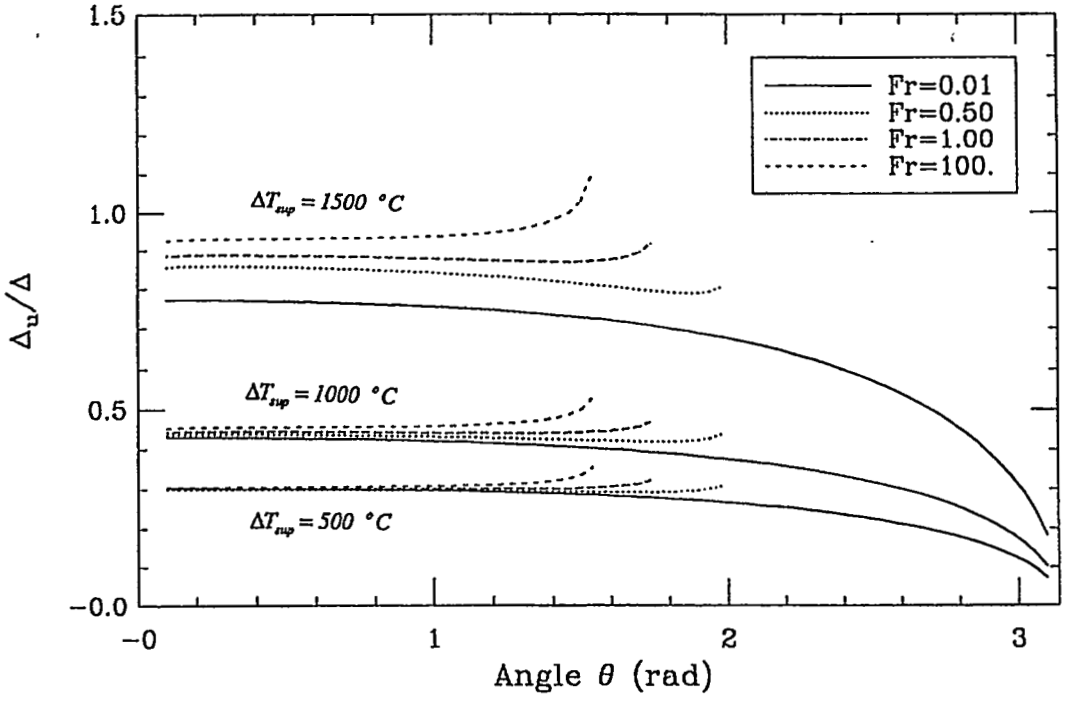

Fig. 5.5. Angular variation of Δ_u/Δ at saturated conditions.

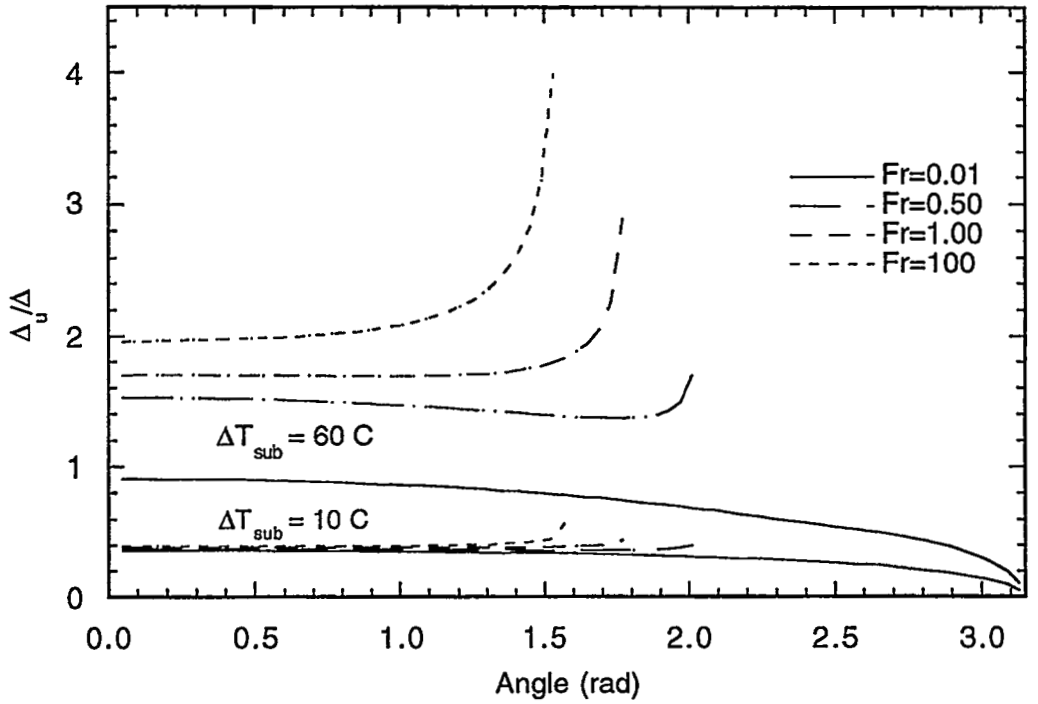

Fig. 5.6. Angular variation of Δ_u/Δ at subcooled conditions.

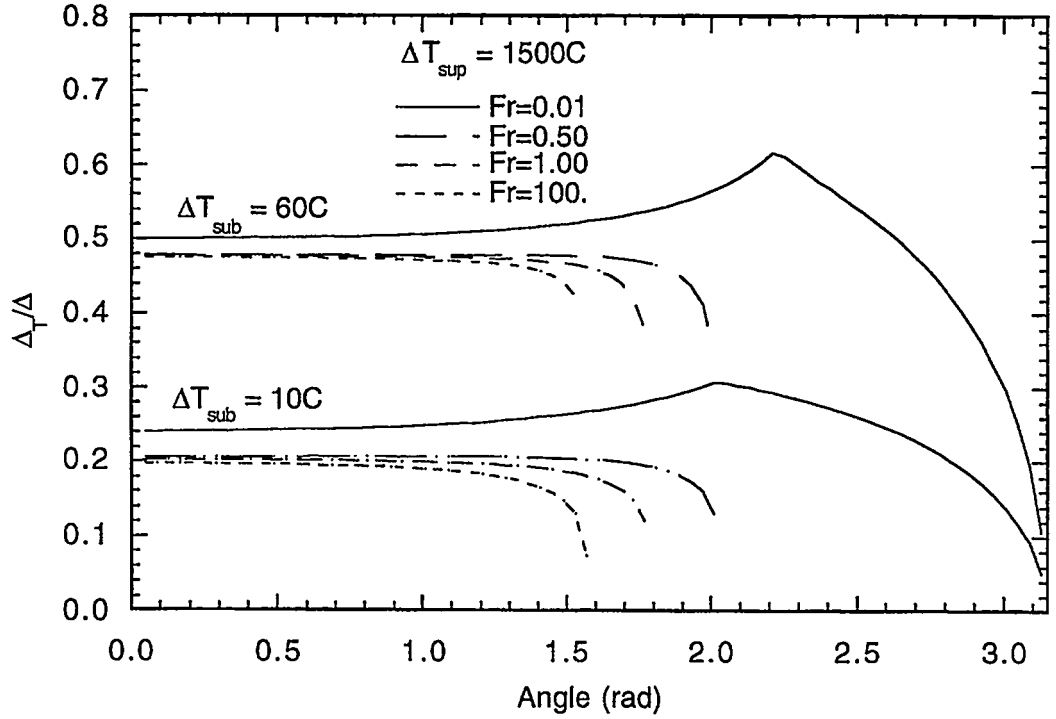

Fig. 5.7. Angular variation of Δ_T/Δ at subcooled conditions.

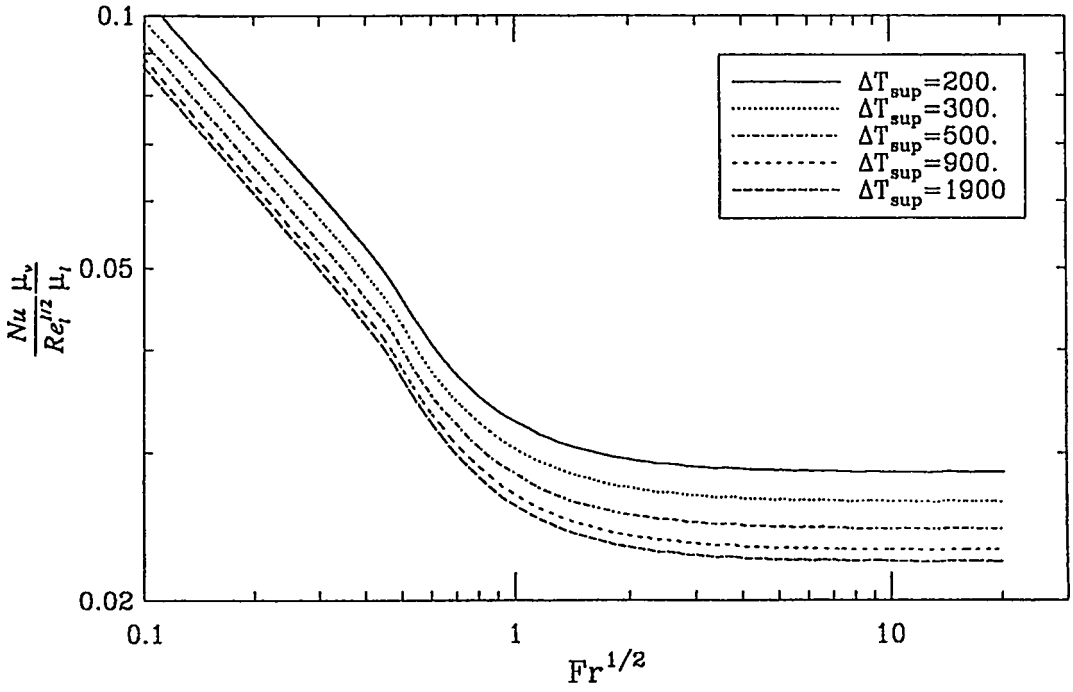

Fig. 5.8. The relationship between $(\mathrm{Nu}/\mathrm{Re}_l^{1/2})(\mu_v/\mu_l)$ and Froude number Fr at saturated film boiling conditions.

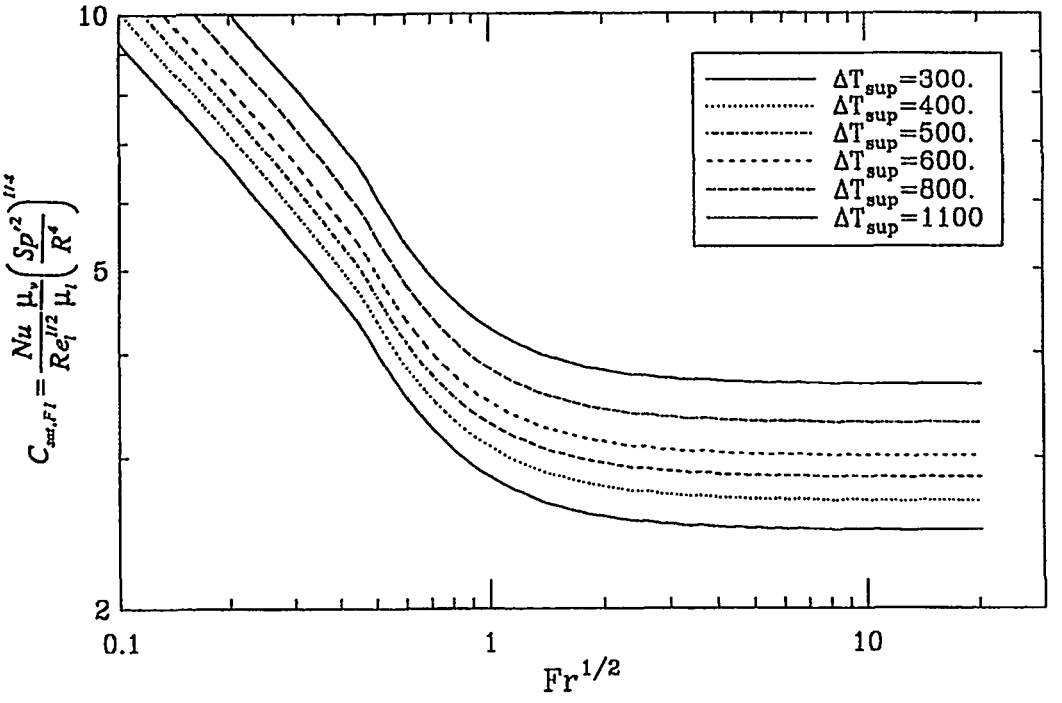

Fig. 5.9. The relationship between $C_{sat,F1}$ and Froude number Fr at saturated film boiling conditions.

for natural free convection and forced convection respectively. The dependences of these two heat transfer characteristics on $Fr^{1/2}$ are shown in Fig. 5.10 at two significantly different superheat conditions. It shows that they are much less dependent on the superheat than are the $(Nu/Re_l^{1/2})(\mu_v/\mu_l)$ and $C_{sat,F1} = (Nu/Re_l^{1/2})(\mu_v/\mu_l)(Sp'^2/R^4)^{1/4}$.

In the pool film boiling regime, $C_{sat,N}$ is about 0.6, which can be compared with the value of 0.58 from Ito, Nishikawa and Shigechi's (1981) analysis for a cylinder, 0.62 from Bromley's (1950) experimental data for cylinders, 0.586 from Frederking's (1963) analysis for a sphere and ~0.60 from Michiyosh's (1988) analysis for a sphere. On the other hand, for forced convection, $C_{sat,F}$ is about 0.5, which is very close to the values of 0.46 obtained by Ito, Nishikawa and Shigechi (1981), 0.454 form Kobayasi's (1965) theory for spheres and 0.553 from Epstein and Hauser's (1980) analysis for a sphere and cylinder.

Figures 5.11 and 5.12 compared two sets of our experimental data with the theory in terms of $C_{sat,N}$ and $C_{sat,F}$ respectively. They indicate that the agreement of the theory with the experiment is perfect in the forced convection regime. However, in the pool film boiling regime, the experimental data are about 10-20% higher than the theory.

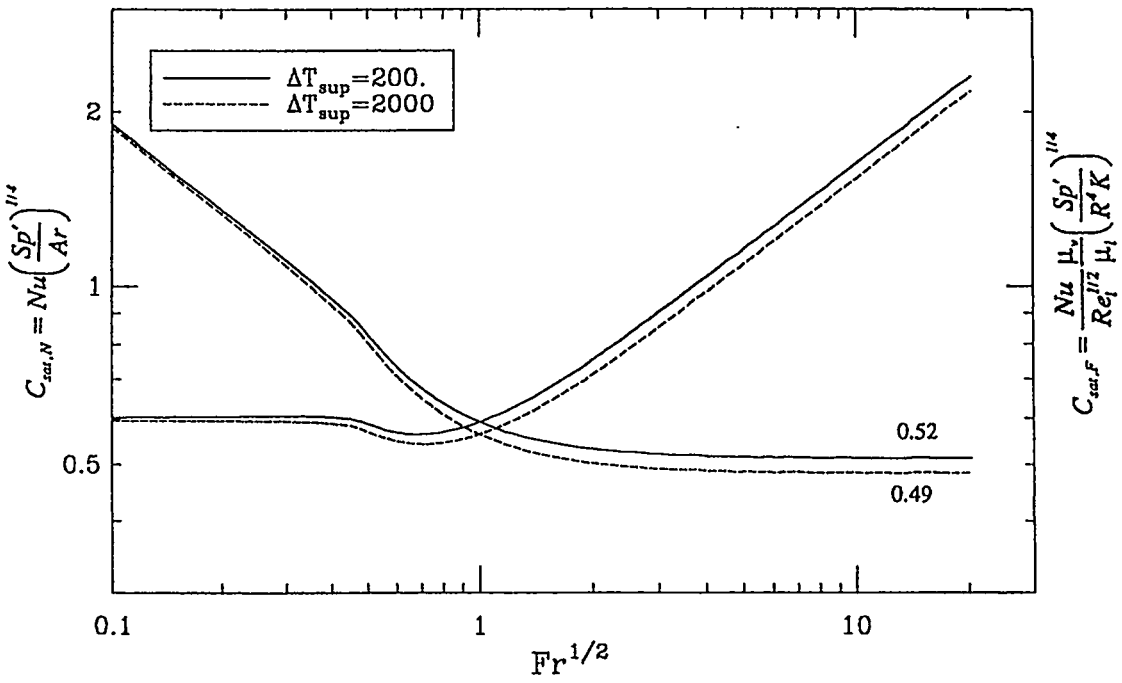

Fig. 5.10. The dependence of $C_{sat,N}$ and $C_{sat,F}$ on Froude number Fr at saturated film boiling conditions.

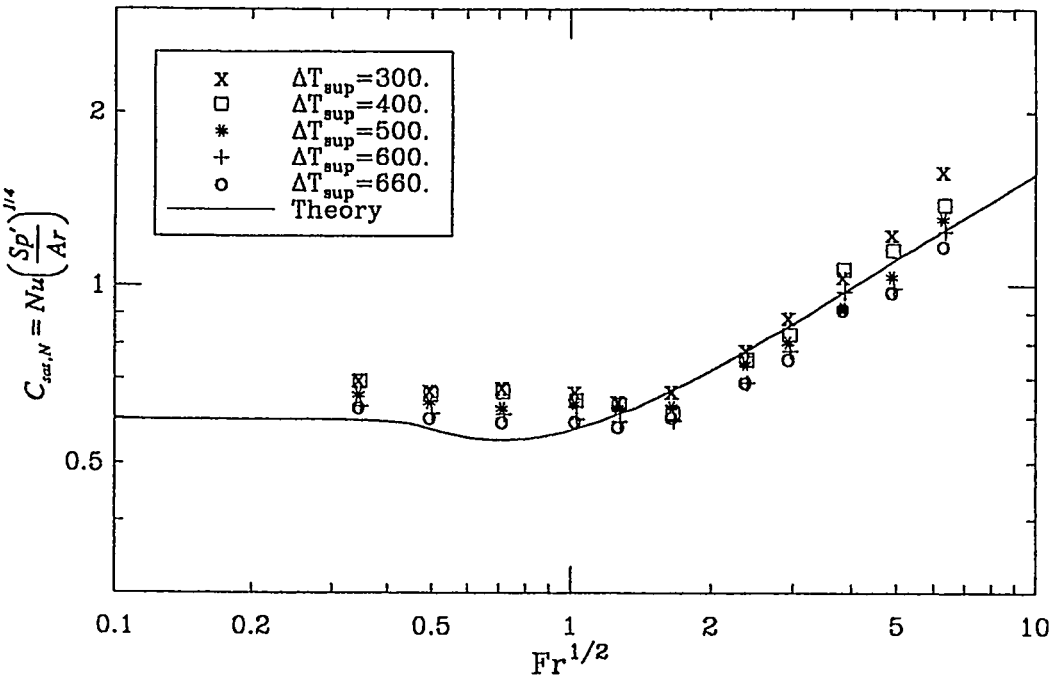

Fig. 5.11. A comparison of saturated experimental data with the theory in terms of $C_{sat,N}$.

In the theoretical model , the equivalent film thickness beyond the separation point is arbitrarily assumed to be two times that of the film thickness at the separation point, i.e., $\Delta_e = \Delta_s$. It is interesting to see what would be the result if the Δ_e is assumed to be infinity, i.e. no heat transfer contribution from the region beyond the separation. The comparison is shown in Fig. 5.13. It shows that with the assumption of $\Delta_e = \Delta_s$, the rear part of the sphere contributes about 16% in the overall heat transfer in forced convection regime for this particular case.

In conclusion, for saturated film boiling, our theoretical analysis agrees well with the existing analyses either for spheres or for cylinders and also agrees well with our experiment.

Heat Transfer Results at Subcooled Conditions

Figures 5.14 and 5.15 show the dependence of $(\mathrm{Nu}/\mathrm{Re}_l^{1/2})(\mu_v/\mu_l)$ on the Froude number with subcooling ΔT_{sub} as the parameter at superheat ΔT_{sup} of 600 °C and 1200 °C respectively. These two figures indicate that the effect of subcooling is more remarkable for the larger Froude number Fr and the smaller superheat ΔT_{sup}.

Based on the discussion in the previous chapters, the following two heat transfer characteristics are the best choices to correlate the subcooled film boiling heat transfer

$$C_{sat,N} = \mathrm{Nu}\left(\frac{Sp'}{\mathrm{Ar}M_c}\right)^{1/4} \qquad \text{for pool film boiling} \tag{5.71}$$

$$C_{sub,F} = \frac{\mathrm{Nu}}{\mathrm{Re}_l^{1/2}}\frac{\mu_v}{\mu_l}\frac{Sp'}{Sc'}\frac{1}{\mathrm{Pr}_l^{1/2}} \qquad \text{for forced convection} \tag{5.72}$$

where M_c in Eq. (5.71) is a complicated function of subcooling ΔT_{sub}, superheat ΔT_{sup} and sphere diameter d, which is given by Eq. (4.5). The variation of these two dimensionless groups are shown in Fig. 5.16 at three conditions. It is obvious that $C_{sub,N}$ is less dependent on the subcooling ΔT_{sub}, superheat ΔT_{sub} and the Froude number Fr in the natural free convection regime ($\mathrm{Fr}^{1/2} < 0.2$), and $C_{sub,F}$ is less dependent on the subcooling ΔT_{sub}, superheat ΔT_{sub} and the Froude number Fr in the forced convection regime ($\mathrm{Fr}^{1/2} > 1.0$).

For pool film boiling, the variation of $C_{sub,N}$ against subcooling ΔT_{sub} is plotted in Fig. 5.17 with superheat ΔT_{sup} as the parameter. When ΔT_{sub} equals 0, i.e., at a saturated condition, $C_{sub,N}$ equals 0.696, which is exactly the same as that obtained by Michiyosh (1988). However, it increases slightly when the subcooling increases. Figure 5.17 indicates that, even when the Froude number is as small as 0.01, the $C_{sub,N}$ is not invariant of

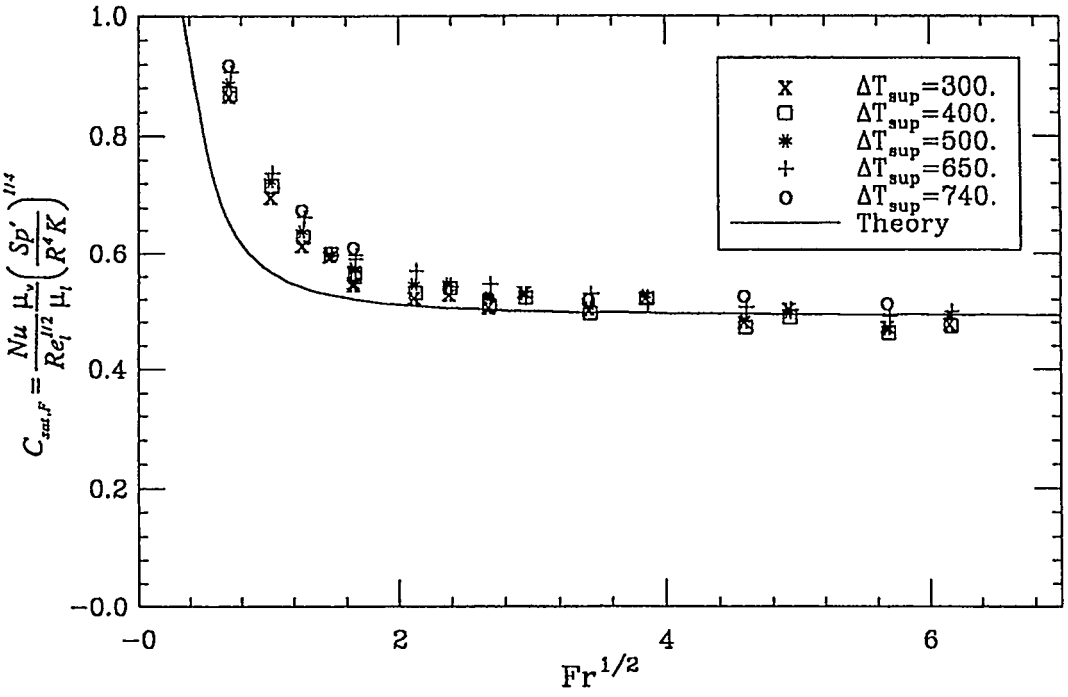

Fig. 5.12. A comparison of saturated experimental data with the theory in terms of $C_{sat,F}$.

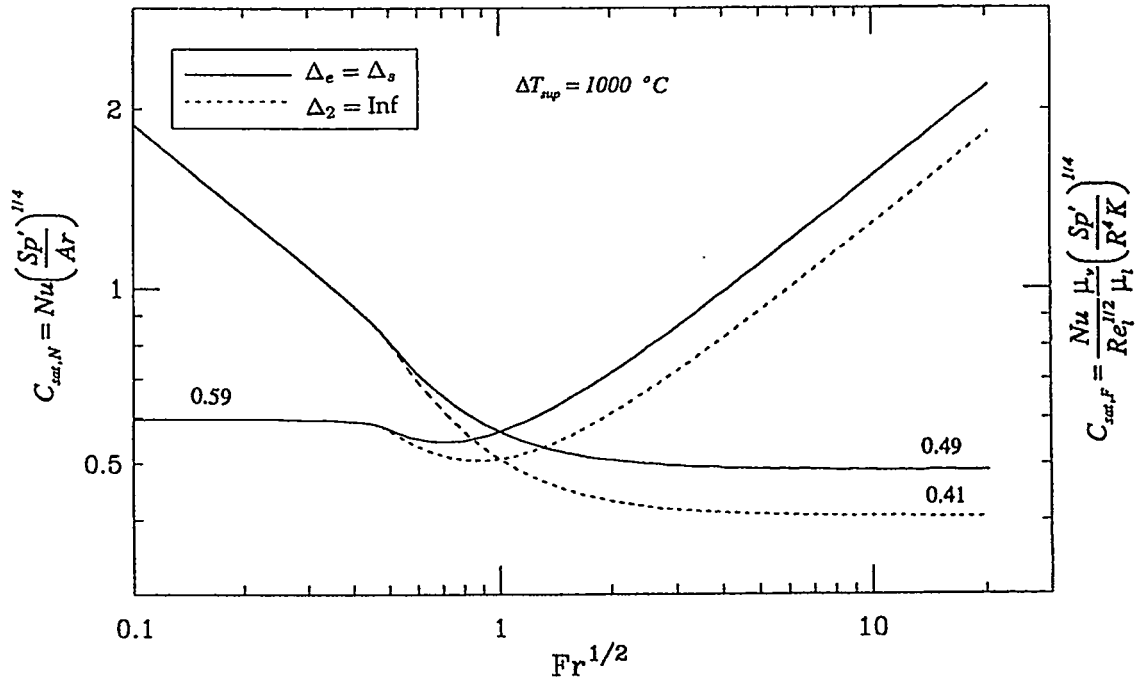

Fig. 5.13. The influence of the equivalent film thickness Δ_e on the overall heat transfer results at saturated film boiling conditions.

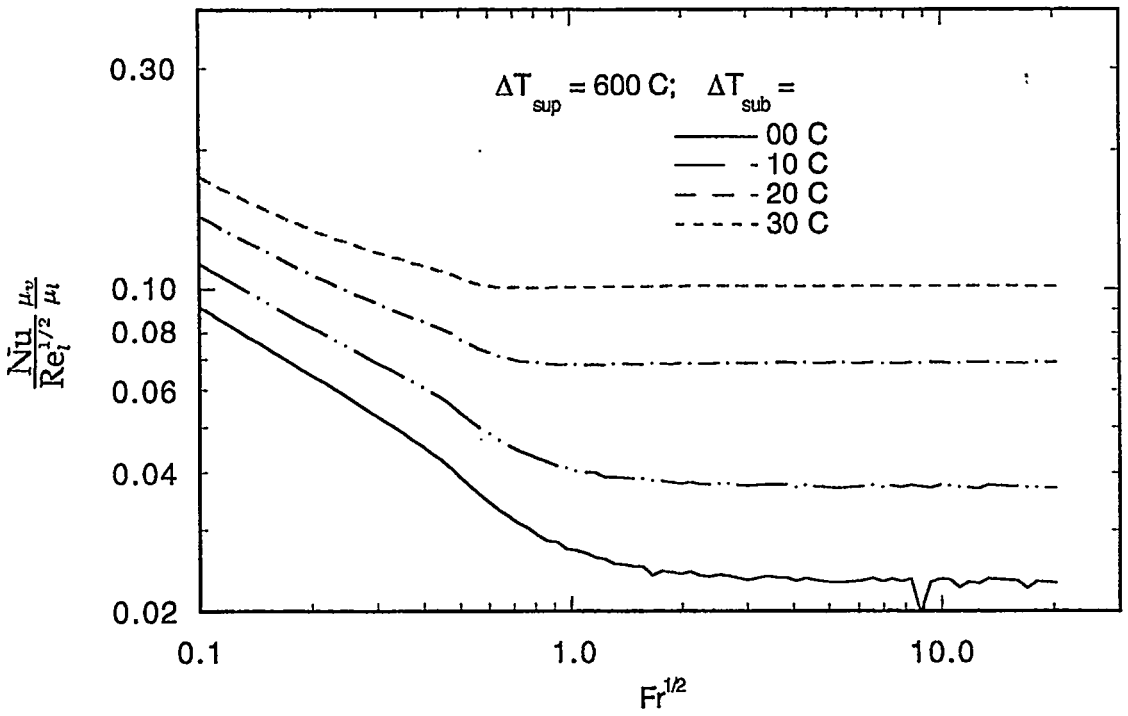

Fig. 5.14. The relationship between $(\mathrm{Nu}/\mathrm{Re}_l^{1/2})(\mu_v/\mu_l)$ and Froude number Fr at subcooled film boiling conditions with $\Delta T_{sup} = 600$ °C.

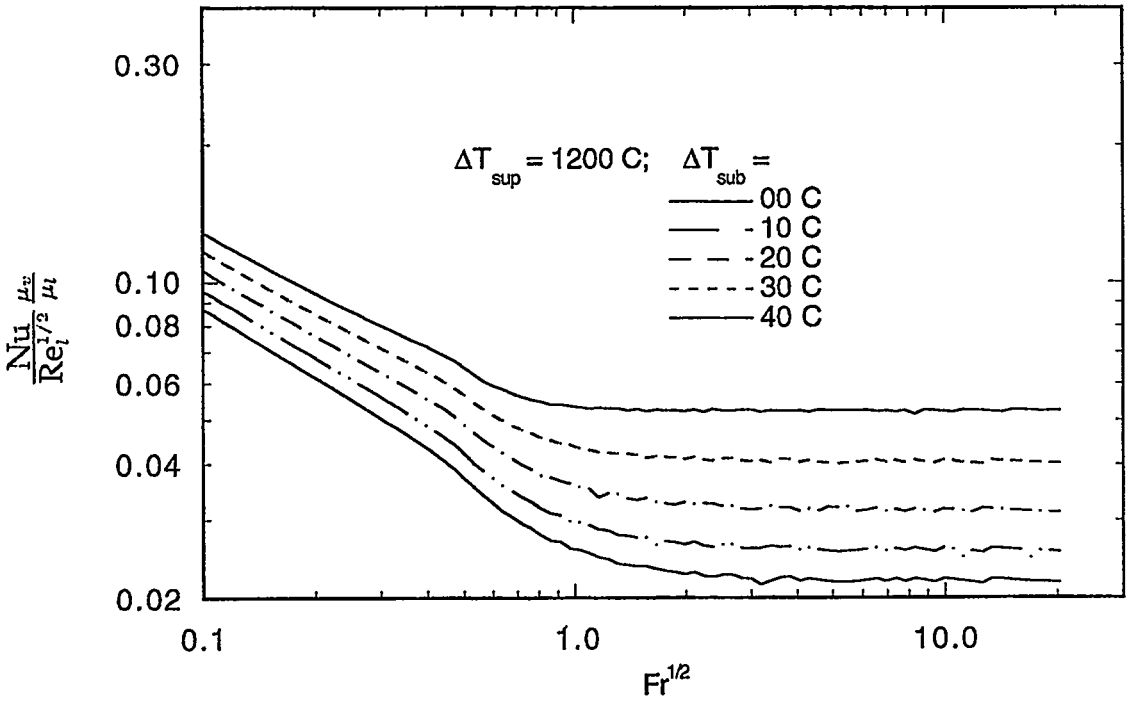

Fig. 5.15. The relationship between $(\mathrm{Nu}/\mathrm{Re}_l^{1/2})(\mu_v/\mu_l)$ and Froude number Fr at subcooled film boiling conditions with $\Delta T_{sup} = 1200$ °C.

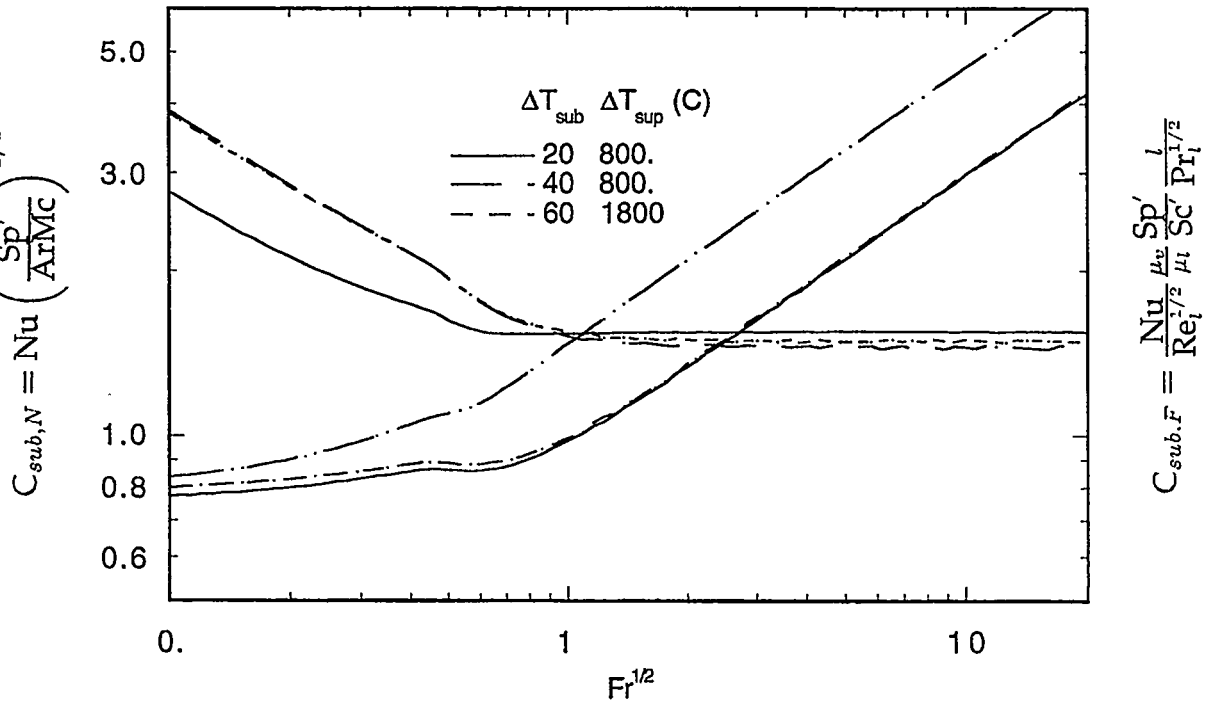

Fig. 5.16. The dependence of $C_{sub,N}$ and $C_{sub,F}$ on Froude number Fr at subcooled film boiling conditions.

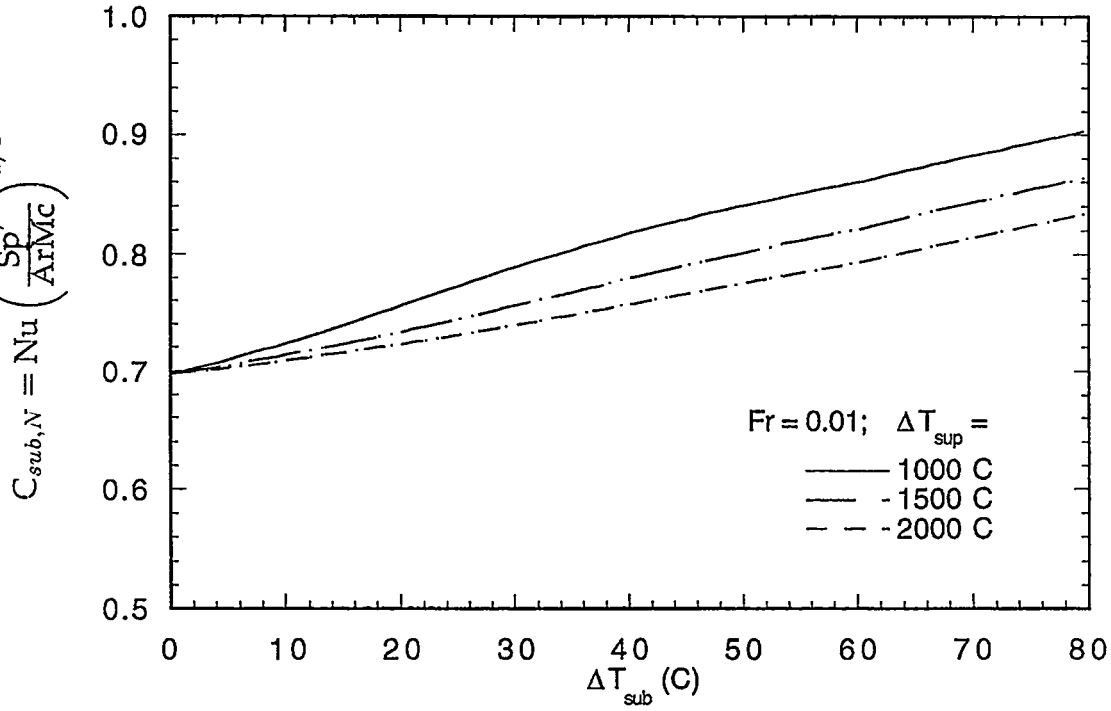

Fig. 5.17. The dependence of $C_{sub,N}$ on subcooling ΔT_{sub} in natural free convection film boiling.

subcooling, superheat and Froude number. In an approximation sense, the $C_{sub,N}$ may be regarded as a constant (about 0.72) if the subcooling is lower than 20°C.

In the case of forced convection, the variations of $C_{sub,F}$ and $C_{sat,F}$ against subcooling ΔT_{sub} are shown in Fig. 5.18 with the superheat ΔT_{sup} as the parameter. It indicates that the higher the superheat, the less the $C_{sat,F}$ depends on subcooling. This means that when the superheat is very high, the saturated forced convection correlation may be approximately used for the subcooled condition. It also shows that the lower the superheat, the earlier the $C_{sub,F}$ levels out (i.e., $C_{sub,F}$ tends to be a constant at smaller subcooling). The constant that the $C_{sub,F}$ tends to reach is about 1.5. In comparison, the $C_{sub,F}$ obtained by Shigechi, Ito and Nishikawa (1983) for a cylinder is 1.16, and the one obtained from Epstein and Hauser's (1980) analysis for a sphere and cylinder is 0.977.

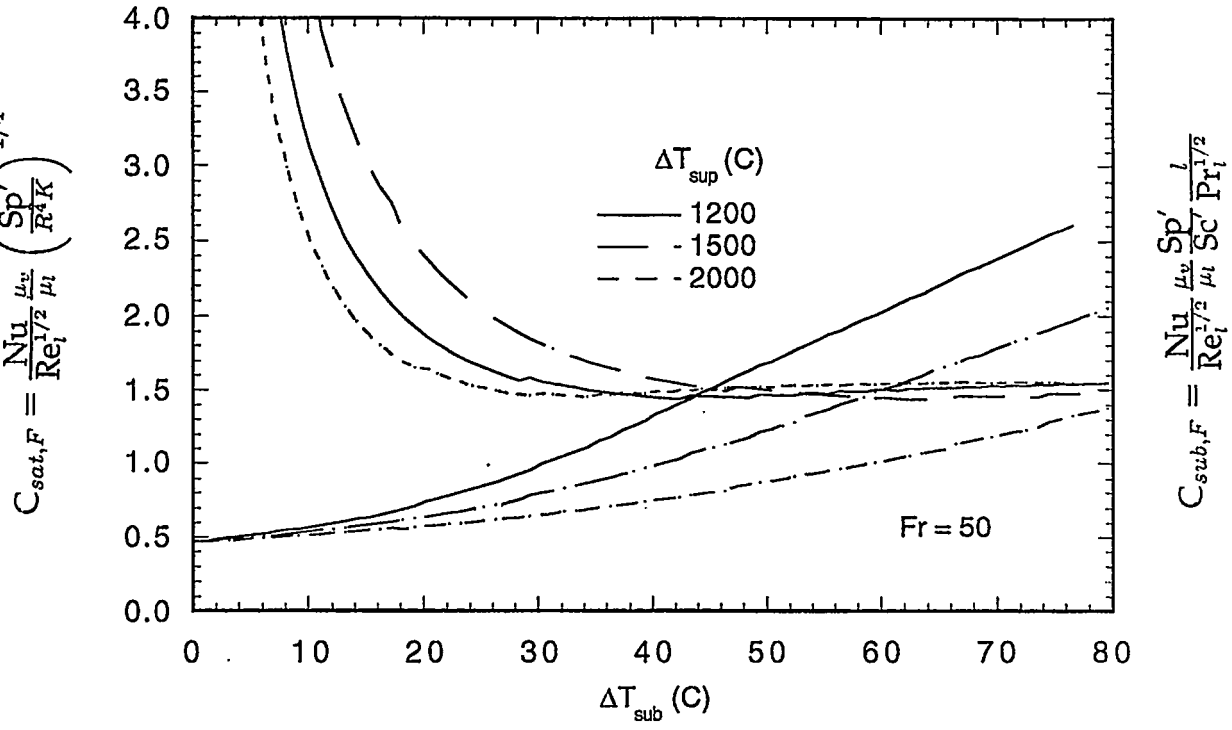

Fig. 5.18. The dependence of $C_{sat,F}$ and $C_{sub,F}$ on subcooling ΔT_{sub} in forced convection film boiling.

The comparisons of the experimental data of this work with the predictions of the theory in terms of $C_{sub,F}$ are shown in Figs. 5.19 (a) and 5.19 (b) for two subcooling conditions respectively. The comparisons indicate that in the natural convection and transition regimes ($Fr^{1/2} < 2.0$), contrary to the saturated case, the theoretical predictions are about 20% higher than the experimental data especially when the superheat is low.

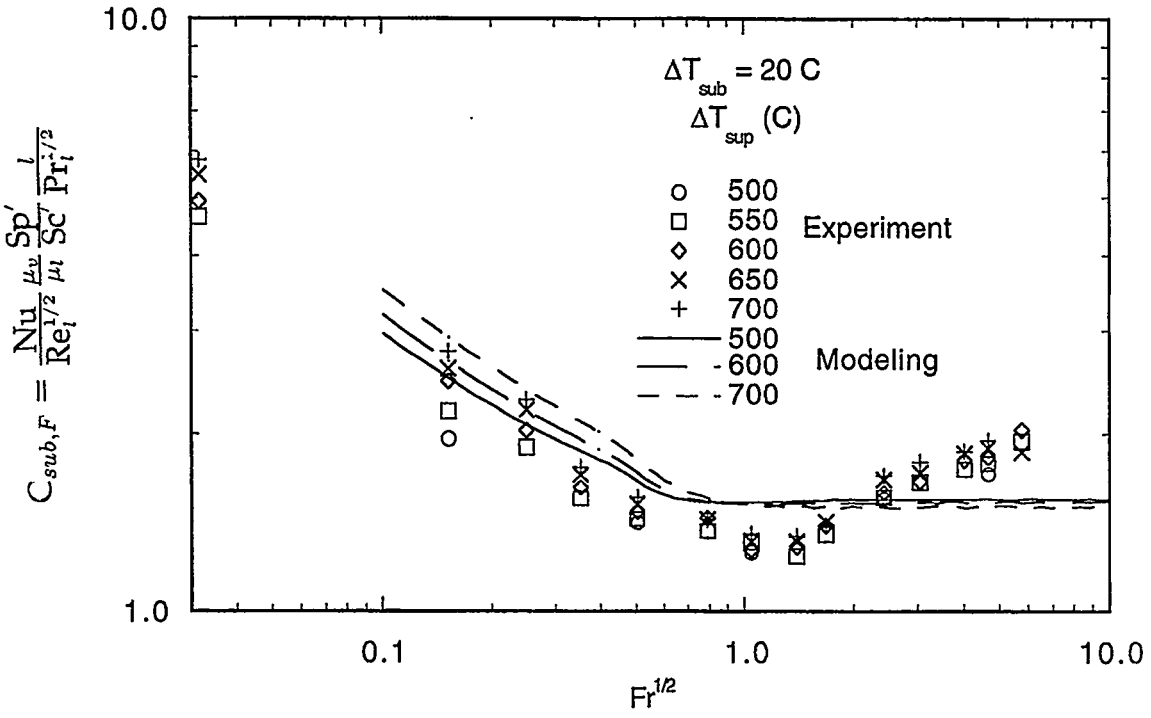

Fig. 5.19(a). A comparison of 20 °C subcooled experimental data with the preliminary theory in terms of $C_{sub,F}$.

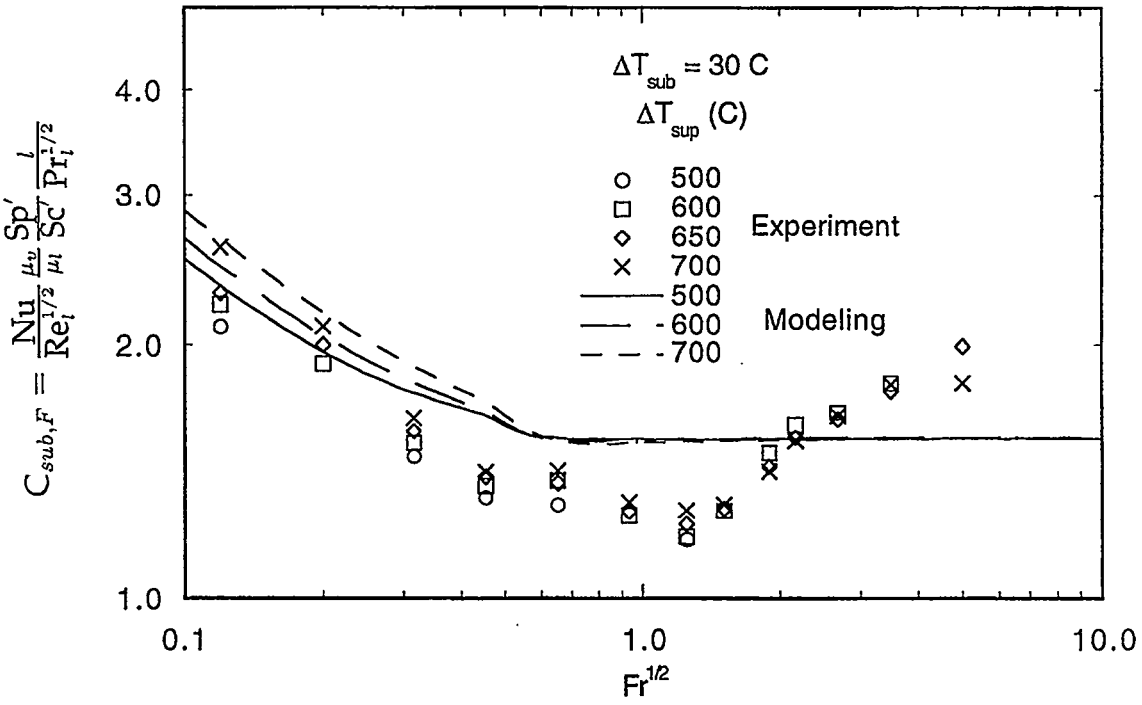

Fig. 5.19(b). A comparison of 30 °C subcooled experimental data with the preliminary theory in terms of $C_{sub,F}$.

But when the $Fr^{1/2}$ is larger than 2.0, the prediction is lower than the experimental data. The comparisons also clearly show that the turning point of the theory happens at a lower Fr than the experimental data. The reason for this difference may be that the vapor film separates at a larger angle in reality than the mode predicted. The experimental data also clearly exhibit a higher power dependency on the Reynolds number than the 0.5 that is predicted by the theory as given by Eq. (5.72).

When subcooling in forced convection conditions is high, the overall heat transfer result is very sensitive to the choice of the equivalent film thickness of the rear part because the film that covers the rear part of the sphere is thin. As indicated earlier, in our preliminary model, the assumption $\Delta_e = \Delta_s$ is completely arbitrary, so it certainly cannot predict the experiment well.

In conclusion, when there is no separation (i.e., for the pool film boiling), the two-phase laminar boundary-layer theory agrees well with the experiment, some previous analyses and correlations. This preliminary model also works well for saturated forced convection film boiling, even when there is separation. However, this preliminary model does not work well in the subcooled forced convection and transition regimes because it does not model the heat transfer in the rear part correctly. A model that considers the heat transfer in the rear separated region for subcooled forced convection film boiling, therefore, developed next.

5.5 A Turbulent Heat Transfer Model for the Separated Rear Region

As mentioned in Chapter 4 Section 1, the experimental observation shows that a thin vapor film covers all of the sphere in the case of subcooled forced convection. The film on the front part is always smooth, but wavy on the rear side. So, we may still use the laminar model to calculate the heat transfer for the front unseparated region, and use a turbulent eddy model to calculate the heat transfer in the rear separated region.

Theofanous, Houze and Brumfield (1976) studied the turbulent mass transfer at the free gas-liquid interface. By a dimensional analysis or an *unsteady mass transfer eddy model*, they obtained two mass transfer coefficient correlations, with the constants being determined by experiments. This model can be readily converted to a heat transfer situation, and Liang and Peter-Griffith (1994) did so by applying this model to calculate the condensation of steam in subcooled water. In the following, the same model will be extended to calculate the turbulent heat transfer across the vapor-water interface in the rear separated region when the Froude number Fr is larger than 6.

It is reasonable to consider the flow behind the sphere as large turbulent eddies, with length scale $l = r$ and velocity $u = cU$, where U is the main stream flow velocity and c is a constant. Because of the viscous dissipation, it may also be assumed that the large eddies break down to Kolmogorov microscale eddies with their length and velocity being

$$l_k = \left(\frac{\upsilon_l^3}{\epsilon}\right)^{1/4} \qquad \text{and} \qquad u_k = (\upsilon_l \epsilon)^{1/4} \tag{5.73}$$

Because of the existence of film on the sphere surface, the eddies behind the sphere behave like eddies in a free stream. Therefore, the dissipation rate may be related with the large turbulent eddies by the well known empirical formula [Tennekes and Lumley (1972)],

$$\epsilon = u^3/l \tag{5.74}$$

The small eddies are carried by the large eddies to the free vapor-water interface on the back of the sphere to participate in heat transfer from time $t = 0$ to $t_{exp} = r/u$. Following the analysis of Theofanous et al., (1976), unsteady heat transfer into the small eddy is calculated by taking the velocity field around the small eddy to be that of the Fortescue-Pearson (1970) roll cell. The mathematical governing equation, then, is

$$\frac{\partial T}{\partial t} + \left(u_m sin\frac{\pi x}{l_k}\right)\frac{\partial T}{\partial x} + \left(-\frac{\pi u_m y}{l_k} cos\frac{\pi x}{l_k}\right)\frac{\partial T}{\partial y} = \alpha_l \frac{\partial^2 T}{\partial y^2} \tag{5.75}$$

where $u_m = 2^{1/2} u_k$. The initial and boundary conditions are

$$\begin{aligned} T = T_l - T_w = 0 \qquad & \text{at } t = 0, \\ T = 0 \qquad & \text{at } y = \infty, \\ T = \Delta T_{sub} \qquad & \text{at } y = 0,\ t > 0. \end{aligned}$$

Defining $\eta = y/\delta(x,t)$, the problem becomes a search for $T = T(\eta)$ with the following two ordinary differential equations

$$-T'\eta\xi = \alpha_l T'' \tag{5.76}$$

$$\frac{1}{2}\frac{\partial(\delta^2)}{\partial t} + \frac{u_m}{2} sin\frac{\pi x}{l_k}\frac{\partial(\delta^2)}{\partial x} + \frac{\pi u_m}{l_k} cos\frac{\pi x}{l_k}\delta^2 = \xi \tag{5.77}$$

where ξ is an arbitrary constant. The solution is

$$T = \Delta T_{sub} erfc\left\{\frac{y}{2}\left[\frac{\pi u_m}{\alpha_l l_k}\left(coth\left(\frac{\pi u_m t}{l_k}\right) + cos\left(\frac{\pi x}{l_k}\right)\right)\right]^{1/2}\right\} \tag{5.78}$$

Hence, the average heat transfer coefficient h is

$$h = \frac{1}{l_k t_{exp} \Delta T_{sub}} \int_{t=0}^{t_{sub}} \int_{x=0}^{l_k} k_l \frac{\partial T}{\partial y} |_{y=0} \, dt dx = 1.07 \rho_l C_{p,l} F(\tau) \left(\frac{\alpha_l u_k}{l_k} \right)^{1/2} \tag{5.79}$$

where

$$F(\tau) = \frac{\pi}{2\sqrt{2}\tau} \int_0^{\tau} \int_0^{l} (coth\pi t' + cos\pi x')^{1/2} \, dx' dt' \tag{5.80}$$

and

$$\tau = \sqrt{2} t_{exp} u_k / l_k \tag{5.81}$$

In the case when Fr > 6, ($Fr^{1/2} > 2.5$), Re > 10000 and

$$\tau = \sqrt{2} \frac{r/u}{l_k/u_k} >> 1 \tag{5.82}$$

So, $F(\tau)$ is constant and is equal to one.

As done by Theofanous et al., (1976), the experimental constant of 0.25 is used instead of the analytical constant of 1.07. Finally, the heat transfer coefficient for the rear separated region is

$$\begin{aligned} h_{top} &= 0.25 \rho_l C_{p,l} \left(\frac{\alpha_l u_k}{l_k} \right)^{1/2} = 0.25 \rho_l C_{p,l} \mathrm{Pr}_l^{-1/2} \left(\frac{\upsilon_l c^3 U^3}{r} \right)^{1/4} \\ &= 0.25 \rho_l C_{p,l} \mathrm{Pr}_l^{-1/2} \left(4 \upsilon_l^2 c^6 g^3 d \right)^{1/8} \mathrm{Fr}^{3/8} \end{aligned} \tag{5.83}$$

In this formula, the only unknown is the constant c, which turned out to be 0.23 ± 0.1 by matching the computation with the experimental data.

Eq. (5.83) is only good for forced convection film boiling when Fr > 6.0. Applying this model to the transition region (from Fr = 2/9 to 6) will result in a 10–20% higher heat transfer in comparison to the experimental data. For a better prediction in the transition regime, the following equation is used

$$h_{top} = h_{Fr=6} \left(\frac{\mathrm{Fr}}{6} \right)^n \tag{5.84}$$

where $h_{Fr=6}$ is calculated from Eq. (5.83) with Fr = 6, and n is 3/4, which is determined by matching the calculated Nusselt number with experimental data in the transition regime.

The results of the new model are compared with the experiment data in Figs. 5.20(a) and 5.20(b) for the cases of 20 °C and 30 °C subcooling respectively. The new model

agrees with the experiment much better than the preliminary model of the previous section. However the experimental data still show a little higher power dependency on the velocity (or the Froude number) than the theory. There may be two reasons for this discrepancy. First, the heat transfer in the unseparated front part may also be affected by the turbulence in the coming flow. Secondly, this rear turbulent model is not good enough to account for the heat transfer perfectly, because the flow and vapor film in this separated region is so complicated.

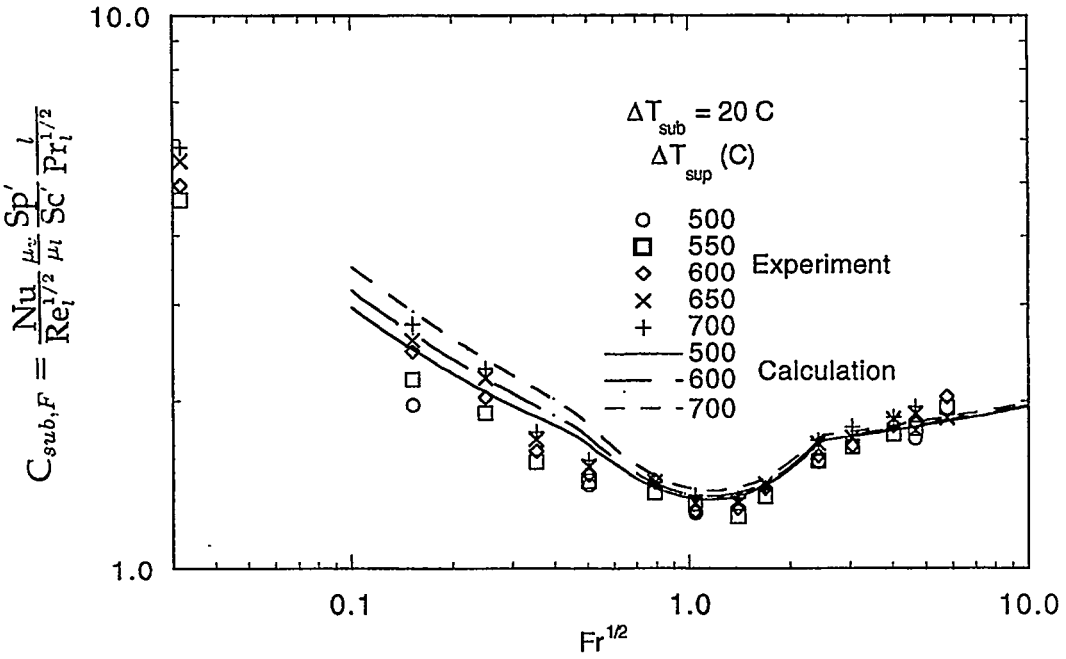

Fig. 5.20(a). A comparison of 20 °C subcooled experimental data with the turbulent model theory in terms of $C_{sub,F}$.

Coupled with the turbulent model, the variation of the two predicted heat transfer characteristics, $C_{sub,N}$ and $C_{sub,F}$, are shown in Fig. 5.21. It indicates that $C_{sub,N}$ and $C_{sub,F}$ are still essentially independent of subcooling ΔT_{sub} and superheat ΔT_{sup} in the free convection and forced convection regimes respectively.

In conclusion, with the laminar model for the front unseparated film and the turbulent eddy model for the rear separated region, the combined theoretical model can predict well all the cases of single-phase film boiling.

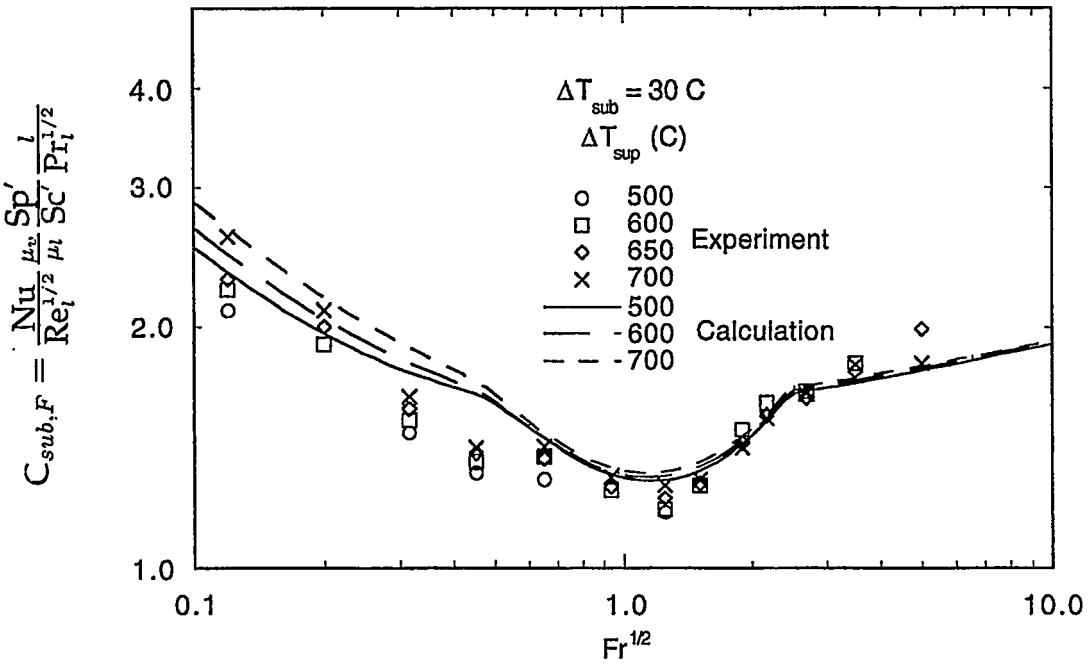

Fig. 5.20(b). A comparison of 30 °C subcooled experimental data with the turbulent model theory in terms of $C_{sub,F}$.

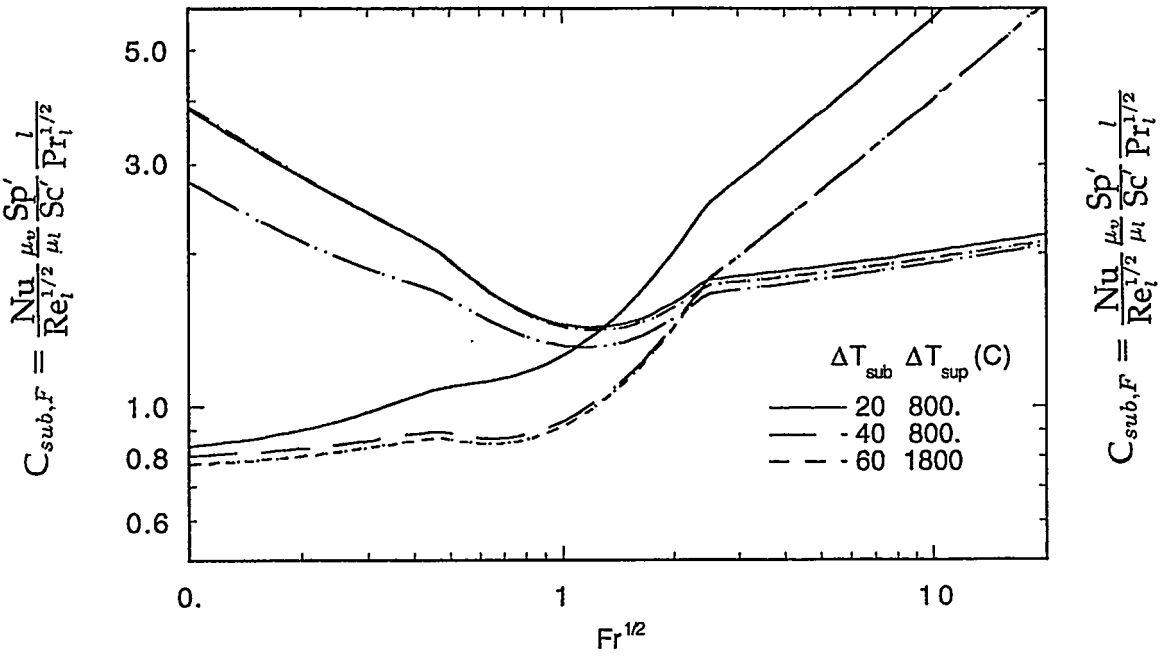

Fig. 5.21. The dependence of $C_{sub,N}$ and $C_{sub,F}$ of modified turbulent model on Froude number Fr at subcooled film boiling conditions.

6 A GENERAL CORRELATION FOR FILM BOILING IN SINGLE-PHASE FLOWS

6.1 Constructing the General Correlation

The experimental data presented in Chapter 4 and theoretical analysis in Chapter 5 indicate that the following "partial" correlations could be well used to correlate and predict the film boiling heat transfer in particular regimes.

Pool Film Boiling Correlation

$$\mathrm{Nu}_p/(1+2/\mathrm{Nu}_p) = K_c(d')(\mathrm{Ar}/Sp')^{1/4}M_c^{1/4} \tag{6.1}$$

$$\begin{aligned}
M_c &= E^3/[1+E/(Sp'\mathrm{Pr}_l)]/(R\mathrm{Pr}_l Sp')^2 \\
E &= (A+CB^{1/2})^{1/3} + (A-CB^{1/2})^{1/3} + (1/3)Sc^* \\
A &= (1/27)Sc^{*3} + (1/3)R^2 Sp'\mathrm{Pr}_l Sc^* + (1/4)R^2 Sp'^2\mathrm{Pr}_l^2 \\
B &= (-4/27)Sc^{*2} + (2/3)Sp'\mathrm{Pr}_l Sc^* - (32/27)Sp'\mathrm{Pr}_l R^2 \\
&\quad + (1/4)Sp'^2\mathrm{Pr}_l^2 + (2/27)Sc^{*3}/R^2 \\
C &= (1/2)R^2 Sp'\mathrm{Pr}_l, \quad Sc^* = 0.93\mathrm{Pr}_l^{0.22}C_{pl}\Delta T_{sub}/h'_{fg}
\end{aligned}$$

$$\begin{aligned}
K_c(d') &= 0.5d'^{-1/4}, && \text{for } d' < 0.14 \\
K_c(d') &= 0.86/(1+0.28d'), && \text{for } 0.14 < d' < 1.25 \\
K_c(d') &= 2.4d'/(1+3.0d'), && \text{for } 1.25 < d' < 6.6 \\
K_c(d') &= 0.47d'^{1/4}, && \text{for } d' > 6.6
\end{aligned}$$

This is applicable for both saturated and subcooled conditions as long as $\mathrm{Fr}^{1/2}$ is smaller than 0.2. The analytical derivation of the base formula of this correlation is given in Appendix A. The $K_c(d')$ ranges from 0.70 to 0.78 as sphere diameter changes from 6.0 to 19.0 mm.

At the saturated condition, $M_c^{1/4}$ is about 0.86, so $[K_c(d')M_c^{1/4}]$ varies from 0.6 to 0.67, and thus Eq. (6.1) becomes

$$\mathrm{Nu}_p = 0.64(\mathrm{Ar}/Sp')^{1/4} \tag{6.2}$$

Forced Convection Film Boiling At Saturated Conditions

$$\mathrm{Nu}_s = 0.5\mathrm{Re}_l^{1/2}\frac{\mu_l}{\mu_v}\left(\frac{KR^4}{Sp'}\right)^{1/4} \tag{6.3}$$

Forced Convection Film Boiling At Subcooled Conditions

$$\mathrm{Nu}_f = \mathrm{Nu}_s + 0.072\mathrm{Re}_l^{0.77}\mathrm{Pr}_l^{0.5}\frac{\mu_l}{\mu_v}\frac{Sc'}{Sp'} \tag{6.4}$$

Eq. (6.4) coupled with Eq. (6.3) could essentially predicate all the forced convection film boiling ($\mathrm{Fr}^{1/2} > 2.5$), including all the saturated, small subcooled and large subcooled cases. The comparisons of the forced convection film boiling experimental data with the predication of Eq. (6.4) are given in Figs. 6.1, 6.2 and 6.3 for saturated, small subcooling ($0 < \Delta T_{sub} < 20$ °C), and large subcooling respectively. The agreements are good in all the three cases.

Now we are ready to construct a general correlation. After some trial and error, we found that Eq. (6.1) and Eq. (6.4) could be combined in the following way for film boiling on spheres in all regimes:

Combined Correlation

$$\mathrm{Nu} = \left[\mathrm{Nu}_p^5 + [F(\mathrm{Fr})\mathrm{Nu}_f]^5\right]^{1/5} \tag{6.5}$$

where the empirical function

$$F(\mathrm{Fr}) = 1 - \frac{0.2}{1 + |\,\mathrm{Fr}^{0.5} - 1\,|}$$

is introduced to correlate the transition data. Figure 6.4 gives the comparison of the experimental data obtained at all conditions with the correlation (6.5), and it shows that most of the data points are in a band within ±15%.

6.2 Comparisons of the General Correlation With the Theory

The Nusselt number calculated from the general correlation Eq. (6.5), at saturated condition, are compared with the theory and experiment in terms of $C_{sat,N}$ and $C_{sat,F}$, in Figs. 6.5 and 6.6 respectively. For subcooled cases, with the modified turbulent model Eq. (5.85) , the comparisons are given in Figs. 6.7 (a) and 6.7 (b) in terms of $C_{sub,F}$. They all show good agreement among the experiment, theory and correlation. For subcooled cases, with the turbulent model Eq. (5.83), comparisons are given in Figs 6.8(a) and 6.8(b).

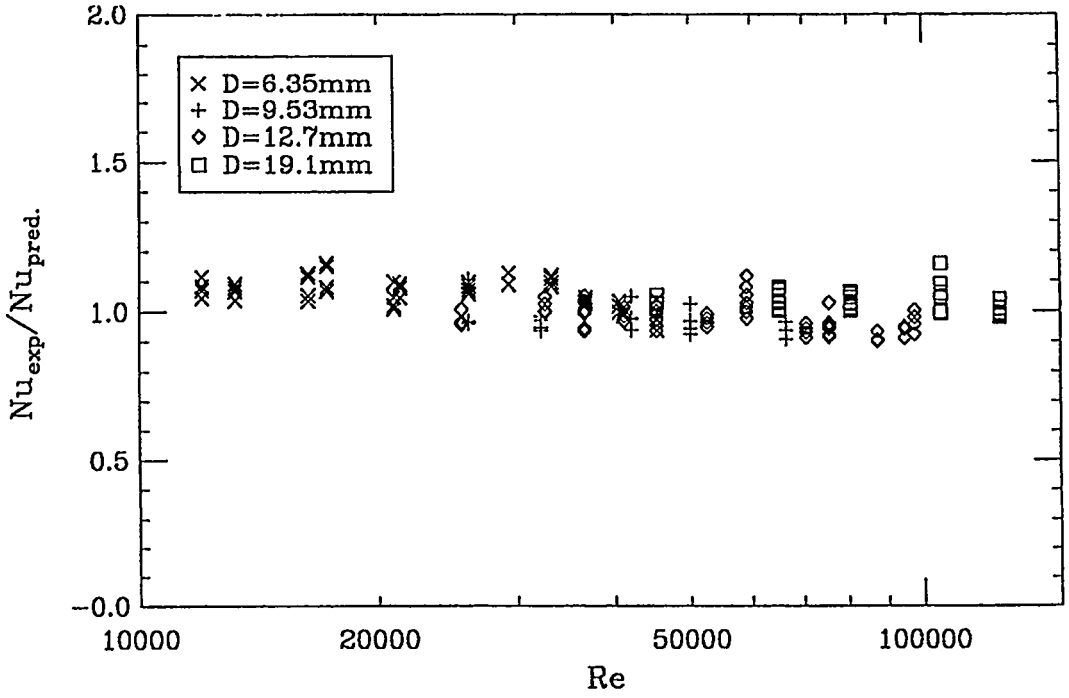

Fig. 6.1. Forced convection data obtained in saturated water flow are compared with Eq. (6.3).

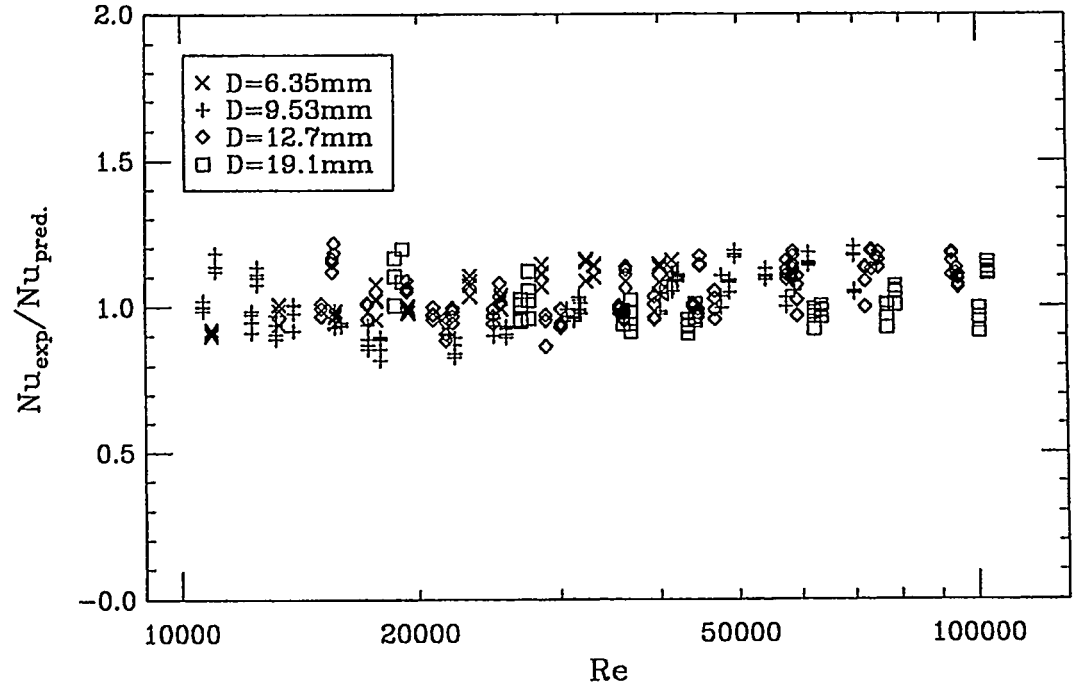

Fig. 6.2. Forced convection data obtained in little subcooled (0–20 °C) water flow are compared with Eq. (6.4).

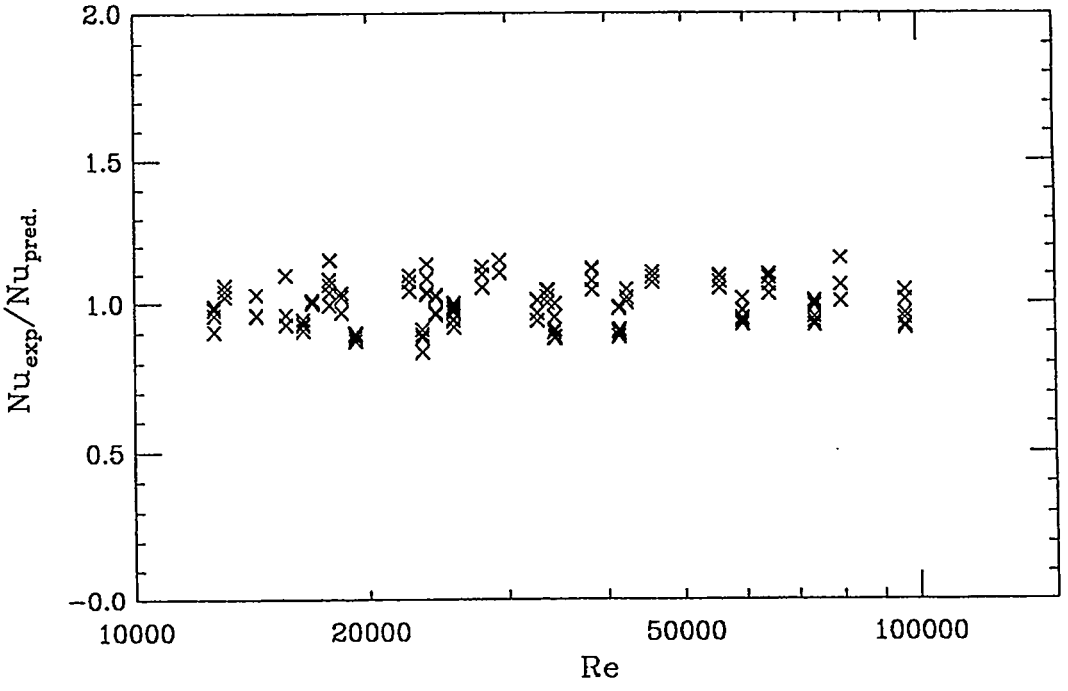

Fig. 6.3. Forced convection data obtained in large subcooled (> 20 °C) water flow are compared with Eq. (6.4).

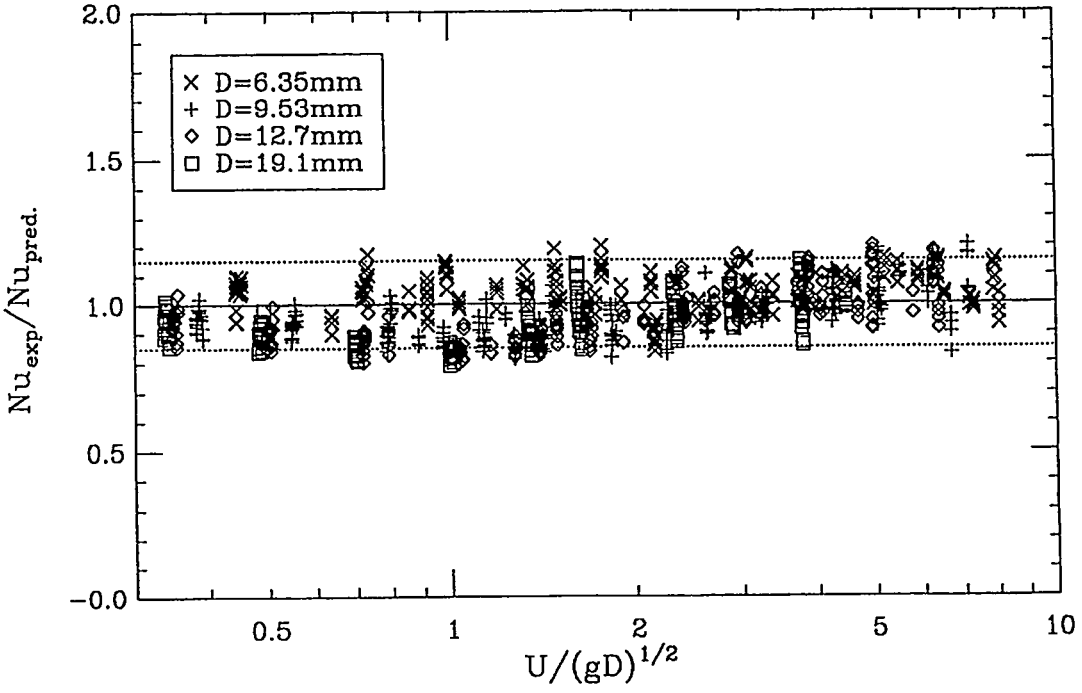

Fig. 6.4. Data obtained at all conditions are compared with correlation (6.5).

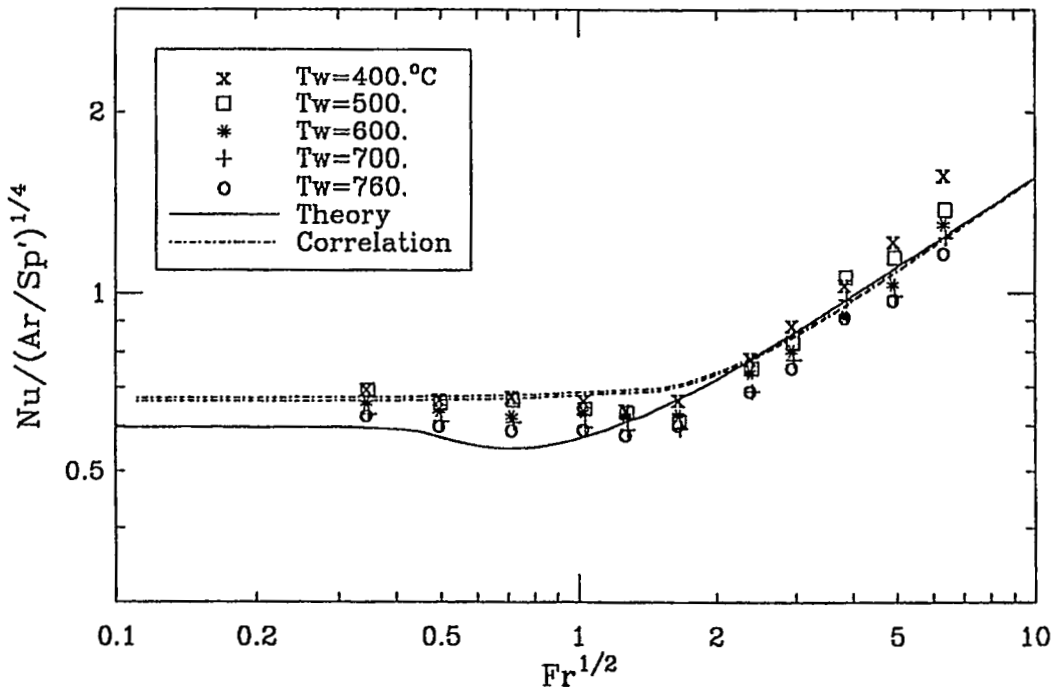

Fig. 6.5. A comparison of the general correlation with the theory and experiment in terms of $C_{sat,N}$ at saturated conditions.

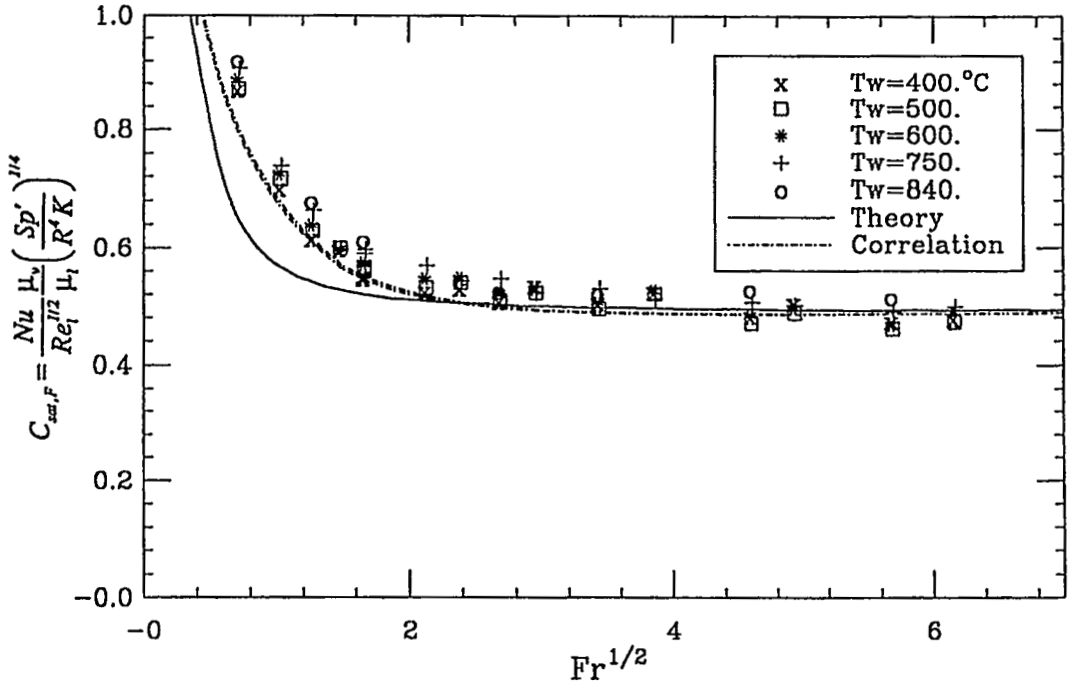

Fig. 6.6. A comparison of the general correlation with the theory and the experiment in terms of $C_{sat,F}$ at saturated conditions.

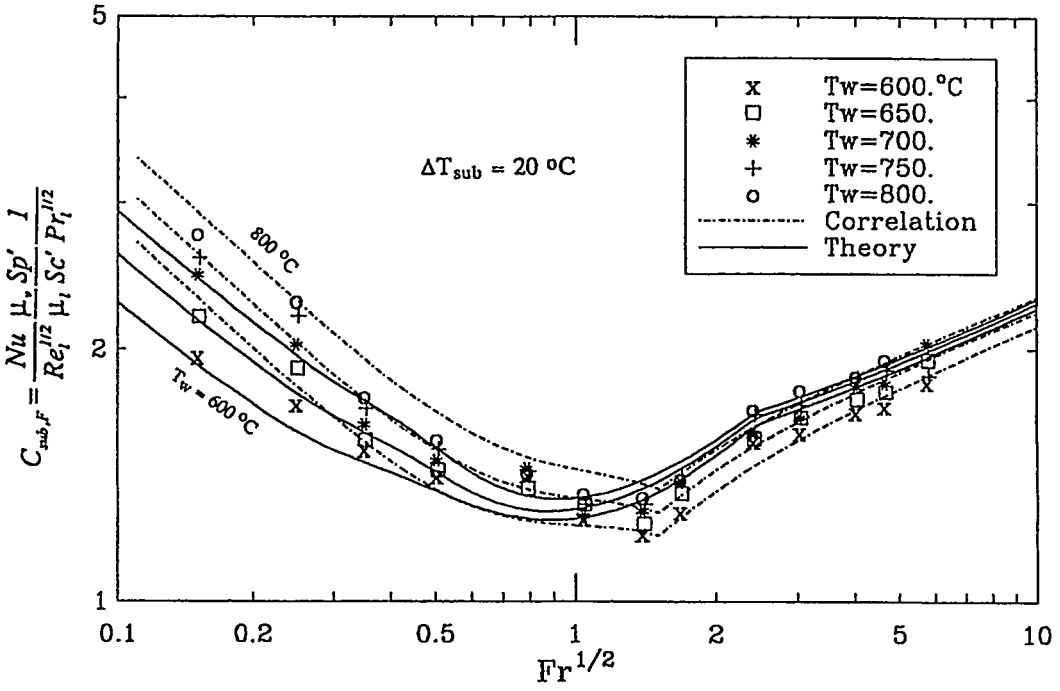

Fig. 6.7(a). A comparison of general correlation with the modified turbulent model theory and the experiment at 20 °C subcooling.

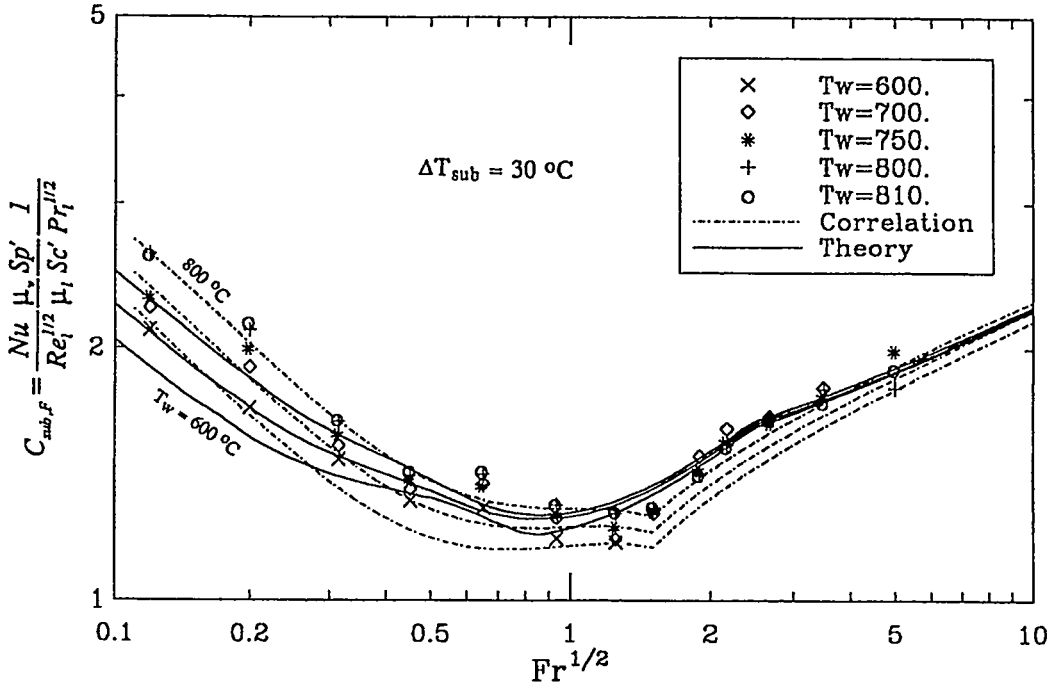

Fig. 6.7(b). A comparison of general correlation with the modified turbulent model theory and the experiment at 30 °C subcooling.

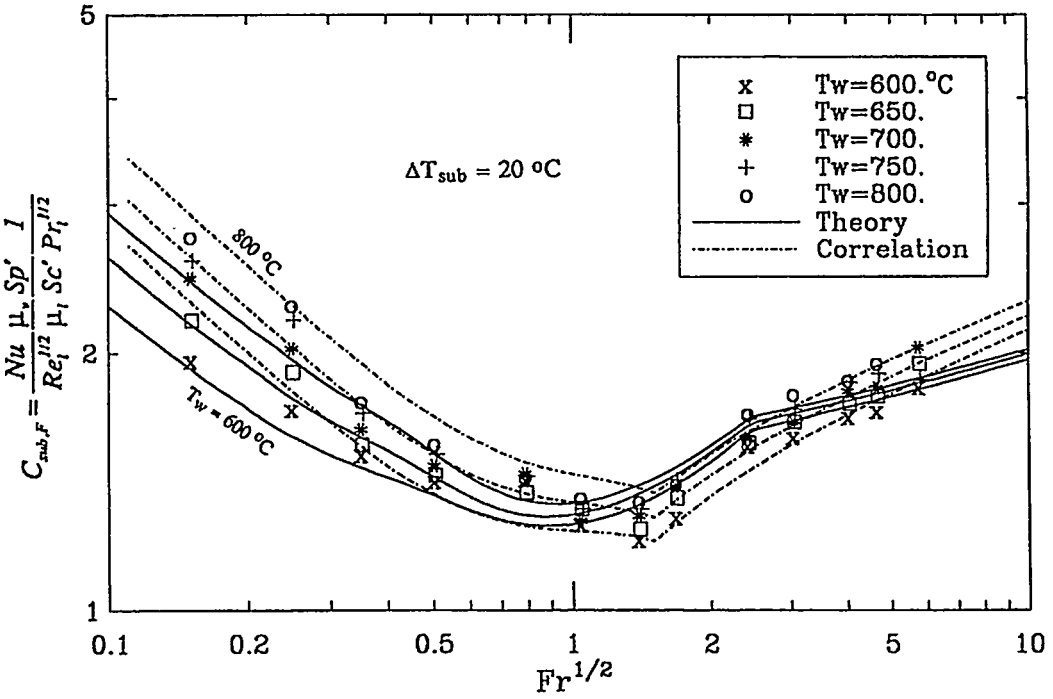

Fig. 6.8(a). A comparison of general correlation with the turbulent model theory and the experiment at 20 °C subcooling.

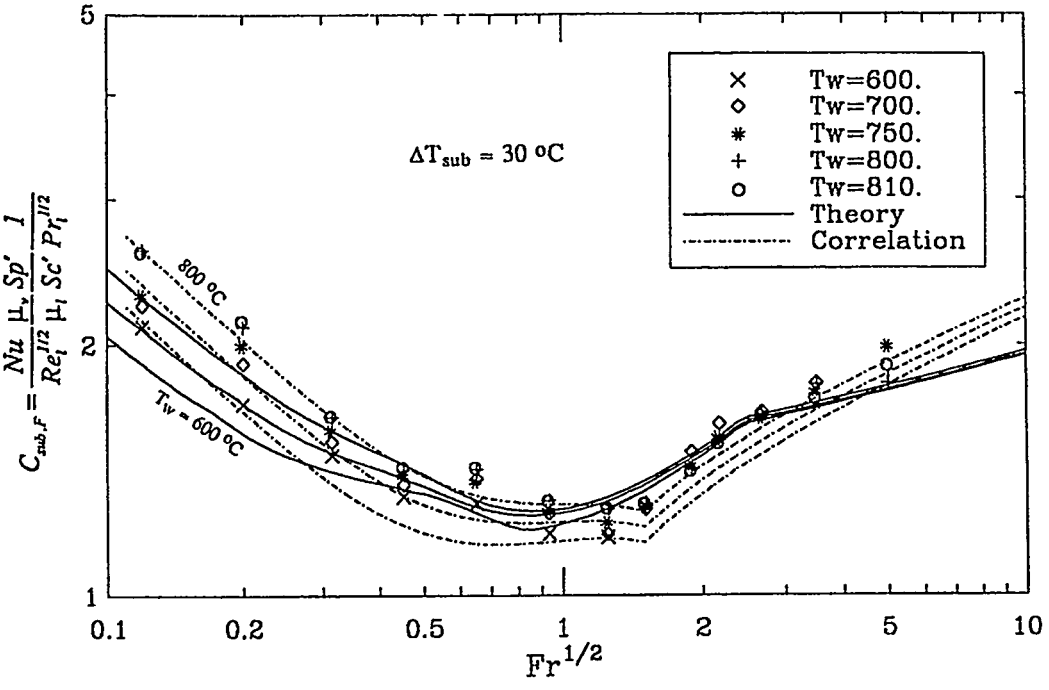

Fig. 6.8(b). A comparison of general correlation with the turbulent model theory and the experiment at 30 °C subcooling.

6.3 Comparisons of the General Correlation with Others

In the case of saturated pool film boiling, the comparison is given in Fig. 6.9; it shows that our correlation is a little lower than Hendrik's correlation (which is for sphere) and a little higher than others. For the subcooled pool film boiling, the comparison at the sphere temperature of 760 °C is shown in Fig. 4.17; it shows our correlation is lower than Farahat's and higher than all others.

For saturated forced convection, the comparison is given in Fig. 6.10. Our correlation is quite close to Bromley's correlation but is only about half of Epstein's et al (1980) correlation. Dhir's et al (1978) correlation, which is not valid for this high velocity case, gives much higher Nusselt number than the others.

Figure 6.11 shows the comparison for the case of subcooled forced convection. It indicates that our correlation agrees very well with Epstein's correlation at high sphere superheat, and about 10–20% lower than it at low superheat (400–600 °C). Compared to our correlation, Dhir's correlation is lower when the sphere temperature is low and higher when the sphere temperature is high. Orozco's correlation is extremely low compared with the others.

Figures 6.12 through 6.14 give more comparisons of our correlation with Epstein's and Dhir's correlations. The general conclusions are: (1) for complete saturated film boiling, both Epstein's and Dhir's correlations give much higher (more than a factor of two) predication than ours; (2) for large subcooling and high velocity, our correlation agrees with Epstein's correlation and is higher than Dhir's correlation. (3) At the transition regime from natural to forced convection with large subcooling, our correlation gives the lowest value and Epstein's gives the highest value.

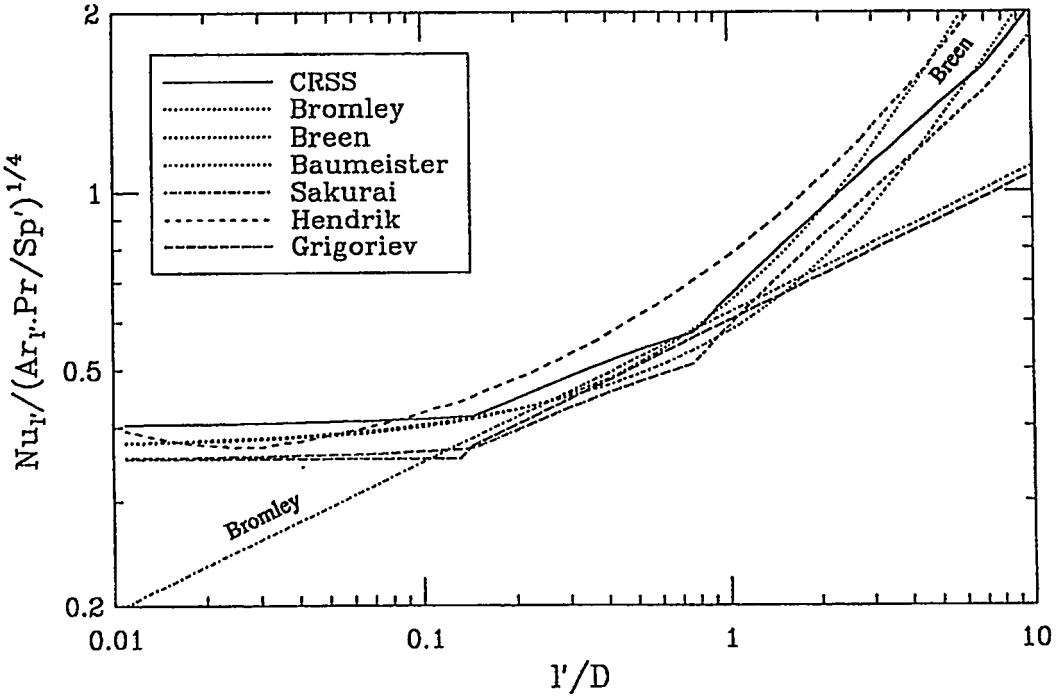

Fig. 6.9. The present general correlation is compared with other saturated pool film boiling correlations.

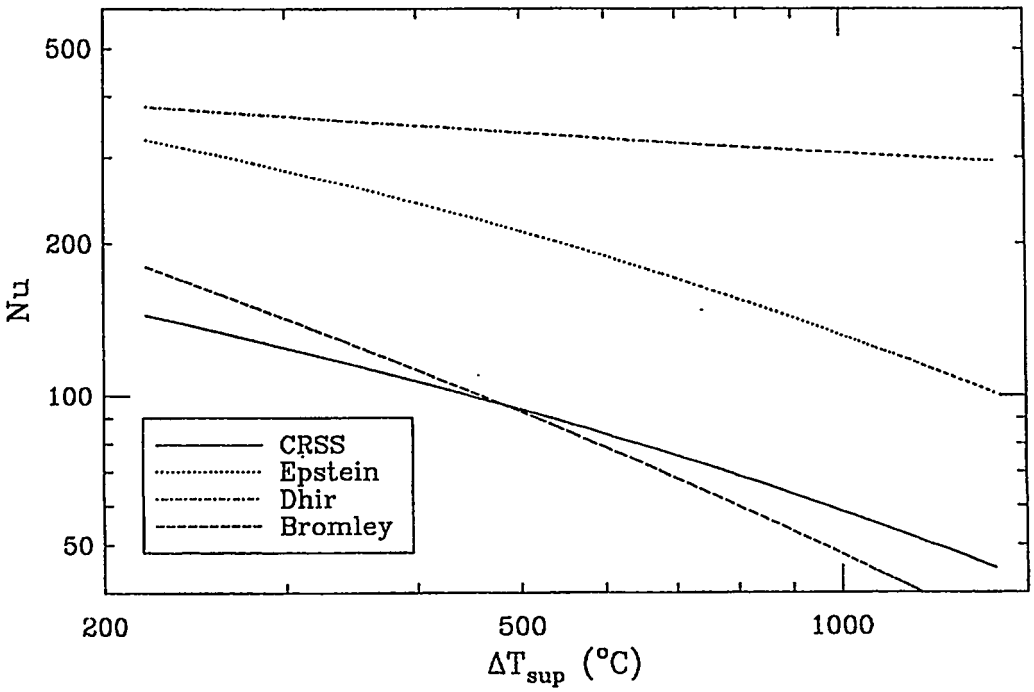

Fig. 6.10. Comparison of our general correlation with other correlations at saturated forced convection condition ($U = 1.5$ m/s).

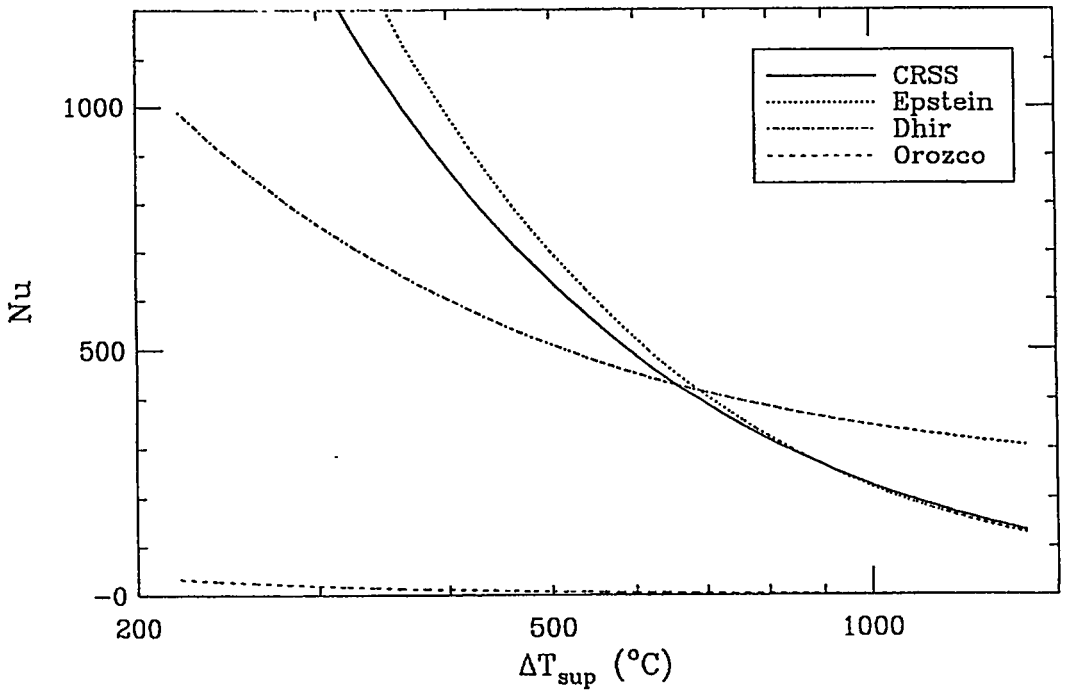

Fig. 6.11. Comparison of our general correlation with other correlations at highly subcooled forced convection condition ($\Delta T_{sub} = 30$ °C, $U = 1.5$ m/s).

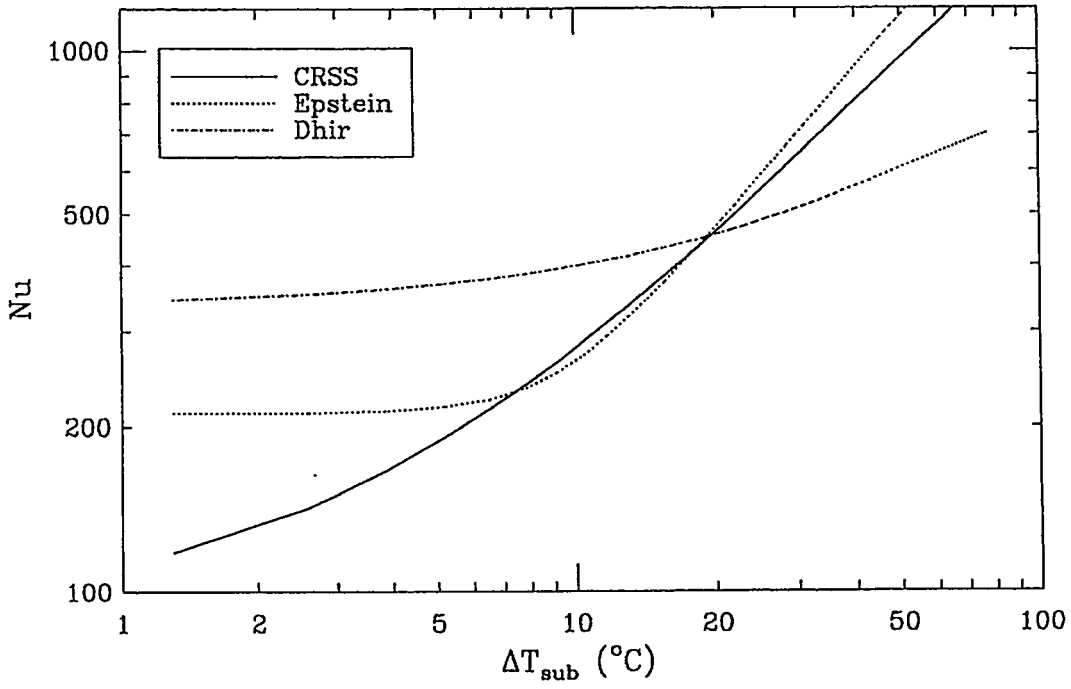

Fig. 6.12. Comparison of our general correlation with other correlation at forced convection regime ($U = 1.5$ m/s).

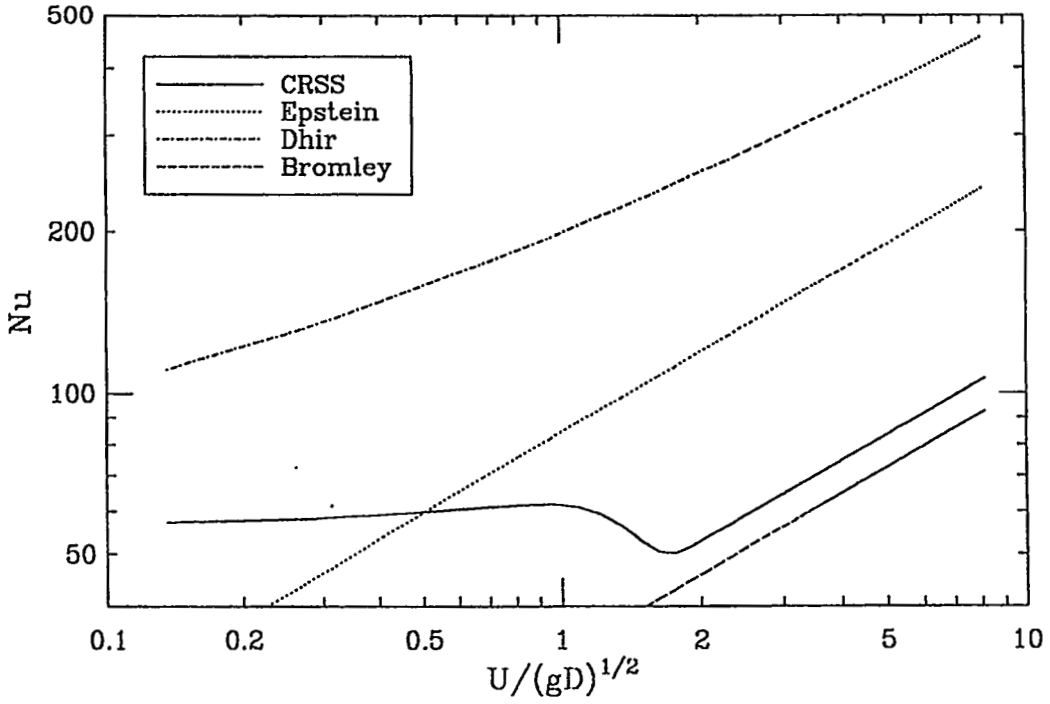

Fig. 6.13. Comparison of our general correlation with other correlation at saturated condition.

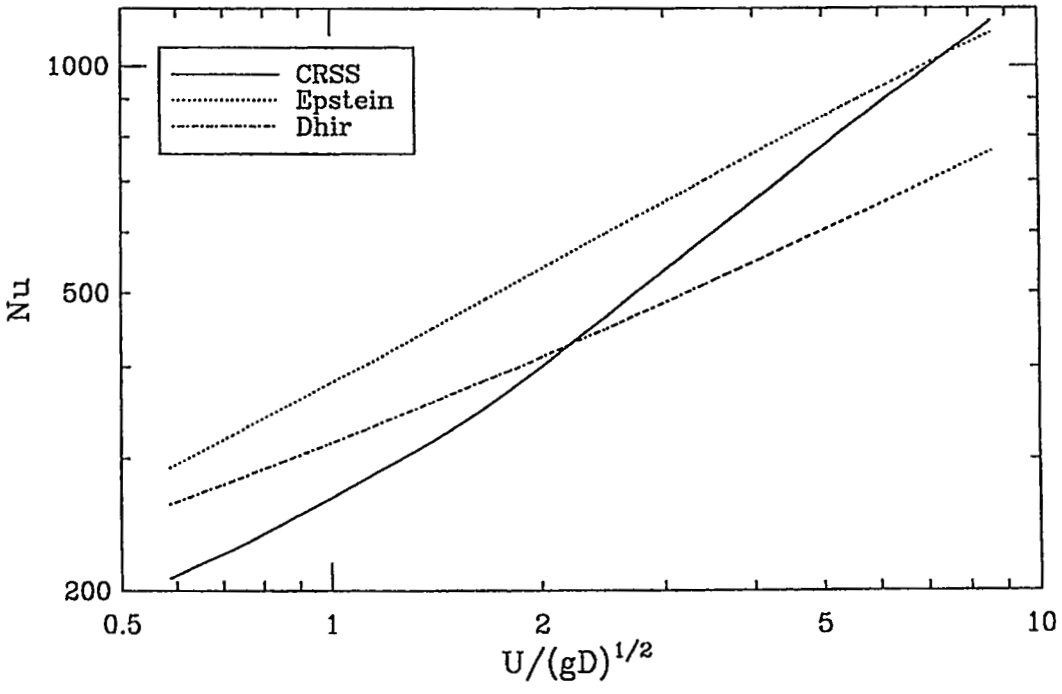

Fig. 6.14. Comparison of our general correlation with other correlation at subcooled condition.

7 FILM BOILING IN TWO-PHASE FLOWS

The film boiling from a sphere in two-phase flows has been studied in two parts, film boiling in upward two-phase flow and film boiling in downward two-phase flow. The experiments were carried out with 316 stainless steel spheres of 12.7 mm in diameter, saturated water and saturated steam in atmospheric pressure.

In both cases, prior to heat transfer tests, the void fractions (or water fraction) in the test section were investigated and measured "off line" by the X-ray radiography. The X-ray radiographs were also taken during the "on line" heat transfer runs. The two-phase flow that we characterize and communicate here is the two-phase flow that comes towards the test sphere, other than the disturbed flow behind the boiling spheres.

All two-phase film boiling heat transfer experiments were conducted by transient mode runs. The experimental data are interpreted and correlated in different ways, and the final experimental correlations are suggested.

7.1 Upward Two-Phase Flow Generation and Void Fraction Measurement

The upward two-phase flows were generated within the two-phase mixer by injecting saturated steam into a saturated upward water flow through the tube-needle assembly, as shown in Fig. 3.2. Only No.1 tube-needle assembly, see Section 3.2, was used in the upward two-phase experiment to generate the two-phase flows.

By varying the water and steam flow rates, different two-phase flows were generated in the test tube. In the our present experiment, the superficial water velocity covers from 0.3 to 1.6 m/s, and the superficial steam velocity varies from 1.4 to 4.5 m/s. The void fractions in the test tube, which can not be determined theoretically, were detected and measured by the X-ray radiographic method, as presented in Section 3.5. For each combination of water and steam flow rates, the radiograph of the generated two-phase flow was taken, and the void fraction was determined by analyzing the darkness of the obtained X-ray pictures. Typical X-ray radiographs of the center part of the test tube obtained at different steam flow rates are shown in Figs. 7.1 through 7.5 respectively. The void fractions in the test section were determined in an "off line" fashion, without the test sphere inside the test section.

The direct observation of two-phase flow inside the test tube and the pictures in Figs. 7.1 through 7.5 indicate that there are three flow regimes: (1) with low water flow rate, especially when the steam flow rate is also low, the two-phase flow is "bubbly" flow with

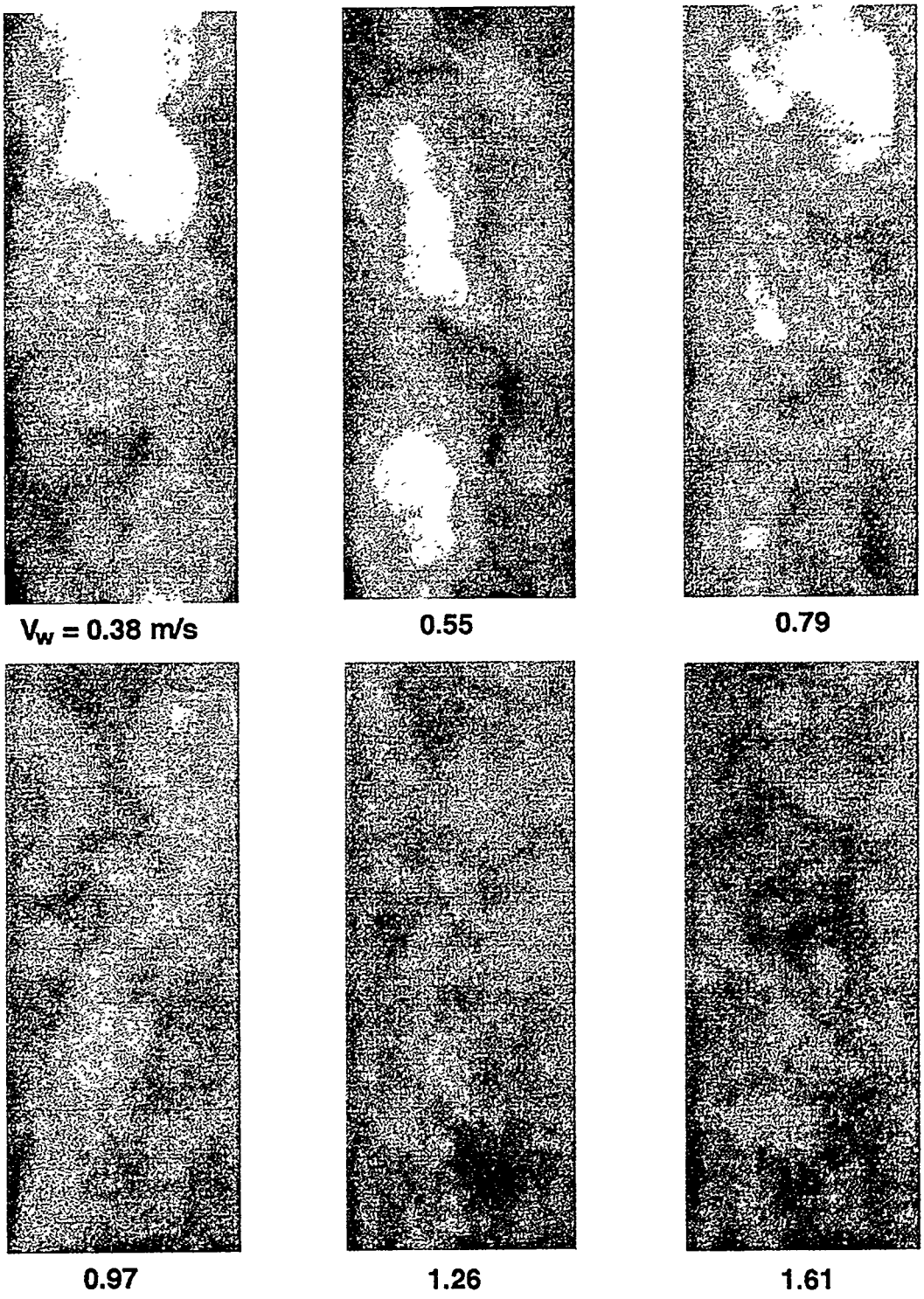

Fig. 7.1 X-Ray radiographs obtained with superficial steam velocity at 1.4 m/s.

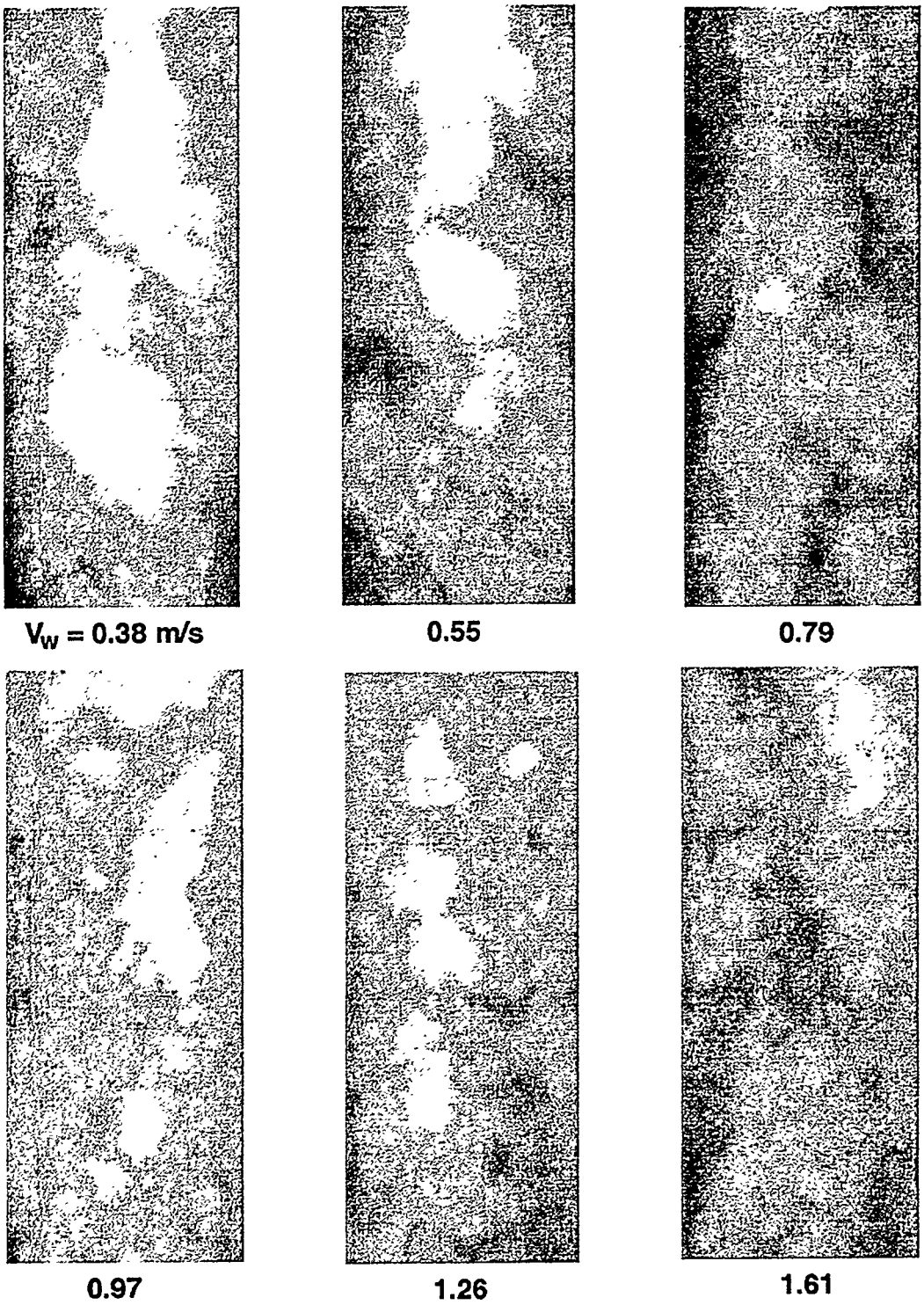

Fig. 7.2 X-Ray radiographs obtained with superficial steam velocity at 2.1 m/s.

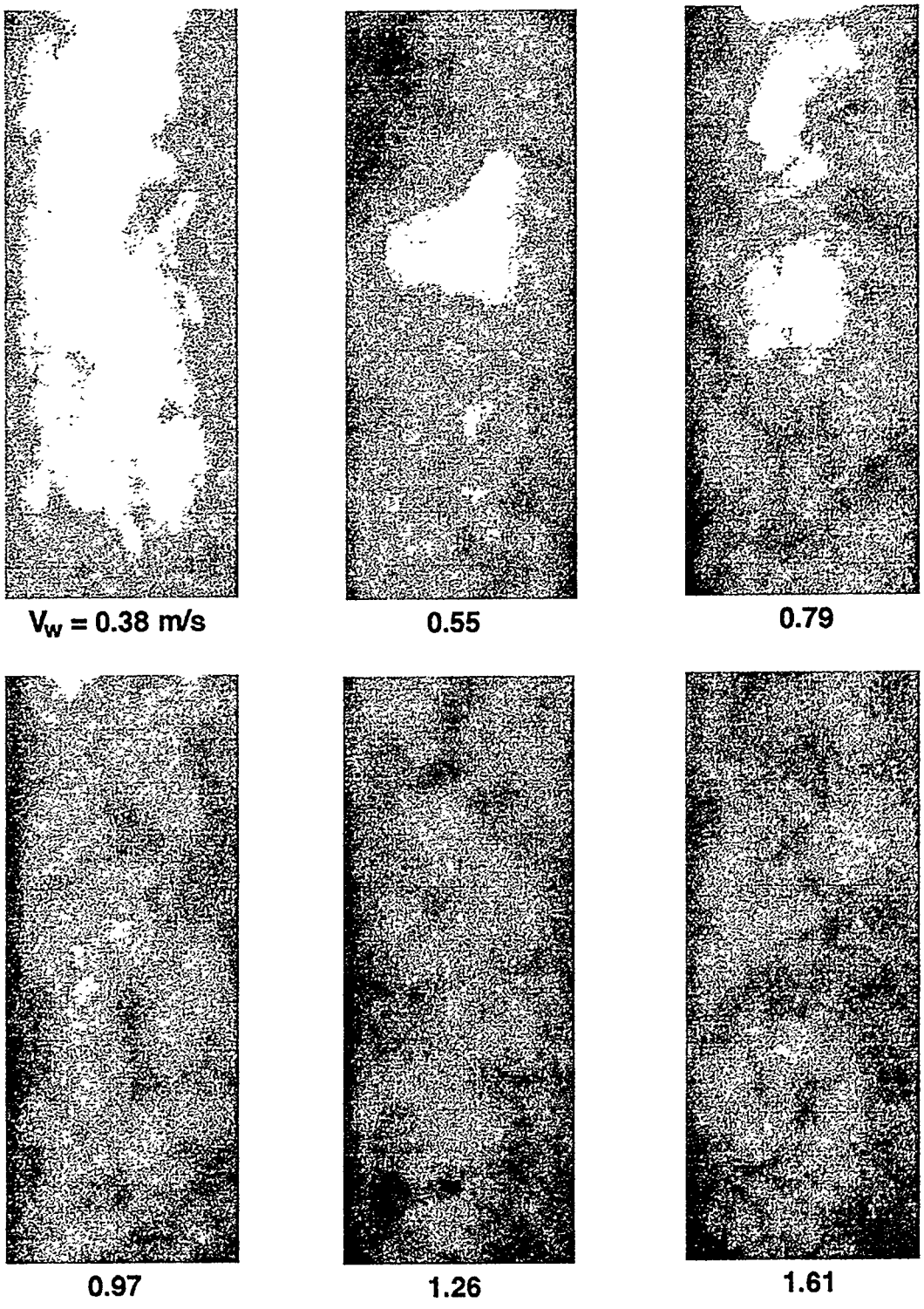

Fig. 7.3 X-Ray radiographs obtained with superficial steam velocity at 2.7 m/s.

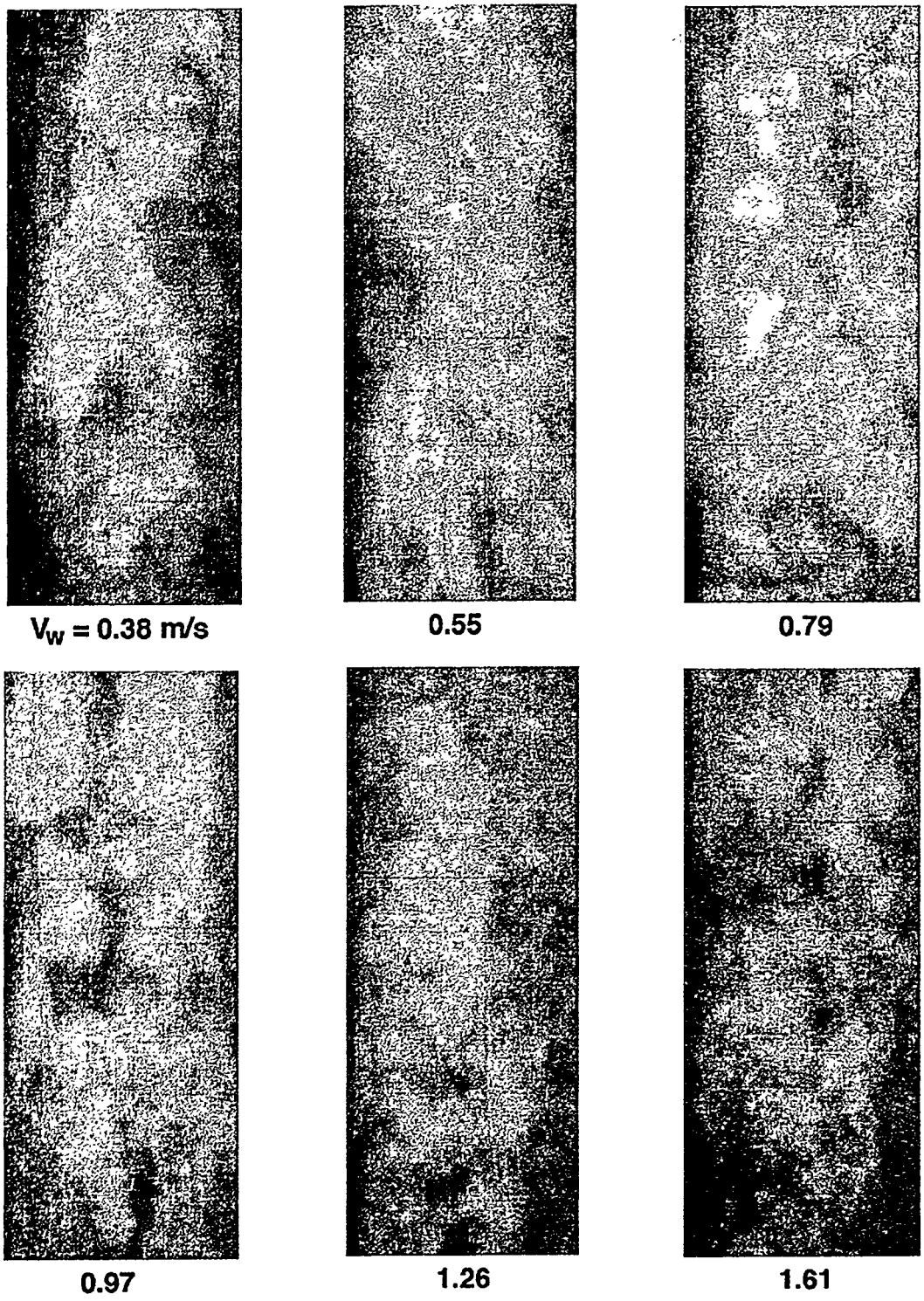

Fig. 7.4 X-Ray radiographs obtained with superficial steam velocity at 3.2 m/s.

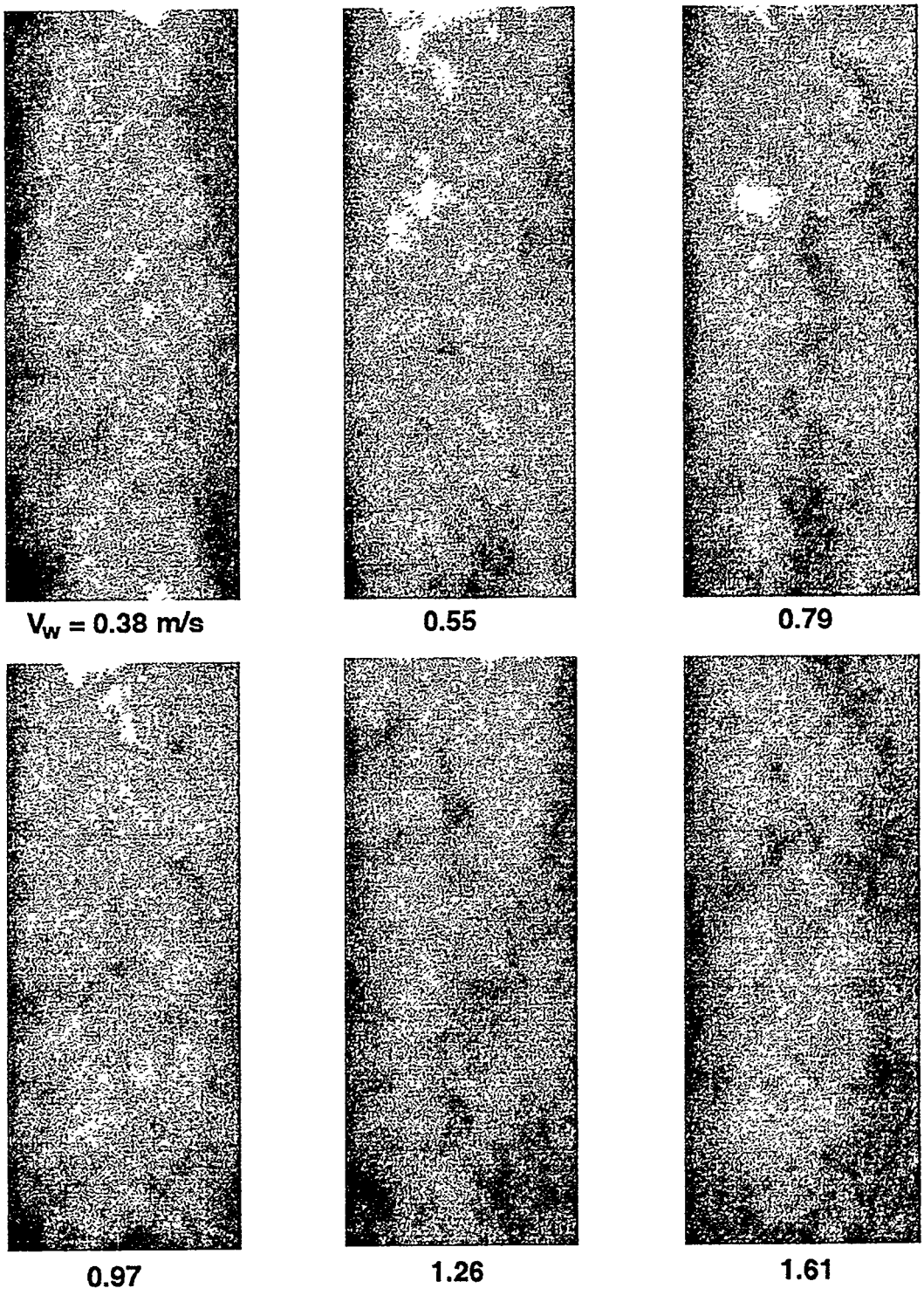

Fig. 7.5 X-Ray radiographs obtained with superficial steam velocity at 4.5 m/s.

void fraction from 0.65 to 0.4; (2) with high water flow rate but low steam flow rate, the flow looks like a single-phase flow with lots of small bubbles; (3) with both high water flow rate and high steam flow rate, the two-phase flow appears as an upward mist-jet flow with void fraction about 0.5.

Because of the variant nature of the two-phase flows (both in time and in space), especially for the bubbly flow case, several X-ray pictures were taken for each water/steam flow combination to get the average void fraction for that flow condition. The obtained water fractions at superficial steam velocities of 1.4, 2.1, 2.7, 3.2 and 4.5 m/s are shown in Figs. 7.6 through 7.10, respectively. The water fraction covers range from 35% to 80%.

After knowing the superficial water and steam velocities (V_w and V_s) and the void fraction of the two-phase flow (a) the water and the steam velocities can be calculated by

$$U_w = V_w/\alpha_w = V_w/(1-\alpha) \tag{7.1}$$

$$U_s = V_s/\alpha = V_s/(1-\alpha_w) \tag{7.2}$$

In our present experiment, the water velocity varies from 0.6 to 3.2 m/s and the steam velocity varies from 3.0 to 9.0 m/s.

Typical radiographs of film boiling on sphere in two-phase flow are shown in Fig. 7.11. For most two-phase cases, it is impossible to distinguish the vapor film from the steam void of the coming two-phase flow, except the cases when the void fraction is very low. For comparison, the radiographs of film boiling on a sphere in saturated single-phase flow are also shown in Fig. 7.11. It is very clear that the film configuration in single-phase flow observed from X-ray pictures are completely consistent with those from photo pictures.

7.2 Film Boiling in Upward Two-Phase Flows

Setting the steam flow rate at certain level, the film boiling heat transfer experiment was carried out by adjusting the water flow rate from one value to another. The water and steam velocities were calculated by Eqs. (7.1) and (7.2). Typical experiment data are tabled in Appendix E.

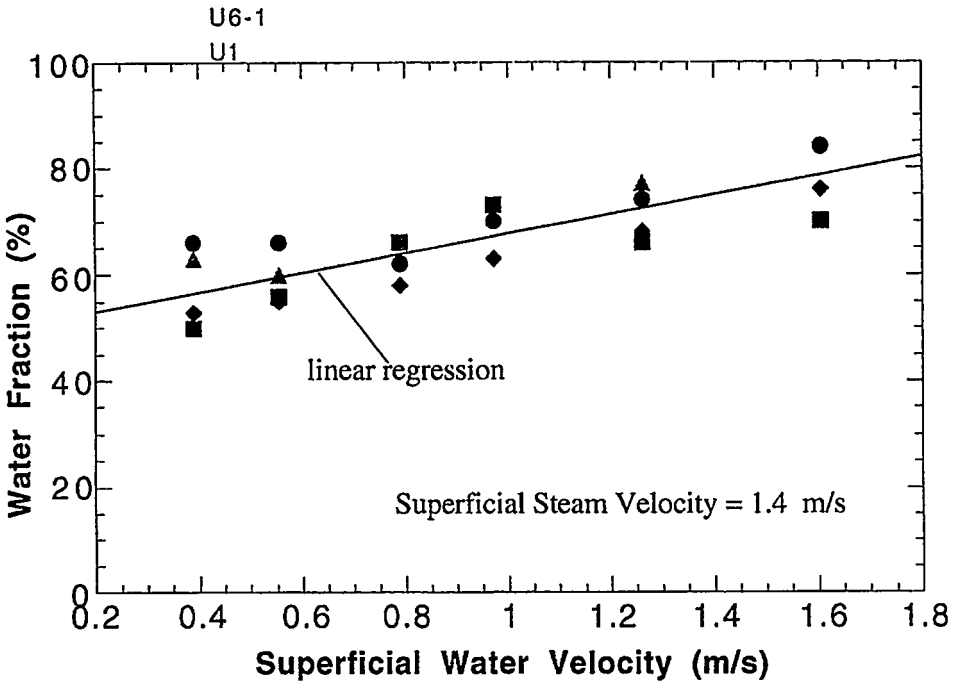

Fig. 7.6. Measured water fraction. The symbols represent measurements obtained at different times.

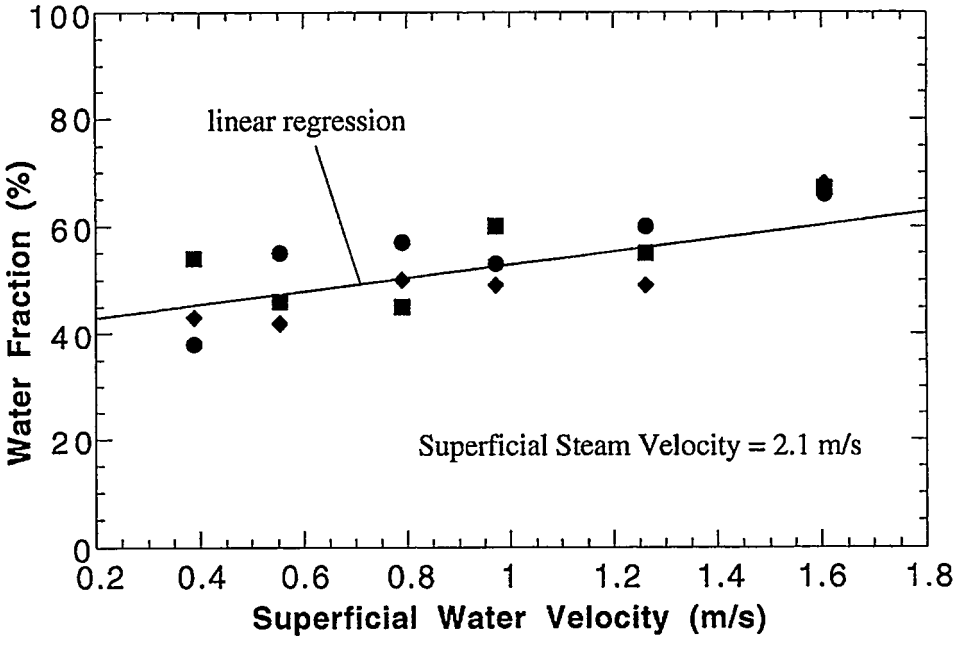

Fig. 7.7. Measured water fraction. The symbols represent measurements obtained at different times.

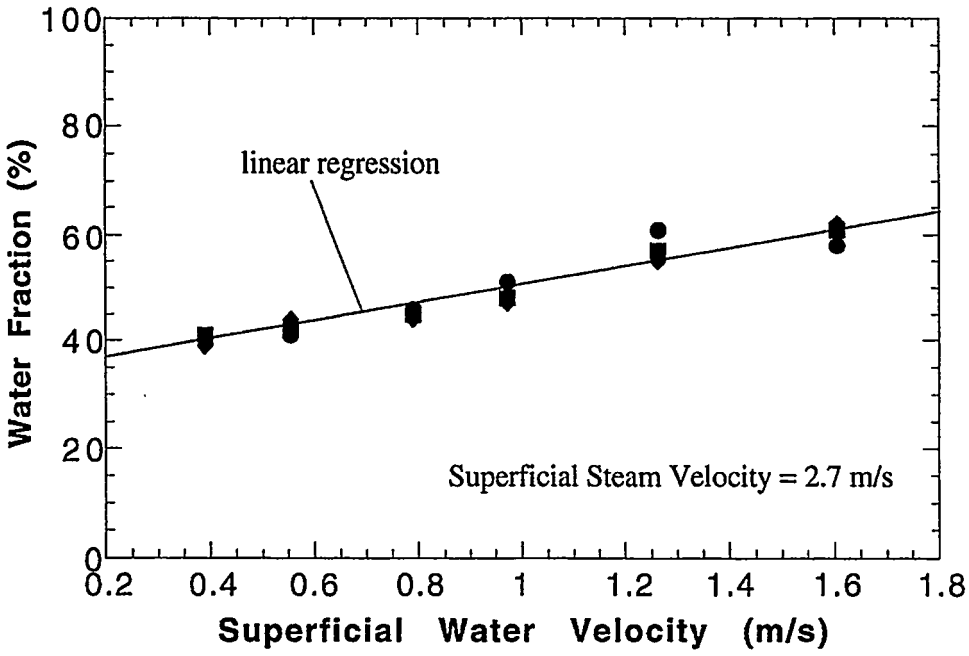

Fig. 7.8. Measured water fraction. The symbols represent measurements obtained at different times.

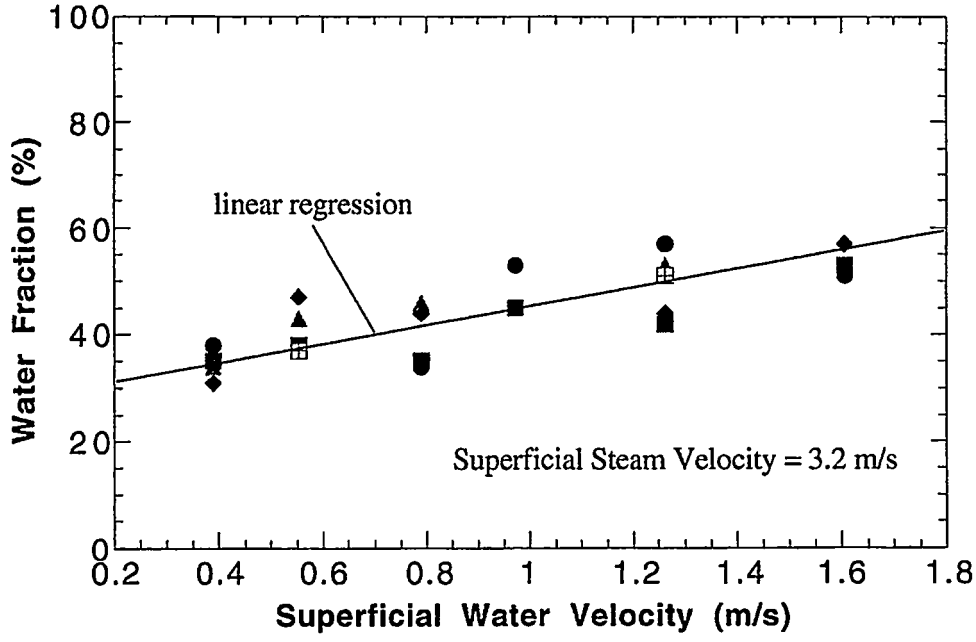

Fig. 7.9. Measured water fraction. The symbols represent measurements obtained at different times.

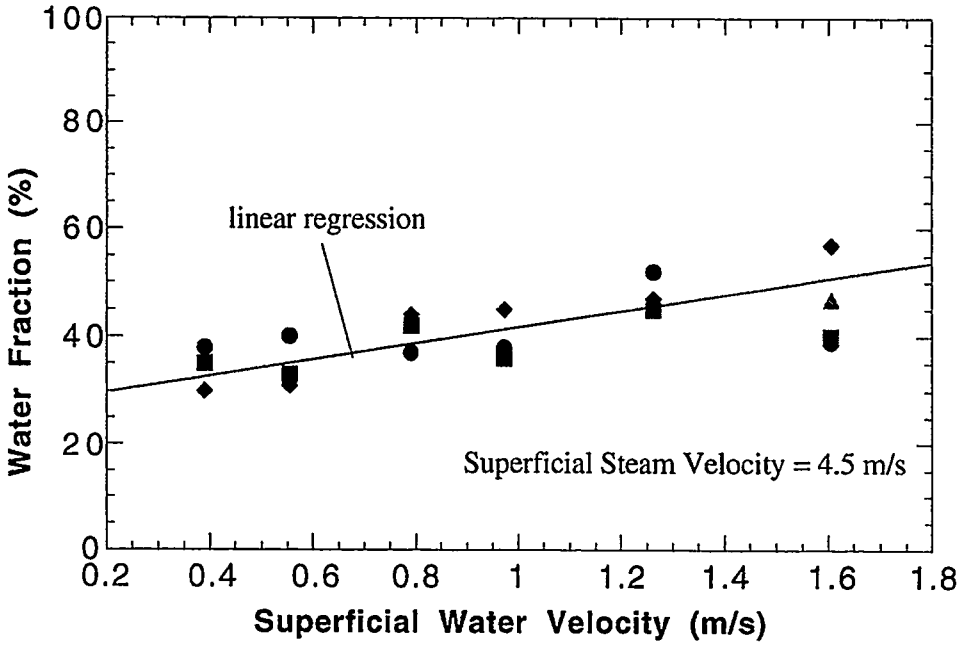

Fig. 7.10. Measured water fraction. The symbols represent measurements obtained at different times.

Choosing the superficial water velocity V_w as the characteristic flow velocity and defining the Reynolds number as

$$\mathrm{Re} = \frac{V_w/D}{\upsilon_l} \tag{7.3}$$

the experimental Nusselt numbers

$$\mathrm{Nu} = \frac{hD}{k_l} \tag{7.4}$$

were plotted in Fig. 7.12 and 7.13 for two steam flow rates respectively. As in the case of single-phase film boiling, the Nu number depends both on the superficial water velocity and the sphere superheat. The comparison of Fig. 7.12 with Fig. 7.13 also indicates that the higher the steam flow rate, the higher the Nu number. In terms of the saturated single-phase film boiling heat transfer characteristic

$$C'_{sat,F} = \frac{\mathrm{Nu}}{\mathrm{Re}^{1/2}} \frac{\mu_v}{\mu_l} \left(\frac{Sp'}{R^4 K} \right)^{1/4} \tag{7.5}$$

the data that are plotted in Figs. 7.12 and 7.13 were re-plotted in Figs. 7.14 and 7.15, respectively. In the same way, more data obtained with other steam flow rates are shown in Fig. 7.16. They show that the sphere superheat effect is well correlated in all the upward two-phase cases as in the case of single-phase flow. However, the $C'_{sat,F}$ is no longer a constant of 0.5 as in the case of single-phase flow, and it varies from 0.45 to 0.95. They also show that the heat transfer characteristic $C'_{sat,F}$ decreases with Re and increases with the superficial steam velocity. It is obvious that the superficial water velocity is not a good characteristic velocity for the upward two-phase film boiling.

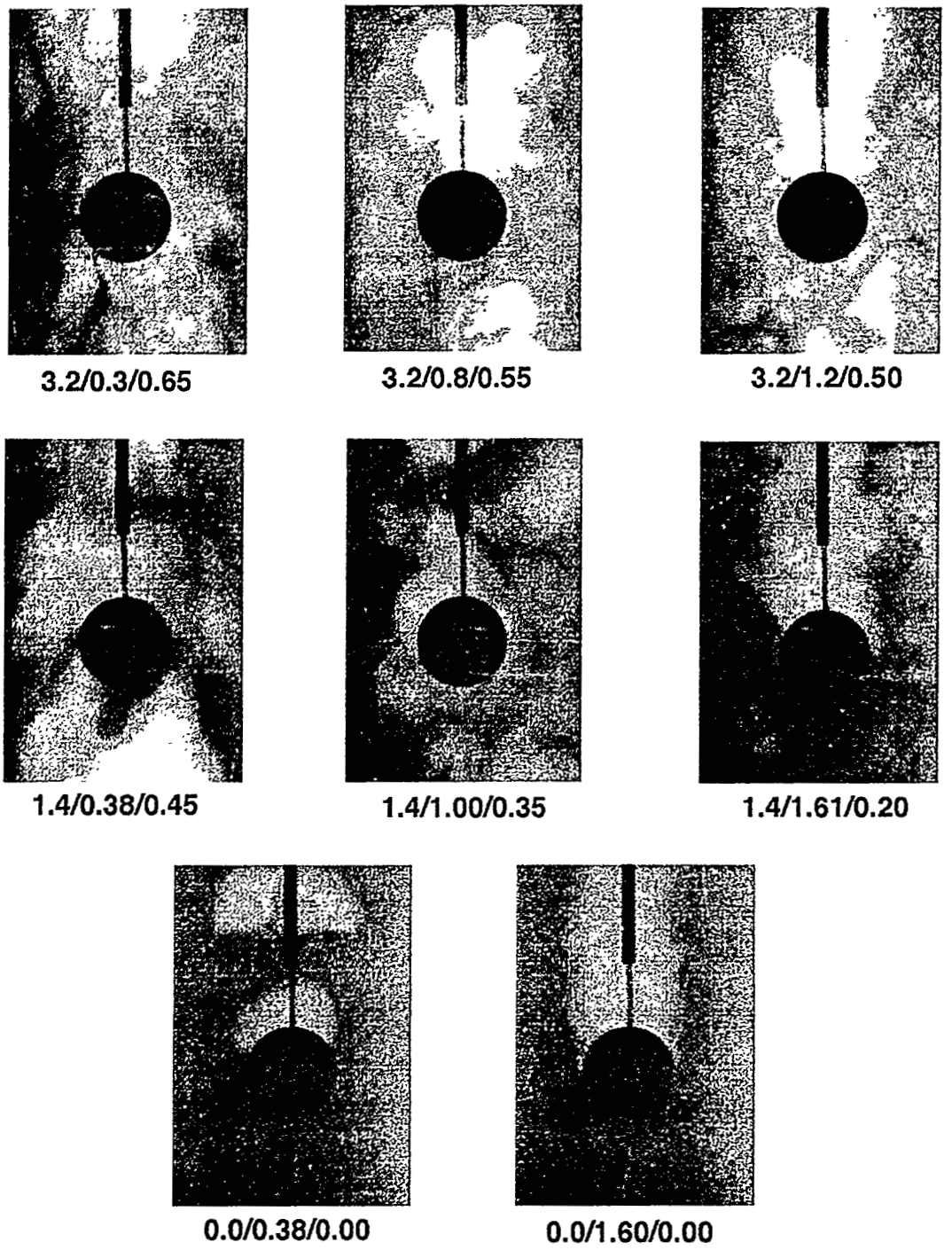

Fig. 7.11 X-Ray radiographs of film boiling from sphere in upward two- and single- phase flow. The numbers stand for: superficial Steam velocity/superficial water velocity/void fraction.

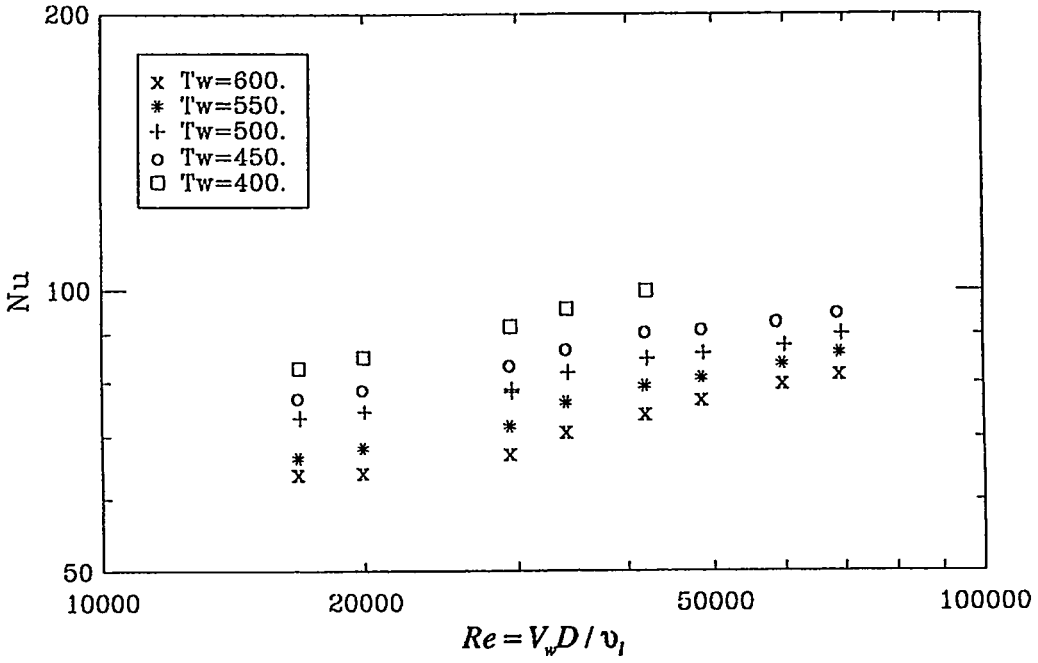

Fig. 7.12. Film boiling Nusselt number obtained in upward two-phase flow with superficial steam velocity at 1.4 m/s.

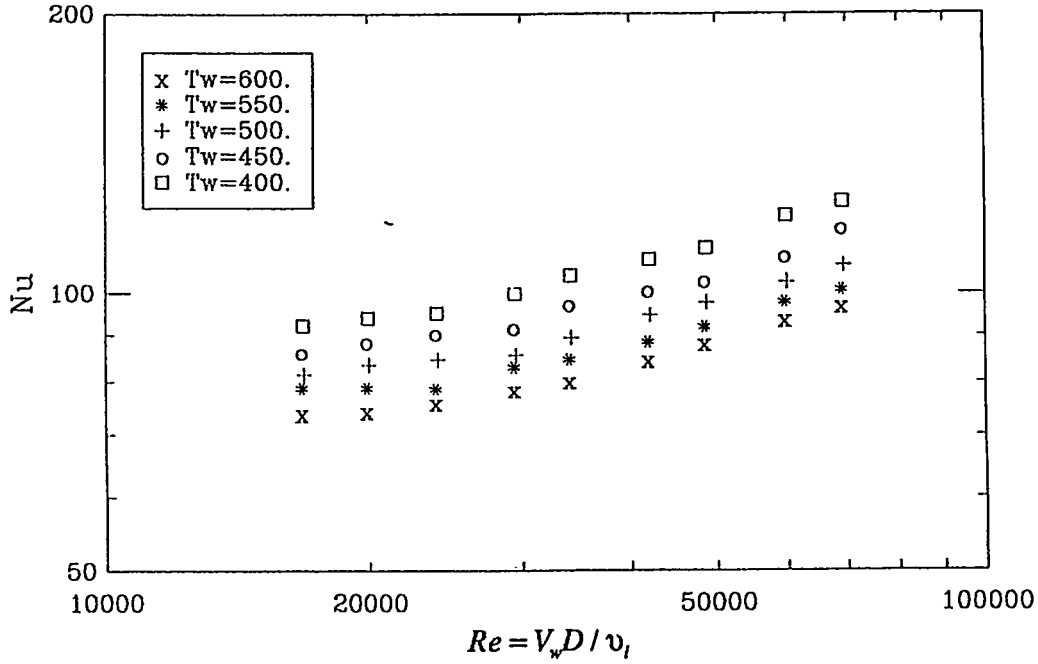

Fig. 7.13. Film boiling Nusselt number obtained in upward two-phase flow with superficial steam velocity at 4.5 m/s.

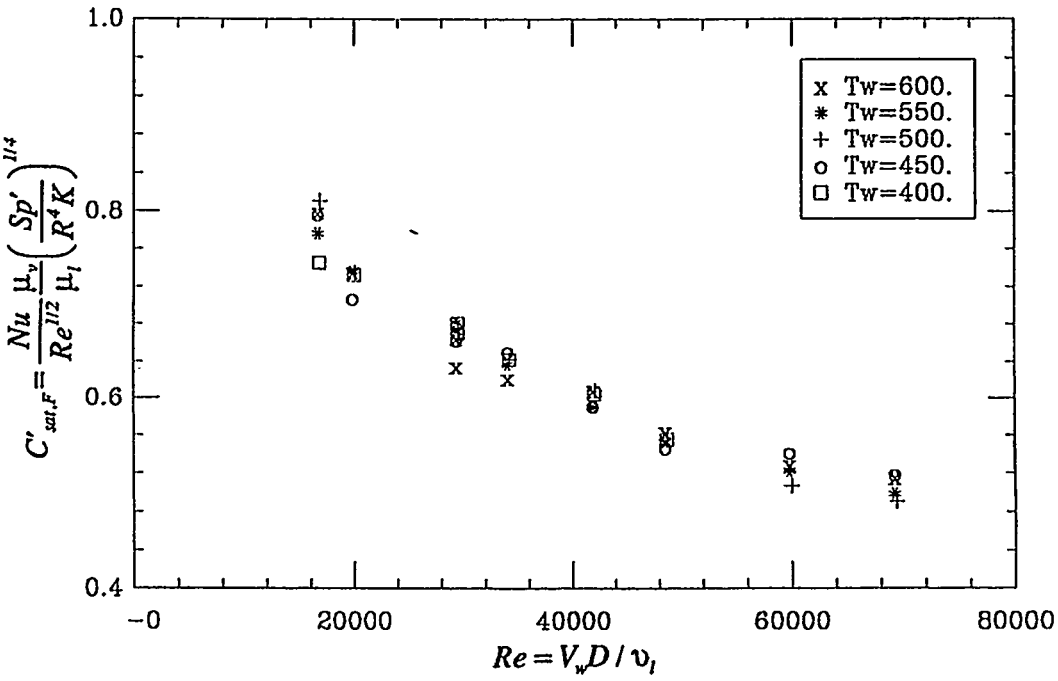

Fig. 7.14. Film boiling Nusselt number obtained in upward two-phase flow with superficial steam velocity at 1.4 m/s.

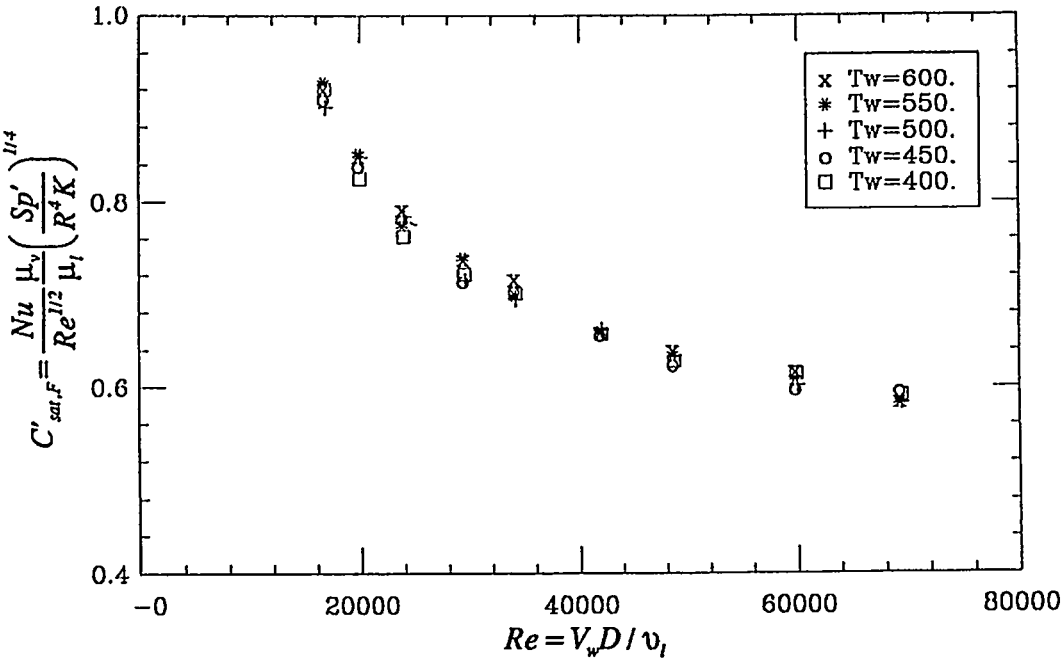

Fig. 7.15. Film boiling Nusselt number obtained in upward two-phase flow with superficial steam velocity at 4.5 m/s.

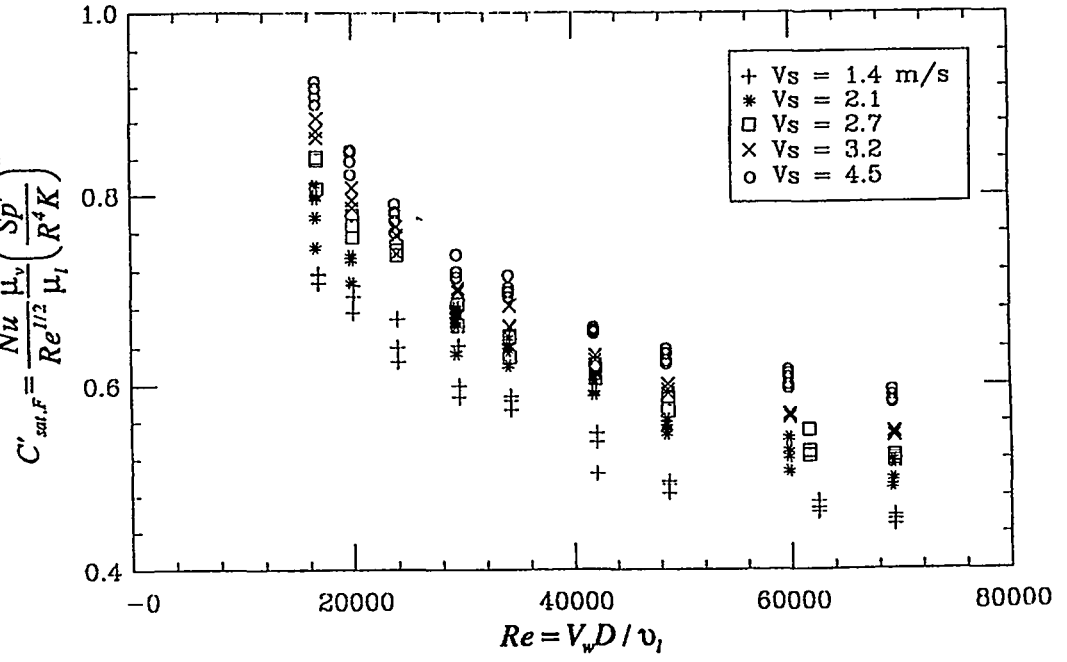

Fig. 7.16. All the film boiling heat transfer data obtained in upward two-phase flow, plotted in terms of superficial water velocity V_w. Repeated symbols represent data of different sphere superheats.

Instead of using the superficial water velocity, now, the water velocity (or called water phase velocity) U_w calculated from Eq. (7.1) is used as the characteristic velocity to define the Reynolds number

$$\mathrm{Re}_l = \frac{U_w D}{\upsilon_l} \tag{7.6}$$

Based on this definition, all the experiment data were re-plotted in Fig. 7.17 in terms of

$$C_{sat,F} = \frac{\mathrm{Nu}}{\mathrm{Re}_l^{1/2}} \frac{\mu_v}{\mu_l} \left(\frac{Sp'}{R^4 K}\right)^{1/4} \tag{7.7}$$

It shows that the effects of water flow and steam flow are correlated much better in this way, and the $C_{sat,F}$ ranges from 0.4 to 0.5, which is very close to the single-phase flow value of 0.5.

Figure 7.17 also clearly shows that there are two two-phase flow regimes. One is the upward mist-jet flow regime (include the nearly single-phase flow regime) with Reynolds number bigger than 7×10^4. In this regime, the data are well correlated by

$$\mathrm{Nu} = 0.42 \mathrm{Re}_l^{1/2} \frac{\mu_l}{\mu_v} \left(\frac{R^4 K}{Sp'}\right)^{1/4} \tag{7.8}$$

within a $\pm 10\%$ band. The other regime is the upward bubbly two-phase flow regime with the Reynolds number smaller than 7×10^4.

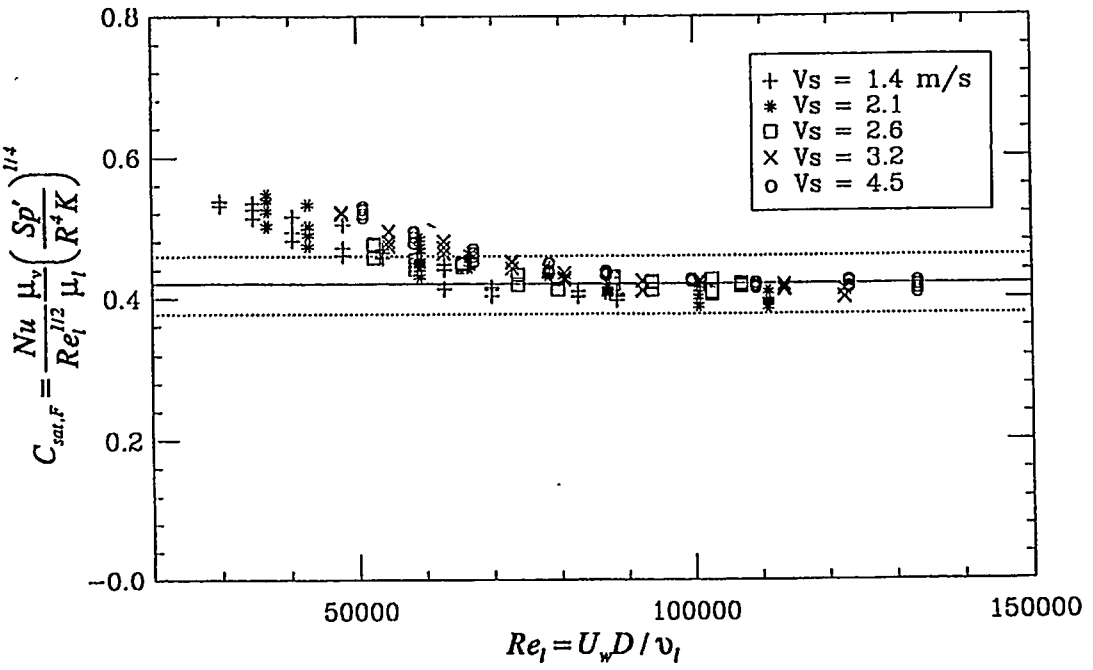

Fig. 7.17. All the film boiling heat transfer data obtained in upward two-phase flow, plotted in terms of superficial water velocity U_w. Repeated symbols represent data of different sphere superheats.

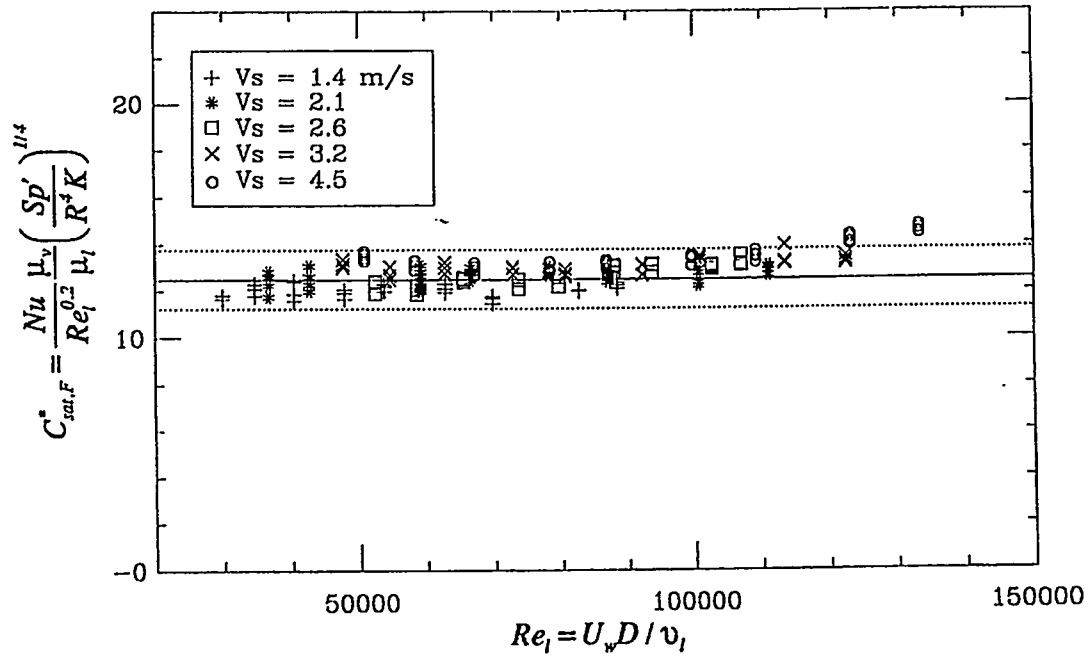

Fig. 7.18. All the film boiling heat transfer data obtained in upward two-phase flow, plotted in terms of Eq. (7.9). Repeated symbols represent data of different sphere superheats.

In order to correlated the data in the bubbly flow regime better, we tried to adjust the exponent on the Reynolds number in Eq. (7.7) to fit the experiment data. With an exponent of 0.2 on Reynolds number, all the experiment data are re-plotted in Fig. 7.18. The thus resulted correlation is

$$\mathrm{Nu} = 12.5\mathrm{Re}_l^{0.2}\frac{\mu_l}{\mu_v}\left(\frac{R^4K}{Sp'}\right)^{1/4} \tag{7.9}$$

which correlates the data within a ±10% band, for Reynolds number less than 1.2×10^5.

7.3 Downward Two-Phase Flow Generation, Void Fraction Measurement and Prediction

The downward two-phase flows were generated by injecting water jets into a downward steam flow. All the three tube-needle assemblies (see Section 3.2) were used as the water injector. Both water and steam flow rates can be adjusted independently to produce the downward two-phase flows. The superficial water velocity varies from 0.07 to 1.6 m/s, and the superficial steam velocity changes from 1.0 to 4.5 m/s.

The water jet velocity and the void fraction at the test sphere location can be predicated based on the geometry of the tube-needle assembly and the acceleration of the water due to the gravity and the drag force of the steam flow. The equations that govern the acceleration of the water drop are

$$\frac{dU_w}{dt} = g + \frac{3}{4}\frac{C_D}{D}\frac{\rho_v}{\rho_w} \mid U_s - U_w \mid (U_s - U_w) \tag{7.10}$$

$$\frac{dh}{dt} = U_w \tag{7.11}$$

where D is the sphere diameter and C_D is the drag coefficient.

In the computation, the inner diameter of the tube-needle was used to approximate the diameter of the water drops in the test section, and a value of 0.5 was chosen for the drag coefficient C_D. The drag force of the water-steam interaction is much smaller than the gravity in our case. So the calculation is not sensitive to the selections of the drop diameter and the drag coefficient. Once the water jet velocity at the tube outlet $U_{w,0}$ (calculated based on the water flow rate and tube-needle inner diameter) and the water drop-jet velocity at the test sphere location U_w are known, the water fraction and the void fraction can be calculated as follows

$$\alpha_w = \frac{U_{w,0}}{U_w}\frac{A_{hole}}{A_{base}} \tag{7.12}$$

$$\alpha = 1 - \alpha_w \tag{7.13}$$

The void fractions of the downward two-phase flow are also measured by the X-ray radiography as in the case of upward two-phase flow. Figures 7.19, 7.20 and 7.21 show the X-ray pictures of the downward two-phase flows at the center part of the test section (where the test sphere is located) with No.1, No.2 and No.3 tube-needle assemblies respectively. These radiographs are obtained with the superficial steam velocity at 4.5 m/s, and the radiographs with other superficial steam velocities 1.0, 1.4, 2.1 and 3.2 m/s are quite the same. These radiographs clearly show that when the water jet velocity is low, the two-phase flow looks more like a droplet flow; and when the water jet velocity is high, the two-phase flow shows more like a jet flow.

Figure 7.22 shows typical X-ray pictures of the sphere film boiling in downward two-phase flow. We cannot get detailed information of the vapor film on the sphere, although somewhat higher void fraction regions can be seen behind the spheres.

The measured and the predicted void fractions are compared in Figs. 7.23, 7.24 and 7.25 for the two-phase flows generated by No.1, No.2 and No.3 tube-needle assemblies, respectively. They show that the predicted void fractions reasonably agree with the X-ray measurements. Therefore, Eqs. (7.10) through (7.13) can be used to calculate the water velocity and void fraction of the two-phase flow at the test sphere location.

With all combinations of the water flow rate and steam flow rate, the downward two-phase flows cover void fraction range from 70% to 95%, with the water velocity ranges from 1.9 to 6.5 m/s and the steam velocity ranges from 1.1 to 9.0 m/s.

7.4 Film Boiling of Downward Two-Phase Flows

All the three tube-needle assemblies are used in the downward two-phase flow film boiling heat transfer experiment. With each tube-needle assembly, the superficial steam flow rate were first set at one of following values 1.0, 1.4, 2.1, 3.2 and 4.5 m/s, then transient mode runs were carried out by varying the water flow rate. Typical downward two-phase heat transfer experimental data are tabled in Appendix F.

Defining the Reynolds number with the superficial water velocity, as in Eq. (7.3), the experiment data are plotted in terms of the saturated single-phase film boiling heat transfer characteristic $C'_{sat,F}$ in Figs. 7.26, 7.27 and 7.28 for No.1, No.2 and No.3 tube-needle assemblies respectively. In these figures the superficial steam velocity are shown as the parameters, and the repeated symbols represent data of different sphere superheats (from 400 to 800 °C). These figures indicate that, as in the case of upward single- and two-phase flows, the effect of sphere superheat is well correlated in all the cases of downward

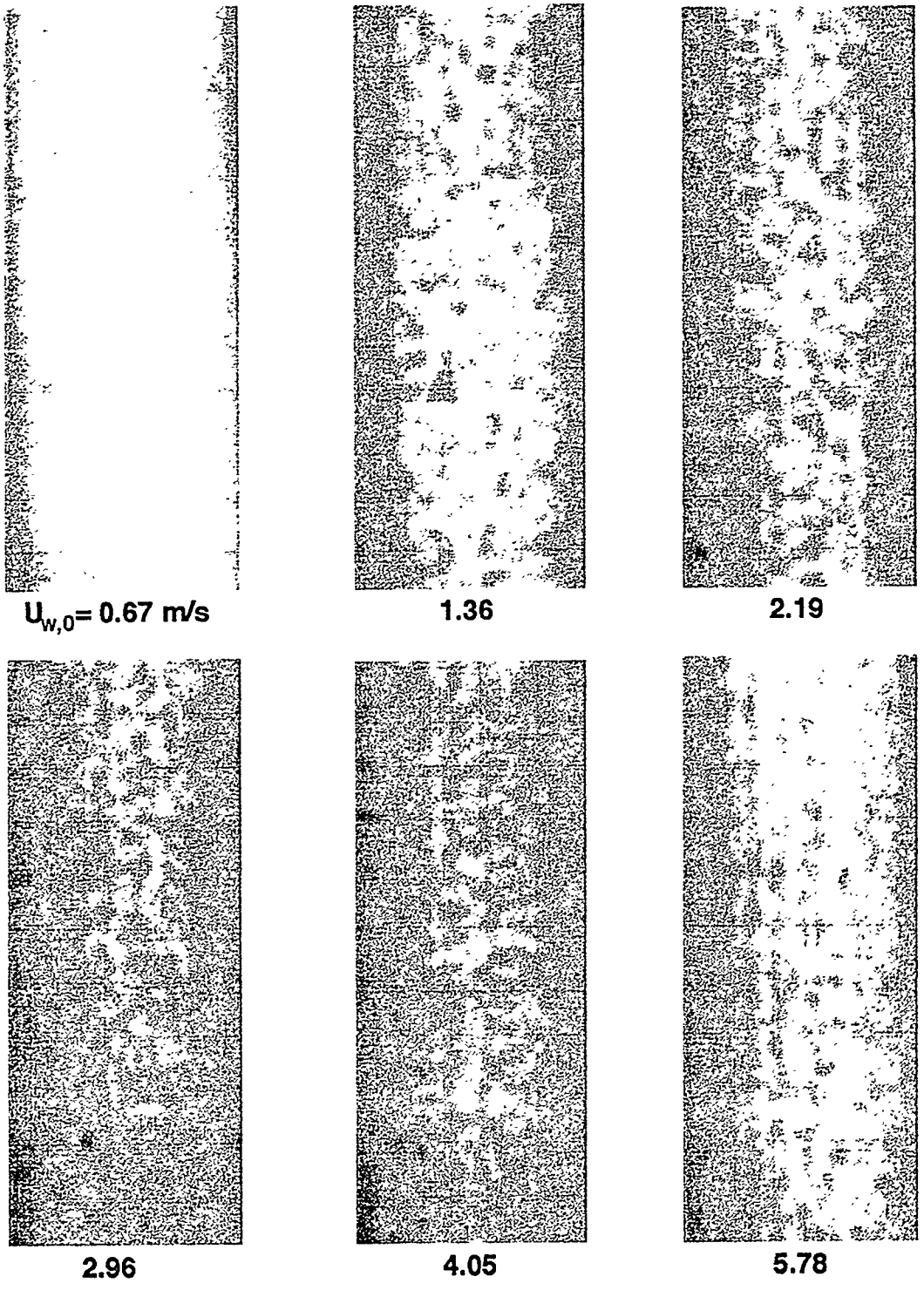

Fig. 7.19 X-Ray radiographs of downwrd two-phase flow generated by No. 1 tube-needle assembly.

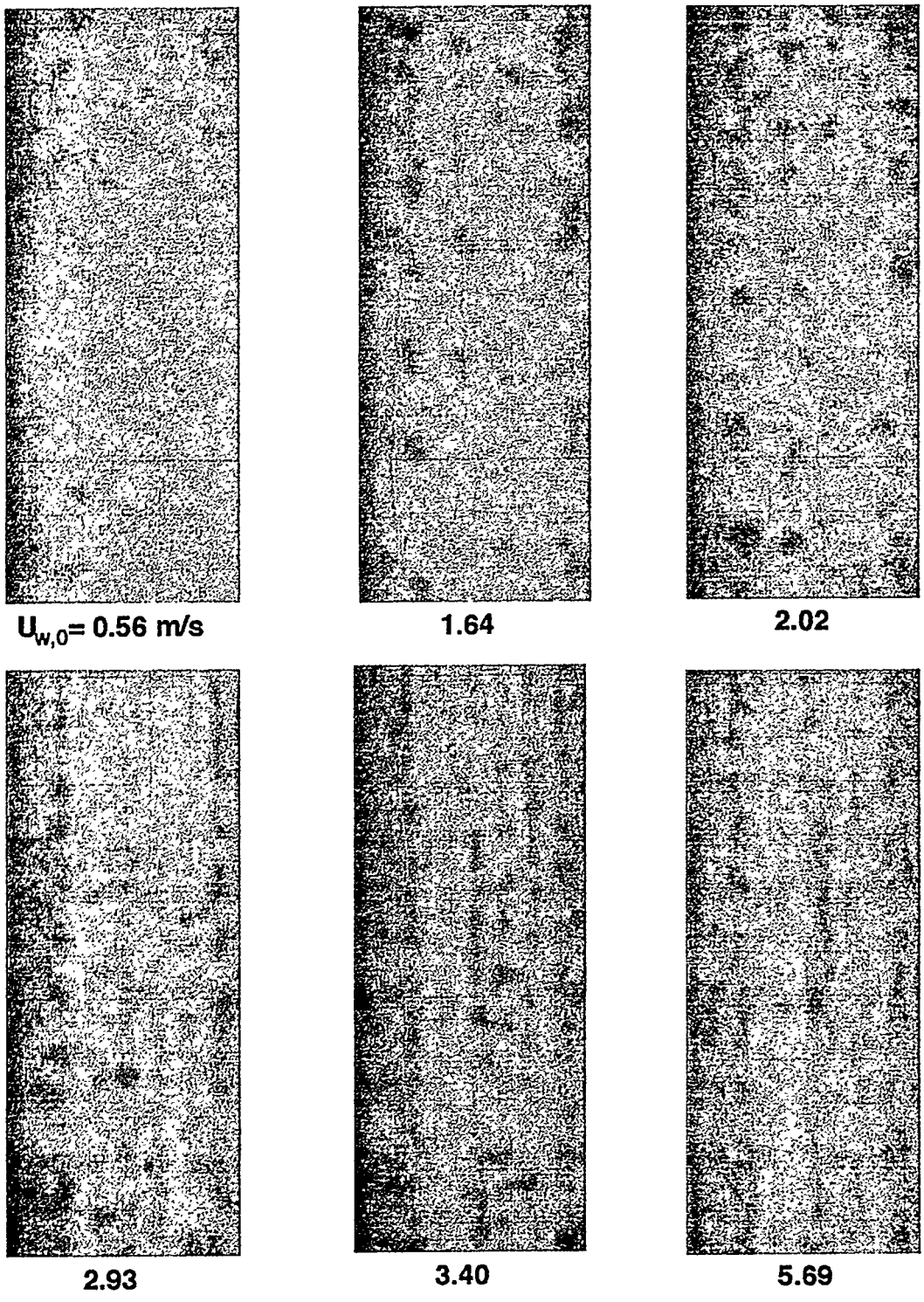

Fig. 7.20 X-Ray radiographs of downwrd two-phase flow generated by No. 2 tube-needle assembly.

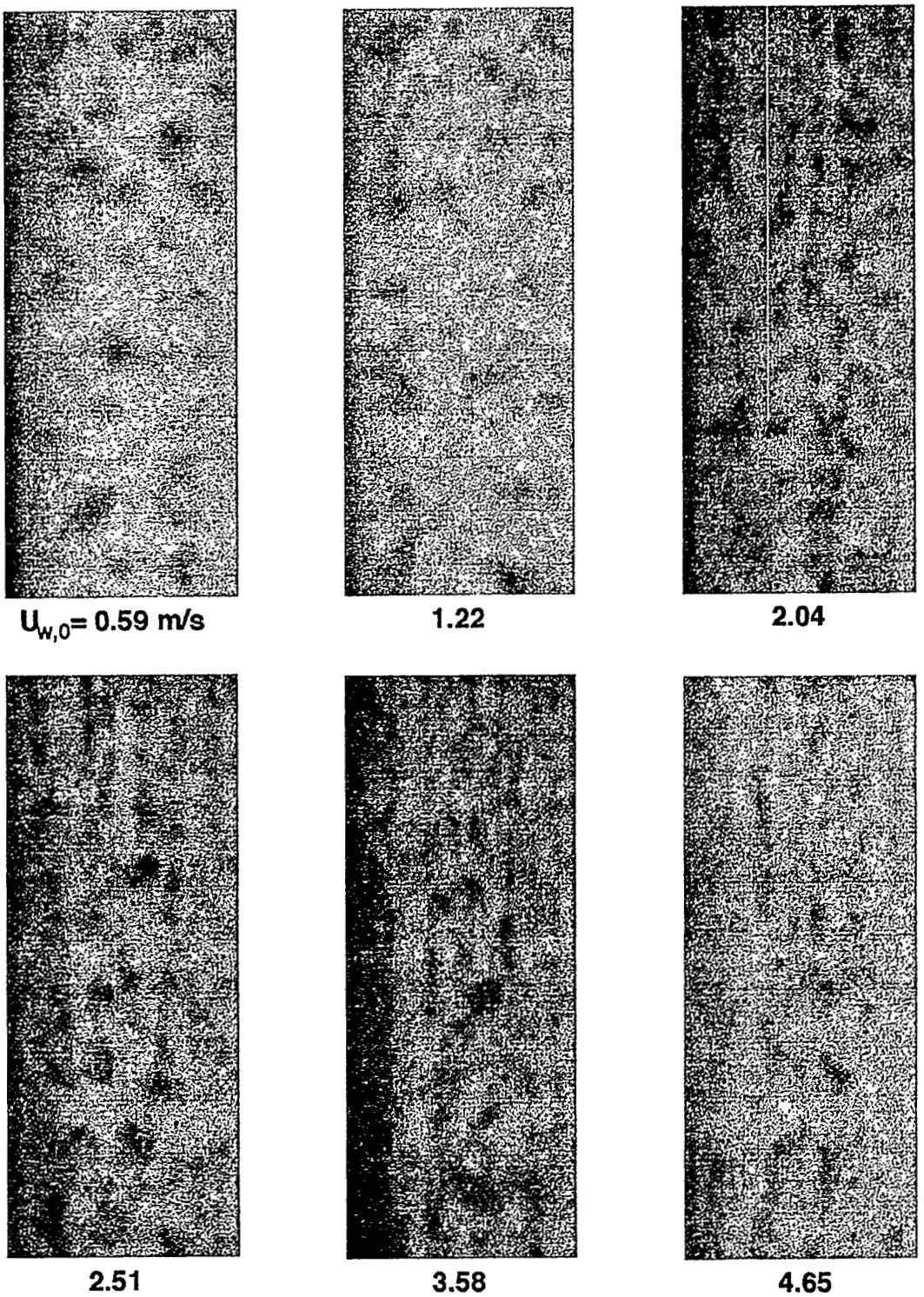

Fig. 7.21 X-Ray radiographs of downwrd two-phase flow generated by No. 3 tube-needle assembly.

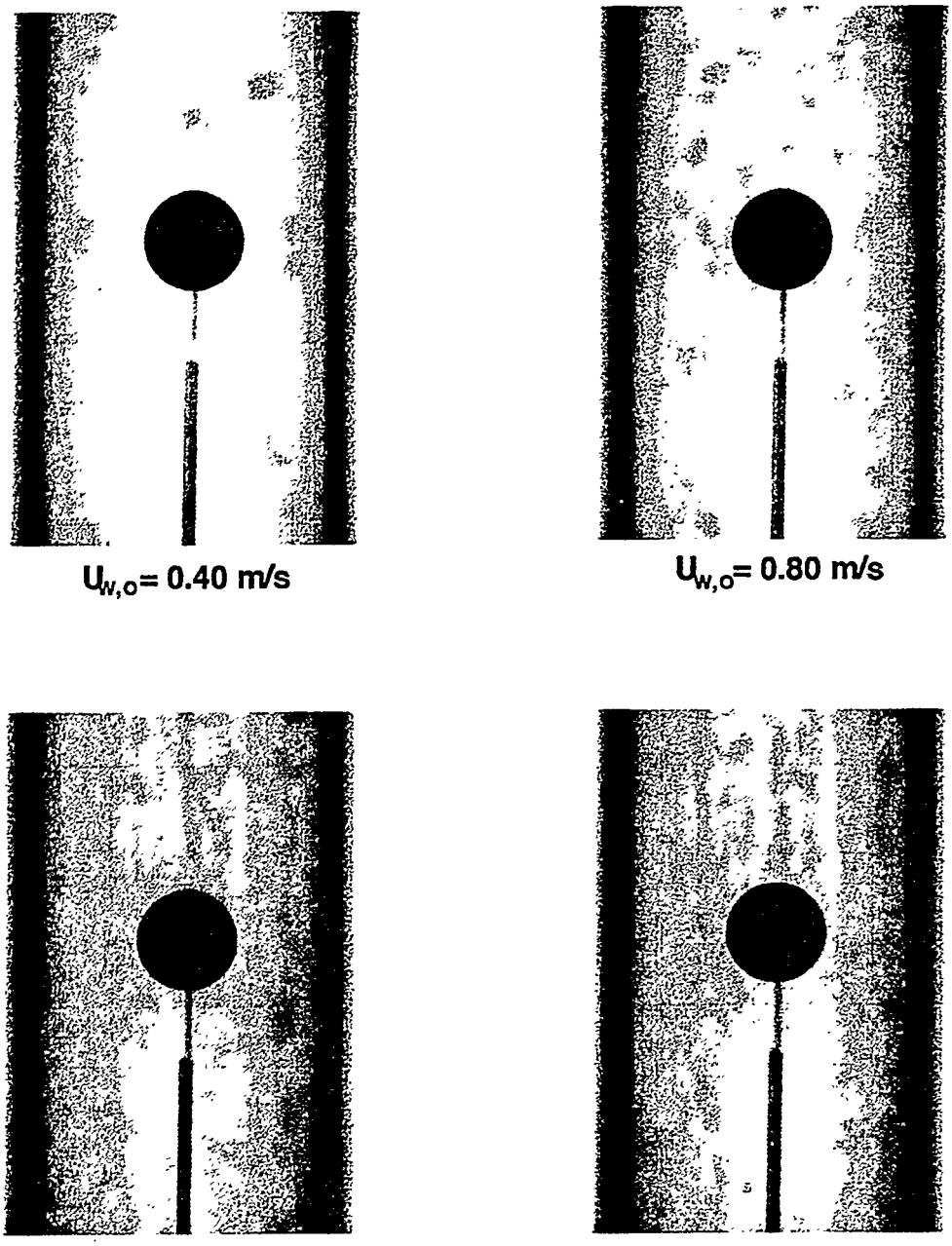

Fig. 7.22 X-Ray radiographs of film boiling on sphere in downward two-phase flow generated by No. 1 tube-needle assembly.

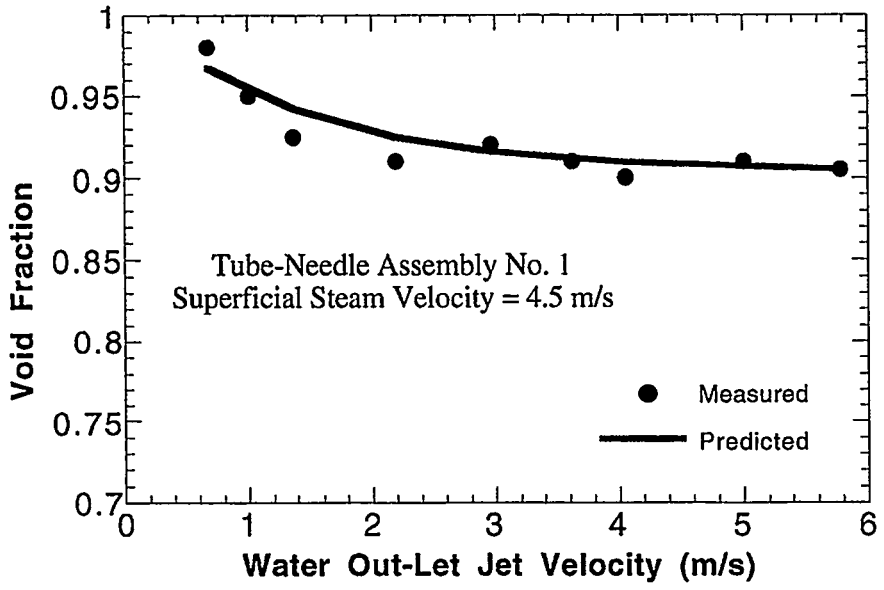

Fig. 7.23. Comparison of measured void fraction with the predicted.

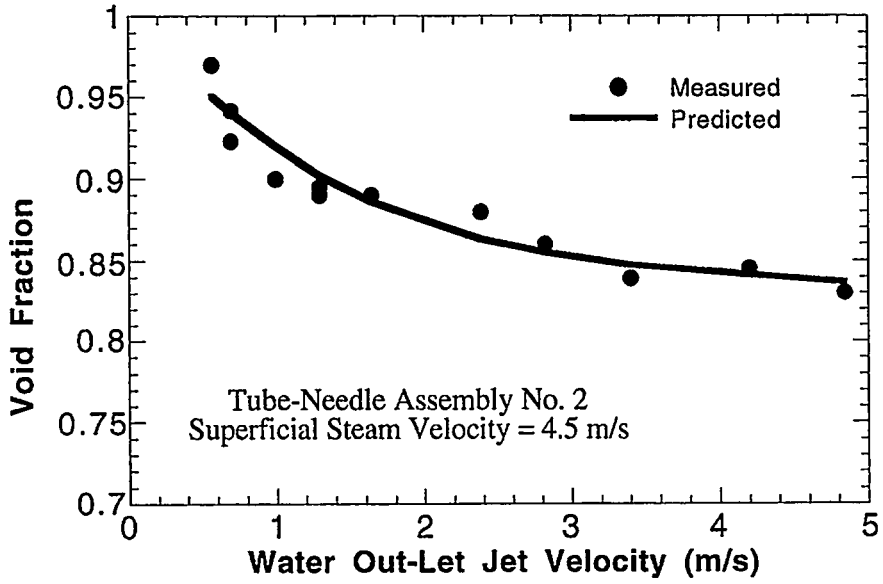

Fig. 7.24. Comparison of measured void fraction with the predicted.

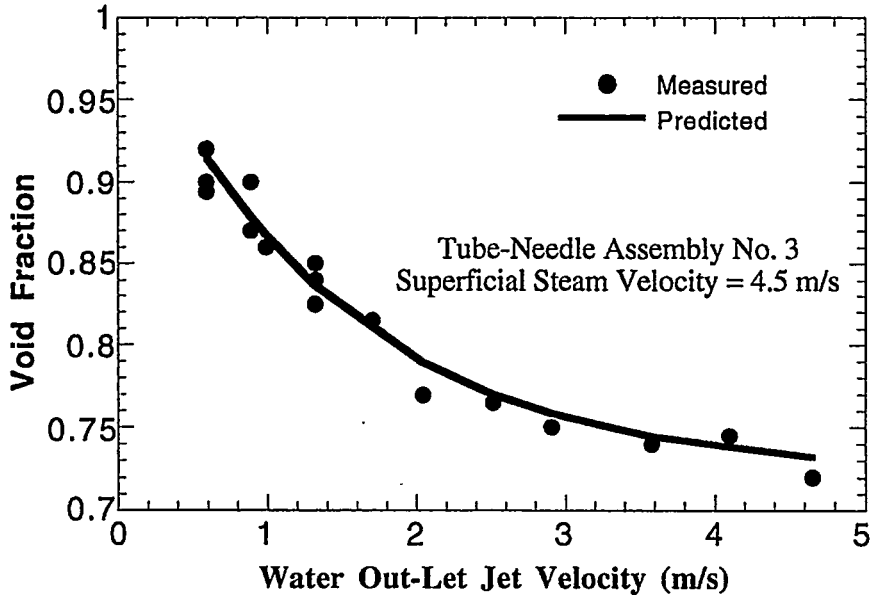

Fig. 7.25. Comparison of measured void fraction with the predicted.

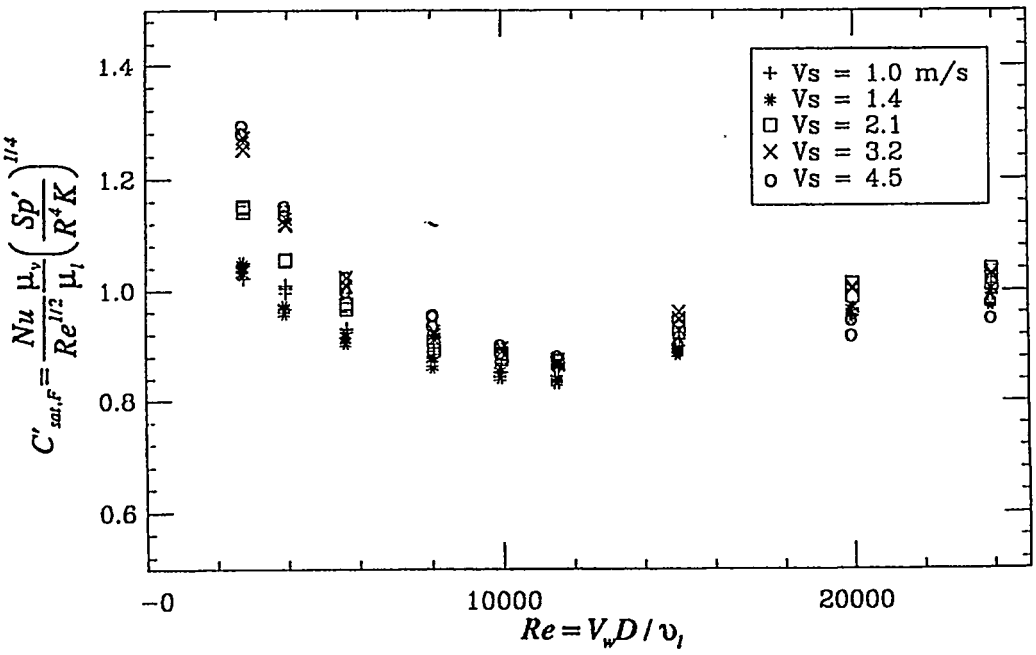

Fig. 7.26. Film boiling heat transfer data obtained in downward two-phase flow generated by No.1 tube-needle assembly, plotted in terms of superficial water velocity V_w.

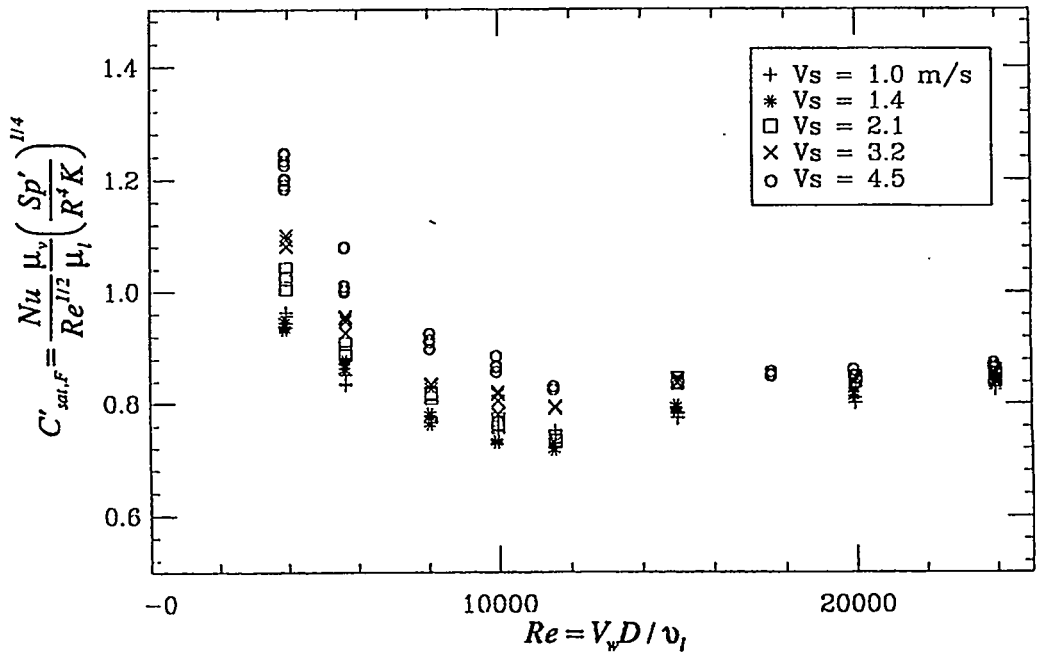

Fig. 7.27. Film boiling heat transfer data obtained in downward two-phase flow generated by No.2 tube-needle assembly, plotted in terms of superficial water velocity V_w.

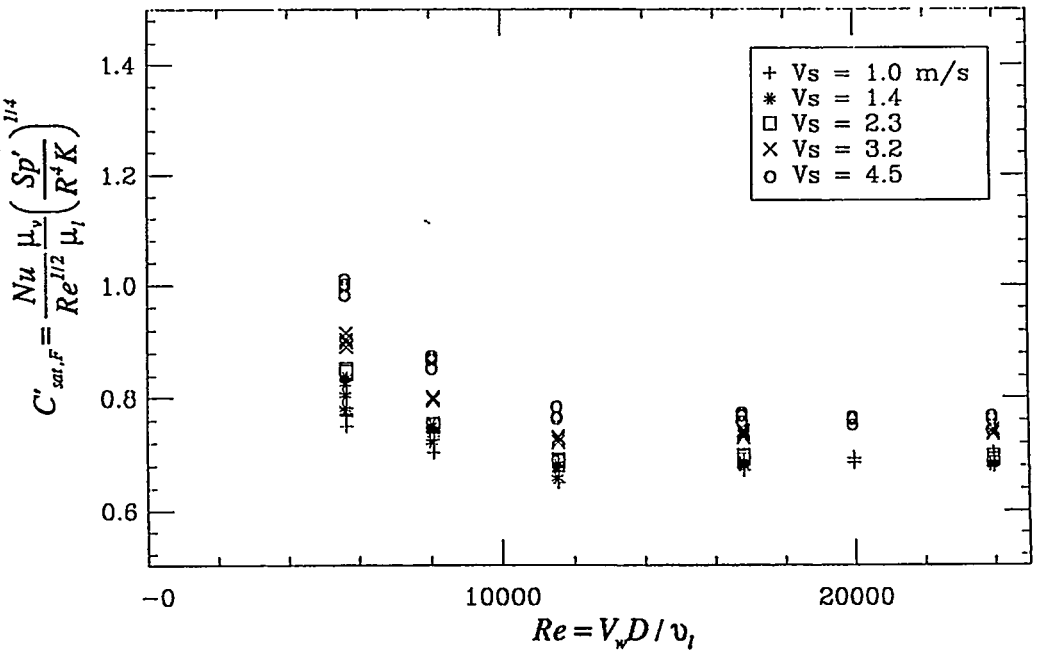

Fig. 7.28. Film boiling heat transfer data obtained in downward two-phase flow generated by No.3 tube-needle assembly, plotted in terms of superficial water velocity V_w.

two-phase flows. They also show that the heat transfer characteristic $C'_{sat,F}$ is no longer a constant of 0.5, and it varies from 0.7 to 1.3. When the Reynolds number is high, the steam velocity has very little or no effect on the $C'_{sat,F}$; but when the Reynolds number is small, the steam velocity has a significant effect on the $C'_{sat,F}$. Comparing the three figures that obtained with different tube-needle assemblies, it is obvious that the smaller the tube inner diameter, the higher the heat transfer characteristic $C'_{sat,F}$.

As in the case of upward two-phase flow, we now define the Reynolds number Re_l based on the water velocity at the test sphere location, which is calculated by Eqs. (7.10) through (7.13). In terms of the heat transfer characteristic $C_{sat,F}$, the data obtained with superficial steam velocities at 1.0 and 4.5 m/s are plotted in Figs. 7.29 and 7.30 respectively, with the number of tube-needle assembly as the parameter. It is obvious that: the $C_{sat,F}$ is still not a constant; it increases with the Reynolds number; the smaller the diameter of the tube diameter, the higher is the $C_{sat,F}$; the steam velocity almost has no influence on the $C_{sat,F}$. In general, based on the water-phase velocity, unlike the upward two-phase flow, $C_{sat,F}$ is not a proper heat transfer characteristic to correlate the downward two-phase flow heat transfer data.

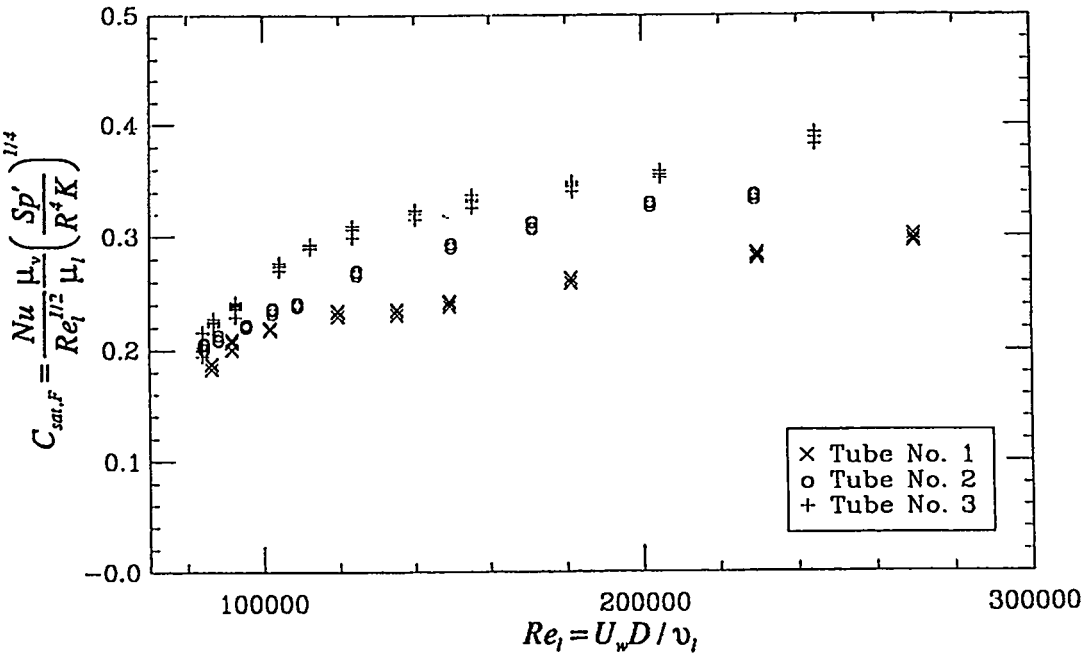

Fig. 7.29. Film boiling heat transfer data obtained in downward two-phase flow with superficial steam velocity at 1.0 m/s, plotted in terms of $C_{sat.F}$.

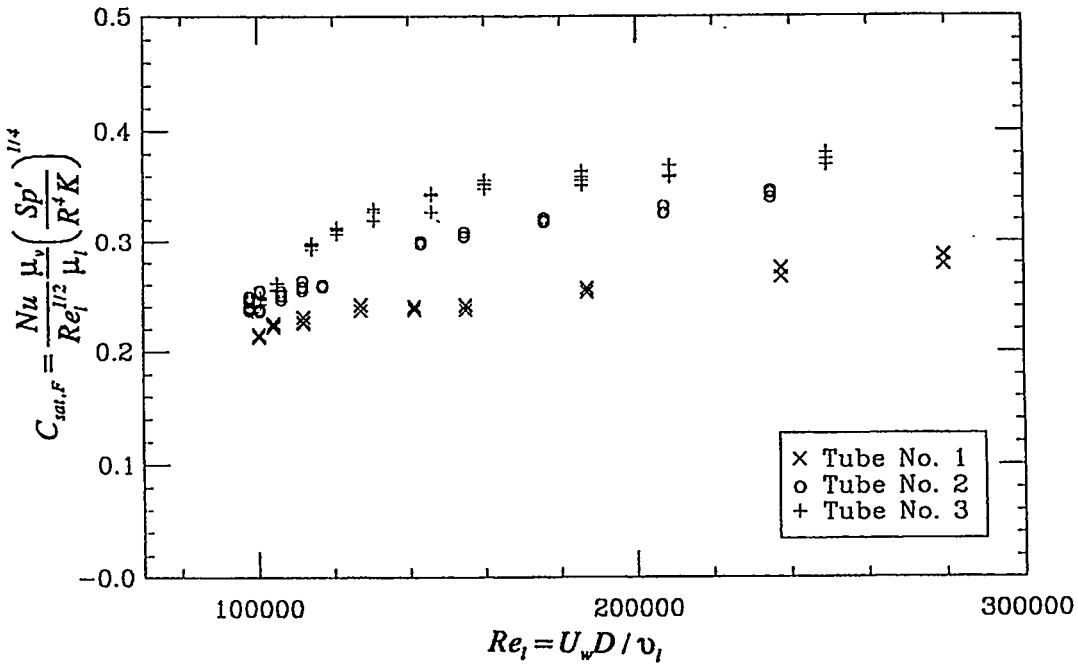

Fig. 7.30. Film boiling heat transfer data obtained in downward two-phase flow with superficial steam velocity at 4.5 m/s, plotted in terms of $C_{sat.F}$.

There are reasons for this. First, in the upward two-phase flows the water fractions are higher (from 35% to 80%) than those in the downward two-phase flows (from 5% to 30%). Secondly, in the case of upward two-phase flows, the gravity is opposite to the flow direction, so it helps to accumulate more water at the front stagnation point than in the case of downward two-phase flows. So for the film boiling in upward two-phase flows, from the sphere point of view, it is like in a saturated single-phase water flow. This is why the saturated single-phase film boiling heat transfer characteristic $C_{sat,F}$ still works well for the film boiling in upward two-phase flows. On the other hand, in the downward two-phase flows, there is no much water accumulated at the front stagnation point, and the film boiling may be thought as in a low density single-phase flow with an equivalent density

$$\rho_e = \alpha_w \rho_{water} \tag{7.14}$$

Substituting this equivalent density as the liquid phase density into the heat transfer characteristic $C_{sat,F}$, Eq. (7.7), we have new heat transfer characteristic

$$C_{D,two} = \frac{\mathrm{Nu}}{\mathrm{Re}_l^{1/2}} \frac{\mu_v}{\mu_l} \left(\frac{Sp'}{R^4 K} \right)^{1/4} \frac{1}{\alpha_w^{1/4}} \tag{7.15}$$

which is just the $C_{sat,F}$ divided by a factor of $\alpha_w^{1/4}$.

With the new heat transfer characteristic $C_{D,two}$, the experiment data that plotted in Figs. 7.29 and 7.30 are re-plotted in Figs. 7.31 and 7.32 respectively. In the same way, Fig. 7.33 shows all the data of downward two-phase flow, which represents all the data obtained with different sphere superheats, different tube-needle assemblies, and different steam and water velocities. It is obvious that this heat transfer characteristic correlates well all the effects, except that it increases slightly with the Reynolds number Re_l (or water-phase velocity). Moreover, the $C_{D,two}$ only varies only from 0.4 to 0.5, and it is very close to the saturated single-phase value $C_{sat,F} = 0.5$. So, in an approximation sense, the heat transfer characteristic Eq. (7.15) can be used to correlate the downward two-phase film boiling heat transfer in the following formula

$$\mathrm{Nu} = 0.45\mathrm{Re}_l^{1/2} \frac{\mu_l}{\mu_w} \left(\frac{R^4 K}{Sp'} \right)^{1/4} \alpha_w^{1/4} \tag{7.16}$$

within a ±20% band.

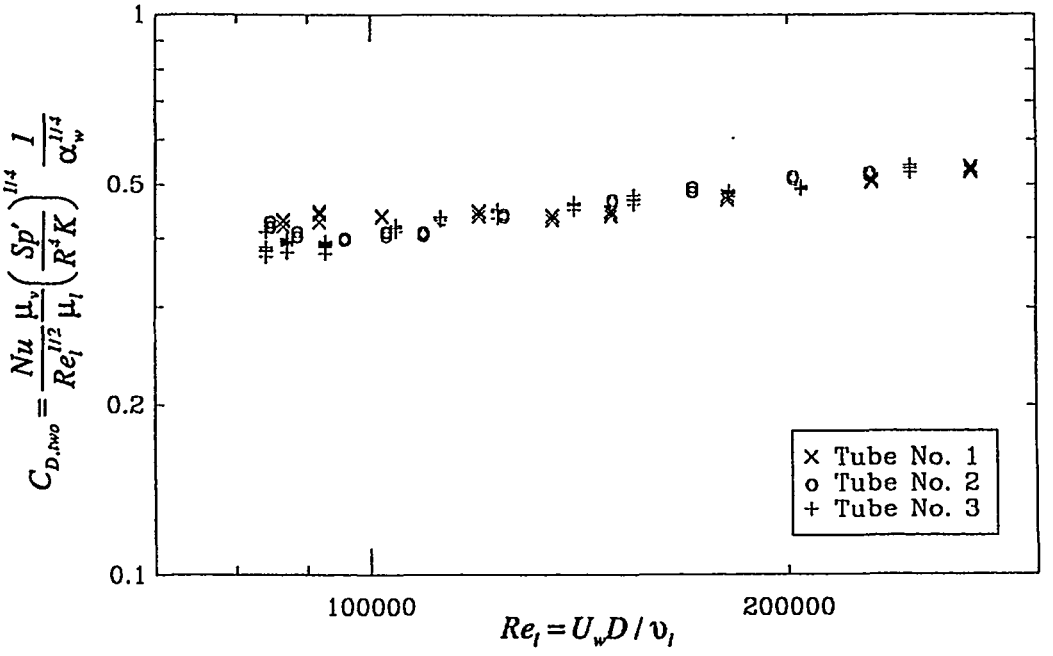

Fig. 7.31. Film boiling heat transfer data obtained in downward two-phase flow with superficial steam velocity at 1.0 m/s, plotted in terms of $C_{D,two}$.

The systematically increasing of the $C_{D,two}$ with Re_l suggests us that the exponent on the Reynolds number in Eqs. (7.15) or (7.16) should be higher. By fitting the correlation with the experimental data, it was found that a power of 0.75 could be used instead of 0.5.

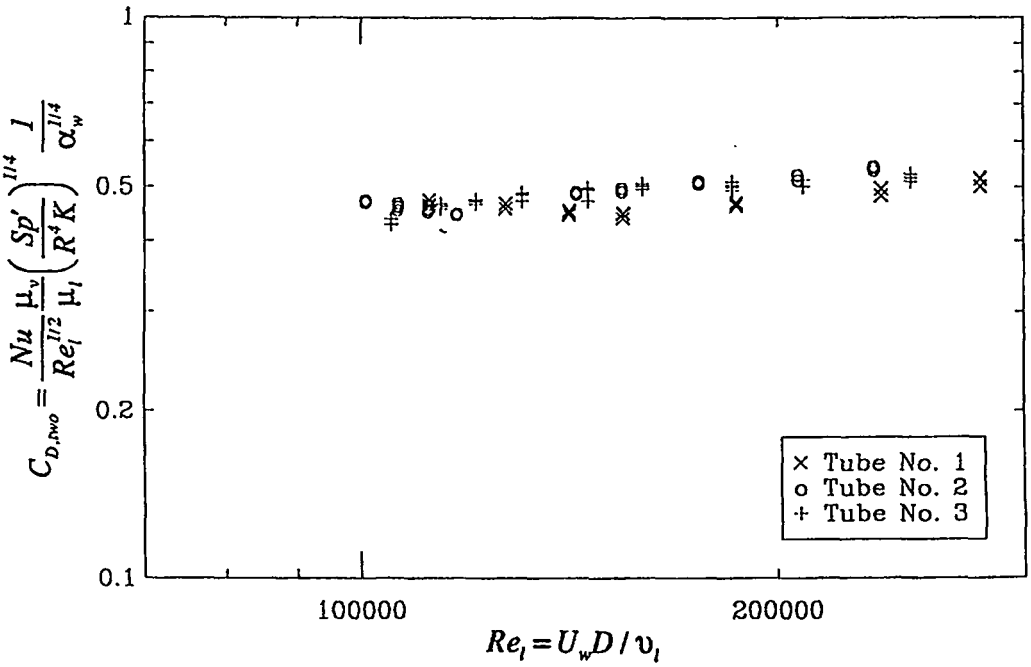

Fig. 7.32. Film boiling heat transfer data obtained in downward two-phase flow with superficial steam velocity at 4.5 m/s, plotted in terms of $C_{D,two}$.

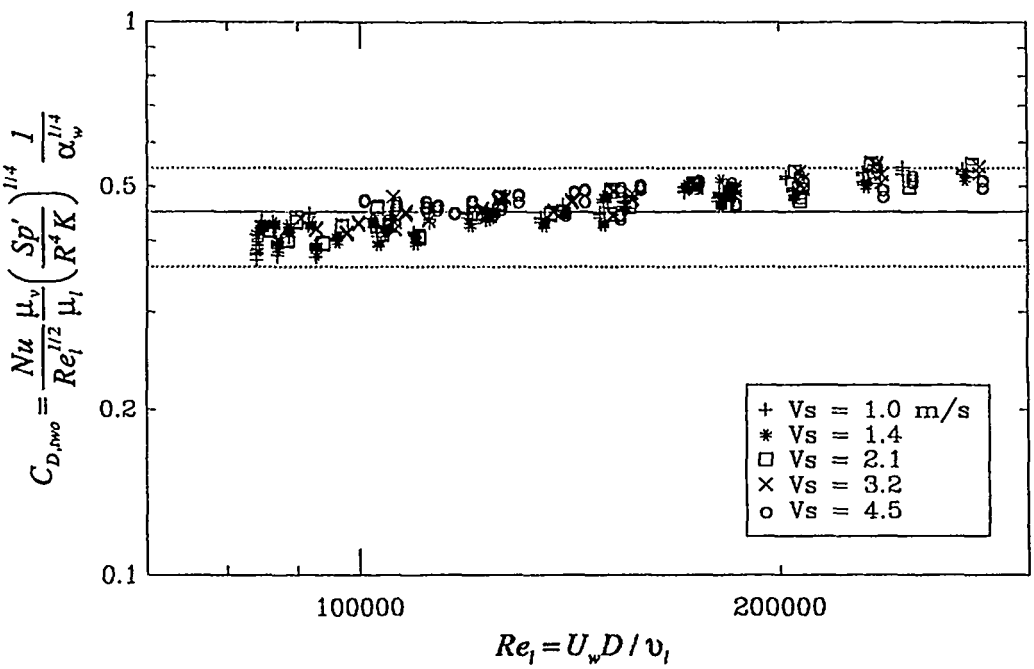

Fig. 7.33. All the film boiling heat transfer data obtained in downward two-phase flow with superficial steam velocity at 1.0 m/s, plotted in terms of $C_{D,two}$. Repeated symbols represent data from different tube-neddle assemblies and with different sphere superheats.

In terms of the further modified new heat transfer characteristic

$$C^*_{D,two} = \frac{\mathrm{Nu}}{\mathrm{Re}_l^{0.75}} \frac{\mu_v}{\mu_l} \left(\frac{Sp'}{R^4 K} \right)^{1/4} \frac{1}{\alpha_w^{1/4}} \tag{7.17}$$

all the downward two-phase data are shown in Fig. 7.34. It correlates the data much better than $C_{D,two}$, and the corresponding correlation is

$$\mathrm{Nu} = 0.0235 \mathrm{Re}_l^{0.75} \frac{\mu_l}{\mu_v} \left(\frac{R^4 K}{Sp'} \right)^{1/4} \alpha_w^{1/4} \tag{7.18}$$

which correlates the data within a ±10% band.

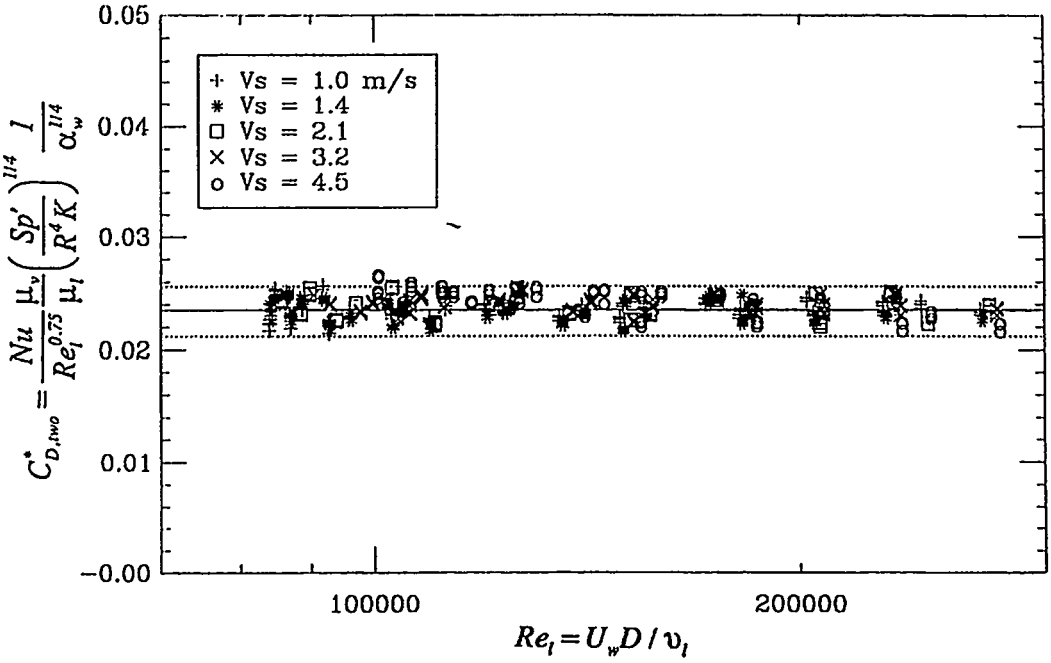

Fig. 7.34. All the film boiling heat transfer data obtained in downward two-phase flow with superficial steam velocity at 4.5 m/s, plotted in terms of $C^*_{D,two}$. Repeated symbols represent data from different tube-neddle assemblies and with different sphere superheats.

7.5 Conclusion

The void fractions of upward and downward two-phase flow were measured by the X-ray radiography. The calculated void fraction of downward two-phase flow, which is based on the acceleration due to the gravity and steam drag, agrees well with the radiographic measurements.

The upward two-phase flows cover void fraction range from 0.2 to 0.65 with the water velocity from 0.6 to 3.2 m/s and the steam velocity from 3.0 to 9.0 m/s. When the water velocity is low, the flow appears like a bubbly flow; when the water velocity is high, the flow shows like a mist-jet flow. Based on the water velocity, the film boiling heat transfer data can be essentially correlated by the saturated single-phase heat transfer characteristic $C_{sat,F}$, with an equation of

$$\mathrm{Nu} = 0.42\mathrm{Re}_l^{1/2}\frac{\mu_l}{\mu_v}\left(\frac{R^4K}{Sp'}\right)^{1/4} \tag{7.19}$$

The modified correlation

$$\mathrm{Nu} = 12.5\mathrm{Re}_l^{0.2}\frac{\mu_l}{\mu_v}\left(\frac{R^4K}{Sp'}\right)^{1/4} \tag{7.20}$$

fits the experimental data better (within a $\pm 10\%$ band), for $3 \times 10^4 < \mathrm{Re}_l < 1.2 \times 10^5$.

The downward two-phase flows are droplet-jet flows and cover void fraction from 0.7 to 0.95 with water velocity from 1.9 to 6.5 m/s and steam velocity from 1.1 to 9.0 m/s. Based on the water phase velocity and with an adjustment factor $\alpha_w^{1/4}$, the saturated single-phase film boiling heat transfer characteristic $C_{sat,F}$ can also correlate all the downward two-phase film boiling heat transfer data within a $\pm 20\%$ band with the equation

$$\mathrm{Nu} = 0.45\mathrm{Re}_l^{1/2}\frac{\mu_l}{\mu_v}\left(\frac{R^4K}{Sp'}\right)^{1/4}\alpha_w^{1/4} \tag{7.21}$$

With an increase of the exponent on the Reynolds number (from 0.5 to 0.75), the following equation fits the experimental data even better (within a $\pm 10\%$ band)

$$\mathrm{Nu} = 0.0235\mathrm{Re}_l^{0.75}\frac{\mu_l}{\mu_v}\left(\frac{R^4K}{Sp'}\right)^{1/4} \tag{7.22}$$

8 FILM BOILING FROM A MULTI-SPHERE ARRAY

In the analysis of fuel-coolant interaction (or premixing), the concern about film boiling is from a group of spheres instead of one sphere. Obviously, the presence of solid spheres and the addition of vapor from the film boiling will change the local water flow velocity and the void fraction. It may be that the single sphere film boiling correlations are not applicable to the film boiling from a multi-sphere group. However, because the local velocity and void fraction around the sphere in question already represent all the effects, as long as they are known, the film boiling correlation for a single sphere in two-phase flow could be used to calculate the film boiling heat transfer from a sphere that is among a multi-sphere group.

In order to verify this, the "on-line" local velocity and void fraction should be measured with multi-sphere array present in the test section and film boiling on. But, it is impossible to get these measurements with the present X-ray radiographic method. However, in this work, as a preliminary step towards the problem of film boiling from multi-sphere arrays, the influence on heat transfer with the presence of four spheres in the front of the test sphere are investigated experimentally.

The experiments have been conducted in upward single-phase flow, upward two-phase flow and downward two-phase flow. The multi-sphere array is constructed as illustrated in Fig. 8.1, with the back-center sphere as the test sphere. All these experiments are carried out with transient mode runs. All the four fore-spheres and the test sphere were heated up and experience cool down transients (in film boiling condition) from 900 °C to quench. In all the multi-sphere experiments, the runs were conducted and the data from the test sphere were reduced in the same way as in the corresponding single sphere cases, and the reduced heat transfer characteristics are compared with those obtained with a single sphere.

8.1 Film Boiling From A Multi-Sphere Array in Saturated Single-Phase Flows

For film boiling from a multi-sphere array in saturated single-phase flows, the superficial water velocity is used to characterize the flow. The experiment data is shown in Fig. 8.2 in terms of the pool film correlation (1/4-power law). It shows that for $Fr^{1/2} < 1.0$, the $Nu/(Ar/Sp')^{1/4}$ values are about 0.87, which is higher than the 0.64 that is obtained for a single sphere. The same data are re-plotted in Fig. 8.3 in terms of forced convection film boiling correlation. For $Fr^{1/2} > 2.0$, the heat transfer characteristic is about 0.4, which is lower than the 0.5 that is obtain for a single sphere.

More clearly, the comparison is given in Fig. 8.4 in terms of the ratios of the multi-sphere experimental data over the general correlation for a single sphere, Eq. (6.5). It is obvious that, in the pool film boiling regime, the multi-sphere data are about 20% higher than that of the single sphere. This is because the boilings on the fore-spheres make the convection in the water more turbulent and thus enhance the film boiling heat transfer on the test sphere. However, in the forced convection regime, the boiling on the fore-spheres creates some void fraction and, possibly, some superheated vapor in the water flow, so the film boiling heat transfer decreases, which is also about 20% .

8.2 Film Boiling From A Multi-Sphere Array in Upward Two-Phase Flows

As in the case of single-sphere film boiling in upward two-phase flows, the upward two-phase flow was created by injecting saturated steam into a saturated water flow through the No. 1 tube-needle assembly. The runs were carried out in three subsets with the superficial steam velocity at 1.4, 2.7 and 4.5 m/s, respectively. For each subset, the superficial water velocity was changed from 0.3 to 1.4 m/s to carry out each run.

Again, as in the case of single-sphere upward two-phase flow, the data were reduced with water and steam properties at film temperatures and with the coming water-phase velocity as the characteristic velocity. In terms of Eq. (7.8), which is more applicable for high Reynolds number, the data are shown in Fig. 8.5. In terms of Eq. (7.9), which is more proper for low Reynolds number, the same data are shown in Fig. 8.6. In these figures, the repeated symbols represent the data of different sphere superheats. They show clearly that, as in the forced convection single-phase flow, the film boiling heat transfer decreases about 15% when four boiling spheres are placed in the front of the test sphere. The reason for this is that the boiling on the fore-spheres increases the void fraction and may produce superheated vapor in the front of the test sphere.

8.3 Film Boiling From A Multi-Sphere Array in Downward Two-Phase Flows

Basically, here we just repeat the film boiling heat transfer experiment in downward two-phase flow with four fore-spheres placed in the front of the test sphere, as shown in Fig. 8.1. The experiment was carried out in three subsets with No. 1, No. 2 and No .3 tube-needle assemblies respectively. For each subset, the superficial steam velocity was set at certain value (1.0, 2.1 or 4.5 m/s) first, and then the water velocity was changed to make each run.

The experiment data are reduced in the same way as in the case of a single-sphere. The data obtained with No. 1, No. 2 and No. 3 tube-needle assemblies are shown in Figs.

8.7 through 8.9 respectively. For each case, the data are plotted in terms of Eq. (7.16) and Eq. (7.18) respectively in (a) and (b), and the repeated symbols represent the data with different sphere superheats. These data indicate that, in all cases, the film boiling heat transfer increases significantly with four boiling spheres placed in the front of the test sphere. They also show that the bigger the tube-needle inner diameter, the higher is the increase. The reason of this enhancement is quite obvious: the presence of the fore-spheres concentrates more water towards the front of the test sphere, which yields high water fraction and high water flow velocity.

8.4 Conclusion

The film boiling from a multi-sphere group has also been investigated through a five-sphere array with four spheres placed in the front of the test sphere. The experiments indicate that: (1) the presence of boiling spheres in the front of the test sphere decreases the film boiling heat transfer in the upward two-phase flow and increases the heat transfer in downward two-phase flow; and (2) in a saturated single-phase upward flow, the presence of boiling spheres in the front of the test sphere increases the heat transfer in pool film boiling regime and decreases the heat transfer in forced convection film boiling regime. These trends are consistent with the expectation using the single-sphere correlation and the theoretical interpretation in conjunction with the flow field changes due to the presence of the four spheres ahead of the test sphere.

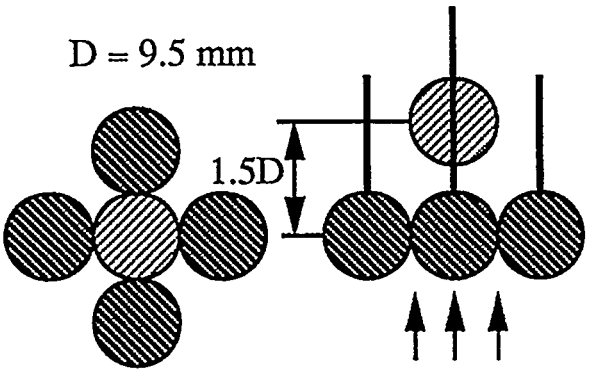

Fig. 8.1. Schematic of the multi-sphere array.

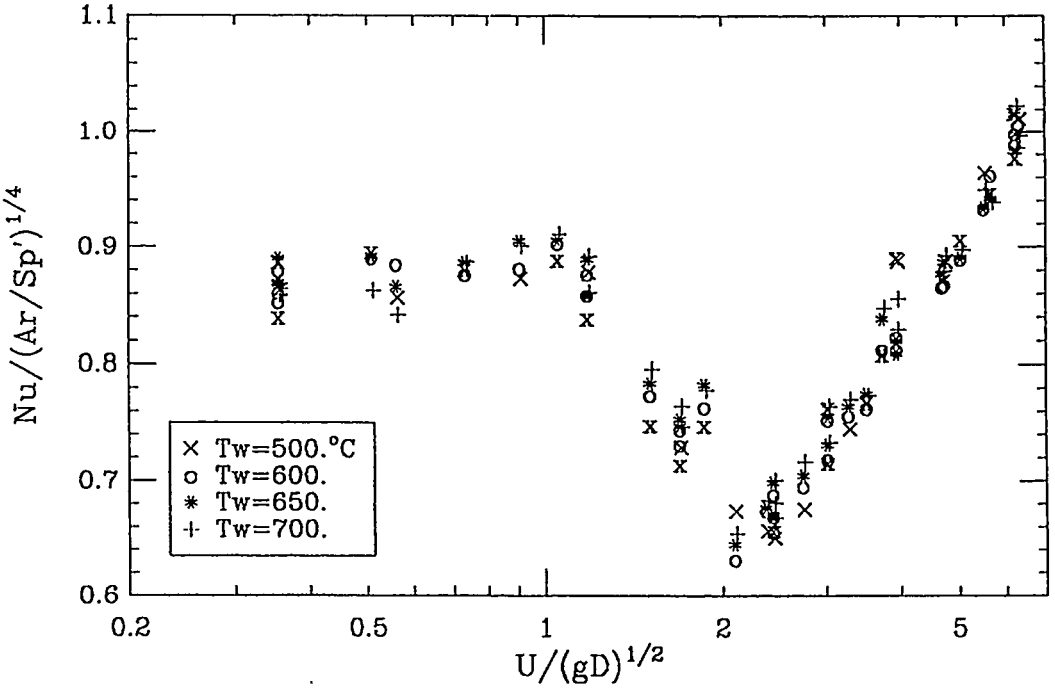

Fig. 8.2. Heat transfer data of film boiling from multi-sphere array in saturated single-phase flow, plotted in terms of pool film boiling correlation.

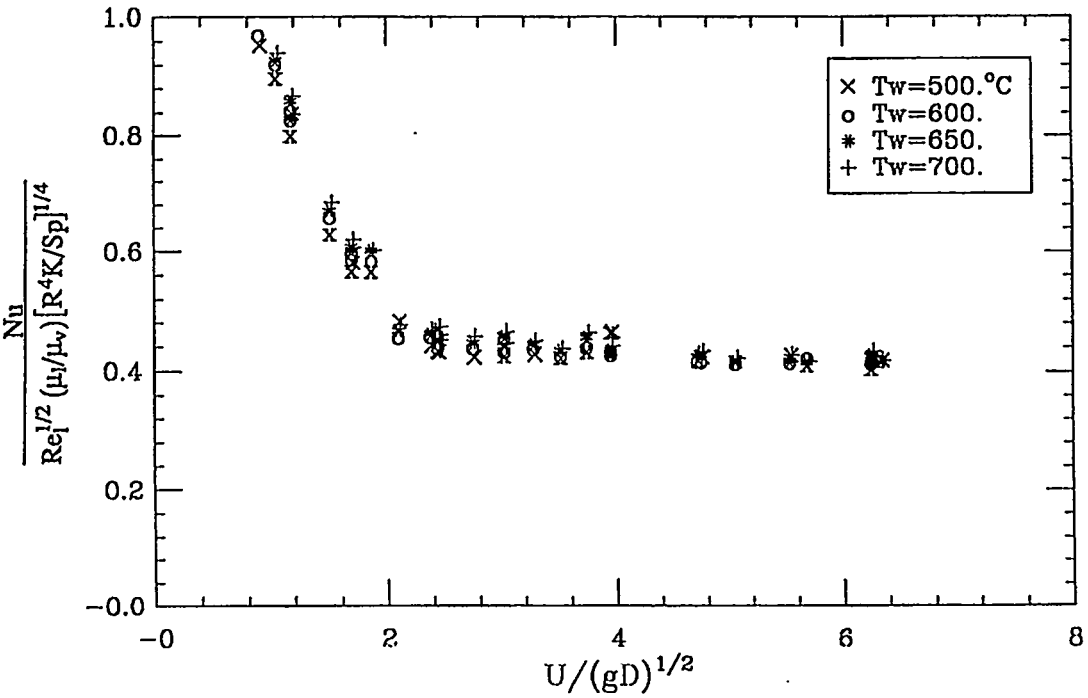

Fig. 8.3. Heat transfer data of film boiling from multi-sphere array in saturated single-phase flow, plotted in terms of forced convection film boiling correlation.

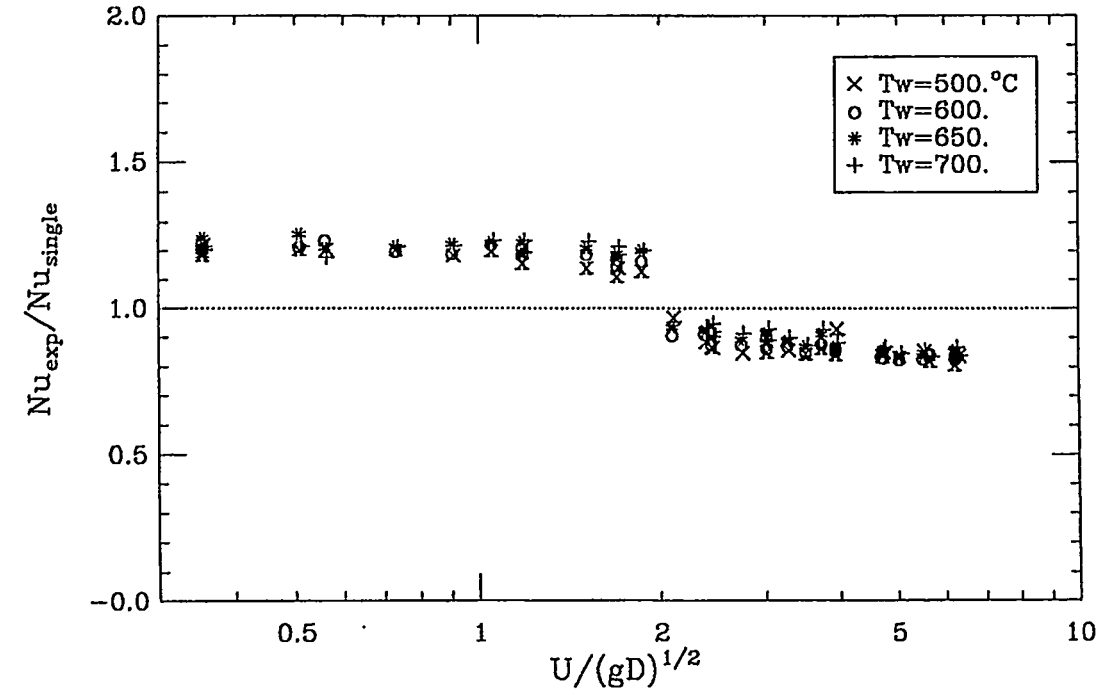

Fig. 8.4. Comparison of the data from multi-sphere array in single-phase flow with the general correlation Eq. (6.5).

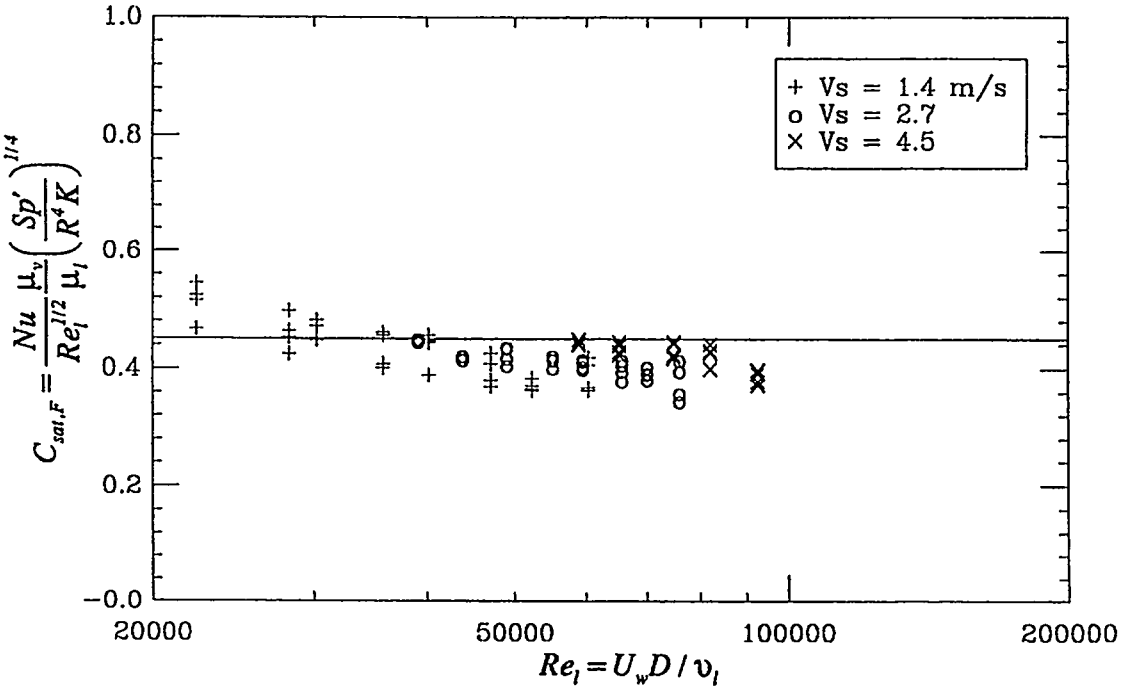

Fig. 8.5. Heat transfer data of film boiling from multi-sphere array in upward two-phase flow, plotted in terms of Eq. (7.8).

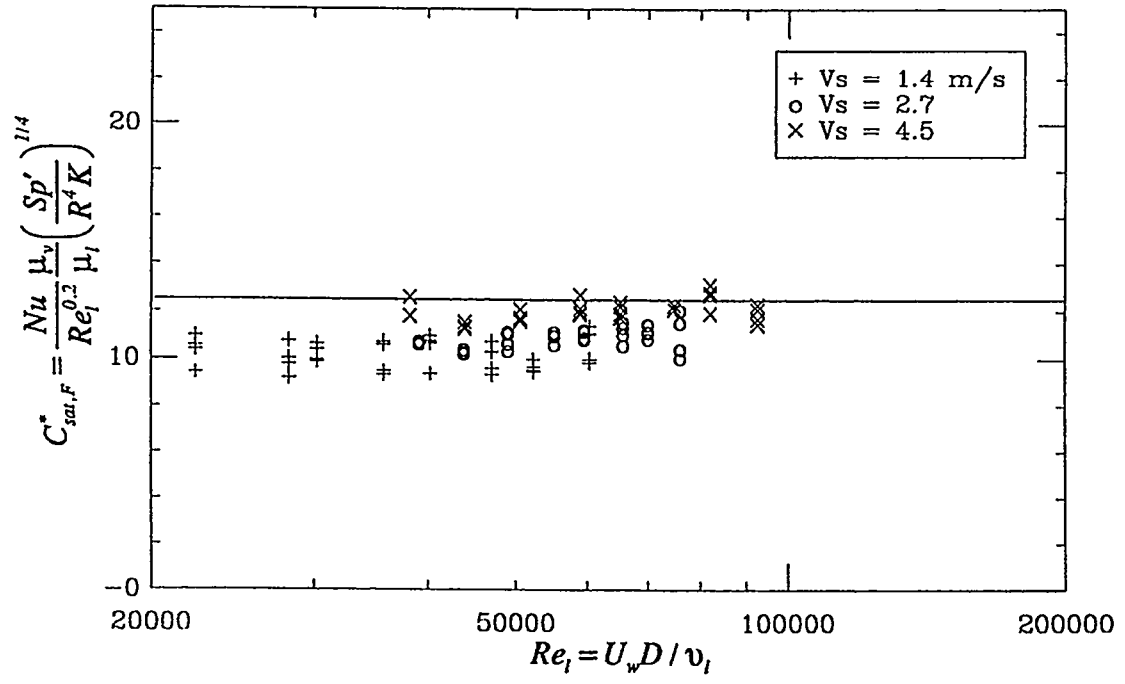

Fig. 8.6. Heat transfer data of film boiling from multi-sphere array in upward two-phase flow, plotted in terms of Eq. (7.9).

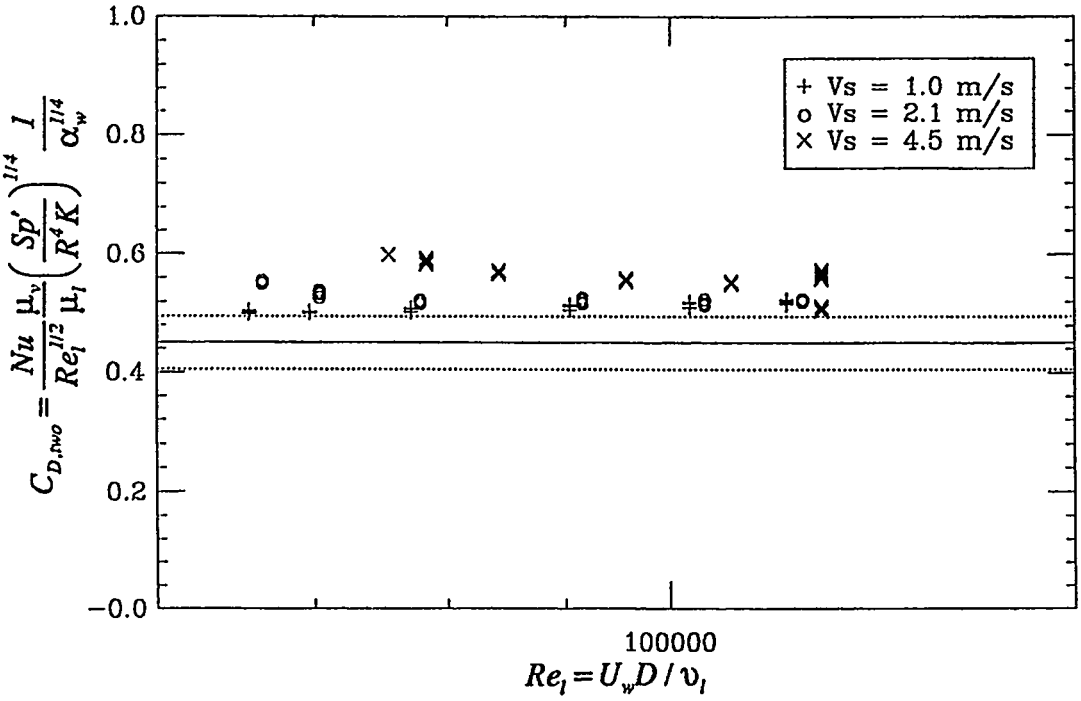

Fig. 8.7(a). Heat transfer data of film boiling from multi-sphere array in downward two-phase flow generated by No. 1 tube-needle assembly, plotted in terms of Eq. (7.16).

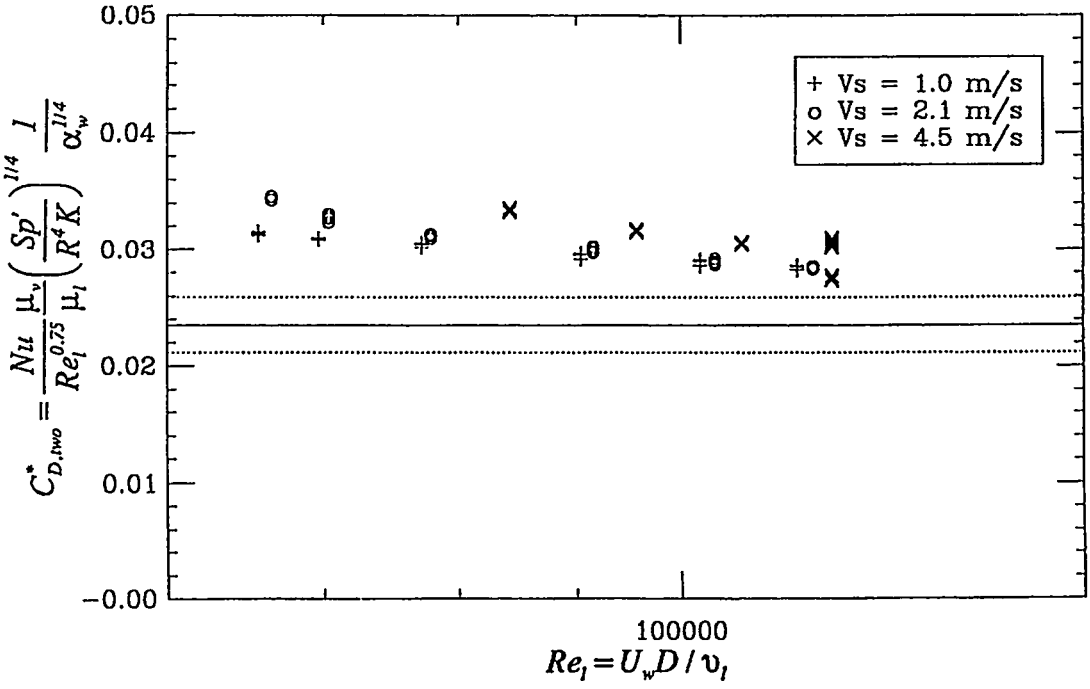

Fig. 8.7(b). Heat transfer data of film boiling from multi-sphere array in downward two-phase flow generated by No. 1 tube-needle assembly, plotted in terms of Eq. (7.18).

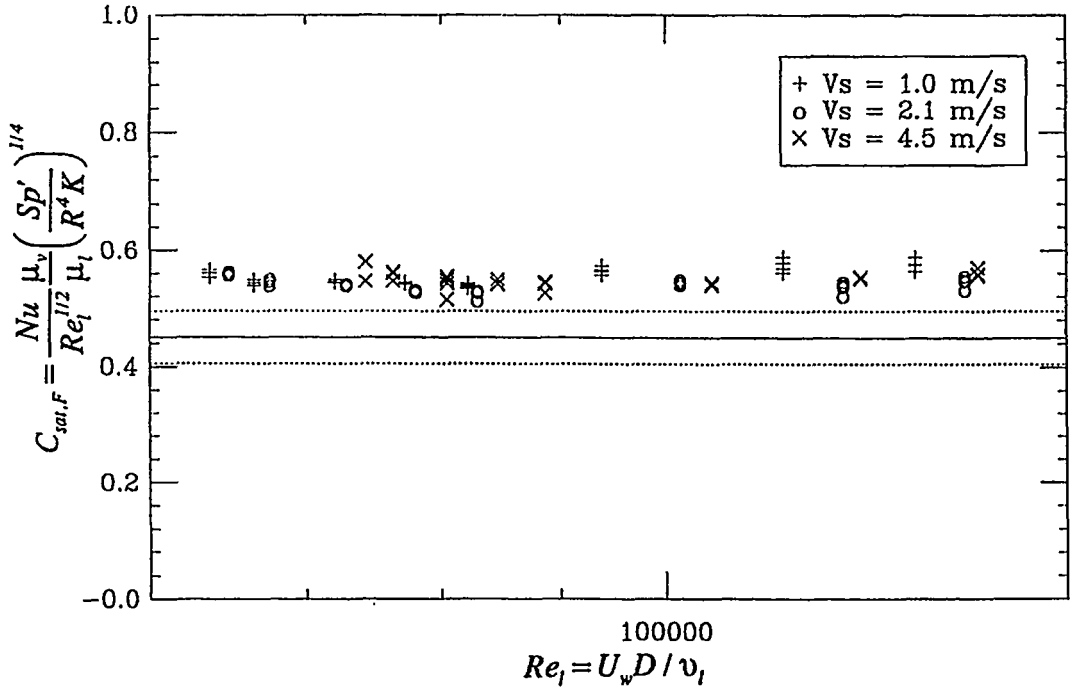

Fig. 8.8(a). Heat transfer data of film boiling from multi-sphere array in downward two-phase flow generated by No. 2 tube-needle assembly, plotted in terms of Eq. (7.16).

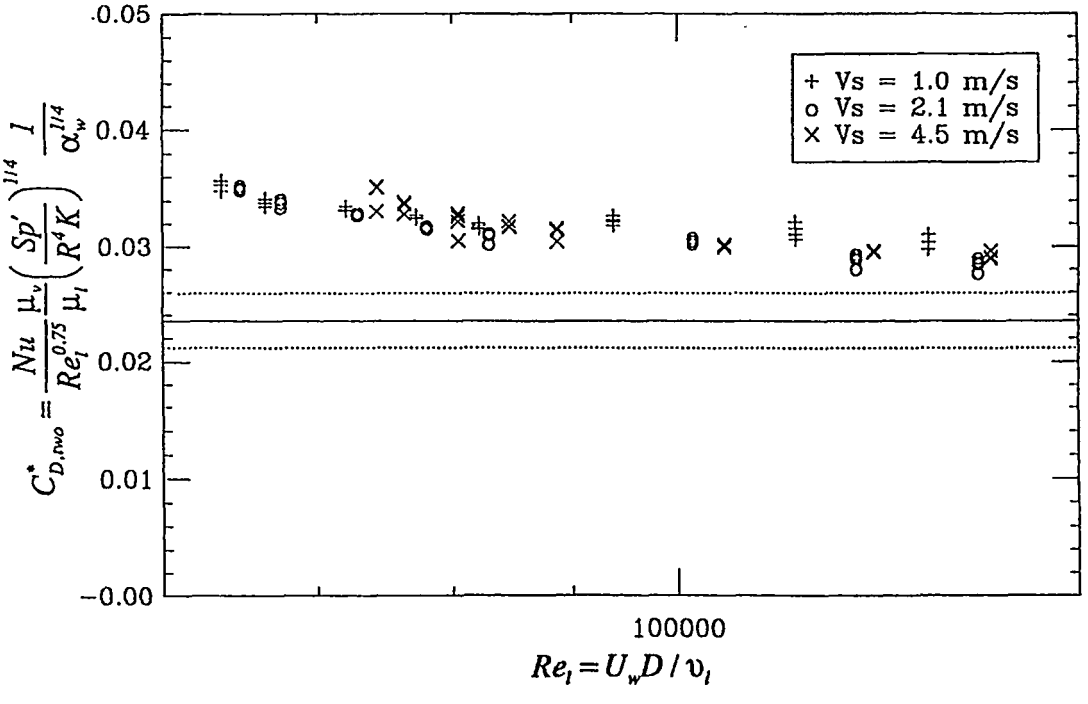

Fig. 8.8(b). Heat transfer data of film boiling from multi-sphere array in downward two-phase flow generated by No. 2 tube-needle assembly, plotted in terms of Eq. (7.18).

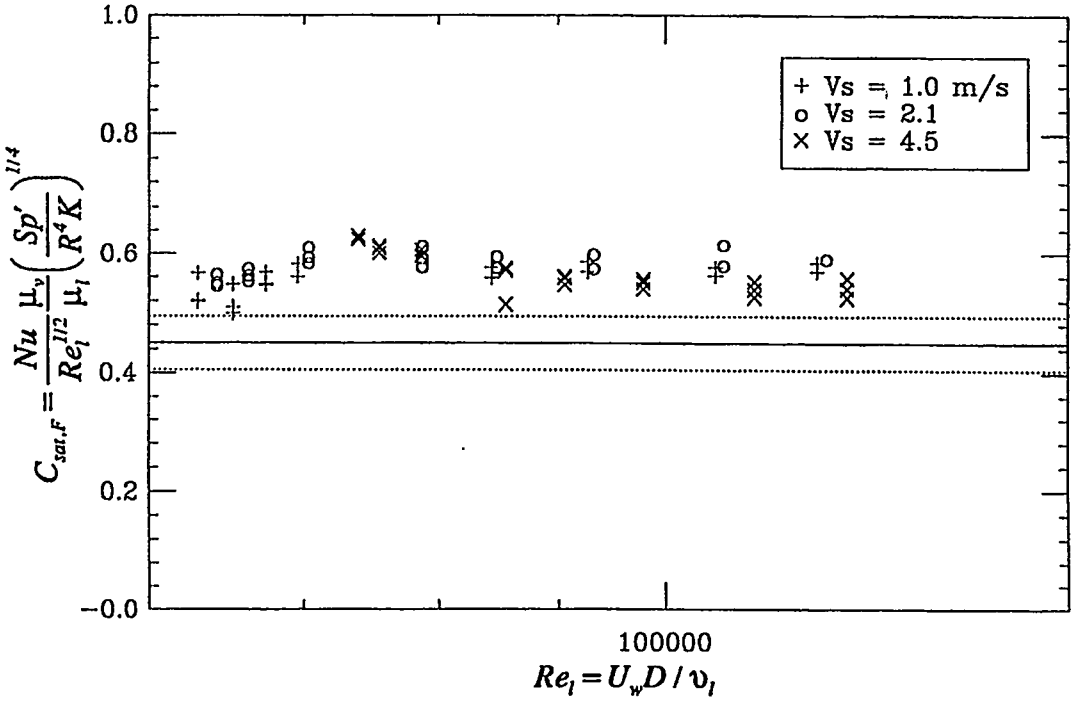

Fig. 8.9(a). Heat transfer data of film boiling from multi-sphere array in downward two-phase flow generated by No. 3 tube-needle assembly, plotted in terms of Eq. (7.16).

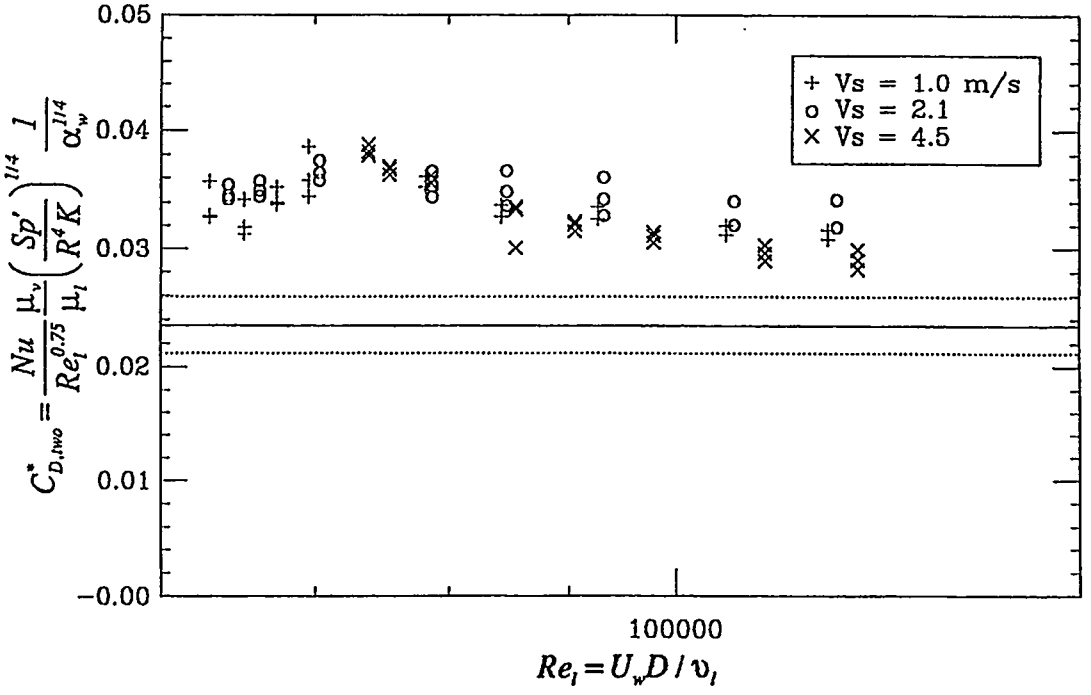

Fig. 8.9(b). Heat transfer data of film boiling from multi-sphere array in downward two-phase flow generated by No. 3 tube-needle assembly, plotted in terms of Eq. (7.18).

9 CONCLUSIONS

1. A flexible experimental system has been built and robust experimental techniques have been developed to test film boiling from very high temperature spheres in a wide variety of two-phase flows.

2. Single-phase film boiling experiments have been conducted systematically (with liquid subcooling from 0 to 40 °C, liquid velocity from 0 to 2 m/s, sphere superheat from 200 to 900 °C, sphere diameter from 6 to 19 mm) to obtain high quality heat transfer data. A general correlation has been developed.

3. Utilizing an two-phase laminar boundary-layer model for the unseparated front film region and a turbulent eddy model for the separated rear region, a theoretical model has been developed to predict the film boiling heat transfer in all single-phase regimes.

4. Two-phase film boiling data have been obtained in a wide variety of flow regimes. The upward two-phase flows cover void fraction from 0.2 to 0.65, water velocity from 0.6 to 3.2 m/s, and steam velocity from 3.0 to 9.0 m/s. The downward two-phase flows cover void fraction from 0.7 to 0.95, water velocity from 1.9 to 6.5 m/s, and steam velocity from 1.1 to 9.0 m/s. The saturated single-phase heat transfer correlation is found to be applicable to the two-phase film boiling data by making use of the actual water velocity (water phase velocity), and an adjustment factor of $(1-\alpha)^{1/4}$ (with a being the void fraction) for downward flow case only.

5. Preliminary experiments on film boiling from a multi-sphere array indicate that: (1) the presence of boiling spheres in the front of the test sphere decrease the heat transfer in upward two-phase flows and increase the heat transfer in downward two-phase flows; and (2) in a saturated single-phase upward flow, the presence of boiling spheres in the front of the test sphere increases the heat transfer in pool film boiling and decreases the heat transfer in forced convection film boiling.

10 REFERENCES

1. Amarasooriya, W.H. and T.G. Theofanous, "Premixing of Steam Explosions: A Three-Fluid Model," Nuclear Engineering and Design, **126**, 23–39 (1991).

2. Aziz, A., G.F. Hewitt and D.B.R. Kenning, "Heat Transfer Regimes in Forced-Convection Film Boiling on Spheres," Proc. 8th Int. Heat Transfer Conference, 2149–2154 (1986).

3. Banchero, J.T., G.E. Barker and R.H. Boll, "Stable Film boiling of Liquid Oxygen Outside Single Horizontal Tubes and Wires," Heat Transfer, Chemical Engineering Progress, Symposium Series, Americal Institute of Chemical Engineers, New York, Vol. 51, p. 21 (1955).

4. Barron, R.F. and A.K. Gorgolis, "Film Boiling of Liquid Nitrogen on a Sphere in an Enclosure," Adv. Cryog. Eng. vol. 23, pp 305–312 (1977).

5. Baumeister, K.J. and T.D. Hamill, "Laminar Flow Analysis of Film Boiling from a Horizontal Wire," NASA TN D-4035 (1967).

6. Bradfield, W.S., "Periodic Contact Behavior in Film Boiling," I& EC Fundamentals, pp 200–204 (1966).

7. Bradfield, W.S., "On the Effect of Subcooling on Wall Superheat in Pool Boiling," J. Heat Transfer, Trans. of the ASME, August, pp 269–270 (1967).

8. Breen, B.P. and J.W. Westwater, "Effect of Diameter of Horizontal Tubes on Film Boiling Heat Transfer," Chemical Engineering Progress, vol. 58, No. 7, July (1962).

9. Bromley, L.A., "Heat Transfer in Stable Film Boiling," Chemical Engineering Progress, Vol. 46, No. 5, pp 221–227, May (1950).

10. Bromley, L.A., N.R. Leroy and J.A. Robbers, "Heat Transfer in Forced Convection Film Boiling," Industrial and Engineering Chemistry, Vol. 45, No. 12, pp 2639–2646 (1953).

11. Bui, T.D. and V.K. Dhiw, "Film Boiling Heat Transfer on an Isothermal Vertical Surface," Trans. of the ASME, J. Heat Transfer, Vol. 107, pp 764–771 (1985).

12. Cess, R.D. and E.M. Sparrow, "Subcooled Forced-Convection Film Boiling on A Flat Plate," J. of Heat Transfer, Trans. of The ASME, pp 377-379, August, (1961).

13. Cess, R.D. and E.M. Sparrow, "Film Boiling in a Forced-Convection Boundary-Layer Flow," J. Heat Transfer, Trans. of ASME, pp 370–376, August (1961).

14. Cess, R.D., "Forced-Convection Film Boiling on a Flat Plate with Uniform Surface Heat Flux," J. Heat Transfer, Trans. of the ASME, p. 395 (1962).

15. Chou, X.S. and L.C. Witte, "A Theoretical Model for Flow Film Boiling Across Horizontal Cylinders," AIAA 92-4051, national Heat Transfer Conference, San Diego (1992).

16. Dhir, V.K. and G.P. Purohit, "Subcooled Film-Boiling Heat Transfer From Spheres," Nuclear Engineering and Design, Vol. 47, pp 49-66, (1978).

17. Dix, D., and J. Orozco, "Film Boiling Heat Transfer From A Sphere in Natural and Forced Convection of Freon-113," Experimental Heat Transfer, Vol. 3, pp 129-148, (1990).

18. Epstein, M. and G.M. Hauser, "Subcooled Forced-Convection Film Boiling in the Forward Stagnation Region of A Sphere or Cylinder," Int. J. of Heat and Mass Transfer, Vol. 23, pp 197-189, (1980).

19. Farahat, M.M. and T.N. Nasr, "Film Boiling Heat Transfer from Small Spherical Particles to Saturated Sodium and Water," Atomkernenergie (ATKE) Bd. 26, Lfg. 2, pp 99–102 (1975).

20. Farahat, M.M. and T.N. Nasr, "Natural Convection Film Boiling from Spheres to Saturated Liquid, An Integral Approach," Int. J. Heat Mass Transfer, Vol. 21, pp 256–258 (1978).

21. Farahat, M.M.K. and D.T. Eggen, "Pool Boiling in Subcooled Sodium at Atmospheric Pressure," Nuclear Science and Engineering, Vol. 53, pp 240–253 (1974).

22. Farahat, M.M.K., "Transient-Boiling Heat Transfer From Spheres To Sodium," ANL-7909, (1972).

23. Fodemski, T.R., "The Influence of Liquid Viscosity and System Pressure on Stagnation Point Vapor Thickness During Forced-Convection Film Boiling," Int. J. Heat and Mass Transfer, Vol. 28, No. 1, pp 69-80 (1985).

24. Fodemski, T.R. and W.B. Hall, "Forced Convection Film boiling on a Sphere in (a) Sub-Cooled or (b) Superheated Liquid," Proc. 7th Heat Transfer Conf., München 4, pp 375–379 (1982).

25. Fodemski, T.R., "Forced Convection Film Boiling in the Stagnation Region of a Molten Drop and Its application to Vapor Explosions," Int. J. Heat & Mass Transfer, Vol. 35, No. 8, pp 2005–2016 (1992).

26. Fortescue, G.E. and J.R.A. Pearson, "On Gas Absorption Into a Turbulent Liquid," Chem. Engng Sci. Vol. 22, pp 1163–1176 (1967).

27. Frederking, T.H.K. and J.A. Clark,"Natural Convection Film Boiling on A Sphere," Adv. Cryog. Eng. Vol.8, pp 501–506, (1963).

28. Frederking, T.H.K., R.C. Chapman and S. Wang, "Heat Transport and Fluid Motion During Cooldown of Single Bodies to Low Temperatures," Adv. Cryog. Eng. vol. 10, Part 2, pp 353-360 (1965).

29. Grigoriev, V.A., V.V. Klimenko and A.G. Shelepen, "Pool Film Boiling from Submerged Sphered," Proc. of 7th Int. Heat Transfer Conf., Munich, Germany, Vol. 4, pp 387–392 (1982).

30. Hamill, T.D. and K.J. Baumeister, "Effect of Subcooling and Radiation on Film-Boiling Heat Transfer from a Flat Plate," NASA TND-3925 (1967).

31. Hendricks, R.C. and K.J. Baumeister, "Film Boiling from Submerged Spheres," NASA TN-5124 (1969).

32. Hendricks, R.C. and K.J. Baumeister, "Similarity and Curvature Effects in Pool Film Boiling," Proc. of the 4th Int. Heat Transfer Conf., Paris-Versailles, Vol. 5, B3.7 (1970).

33. Hesson, J.C. and L.C. Witte, "Comment on 'Film Boiling Heat Transfer Around a Sphere in Forced Convection' by K. Kobayasi," J. Nuclear Science and Technology, Vol. 3, No. 10, pp 448–449 (1966).

34. Hishikawa, K. and T. Ito, "Two-Phase Boundary-Layer Treatment of Free-Convection Film Boiling," Int. J. Heat Mass Transfer, Vol. 9, pp 103–115 (1966).

35. Hsiao, K.H., L.C. Witte and J.E. Cox, "Transient Film Boiling from A Moving Sphere," Int. J. Heat and Mass Transfer, Vol. 18, pp 1343–1350 (1975).

36. Irving, M.E. and J.W. Westwater, "Limitations for obtaining boiling Curves by the Quenching Method with Spheres," Proc. 8th Int. Heat Transfer Conf., Vol. 4, pp 2061–2066 (1986).

37. Ito, T., K. Nishikawa and T. Shigechi, "Forced Convection Film Boiling Heat Transfer From A Horizontal Cylinder to Liquid Cross-flow Upward (1st Report, Saturated Liquid)," Bulletin of the JSME, Vol. 24, No. 198, pp 2107-2114, Dec., (1981).

38. Ito, T. and K. Hishikawa, "Two-Phase Boundary-Layer Treatment of Forced-Convection Film Boiling," Int. J. Heat and Mass Transfer, Vol. 9, pp 117-130 (1966).

39. Jacobs, H.R. and R.F. Boehm, "An Analysis of Effects of Body Force and Forced Convection on Film boiling," Proc. Int. Heat Transfer, Vol. 5, B3.9, pp 1–11 (1970).

40. Jacobson, R.N. and F.H. Shair, "Film Boiling From A Sphere During Forced Convection of Subcooled Water," I&EC Fundamentals Vol. 9, No. 1, (1970).

41. Klimenko, V.V., "Film boiling on a Horizontal Plate—New Correlation," Int. J. Heat and Mass Transfer, Vol. 24, pp 69–79 (1981).

42. Kobayasi, K., "Counter-Comment to Hesson & Witte's Comment on 'Film Boiling Heat Transfer Around A Sphere in Forced Convection'," J. of Nuclear Science and Technology, Vol. 3 , No. 10, pp 449-450, (1966).

43. Kobayasi, K., "Film Boiling Heat Transfer Around a Sphere in Forced Convection," J. Nuclear Science and Technology, Vol. 2, No. 2, pp 62–67 (1965).

44. Liang, J-S. and P. Griffith, "Experimental and Analytical Study of Direct Contact Condensation of Steam in Water," Nuclear Engineering and Design, Vol. 147, pp 425–435 (1994).

45. Liu, C., T.G. Theofanous and W.W. Yuen "Film Boiling From Spheres in Single- and Two-Phase Flow," ANS Proceedings, National Heat Transfer Conference, HTC-Vol. 6, San Diego, August, (1992).

46. Liu, Q.S., and M. Shiotsu and A. Sakurai, "A Correlation for Forced Convection Film Boiling Heat Transfer From A Horizontal Cylinder," HTD-Vol. 197, Two-phase Flow and Heat Transfer, Proceeding of 28th National Heat Transfer Conferece, ASME (1992).

47. Marschall, E. and L.C. Farrar, "Film Boiling from a Partly Submerged Sphere," Int. J. Heat and Mass Transfer, Vol. 18, pp 875–878 (1975).

48. McAdams, W.H., **Heat Transmission**, 3rd ed., McGraw-Hill Book Co., New York, p. 172 (1954).

49. Merte, Jr., H. and J.A. Clark, "Boiling Heat Transfer with Cryogenic Fluids at Standard, Fractional, and Near-Zero Gravity," J. Heat Transfer, Trans. of ASME, pp 351–359, August (1964).

50. Michiyoshi, I., O. Takahashi, and Y. Kikuchi, "Heat Transfer and the Low Limit of Film Boiling," Proc. of the First World Conf. on Experimental Heat Transfer, Fluid Mechanics and Thermodynamics, Dubrovnik, Yugoslavia, pp 1404-1415, (1988).

51. Motte, E.I., L.A. Bromley, "Film Boiling of Flowing Subcooled Liquids," Industrial and Engineering Chemistry, Vol. 49, No. 11, (1957).

52. Nakayama, A. and H. Koyama, "An Integral Method in Laminar Film Pool Boiling from Curved Surfaces," Trans. of the ASME, J. Heat Transfer, Vol. 108, pp 490–493 (1986).

53. Nakayama, A. and H. Koyama, "Analysis of Combined Free and Forced convection Film Boiling Part II: Combined Free and Forced Convection Region," AIChE J., Vol. 32, No. 1, pp 142–145 (1986).

54. Nakayama, A. and H. Koyama, "Analysis of Combined Free and Forced convection Film Boiling Part I: Forced and Free Convection Regions," AIChE J., Vol. 32, No. 1, pp 146–148 (1986).

55. Nakayama, A., "Subcooled Forced-Convection Film boiling in the Presence of a Pressure Gradient," AIAA J., Vol. 24, No. 2, pp 230–236 (1986).

56. Nishikawa, J., T. Ito and T. Kuroki, "Pool Film Boiling Heat Transfer from a Horizontal Cylinder to Saturated Liquids," Int. J. Heat and Mass Transfer, Vol. 15, pp 853–862 (1972).

57. Nishkawa, K., T. Ito and K. Matsumoto, "Investigation of Variable Thermophysical Property Problem Concerning Pool Film Boiling from Vertical Plate with Prescribed Uniform Temperature," Int. J. Heat and Mass Transfer, Vol. 19, pp 1173–1182 (1976).

58. Orozco, J. and H. Francisco, "Free Convection Film Boiling Heat Transfer from a Rotating Surface," J. Heat Transfer, Trans. of the ASME, Vol. 114, August, pp 695–702 (1992).

59. Orozco, J., R. Stellman and D. Poulikakos, "Dynamics Response of a Liquid-Vapor Interface during Flow Film Boiling from a Sphere," J. Heat Transfer, Trans. of the ASME, vol. 109, pp 1051–1055 (1987).

60. Orozco, J. and L.C. Witte,"Flow Film Boiling From A Sphere to Subcooled Freon-11," J. of Heat Transfer. Transactions of ASME, Vol. 108, Nov. (1986).

61. Rhea, L.G. and R.G. Nevins, "Film Boiling Heat Transfer from an Oscillating Sphere," J. Heat Transfer, Trans. of the ASME, pp 267–272, May (1969).

62. Sakurai, A., M. Shiotsu, and K. Hata, "A General Correlation for Pool Film Boiling Heat Transfer From A Horizontal Cylinder to Subcooled Liquid: Part 2 – Experimental Data for Various Liquids and Its Correlation," J. of Heat Transfer, Transactions of the ASME, Vol. 112, pp 441–450, May, (1990b).

63. Sakurai, A. and M. Shiotsu, "Pool Film Boiling Heat Transfer and Minimum Film Boiling Temperature," Pool and Externam Flow Boiling, ASME (1992).

64. Sakurai, A., M. Shiotsu, and K. Hata, "A General Correlation for Pool Film Boiling Heat Transfer From A Horizontal Cylinder to Subcooled Liquid: Part 1 – A Theoretical Pool Film Boiling Heat Transfer Model Including Radiation Contributions and Its Analytical Solution," J. of Heat Transfer, Transactions of the ASME, Vol. 112, pp 430–440, May, (1990a).

65. Sakurai, A., M. Shiotsu and K. Hata, "Effect of System Pressure on Film-Boiling Heat Transfer, Minimum Heat Flux, and Minimum Temperature," Nuclear Science and Engineering, Vol. 88, pp 321–330 (1984).

66. Schmidt, W.E. and L.C. Witte, "Oscillation Effects Upon Film Boiling from a Sphere," J. Heat Transfer, Trans. of the ASME, pp 491–493, Nov. (1972).

67. Sheppard, J.J. and W.S. Bradfield, "Stagnation Free-Convection Film Boiling on a Hemisphere," (1971)

68. Shigechi, T., T. Ito, and K. Nishikawa, "Forced Convection Film Boiling Heat Transfer From a Horizontal Cylinder to Liquid Cross-flow Upward (2nd Report, Subcooled Liquid)," Bulletin of the JSME, Vol. 26, No. 214, pp 554-561, April, (1983).

69. Shih, C. and M.M. El-Wakil, "Film Boiling and Vapor Explosions from Small Spheres," Nuclear Science and Engineering, Vol. 77, pp 470–479 (1981).

70. Siviour, J.B. and A.J. Ede, "Heat Transfer in Subcooled Pool Film Boiling," Proc. 4th Int. Heat Transfer Conf., Vol. 5, B3.12, Paris-Versailles (1970).

71. Sparrow, E.M., "The Effect of Radiation of Film-Boiling Heat Transfer," Int. J. Heat Mass Transfer, Vol. 7, pp 229–238 (1964).

72. Srinivasan, J. and N.S. Rao, "Numerical Study of Heat Transfer in Laminar Film Boiling by the Finite-Difference Method," Int. J. Heat and Mass Transfer, Vol. 27, pp 77–84 (1984).

73. Stevens, J.W. and L.C. Witte, "Destabilization of Vapor Film Boiling Around Spheres," Int. J. Heat and Mass Transfer, Vol. 16, pp 669–678 (1973).

74. Stevens, J.W. and L.C. Witte, "Transient Film and Transition Boiling From A Sphere," J. Of Heat Transfer, Vol. 14, pp 443-450., (1971).

75. Tachibana, F. and S. Fukui, "Heat Transfer in Film Boiling to Subcooled Liquids," Int. Developments in Heat Transfer, ASME, pp 219–223 (1961).

76. Tennekes, H. and J.L. Lumley, **A First Course In Turbulence**, the MIT Press, (1972).

77. Theofanous, T.G., B. Najafi and E. Rumble, "An Assessment of Steam-Explosion-Induced Containment Failure. Part I: Probabilistic Aspects," Nuclear Science and Engineering, Vol. 97, pp 259–281 (1987).

78. Theofanous, T.G., R.N. Houze and L.K. Brumfield, "Turbulent Mass Transfer at Free, Gas-Liquid Interface, With Applications To Open-Channel, Bubble and Jet Flows," Int. J. of Heat Mass Transfer, Vol. 19, pp 613-624, (1976).

79. Theofanous, T.G. and W.H. Amarasooriya, "Premixing of Steam Explosions: A Three-Fluid Model," Nuclear Engineering and Design, Vol. 126, pp 23–39 (1991).

80. Toda, S. and M. Mori, "Subcooled Film Boiling and the Behavior of Vapor Film on a Horizontal Wire and a Sphere," Proc. 7th Int. Heat Transfer Conf., Munich, Germany, Vol. 4, pp 173–178 (1982).

81. Touloukian, Y.S. and E.H. Buyco, "Specific Heat, Metallic Elements and Alloys," Thermophisical Properties of Matter 4, IFI/Plenum, New York (1970).

82. Tso, C.P., H.G. Low, and S. M. Ng, "Pool Film Boiling From Spheres to Saturated and Subcooled Liquids of Freon-12 and Freon-22," Int. J. Heat and Fluid Flow, Vol. 11, No. 2, pp 154-159, (1990).

83. Walford, F.J., "Transient Heat Transfer From A Hot Nickel Sphere Moving Through Water," Int. J. Heat Mass Transfer, pp 1621–1625, (1970).

84. Walsh, S. and S.D. R. Wilson, "Boundary-Layer Flow in Forced-Convection Film-Boiling on a Wedge," Int. J. Heat Mass Transfer, Vol. 22, pp 569-574 (1979).

85. Wang, B.X. and X.F. Peng, "Film Boiling Heat Transfer for Liquid Flowing with High Velocity," Int. J. Heat Mass Transfer, vol. 35, pp 675-682 (1992).

86. Westwater, J.W., J.J. Hwalek and Mark E. Irving, "Suggested Standard Method for Obtaining Boiling Curves by Quenching," Ind. Eng. Chem. Fundamentals, Vol. 25, pp 685-692 (1986).

87. Wilson, S.D.R, "Steady and Transient Film Boiling on a Sphere in Forced Convection," Int. J. Heat Mass Transfer, Vol. 22, pp 207-218 (1979).

88. Witte, L.C. and J. Orozco, "The Effect of Vapor Velocity Profile Shape on Flow Film Boiling from Submerged Bodies," J. Heat Transfer, Trans. of the ASME, Vol. 106, pp 191-197 (1984).

89. Witte, L.C., "Film Boiling From A Sphere," I&EC Fundamentals, pp 517–518, (1968).

90. Yuen, W.W., X. Chen and T.G. Theofanous, "On the Fundamental Microinteractions That Support the Propagation of Steam Explosions," Nuclear Engineering and Design, Vol. 146, pp 133-146 (1994).

91. Yuge, T., "Experiments on Heat Transfer from Spheres Including Combined Natural and Forced Convection," J. Heat Transfer ser. c 82, p 214 (1960).

92. Zvirin, Y., G.F. Hewitt and D.B.R. Kenning, "Boiling on Free-Falling Spheres: Drag and Heat Transfer Coefficients," Experimental Heat Transfer, Vol. 3, pp 185-214 (1990).

93. Zvirin, Y., S. Aziz, G.F. Hewitt and D.B.R. Kenning, "Experimental Investigation of the Transition from Boiling on Free Falling Spheres," ANS Proc. 23rd US National Heat Transfer Conf., Houston, TX, pp 209-216 (1988).

APPENDIX A

A DERIVATION OF THE CORRELATION FOR POOL FILM BOILING ON A SPHERE

APPENDIX A

A DERIVATION OF THE CORRELATION FOR POOL FILM BOILING ON A SPHERE

Figure A1 shows the physical model and coordinates, with the sphere radius, vapor layer thickness and liquid layer thickness being R, Δ, and δ, respectively. Based on the assumptions of thin layer in an incompressible fluid and no radiation effects, the one dimensional laminar momentum and energy boundary layer governing equations for the buoyancy-induced vapor motion are

$$\rho_v u_v \frac{\partial u_v}{\partial x} = g(\rho_l - \rho_v) sin\phi + \mu_v \frac{\partial^2 u_v}{\partial y^2} \tag{A1}$$

$$\rho_v c_{pv} u_v \frac{\partial T_v}{\partial x} = k_v \frac{\partial^2 T_v}{\partial y^2} \tag{A2}$$

The corresponding equations of the free-convection in the liquid boundary layer are

$$\rho_l u_l \frac{\partial u_l}{\partial x} = g\beta_l \rho_l (T_l - T_\infty) sin\phi + \mu_l \frac{\partial^2 u_l}{\partial z^2} \tag{A3}$$

$$\rho_l c_{pl} u_l \frac{\partial T_l}{\partial x} = k_l \frac{\partial^2 T_l}{\partial z^2} \tag{A4}$$

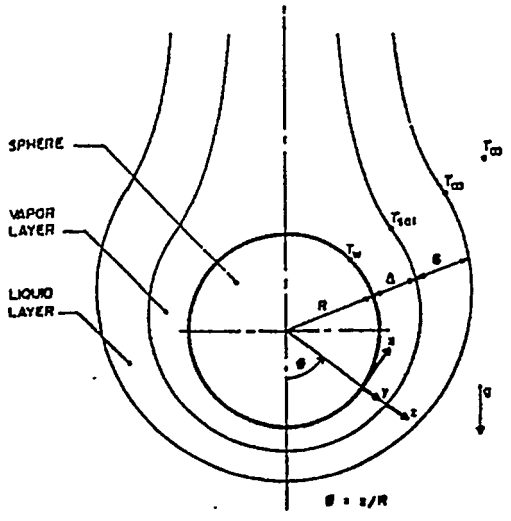

Figure A1. Model and coordinate system for subcooled pool film boiling.

In order to carry out an analytical solution to the above boundary layer equations, further assumptions are made:

(1) Convective terms are neglected, and the effects are compensated by using an effective latent heat of vaporization h'_{fg} in the later on energy integral equation.

(2) The buoyancy term in the liquid momentum equation is neglected.

(3) The wall temperature is uniform at T_w, and the vapor-liquid interface is smooth and is at $T_{sat}(T_w > T_{sat} > T_\infty)$.

(4) The thickness of the momentum boundary layer is assumed to be the same as that of the thermal boundary layer in liquid phase.

The necessary velocity boundary conditions are assumed to be non-slip condition at the wall and at the vapor-liquid interface, continuous interfacial shear, and stationary bulk liquid beyond the boundary of the liquid layer. The full set of conditions are expressed by

At $y = 0$:

$$\begin{aligned} u_v &= 0 \\ T_v &= T_w \end{aligned} \tag{A5}$$

At $y = \Delta$ and $z = \delta$:

$$\begin{aligned} u_v &= u_l \\ \mu_v \frac{\partial u_v}{\partial y} &= \mu_l \frac{\partial u_l}{\partial z} \\ T_v &= T_l = T_{sat} \end{aligned} \tag{A6}$$

At $z = \delta$:

$$\begin{aligned} u_l &= 0 \\ T_l &= T_\infty \end{aligned} \tag{A7}$$

The governing equation may now be solved completely in terms of the unknowns Δ and δ. The results are

$$u_v = \frac{g(\rho_l - \rho_v) sin\phi \Delta^2}{2\mu_v} \left[\left(\frac{f + 2\xi}{f + \xi} \right) \left(\frac{y}{\Delta} \right) - \left(\frac{y}{\Delta} \right)^2 \right] \tag{A8}$$

$$T_v = T_w - \Delta T_{sup}\frac{y}{\Delta} \tag{A9}$$

$$u_l = \frac{g(\rho_l - \rho_v)sin\phi\Delta^2}{2\mu_l}\left(\frac{f\xi}{f+\xi}\right)\left(1-\frac{z}{\delta}\right) \tag{A10}$$

$$T_l = T_{sat} - \Delta T_{sub}\frac{z}{\Delta} \tag{A11}$$

where $f = \mu_l/\mu_v$ and $\xi = \delta/\Delta$. The integral heat balance are performed on the vapor and liquid layers, giving

$$h'_{fg}\frac{d}{dx}\int_0^{\Delta} u_v\rho_v 2\pi R sin\phi dy = 2\pi R sin\phi\left[-k_v\frac{\partial T_v}{\partial y}\mid_{y=0} + k_l\frac{\partial T_l}{\partial z}\mid_{z=0}\right] \tag{A12}$$

$$C_{pl}\frac{d}{dx}\int_0^{\delta} u_l\rho_l(T_l - T_\infty)2\pi R\,\sin\phi dz = 2\pi R\,\sin\phi\left[-k_l\frac{\partial T_l}{\partial z}\mid_{z=0}\right] \tag{A13}$$

Substituting Eqs. (A8) through (A11) into the two integral Eqs. (A12) and (A13), and assuming ξ to be independent of x, yields

$$\frac{d}{dx}(\Delta^3\,sin^2\,\phi) = \left(\frac{f+\xi}{f+4\xi}\right)\left[\frac{12\mu_v k_v\Delta T_{sup}}{g(\rho_l-\rho_v)\rho_v h'_{fg}} - \frac{12\mu_v k_l\Delta T_{sub}}{g(\rho_l-\rho_v)\rho_v h'_{fg}\xi}\right]\frac{sin\,\phi}{\Delta} \tag{A14}$$

$$\frac{d}{dx}(\Delta^3\,sin^2\,\phi) = \left(\frac{f+\xi}{f\xi^2}\right)\left[\frac{6\mu_l k_l}{g(\rho_v-\rho_l)\rho_l C_{pl}\xi}\right]\frac{sin\,\phi}{\Delta} \tag{A15}$$

The solution to Eqs. (A14) and (A15) , respectively, are

$$\Delta = I(\phi)\left\{\left(\frac{f+\xi}{f+4\xi}\right)\left[\frac{16R\mu_v k_v\Delta T_{sup}}{g(\rho_l-\rho_v)\rho_v h'_{fg}} - \frac{16R\mu_v k_l\Delta T_{sub}}{g(\rho_l-\rho_v)\rho_v h'_{fg}\xi}\right]\right\}^{1/4} \tag{A16}$$

$$\Delta = I(\phi)\left\{\left(\frac{f+\xi}{f\xi^2}\right)\left[\frac{8R\mu_l k_l}{g(\rho_v-\rho_l)\rho_l C_{pl}\xi}\right]\right\}^{1/4} \tag{A17}$$

where

$$I(\theta) = \frac{\left[\int sin^{5/3}\,\phi d\theta\right]^{1/4}}{sin^{2/3}\,\phi} \tag{A18}$$

Combining Eqs. (A16) and (A17) produces a cubic equation for ξ, which has at lest one real root:

$$\xi = (W_1 + W_2^{1/2})^{1/3} + (W_1 - W_2^{1/2}) + \frac{k_l\Delta T_{sub}}{3k_v\Delta T_{sup}} \tag{A19}$$

where

$$W_1 = \left(\frac{C_2}{3C_1}\right)^3 + \frac{2C_2C_3}{2C_1^2 f} + \frac{C_3}{2C_1} \tag{A20}$$

$$W_2 = \left(\frac{C_3}{2C_1}\right)^2 + \left(\frac{C_3}{C_1}\right)\left(\frac{C_2}{3C_1}\right)^3 + \left(\frac{C_3^2}{fC_1^3}\right)\left[\frac{2C_2}{3} - \frac{4C_2^2}{27fC_1} - \frac{64C_3}{27f^2}\right] \qquad (A21)$$

$$C_1 = \frac{12\mu_v k_v \Delta T_{sup}}{g(\rho_l - \rho_v)\rho_v h'_{fg}} \quad C_2 = \frac{12\mu_v k_l \Delta T_{sub}}{g(\rho_l - \rho_v)\rho_v h'_{fg}} \quad C_3 = \frac{6\mu_v k_l}{g(\rho_l - \rho_v)\rho_l C_{pl}} \qquad (A22)$$

Now we are ready to evaluate the heat transfer coefficient. The average heat flux from the sphere surface is

$$\overline{q}_x = \frac{1}{4\pi R^2}\int_0^x (2\pi R \sin\phi) R d\phi \left(-k_v \frac{\partial T_v}{\partial y}\mid_{y=0}\right) = 0.5 k_v \Delta T_{sup}\int_0^x \frac{\sin\phi}{\Delta} d\phi \qquad (A23)$$

Hence the average Nusselt number is

$$\mathrm{Nu}_c = \frac{\overline{h} d_s}{k_v} = \left(\frac{\overline{q}_x}{\Delta T_{sup}}\right)\frac{d_s}{k_v} = \frac{1}{2} d_s \int_0^x \frac{\sin\phi}{\Delta} d\phi \qquad (A24)$$

Substituting Eq. (A17) into (A24) yields

$$\mathrm{Nu}_c = 2^{-3/2}(\mathrm{ArPr}_v)^{1/4}\left[\left(\frac{f+\xi}{\xi^3}\right)\left(\frac{k_l C_{pv}\rho_v}{k_v C_{pl}\rho_l}\right)\right]^{1/4}\int_0^x \frac{\sin\phi}{I(\phi)} d\phi \qquad (A25)$$

By using Eq. (A19) and rearranging Eq. (A25), we have

$$\mathrm{Nu}_c = C_0(\mathrm{Ar}/Sp')^{1/4} M_c^{1/4} \qquad (A26)$$

where

$$M_c = E^3/[1 + E/(Sp'\mathrm{Pr}_l)]/(R\mathrm{Pr}_l Sp')^2$$
$$E = (A + CB^{1/2})^{1/3} + (A - CB^{1/2})^{1/3} + (1/3)Sc^*$$
$$A = (1/27)Sc^{*3} + (1/3)R^2 Sp'\mathrm{Pr}_l Sc^* + (1/4)R^2 Sp'^2\mathrm{Pr}_l^2$$
$$B = (-4/27)Sc^{*2} + (2/3)Sp'\mathrm{Pr}_l Sc^* - (32/27)Sp'\mathrm{Pr}_l R^2 + (1/4)Sp'^2\mathrm{Pr}_l^2 + (2/27)Sc^{*3}/R^2$$
$$C = (1/2)R^2 Sp'\mathrm{Pr}_l$$
$$h'_{fg} = h_{fg} + 0.5 C_{pv}\Delta T_{sup}, \qquad Sp' = C_{pv}\Delta T_{sup}/(h'_{fg} Pr_v)$$
$$Sc^* = C_{pl}\Delta T_{sub}/h'_{fg}, \qquad R = [(\mu\rho)_v/(\mu\rho)_l]^{1/2}$$

$$C_0 = 2^{-3/2}\int_0^x \frac{\sin\phi}{I(\phi)} d\phi = 0.696 \qquad (A27)$$

The similar analysis can be carried out for pool film boiling on horizontal cylinder and on vertical plate. The same formulation can be obtained except that the constant C_0 is different; C_0 for cylinder case is 0.61 and for plate case is 0.793.

APPENDIX B

A DERIVATION OF THE CORRELATION FOR FORCED CONVECTION FILM BOILING ON A SPHERE

APPENDIX B

A DERIVATION OF THE CORRELATION FOR FORCED CONVECTION FILM BOILING ON A SPHERE

A sphere of radius R and temperature T_w is held in a uniform stream of liquid which has undisturbed velocity U and temperature T_l. We suppose that T_w is constant but may depend on θ. The temperature at the vapor-liquid interface is the saturation temperature T_s. We suppose that the thickness of the vapor film and of the thermal boundary layer in the liquid phase is small compared with radius R. In these regions thin film theory or boundary-layer theory is applied.

Liquid Layer

It is supposed that the velocity field is given by a potential flow. According to K.H. Hsiao, L.C. Witte and J.E. Cox (1975), in spherical polar coordinates (r, θ, ϕ) centered on the sphere and with θ measured from the direction of the incoming steam, the velocity components are

$$U_l\left[-\left(1-\frac{R^3}{r^3}\right)cos\,\theta, \quad \left(1+\frac{R^3}{2r^3}\right)sin\,\theta, \quad 0\right]$$

We also confine the analysis in the region where the flow remains attached (unseparated).

To find the temperature field, a dimensionless boundary-layer coordinate $y = [(r/R)-1]\mathrm{Pe}^{1/2}$ is introduced, and then the dimensionless energy equation takes the form

$$\frac{3}{2}sin\,\theta\frac{\partial T^*}{\partial\theta} - 3y\,cos\,\theta\frac{\partial T^*}{\partial y} = \frac{\partial^2 T^*}{\partial y^2} \qquad (B1)$$

where

$$T^* = (T-T_l)/(T_s-T_l) = (T-T_l)/\Delta T_{sub}$$

and the boundary condition are

$$T^* = 1 \quad \text{on} \quad y = 0; \qquad T^* = 0 \quad \text{at} \quad y = \infty$$

The solution of this problem is

$$T^* = erfc[yf(\theta)] \qquad (B2)$$

where

$$f(\theta) = \frac{3}{4}sin^2\,\theta\left(1-\frac{3}{2}cos\,\theta+\frac{1}{2}cos^3\,\theta\right) \qquad (B3)$$

A constant of integration has been determined by the requirement that $f(0) \neq 0$; in fact $f(0) = (3/2)^{0.5}$.

Thus, the the temperature gradient at the liquid-vapor interface ($y = 0$) can be found as

$$\left(\frac{\partial T}{\partial r}\right)_{y=0} = -\frac{2\Delta T_{sub}}{\pi^{1/2} R} \mathrm{Pe}^{1/2} f(\theta) = -\frac{\Delta T_{sub}}{R} \frac{1}{\delta_T} \tag{B4}$$

where

$$\delta_T = \frac{\pi^{1/2}}{2\mathrm{Pe}^{1/2}} \frac{1}{f(\theta)} \tag{B5}$$

Vapor Layer

Here we choose coordinates (s, n) where s is length measured around the sphere from $\theta = 0$ and n is length measured normal to the surfaces; thus $s = \theta R$ and $n = r - R$. The velocity components are (u, v). Making the usual boundary-layer approximations, the equations of continuity, momentum and energy take the forms of

$$\frac{1}{sin\,\theta} \frac{\partial}{\partial s}(u\,sin\,\theta) + \frac{\partial v}{\partial n} = 0 \tag{B6}$$

$$u\frac{\partial u}{\partial s} + v\frac{\partial u}{\partial n} = -\frac{1}{\rho_v}\frac{\partial p}{\partial s} + v_v \frac{\partial^2 u}{\partial n^2} \tag{B7}$$

$$0 = -\frac{1}{\rho_v}\frac{\partial p}{\partial n} \tag{B8}$$

$$u\frac{\partial T}{\partial s} + v\frac{\partial T}{\partial n} = k_v \frac{\partial^2 T}{\partial n^2} \tag{B9}$$

The vapor-liquid interface is located at $n = n_i(s)$. The boundary conditions are

$$\begin{aligned} u = 0,\ T = T_w \qquad & \text{on } n = 0 \\ u = U_s = 3/2U\,sin\,\theta,\ T = T_s \qquad & \text{on } n = n_i \end{aligned} \tag{B10}$$

Equation (B8) indicates that the pressure in the vapor layer is independent of n as usual in boundary layer theory, and therefore equals $p(n_i)$, the pressure at the interface. By continuity of normal stress at the interface, this is equal to the pressure in the liquid at the interface, and this in turn may be found from the potential flow of the liquid by means of Bernoulli's equation, which gives

$$p = constant - \frac{1}{2}\rho_l \left(\frac{3}{2} U\,sin\,\theta\right)^2 \tag{B11}$$

To effect an analytical solution, further assumption is made: convective terms (on the left side) in the momentum Eq. (B7) and energy Eq. (B9) are neglected. Thus the solutions can be obtained as

$$u = A_l \frac{n}{n_i} + A_2 \frac{n^2}{n_i^2} \tag{B12}$$

$$T - T_s = \Delta T_{sup} \left(1 - \frac{n}{n_i}\right) \tag{B13}$$

where A_1 and A_2 are determined from the following two equations, one is from momentum Eq. (B7) and the other one is from the boundary condition Eq. (B10).

$$0 = -\frac{1}{\rho_v} n_i \frac{\partial p}{\partial s} + \frac{2A_2 v_v}{n_i} \tag{B14}$$

$$A_1 + A_2 = U_s \tag{B15}$$

Integrating continuity Eq. (B6) from $n = 0$ to $n = n_i$ gives

$$\frac{1}{\sin\theta} \frac{d}{ds} \left[\sin\theta \int_0^{n_i} u dn\right] = \left(u \frac{dn_i}{ds} - v\right)_{n_i} = G_v \tag{B16}$$

where G_v is the volume rate of evaporation of liquid at the location θ per unit interface area. G_v is coupled to the temperature fields by means of heat balance and evaporation at the interface, thus it gives

$$\frac{1}{\sin\theta} \frac{d}{ds} \left[\sin\theta \int_0^{n_i} u dn\right] = G_v = \frac{1}{\rho_v h_{fg}} \left[\left(k_l \frac{\partial T}{\partial r}\right)_{y=0} - \left(k_v \frac{\partial T}{\partial n}\right)_{n_i}\right] \tag{B17}$$

Substituting Eqs. (B4), (B12) and (B13) into Eq. (B17) yields

$$\frac{1}{\sin\theta} \frac{d}{d\theta} \left[\sin\theta \left(\frac{A_1 n_i}{2} + \frac{A_2 n_i}{3}\right)\right] = \frac{1}{\rho_v h_{fg}} \left(\frac{k_v \Delta T_{sup}}{n_i} - \frac{k_l \Delta T_{sub}}{R\delta_T}\right) \tag{B18}$$

A_1 and A_2 can be eliminated by means of Eqs. (B14) and (B15). Then, in terms of the dimensionless vapor film thickness $n^* = n_i/R$ Eq. (B18) becomes

$$\frac{1}{\sin\theta} \frac{d}{d\theta} \left[\sin\theta \left(n^{*3} \sin\theta \cos\theta + \alpha n^* \sin\theta\right)\right] = \frac{\beta}{n^*} - \gamma f(\theta) \tag{B19}$$

where

$$\alpha = \frac{4\mu_v}{UR\rho_l}$$

$$\beta = \frac{16}{3} \frac{k_v \mu_v \Delta T_{sup}}{\rho_v \rho_l U^2 R^2 h_{fg}}$$

$$\gamma = \frac{16}{3} \frac{k_l \mu_v \Delta T_{sub}}{\rho_v \rho_l U^2 R^2 h_{fg}} \frac{2}{\pi^{1/2}} \mathrm{Pe}^{1/2}$$

Equation (B19) cannot be solved in closed form, but can be integrated numerically in any particular case. However, this is not convenient for practical uses and not helpful for developing general correlations. So, instead we will show how the equation may be simplified in two special cases and then integrate it analytically. Therefore, we can gain more insight into which terms are likely to be important. Furthermore, the simplified solutions have the great advantage to provide dimensionless groups for developing correlations with only the constant to be determined by experiment.

Large Subcooling Case

Here we begin by supposing that the left hand side of Eq. (B19) is negligible, and the main balance is between the two terms on the right. This express mathematically the situation in which almost all the heat arriving at the interface is convected away in the liquid, and very little is used to produce vapor. This can be justified by following. First we suggest that the order of magnitude of n^* is β/γ,

$$n^* = \frac{\beta}{\gamma} H \qquad (B20)$$

Thus, after some rearrangement of (B19) we have

$$\epsilon \frac{1}{sin\,\theta} \frac{d}{d\theta} \left[sin\,\theta \left(H^3\, sin\,\theta\, cos\,\theta + AH\, sin\,\theta \right) \right] = \frac{1}{H} - f(\theta) \qquad (B21)$$

where

$$\epsilon = \frac{\beta^3}{\gamma^4} = \frac{3\pi^2 k_v^3 \rho_v \rho_l \alpha_l^2 h_{fg} (\Delta T_{sup})^3}{256 k_l^4 \mu_v (\Delta T_{sub})^4} \equiv 5 \times 10^{-5} \frac{\Delta T_{sup}^3}{\Delta T_{sub}^4}$$

$$A = \frac{\alpha \gamma^2}{\beta^2} = \frac{16 \mu_v k_l^2 (\Delta T_{sub})^2}{\pi \rho_l k_v^2 \alpha_l (\Delta T_{sup})^2} \equiv 1.6 \times 10^2 \frac{\Delta T_{sub}^2}{\Delta T_{sup}^2}$$

If ϵ is small and A is not large, the left hand side of Eq. (B21) could be reasonably be neglected. It is easy to see that these requirements can be met in the case of large subcooling. For water/steam system, if ΔT_{sup} = 800 °C, ΔT_{sub} need only be 20 °C to give $\epsilon = 0.16$ and $A = 0.1$. The higher is the subcooling and the lower is the sphere superheat the better is the approximation.

So the solution is simply

$$H = \frac{1}{f(\theta)} \qquad (B22)$$

to the first approximation.

It is easily to show that the Nusselt number is essentially the reciprocal of the nondimensional film thickness

$$\mathrm{Nu}_\theta = \frac{1}{n^*} \tag{B23}$$

Therefore, for the case of large subcooling

$$\mathrm{Nu}_\theta = \frac{1}{n^*} = \frac{1}{H(\theta)}\frac{\gamma}{\beta} = \frac{2}{\pi^{1/2}H(\theta)}\mathrm{Re}_l^{1/2}\mathrm{Pr}_l^{1/2}\frac{\mu_l}{\mu_v}\frac{Sc}{Sp} \tag{B24}$$

This the local Nusselt number. The average Nusselt number is defined as

$$\mathrm{Nu} = \frac{\int_0^{\theta_s}\mathrm{Nu}_\theta dA}{4\pi R^2} = \frac{1}{2}\int_0^{\theta_s} sin\,\theta \mathrm{Nu}_\theta d\theta \tag{B25}$$

Where θ_s is the angle of separation, which is π for the case of large subcooling. Thus, the average Nusselt number is in the form of

$$\mathrm{Nu} = C\mathrm{Re}_l^{1/2}\frac{\mu_l}{\mu_v}\frac{Sc}{Sp} \tag{B26}$$

where

$$C = \frac{1}{\pi^{1/2}}\int_0^x \frac{sin\,\theta}{H(\theta)}d\theta = 0.5642 \tag{B27}$$

This constant is much smaller than the experimental constant of 1.5 to 2.0.

Saturated Case

In this case we begin by neglecting the subcooling altogether, so that we set $\gamma = 0$ in Eq. (B21). After some trial and error it is found that the main balance is between the first term in the bracket on the left, which comes from the pressure gradient, and the term in β/n^* on the right. This suggests that the order of magnitude of n^* is $\beta^{1/4}$, and it gives

$$n^* = \beta^{1/4}\Psi \tag{B28}$$

Substituting it into Eq. (B19) yields

$$\frac{1}{sin\,\theta}\frac{d}{d\theta}\left[sin\,\theta\left(\Psi^3\,sin\,\theta\,cos\,\theta + \delta\Psi\,sin\,\theta\right)\right] = \frac{1}{\Psi} \tag{B29}$$

where the δ is given by

$$\delta = \frac{\alpha}{\beta^{1/2}} = \left(\frac{3\mu_v\rho_l h_{fg}}{k_v\rho_v}\right)^{1/2}\frac{1}{\Delta T_{sup}^{1/2}} \equiv 1.1 \times \frac{1}{\Delta T_{sup}^{1/2}} \tag{B30}$$

where the numerical values are appropriate for water/steam system. δ is small as long as ΔT_{sup} is large, so the term with δ in Eq. (B29) is clearly negligible in most cases. Thus the analytical solution for Ψ is

$$\Psi^4 = \frac{4}{3}(sin\,\theta)^{-8/3}(cos\,\theta)^{-4/3}\int_0^{\theta}(sin\,\theta')^{5/3}(cos\,\theta')^{1/3}d\theta' \qquad (B31)$$

It should be noted that this solution is valid only in the region $\theta < \pi/2$. Actually, for saturated forced convection film boiling, the vapor film gradually develops into a big vapor wake/dome, starting from the region near $\theta \equiv \pi/2$.

Therefore for small subcooling (or saturated) cases, the Nusselt number can be expressed as

$$\mathrm{Nu}_\theta = \frac{1}{n^*} = \frac{1}{\Psi(\theta)}\frac{1}{\beta^{1/4}} = \left(\frac{3}{64}\right)^{1/4}\frac{1}{\Psi(\theta)}\mathrm{Re}_l^{1/2}\left(\frac{1}{Sp}\frac{\mu_l^2\rho_v}{\mu_v^2\rho_l}\right)^{1/4} \qquad (B32)$$

By the definition of Eq. (B25) and integration from $\theta = 0$ to $\pi/2$, the average Nusselt number may be correlated in the form of

$$\mathrm{Nu} = C\mathrm{Re}_l^{1/2}\left(\frac{1}{Sp}\frac{\mu_l^2\rho_v}{\mu_v^2\rho_l}\right)^{1/4} = C\mathrm{Re}_l^{1/2}\frac{\mu_l}{\mu_v}\left(\frac{R^4K}{Sp}\right)^{1/4} \qquad (B33)$$

where

$$R = \left(\frac{\mu_v\rho_v}{\mu_l\rho_l}\right)^{1/2}, \qquad K = \frac{\rho_l}{\rho_v}$$

and

$$C = \frac{1}{2}\left(\frac{3}{64}\right)^{1/4}\int_0^{x/2}\frac{sin\,\theta}{\Psi}d\theta = 0.198 \qquad (B34)$$

As in the case of large subcooling, this theoretical constant is considerably low, comparing with the constant 0.5 which is obtained from the experiment.

APPENDIX C

TYPICAL SATURATED SINGLE-PHASE EXPERIMENT DATA

APPENDIX C

TYPICAL SATURATED SINGLE-PHASE EXPERIMENT DATA

Test Sphere Diameter: 6.35 mm
Support Thermocouple Wire Diameter: 0.51 mm
Test Sphere Material: 316 Stainless Steel

RUN 1 T_l=100.1(C) V_l=0.010(m/s) Fr= 0.002 Re= 225.1

T_w(C)	q_t(kW/m^2)	q_c	h_t (W/m^2/C)	h_c	Nu_t	Nu_c
672	162.33	138.92	284.21	243.22	29.88	29.88
790	190.06	152.30	275.99	221.16	24.02	24.02
575	133.30	118.33	281.21	249.64	34.22	34.22
493	109.65	99.87	279.45	254.51	38.48	38.48
426	87.36	80.78	269.00	248.73	40.87	40.87
369	72.60	68.08	271.12	254.25	45.05	45.05
320	61.57	58.44	281.12	266.80	50.63	50.63
278	52.26	50.06	294.91	282.54	56.93	56.93

RUN 2 T_l=100.0(C) V_l=0.112(m/s) Fr= 0.197 Re= 2500.1

T_w(C)	q_t(kW/m^2)	q_c	h_t (W/m^2/C)	h_c	Nu_t	Nu_c
698	182.60	156.47	305.94	262.16	31.33	31.33
600	146.54	129.68	293.79	259.98	34.64	34.64
518	121.16	109.97	290.49	263.66	38.67	38.67
448	100.64	93.07	289.56	267.79	42.75	42.75
389	83.35	78.15	289.17	271.14	46.74	46.74
338	70.33	66.72	296.30	281.06	51.94	51.94
294	60.35	57.82	312.20	299.11	58.93	58.93

RUN 3 T_l=100.1(C) V_l=0.216(m/s) Fr= 0.730 Re= 4815.2

T_w(C)	q_t(kW/m^2)	q_c	h_t (W/m^2/C)	h_c	Nu_t	Nu_c
814	226.60	185.18	317.74	259.66	27.52	27.52
693	175.58	149.95	296.43	253.15	30.40	30.40
595	140.68	124.21	284.85	251.49	33.70	33.70
513	115.77	104.88	281.08	254.66	37.59	37.59
442	99.30	92.03	291.21	269.87	43.44	43.44
380	83.27	78.37	298.09	280.57	48.94	48.94
328	70.18	66.85	309.61	294.91	55.35	55.35
284	57.01	54.70	311.88	299.26	59.82	59.82

RUN 4 T_l=100.3(C) V_l=0.232(m/s) Fr= 0.839 Re= 5167.1

T_w(C)	q_t(kW/m^2)	q_c	h_t (W/m^2/C)	h_c	Nu_t	Nu_c
750	202.52	170.10	311.79	261.89	29.60	29.60
645	167.30	146.56	307.75	269.61	34.13	34.13
556	134.94	121.34	296.78	266.89	37.41	37.41
481	110.53	101.40	290.97	266.94	40.96	40.96
417	94.14	87.90	297.83	278.10	46.22	46.22
362	79.26	74.95	303.47	286.97	51.31	51.31
315	67.33	64.31	314.19	300.11	57.34	57.34
275	55.10	52.96	315.67	303.41	61.36	61.36

RUN 5 T_l=100.5(C) V_l=0.333(m/s) Fr= 1.733 Re= 7426.9

T_w(C)	q_t(kW/m^2)	q_c	h_t (W/m^2/C)	h_c	Nu_t	Nu_c
758	207.37	173.98	315.64	264.82	29.70	29.70
644	164.20	143.50	302.23	264.12	33.45	33.45
550	136.22	122.98	303.09	273.63	38.59	38.59
472	111.28	102.60	299.95	276.56	42.90	42.90
406	91.36	85.53	299.12	280.06	47.20	47.20
351	73.58	69.61	294.64	278.76	50.63	50.63
304	62.92	60.18	310.35	296.82	57.69	57.69
265	51.50	49.57	314.32	302.52	62.12	62.12

RUN 6 T_l=100.5(C) V_l=0.446(m/s) Fr= 3.110 Re= 9951.5

T_w(C)	q_t(kW/m^2)	q_c	h_t (W/m^2/C)	h_c	Nu_t	Nu_c
857	236.82	188.44	313.40	249.38	25.34	25.34
709	189.31	161.93	311.34	266.31	31.45	31.45
593	143.73	127.37	291.90	258.67	34.72	34.72
499	117.28	107.20	294.79	269.43	40.47	40.47
421	93.78	87.38	292.90	272.92	45.11	45.11
357	75.46	71.30	294.49	278.25	50.09	50.09
305	59.64	56.87	292.49	278.91	54.12	54.12
262	49.25	47.37	306.22	294.55	60.75	60.75
226	40.36	39.07	321.94	311.68	67.75	67.75

RUN 7 T_l=100.6(C) V_l=0.538(m/s) Fr= 4.515 Re= 11998.0

T_w(C)	q_t(kW/m^2)	q_c	h_t (W/m^2/C)	h_c	Nu_t	Nu_c
739	207.11	176.19	324.74	276.25	31.61	31.61
620	157.80	139.21	303.73	267.96	34.86	34.86
525	127.03	115.45	299.87	272.52	39.65	39.65
446	100.79	93.35	292.36	270.77	43.38	43.38
379	80.17	75.31	287.87	270.40	47.22	47.22
325	71.28	68.01	317.94	303.37	57.14	57.14
280	55.18	52.96	308.35	295.91	59.47	59.47
242	46.00	44.46	325.60	314.72	66.79	66.79
211	37.31	36.24	340.01	330.32	73.55	73.55

RUN 8 T_l=100.7(C) V_l=0.772(m/s) Fr= 9.319 Re= 17244.8

T_w(C)	q_t(kW/m^2)	q_c	h_t (W/m^2/C)	h_c	Nu_t	Nu_c
769	245.55	210.68	367.54	315.33	34.97	34.97
674	212.47	188.83	370.55	329.32	40.36	40.36
590	177.25	161.13	362.20	329.26	44.34	44.34
519	148.61	137.37	355.62	328.72	48.16	48.16
458	124.43	116.43	348.60	326.19	51.47	51.47
406	105.96	100.15	347.34	328.30	55.35	55.35
360	91.65	87.40	353.55	337.15	60.44	60.44
320	77.26	74.12	352.08	337.75	64.05	64.05

RUN 9 T_l=100.7(C) V_l=0.955(m/s) Fr= 14.240 Re= 21316.6

T_w(C)	q_t(kW/m^2)	q_c	h_t (W/m^2/C)	h_c	Nu_t	Nu_c
788	253.93	216.40	369.57	314.95	34.26	34.26
692	237.11	211.58	400.92	357.75	43.01	43.01
608	204.65	187.16	403.94	369.40	48.78	48.78
535	168.64	156.38	388.14	359.92	51.68	51.68
473	142.79	134.06	383.88	360.42	55.84	55.84
419	123.78	117.48	389.51	369.67	61.30	61.30
371	101.88	97.28	376.78	359.77	63.52	63.52
330	92.09	88.70	402.30	387.49	72.48	72.48

RUN 10 T_l=100.8(C) V_l=1.310(m/s) Fr= 26.835 Re= 29274.4

T_w(C)	q_t(kW/m^2)	q_c	h_t (W/m^2/C)	h_c	Nu_t	Nu_c
786	247.84	210.54	361.58	307.17	33.47	33.47
700	281.92	255.52	470.46	426.41	50.84	50.84
619	239.14	220.66	461.40	425.75	55.47	55.47
549	202.32	189.15	451.24	421.88	59.58	59.58
488	178.65	169.17	462.08	437.56	66.60	66.60
432	150.99	144.13	455.67	434.97	70.88	70.88
385	135.16	130.10	475.53	457.73	79.32	79.32
343	122.96	119.23	508.76	493.30	90.61	90.61

RUN 11 T_l=100.8(C) V_l=1.645(m/s) Fr= 42.304 Re= 36756.3

T_w(C)	q_t(kW/m^2)	q_c	h_t (W/m^2/C)	h_c	Nu_t	Nu_c
768	198.48	163.74	297.53	245.46	27.25	27.25
696	289.39	263.44	486.17	442.57	52.99	52.99
624	250.98	232.10	479.87	443.77	57.50	57.50
560	211.77	197.90	461.73	431.49	60.20	60.20
503	187.73	177.38	466.42	440.71	65.82	65.82
454	162.16	154.37	459.90	437.78	69.45	69.45
409	143.75	137.82	466.65	447.42	75.14	75.14
369	130.60	126.08	487.86	471.00	83.46	83.46

RUN 12 T_l=100.8(C) V_l=1.838(m/s) Fr= 52.767 Re= 41045.8

T_w(C)	q_t(kW/m^2)	q_c	h_t (W/m^2/C)	h_c	Nu_t	Nu_c
726	286.09	256.71	457.60	410.59	47.60	47.60
650	267.38	246.11	486.73	448.01	56.36	56.36
582	230.48	215.01	479.40	447.23	60.82	60.82
520	203.93	192.62	486.63	459.64	67.25	67.25
465	176.21	167.85	483.34	460.40	71.97	71.97
418	154.54	148.26	487.13	467.33	77.55	77.55
376	134.28	129.54	488.40	471.13	82.67	82.67

Test Sphere Diameter: 9.53 mm
Support Thermocouple Wire Diameter: 0.51 mm
Test Sphere Material : 316 Stainless Steel

RUN 1 T_l=100.5(C) V_l=0.010(m/s) Fr= 0.001 Re= 340.5

T_w(C)	q_t(kW/m^2)	q_c	h_t (W/m^2/C)	h_c	Nu_t	Nu_c
731	154.77	124.74	245.45	197.82	33.26	33.26
636	128.44	108.48	240.00	202.70	37.79	37.79
554	106.69	93.18	235.34	205.55	42.09	42.09
484	87.99	78.70	229.74	205.49	45.82	45.82
424	75.85	69.35	235.00	214.85	51.63	51.63
372	63.03	58.41	232.64	215.60	55.48	55.48
327	53.55	50.23	236.60	221.92	60.78	60.78
289	46.84	44.42	249.18	236.33	68.42	68.42
256	43.47	41.70	281.01	269.60	81.83	81.83

RUN 2 T_l=100.5(C) V_l=0.116(m/s) Fr= 0.145 Re= 3782.8

T_w(C)	q_t(kW/m^2)	q_c	h_t (W/m^2/C)	h_c	Nu_t	Nu_c
743	158.87	127.44	247.55	198.59	33.00	33.00
643	129.33	108.71	238.46	200.45	37.07	37.07
559	108.78	94.96	237.54	207.37	42.24	42.24
487	90.21	80.77	233.80	209.34	46.52	46.52
425	76.82	70.26	236.87	216.62	51.95	51.95
373	64.31	59.66	236.57	219.47	56.41	56.41
328	53.56	50.22	235.82	221.11	60.48	60.48
289	45.51	43.08	241.31	228.44	66.07	66.07
256	40.60	38.83	262.07	250.64	76.05	76.05

RUN 3 T_l=100.6(C) V_l=0.167(m/s) Fr= 0.299 Re= 5435.6

T_w(C)	q_t(kW/m^2)	q_c	h_t (W/m^2/C)	h_c	Nu_t	Nu_c
731	154.88	124.89	245.77	198.18	33.34	33.34
640	128.07	107.79	237.75	200.11	37.16	37.16
560	109.44	95.51	238.14	207.82	42.25	42.25
492	92.87	83.13	237.18	212.29	46.86	46.86
434	77.61	70.69	233.22	212.42	50.40	50.40
383	67.05	62.06	237.71	220.03	55.78	55.78
339	57.72	54.08	242.32	227.04	61.14	61.14
301	49.04	46.36	245.39	231.99	66.06	66.06
267	42.73	40.76	257.30	245.41	73.27	73.27

RUN 4 T_l=100.6(C) V_l=0.240(m/s) Fr= 0.617 Re= 7812.0

T_w(C)	q_t(kW/m^2)	q_c	h_t (W/m^2/C)	h_c	Nu_t	Nu_c
725	151.27	122.03	242.44	195.58	33.12	33.12
636	128.93	108.99	241.00	203.72	37.99	37.99
559	107.21	93.36	233.88	203.66	41.46	41.46
493	91.33	81.58	233.14	208.24	45.96	45.96
435	79.16	72.20	237.11	216.24	51.23	51.23
384	67.88	62.86	239.66	221.92	56.17	56.17
340	59.09	55.43	247.16	231.83	62.35	62.35
302	49.94	47.25	248.96	235.53	66.99	66.99
268	44.07	42.08	264.41	252.49	75.32	75.32

RUN 5 T_l=100.6(C) V_l=0.345(m/s) Fr= 1.273 Re= 11221.3

T_w(C)	q_t(kW/m^2)	q_c	h_t (W/m^2/C)	h_c	Nu_t	Nu_c
745	164.63	132.90	255.56	206.29	34.20	34.20
649	134.18	112.99	244.66	206.03	37.85	37.85
567	110.52	96.09	236.89	205.97	41.53	41.53
497	92.88	82.90	234.55	209.34	45.97	45.97
436	79.19	72.17	236.27	215.32	50.93	50.93
384	65.69	60.67	232.27	214.54	54.34	54.34
338	57.70	54.08	242.88	227.63	61.35	61.35
299	49.79	47.15	251.08	237.76	67.85	67.85
265	43.15	41.21	263.25	251.45	75.31	75.31

RUN 6 T_l=100.6(C) V_l=0.426(m/s) Fr= 1.945 Re= 13870.7

T_w(C)	q_t(kW/m^2)	q_c	h_t (W/m^2/C)	h_c	Nu_t	Nu_c
760	159.92	126.24	242.58	191.48	31.25	31.25
656	136.67	114.89	246.39	207.13	37.79	37.79
567	107.35	92.93	230.16	199.25	40.19	40.19
493	95.51	85.73	243.55	218.62	48.22	48.22
429	73.89	67.15	225.00	204.49	48.79	48.79
375	63.89	59.18	233.23	216.01	55.36	55.36
328	52.66	49.31	231.64	216.92	59.32	59.32
288	44.82	42.42	239.21	226.39	65.59	65.59
254	38.93	37.19	253.96	242.60	73.79	73.79

RUN 7 T_l=100.6(C) V_l=0.557(m/s) Fr= 3.318 Re= 18118.4

T_w(C)	q_t(kW/m^2)	q_c	h_t (W/m^2/C)	h_c	Nu_t	Nu_c
766	168.47	133.99	253.26	201.43	32.68	32.68
668	142.07	119.04	250.39	209.80	37.75	37.75
585	113.92	98.23	235.53	203.10	40.16	40.16
513	99.95	89.07	242.64	216.21	46.55	46.55
451	81.68	74.00	233.35	211.41	49.08	49.08
398	70.95	65.45	239.07	220.53	54.83	54.83
351	59.20	55.21	236.48	220.56	58.39	58.39
311	54.59	51.68	259.99	246.12	69.03	69.03
276	46.97	44.82	268.18	255.90	75.43	75.43

RUN 8 T_l=100.6(C) V_l=0.800(m/s) Fr= 6.850 Re= 26031.1

T_w(C)	q_t(kW/m^2)	q_c	h_t (W/m^2/C)	h_c	Nu_t	Nu_c
750	211.72	179.34	326.07	276.19	45.54	45.54
663	165.94	143.42	295.14	255.09	46.15	46.15
587	135.96	120.06	279.49	246.81	48.65	48.65
521	119.34	107.94	283.75	256.65	54.67	54.67
465	98.21	89.88	269.97	247.09	56.40	56.40
414	86.31	80.19	275.49	255.93	62.26	62.26
370	76.04	71.49	282.80	265.87	68.61	68.61
330	67.28	63.89	293.69	278.87	76.07	76.07
295	59.34	56.79	305.43	292.29	83.88	83.88

RUN 9 T_l=100.6(C) V_l=0.988(m/s) Fr= 10.466 Re= 32181.8

T_w(C)	q_t(kW/m^2)	q_c	h_t (W/m^2/C)	h_c	Nu_t	Nu_c
786	205.97	168.70	300.57	246.19	39.14	39.14
696	178.68	152.77	300.38	256.83	44.87	44.87
617	154.66	136.37	299.67	264.23	50.34	50.34
548	136.53	123.46	305.50	276.25	57.00	57.00
488	113.30	103.82	293.00	268.47	59.61	59.61
434	101.81	94.89	305.82	285.02	67.61	67.61
386	85.78	80.67	300.50	282.62	71.33	71.33
343	79.13	75.39	327.20	311.73	83.51	83.51
304	72.95	70.21	359.90	346.37	98.20	98.20

RUN 10 T_l=100.7(C) V_l=1.291(m/s) Fr= 17.852 Re= 42046.9

T_w(C)	q_t(kW/m^2)	q_c	h_t (W/m^2/C)	h_c	Nu_t	Nu_c
813	241.06	199.84	338.64	280.74	43.45	43.45
722	206.01	177.14	331.82	285.33	48.48	48.48
644	184.71	164.07	340.41	302.37	55.90	55.90
574	162.86	147.99	344.47	313.01	62.67	62.67
511	137.52	126.71	334.98	308.66	66.57	66.57
457	127.86	119.92	359.54	337.22	77.75	77.75
406	111.91	106.11	367.30	348.28	85.69	85.69
359	100.55	96.33	389.28	372.93	97.64	97.64
317	90.41	87.33	417.46	403.26	112.02	112.02

RUN 11 T_l=100.7(C) V_l=1.539(m/s) Fr= 25.381 Re= 50130.4

T_w(C)	q_t(kW/m^2)	q_c	h_t (W/m^2/C)	h_c	Nu_t	Nu_c
766	219.15	184.68	329.49	277.66	45.05	45.05
686	217.96	193.06	372.27	329.74	58.18	58.18
615	186.47	168.33	362.51	327.24	62.46	62.46
551	162.63	149.32	360.98	331.43	68.10	68.10
494	146.50	136.70	373.05	348.08	76.73	76.73
441	133.70	126.44	392.63	371.33	87.24	87.24
393	117.93	112.59	403.54	385.26	96.36	96.36
349	104.87	100.96	423.20	407.42	108.23	108.23
309	97.10	94.24	467.11	453.34	127.55	127.55

RUN 12 T_l=100.6(C) V_l=2.040(m/s) Fr= 44.599 Re= 66428.8

T_w(C)	q_t(kW/m^2)	q_c	h_t (W/m^2/C)	h_c	Nu_t	Nu_c
784	244.07	207.07	357.14	302.99	48.26	48.26
700	236.96	210.62	395.73	351.73	61.20	61.20
554	178.63	165.17	394.62	364.89	74.78	74.78
493	159.60	149.80	406.62	381.66	84.15	84.15
438	143.75	136.63	426.13	405.04	95.54	95.54
388	125.55	120.40	437.76	419.80	105.76	105.76
345	105.76	101.96	433.81	418.24	111.73	111.73

Test Sphere Diameter: 12.7 mm
Support Thermocouple Wire Diameter: 0.81 mm
Test Sphere Material : 316 Stainless Steel

RUN 1 T_l=100.1(C) V_l=0.011(m/s) Fr= 0.001 Re= 478.2

T_w(C)	q_t(kW/m^2)	q_c	h_t (W/m^2/C)	h_c	Nu_t	Nu_c
748	145.70	118.92	225.06	183.69	40.46	40.46
655	124.72	106.62	225.11	192.44	46.84	46.84
574	102.06	89.67	215.91	189.69	50.64	50.64
503	88.15	79.56	219.34	197.95	57.54	57.54
441	74.13	68.09	217.83	200.09	62.69	62.69
387	63.96	59.68	223.39	208.45	70.07	70.07
340	54.75	51.69	228.69	215.91	77.38	77.38
300	47.00	44.79	236.65	225.54	85.78	85.78
265	38.87	37.26	236.86	227.02	90.63	90.63

RUN 2 T_l=100.0(C) V_l=0.123(m/s) Fr= 0.121 Re= 5309.8

T_w(C)	q_t(kW/m^2)	q_c	h_t (W/m^2/C)	h_c	Nu_t	Nu_c
832	172.69	135.80	236.19	185.73	37.60	37.60
713	136.38	113.15	222.73	184.81	42.25	42.25
613	113.77	98.78	221.96	192.71	49.15	49.15
528	95.47	85.64	223.51	200.48	56.48	56.48
455	79.94	73.39	225.91	207.41	63.90	63.90
393	65.07	60.63	223.02	207.82	69.35	69.35
341	53.18	50.10	221.22	208.39	74.58	74.58
298	44.97	42.79	228.10	217.04	82.72	82.72

RUN 3 T_l=100.4(C) V_l=0.176(m/s) Fr= 0.249 Re= 7640.1

T_w(C)	q_t(kW/m^2)	q_c	h_t (W/m^2/C)	h_c	Nu_t	Nu_c
824	166.24	130.43	229.92	180.40	36.82	36.82
712	133.78	110.68	218.97	181.17	41.48	41.48
617	111.93	96.69	216.90	187.37	47.60	47.60
535	93.50	83.29	215.29	191.78	53.57	53.57
465	78.69	71.76	216.37	197.31	60.05	60.05
404	65.93	61.14	217.34	201.56	66.24	66.24
353	54.91	51.54	217.61	204.26	71.90	71.90
309	46.71	44.31	224.03	212.53	79.66	79.66

RUN 4 T_l=100.6(C) V_l=0.253(m/s) Fr= 0.514 Re= 10982.2

T_w(C)	q_t(kW/m^2)	q_c	h_t (W/m^2/C)	h_c	Nu_t	Nu_c
724	134.36	110.10	215.70	176.76	39.95	39.95
637	114.53	97.82	213.58	182.41	45.28	45.28
561	99.08	87.43	215.21	189.89	51.42	51.42
494	85.07	76.86	216.13	195.27	57.33	57.33
436	73.62	67.77	219.69	202.24	63.79	63.79
385	63.52	59.32	223.78	208.96	70.46	70.46
340	54.14	51.09	226.42	213.65	76.60	76.60
301	46.80	44.57	233.92	222.75	84.54	84.54
267	40.44	38.80	244.02	234.12	93.25	93.25

RUN 5 T_l=100.7(C) V_l=0.364(m/s) Fr= 1.062 Re= 15784.2

T_w(C)	q_t(kW/m^2)	q_c	h_t (W/m^2/C)	h_c	Nu_t	Nu_c
749	140.09	113.19	216.03	174.55	38.41	38.41
655	117.71	99.61	212.44	179.77	43.76	43.76
574	100.27	87.88	212.16	185.95	49.65	49.65
502	84.87	76.31	211.60	190.27	55.36	55.36
440	72.39	66.38	213.24	195.55	61.34	61.34
387	61.49	57.23	215.09	200.17	67.32	67.32
340	53.16	50.10	222.14	209.35	75.04	75.04
300	45.44	43.22	228.05	216.90	82.42	82.42
265	38.80	37.18	236.47	226.63	90.48	90.48

RUN 6 T_l=100.7(C) V_l=0.449(m/s) Fr= 1.622 Re= 19512.3

T_w(C)	q_t(kW/m^2)	q_c	h_t (W/m^2/C)	h_c	Nu_t	Nu_c
780	147.28	116.97	216.93	172.29	36.75	36.75
678	120.84	100.83	209.43	174.76	41.49	41.49
590	102.18	88.74	208.75	181.28	47.48	47.48
515	86.36	77.17	208.49	186.32	53.33	53.33
450	72.84	66.48	208.73	190.51	59.05	59.05
394	62.94	58.47	214.86	199.60	66.50	66.50
345	53.01	49.85	217.35	204.37	72.78	72.78
303	44.89	42.62	222.26	211.02	79.86	79.86
266	38.74	37.10	234.03	224.14	89.30	89.30

RUN 7 T_l=100.7(C) V_l=0.587(m/s) Fr= 2.768 Re= 25491.9

T_w(C)	q_t(kW/m^2)	q_c	h_t (W/m^2/C)	h_c	Nu_t	Nu_c
750	140.26	113.35	216.25	174.75	38.45	38.45
661	118.57	100.01	211.83	178.67	43.22	43.22
583	101.05	88.08	209.61	182.70	48.25	48.25
515	86.04	76.85	207.70	185.53	53.10	53.10
456	76.12	69.53	214.48	195.93	60.28	60.28
402	65.66	60.93	217.76	202.07	66.57	66.57
356	57.16	53.72	224.07	210.60	73.84	73.84
316	48.46	45.93	225.69	213.93	79.45	79.45
280	42.62	40.76	237.72	227.34	88.82	88.82

RUN 8 T_l=100.8(C) V_l=0.843(m/s) Fr= 5.713 Re= 36629.8

T_w(C)	q_t(kW/m^2)	q_c	h_t (W/m^2/C)	h_c	Nu_t	Nu_c
774	166.57	136.90	247.35	203.28	43.60	43.60
684	140.91	120.37	241.64	206.42	48.68	48.68
605	123.67	109.26	245.31	216.72	55.81	55.81
534	105.63	95.46	243.62	220.16	61.55	61.55
473	91.05	83.77	244.71	225.16	67.84	67.84
419	77.49	72.22	243.37	226.81	73.08	73.08
372	68.91	65.07	254.48	240.29	82.46	82.46
330	59.70	56.88	260.84	248.50	90.41	90.41
293	52.03	49.95	271.39	260.54	100.04	100.04

RUN 9 T_l=100.8(C) V_l=1.042(m/s) Fr= 8.729 Re= 45285.8

T_w(C)	q_t(kW/m^2)	q_c	h_t (W/m^2/C)	h_c	Nu_t	Nu_c
781	183.35	152.87	269.46	224.65	47.85	47.85
695	158.66	137.18	267.26	231.07	53.90	53.90
617	139.24	123.99	269.74	240.20	61.00	61.00
548	118.50	107.57	264.78	240.36	66.08	66.08
488	105.26	97.35	272.05	251.60	74.46	74.46
434	90.55	84.78	272.00	254.66	80.55	80.55
386	78.67	74.42	275.83	260.95	87.84	87.84

RUN 10 T_l=100.8(C) V_l=1.361(m/s) Fr= 14.890 Re= 59158.8

T_w(C)	q_t(kW/m^2)	q_c	h_t (W/m^2/C)	h_c	Nu$_t$	Nu$_c$
784	196.34	165.48	287.24	242.10	51.40	51.40
701	195.98	173.94	326.74	289.99	67.20	67.20
630	155.35	139.21	293.90	263.36	65.95	65.95
567	144.56	132.59	310.43	284.73	76.63	76.63
504	137.12	128.45	339.77	318.29	92.32	92.32
451	110.81	104.39	316.14	297.84	92.14	92.14
404	100.75	95.96	331.98	316.19	103.90	103.90
361	91.12	87.57	350.71	337.02	117.40	117.40
320	87.82	85.21	400.73	388.79	143.45	143.45

RUN 11 T_l=100.7(C) V_l=1.741(m/s) Fr= 24.348 Re= 75589.7

T_w(C)	q_t(kW/m^2)	q_c	h_t (W/m^2/C)	h_c	Nu$_t$	Nu$_c$
807	215.58	181.92	305.16	257.51	53.44	53.44
723	206.65	182.52	332.43	293.61	66.45	66.45
646	182.90	165.49	335.41	303.49	74.59	74.59
577	160.02	147.41	336.00	309.53	82.30	82.30
514	146.44	137.30	354.36	332.24	95.22	95.22
456	127.59	121.01	359.54	340.99	104.92	104.92
404	116.49	111.70	384.19	368.42	121.10	121.10
355	106.47	103.05	418.42	404.97	142.12	142.12
312	90.86	88.42	431.15	419.55	156.72	156.72

RUN 12 T_l=100.3(C) V_l=2.244(m/s) Fr= 40.476 Re= 97295.1

T_w(C)	q_t(kW/m^2)	q_c	h_t (W/m^2/C)	h_c	Nu$_t$	Nu$_c$
892	145.39	99.76	183.86	126.15	24.12	24.12
796	275.51	243.22	396.15	349.72	73.38	73.38
707	242.23	219.64	399.93	362.63	83.49	83.49
625	213.88	198.06	407.95	377.76	95.06	95.06
551	188.78	177.69	419.08	394.46	108.07	108.07
484	170.23	162.47	444.01	423.77	125.94	125.94
423	152.98	147.59	475.28	458.54	147.09	147.09
367	133.86	130.15	503.70	489.73	169.22	169.22
317	115.96	113.40	535.70	523.88	194.05	194.05

Test Sphere Diameter: 19.1 mm
Support Thermocouple Wire Diameter: 0.81 mm
Test Sphere Material : 316 Stainless Steel

RUN 1 T_l=100.8(C) V_l=0.004(m/s) Fr= 0.000 Re= 255.7

T_w(C)	q_t(kW/m^2)	q_c	h_t (W/m^2/C)	h_c	Nu_t	Nu_c
782	178.04	129.21	261.55	189.81	60.63	60.63
676	138.22	106.49	240.41	185.22	66.11	66.11
589	112.58	91.27	230.88	187.17	73.68	73.68
515	90.67	75.98	218.95	183.48	78.79	78.79
453	77.49	67.15	220.37	190.97	88.49	88.49
399	64.51	57.09	216.16	191.30	94.92	94.92
354	54.00	48.59	213.66	192.26	101.45	101.45
314	47.34	43.36	222.23	203.54	113.66	113.66

RUN 4 T_l=100.8(C) V_l=0.300(m/s) Fr= 0.482 Re= 19538.6

T_w(C)	q_t(kW/m^2)	q_c	h_t (W/m^2/C)	h_c	Nu_t	Nu_c
782	164.04	115.11	240.79	168.97	53.94	53.94
679	127.12	95.01	220.04	164.46	58.52	58.52
593	106.47	84.70	216.39	172.14	67.43	67.43
520	87.23	72.13	208.01	171.99	73.38	73.38
458	74.10	63.40	207.22	177.29	81.55	81.55
405	62.32	54.61	204.74	179.41	88.32	88.32
359	53.75	48.13	208.33	186.56	97.73	97.73
318	45.95	41.82	211.21	192.22	106.63	106.63
283	41.06	38.01	225.77	209.00	122.04	122.04

RUN 5 T_l=100.8(C) V_l=0.431(m/s) Fr= 0.994 Re= 28074.0

T_w(C)	q_t(kW/m^2)	q_c	h_t (W/m^2/C)	h_c	Nu_t	Nu_c
797	167.48	115.65	240.53	166.09	52.23	52.23
696	122.60	87.98	205.93	147.78	51.61	51.61
612	108.45	84.63	212.21	165.61	63.47	63.47
540	88.71	71.99	202.15	164.05	68.36	68.36
478	78.35	66.36	207.68	175.89	78.99	78.99
424	67.01	58.32	207.36	180.46	86.69	86.69
377	58.20	51.81	210.67	187.54	95.83	95.83
337	48.96	44.20	207.77	187.57	101.38	101.38
301	42.76	39.20	214.15	196.30	111.81	111.81

RUN 6 T_l=100.8(C) V_l=0.577(m/s) Fr= 1.785 Re= 37621.8

T_w(C)	q_t(kW/m^2)	q_c	h_t (W/m^2/C)	h_c	Nu_t	Nu_c
791	162.22	111.69	235.22	161.94	51.26	51.26
695	138.62	104.23	233.45	175.53	61.40	61.40
613	109.24	85.27	213.19	166.41	63.68	63.68
542	93.84	76.94	212.80	174.46	72.51	72.51
427	70.44	61.61	216.31	189.20	90.60	90.60
380	62.05	55.53	222.38	199.05	101.34	101.34
339	54.77	49.91	229.91	209.53	112.83	112.83
303	46.72	43.08	231.30	213.31	121.08	121.08

RUN 7 T_l=100.8(C) V_l=0.696(m/s) Fr= 2.591 Re= 45337.7

T_w(C)	q_t(kW/m^2)	q_c	h_t (W/m^2/C)	h_c	Nu_t	Nu_c
776	175.41	127.69	259.96	189.24	60.80	60.80
684	135.28	102.40	231.95	175.57	62.11	62.11
607	112.36	89.08	221.98	175.99	67.83	67.83
541	95.26	78.45	216.56	178.35	74.22	74.22
484	81.47	69.06	212.55	180.19	80.33	80.33
431	72.53	63.45	219.62	192.12	91.46	91.46
386	61.01	54.23	214.05	190.24	96.08	96.08
344	57.81	52.77	237.69	216.97	116.02	116.02
307	48.69	44.92	236.04	217.77	122.83	122.83

RUN 8 T_l=100.9(C) V_l=0.999(m/s) Fr= 5.349 Re= 65142.0

T_w(C)	q_t(kW/m^2)	q_c	h_t (W/m^2/C)	h_c	Nu_t	Nu_c
806	201.25	147.64	285.36	209.34	65.24	65.24
711	159.27	122.45	261.07	200.72	69.00	69.00
631	138.08	112.04	260.33	211.23	79.19	79.19
563	115.71	96.93	250.58	209.90	85.12	85.12
503	97.60	83.82	242.61	208.35	90.79	90.79
452	80.41	70.13	229.28	199.98	92.78	92.78
406	75.31	67.56	246.85	221.45	108.92	108.92
366	63.82	57.92	241.09	218.82	113.58	113.58
328	55.25	50.81	243.64	224.04	122.64	122.64

RUN 9 T_l=100.9(C) V_l=1.235(m/s) Fr= 8.173 Re= 80534.8

T_w(C)	q_t(kW/m^2)	q_c	h_t (W/m^2/C)	h_c	Nu_t	Nu_c
823	222.48	165.38	308.07	229.00	70.16	70.16
730	182.86	143.06	290.69	227.42	76.61	76.61
652	150.14	121.61	272.62	220.81	80.92	80.92
584	128.22	107.38	265.48	222.33	87.99	87.99
525	110.96	95.46	261.57	225.04	95.45	95.45
474	96.00	84.31	257.47	226.10	102.08	102.08
428	84.49	75.56	257.95	230.68	110.20	110.20
388	73.60	66.74	256.79	232.87	117.36	117.36
350	66.58	61.29	266.74	245.57	130.15	130.15

RUN 10 T_l=100.9(C) V_l=1.613(m/s) Fr= 13.942 Re=105200.9

T_w(C)	q_t(kW/m^2)	q_c	h_t (W/m^2/C)	h_c	Nu_t	Nu_c
832	251.01	191.93	343.18	262.40	79.66	79.66
744	206.10	163.92	320.30	254.74	84.52	84.52
669	177.53	146.72	312.44	258.20	92.83	92.83
602	156.04	133.28	311.24	265.84	103.04	103.04
542	139.19	122.29	315.65	277.31	115.26	115.26
487	119.36	106.72	308.75	276.06	122.60	122.60
438	110.84	101.38	329.01	300.93	142.05	142.05
393	98.76	91.66	338.47	314.15	157.25	157.25

APPENDIX D

TYPICAL SUBCOOLED SINGLE-PHASE EXPERIMENT DATA

APPENDIX D

TYPICAL SUBCOOLED SINGLE-PHASE EXPERIMENT DATA

Test Sphere Diameter: 12.7 mm
Support Thermocouple Wire Diameter: 0.81 mm
Test Sphere Material: 316 Stainless Steel

RUN 1 T_l= 95.4(C) V_l=0.011(m/s) Fr= 0.001 Re= 468.4

T_w(C)	q_t(kW/m^2)	q_c	h_t (W/m^2/C)	h_c	Nu_t	Nu_c
768	167.33	138.33	250.66	207.21	44.71	44.71
669	138.72	119.44	244.03	210.11	50.34	50.34
584	117.89	104.87	244.17	217.21	57.32	57.32
510	97.53	88.61	238.60	216.78	62.47	62.47
444	84.76	78.60	246.68	228.76	71.38	71.38
388	72.34	68.04	252.00	237.02	79.59	79.59
339	60.77	57.74	255.42	242.70	87.17	87.17
297	50.54	48.38	257.41	246.38	94.00	94.00
262	43.33	41.76	269.12	259.39	104.02	104.02

RUN 2 T_l= 95.1(C) V_l=0.123(m/s) Fr= 0.122 Re= 5195.7

T_w(C)	q_t(kW/m^2)	q_c	h_t (W/m^2/C)	h_c	Nu_t	Nu_c
741	169.27	143.27	264.50	223.87	49.70	49.70
653	146.58	128.63	265.46	232.96	56.82	56.82
576	123.79	111.27	260.75	234.39	62.43	62.43
508	106.10	97.25	260.50	238.78	68.94	68.94
448	93.32	87.02	268.51	250.37	77.74	77.74
395	82.66	78.16	281.24	265.93	88.49	88.49
347	74.11	70.90	301.70	288.64	102.55	102.55
303	64.38	62.11	318.59	307.34	116.29	116.29
264	58.83	57.24	361.52	351.73	140.69	140.69

RUN 3 T_l= 95.3(C) V_l=0.177(m/s) Fr= 0.251 Re= 7472.2

T_w(C)	q_t(kW/m^2)	q_c	h_t (W/m^2/C)	h_c	Nu_t	Nu_c
743	169.55	143.31	263.99	223.14	49.42	49.42
654	145.79	127.75	263.48	230.87	56.24	56.24
576	124.95	112.40	262.89	236.48	62.94	62.94
507	107.48	98.70	264.77	243.13	70.31	70.31
445	94.16	87.98	273.67	255.72	79.75	79.75
390	83.61	79.25	289.31	274.24	91.85	91.85
341	73.36	70.29	306.15	293.35	105.11	105.11
296	65.28	63.14	334.61	323.63	123.69	123.69
255	60.89	59.43	394.55	385.05	155.91	155.91

RUN 4 T_l= 95.5(C) V_l=0.254(m/s) Fr= 0.519 Re= 10741.7

T_w(C)	q_t(kW/m^2)	q_c	h_t (W/m^2/C)	h_c	Nu_t	Nu_c
741	175.94	149.96	274.98	234.37	52.04	52.04
656	150.70	132.53	271.55	238.80	58.07	58.07
581	131.49	118.65	273.95	247.20	65.44	65.44
514	114.15	105.01	276.20	254.09	72.82	72.82
455	99.15	92.61	280.27	261.78	80.65	80.65
402	87.01	82.30	289.35	273.70	90.27	90.27
354	77.17	73.79	305.34	291.97	102.71	102.71
310	72.01	69.61	345.18	333.68	125.04	125.04
268	68.23	66.56	407.71	397.75	158.06	158.06

RUN 5 T_l= 95.5(C) V_l=0.410(m/s) Fr= 1.352 Re= 17345.6

T_w(C)	q_t(kW/m^2)	q_c	h_t (W/m^2/C)	h_c	Nu_t	Nu_c
766	191.84	163.17	288.63	245.48	53.13	53.13
683	159.64	139.16	274.07	238.90	56.39	56.39
609	146.27	131.61	288.07	259.20	66.48	66.48
541	125.73	115.22	285.76	261.87	72.65	72.65
480	112.60	105.02	296.88	276.89	82.70	82.70
425	99.78	94.32	307.86	291.00	93.08	93.08
374	94.64	90.74	346.90	332.60	113.83	113.83
326	85.82	83.08	381.52	369.35	135.14	135.14
282	76.10	74.21	420.45	410.00	159.81	159.81

RUN 8 T_l= 95.3(C) V_l=0.525(m/s) Fr= 2.210 Re= 22162.5

T_w(C)	q_t(kW/m^2)	q_c	h_t (W/m^2/C)	h_c	Nu_t	Nu_c
847	230.89	192.00	309.65	257.50	51.39	51.39
750	197.83	170.91	304.95	263.44	57.95	57.95
663	177.59	158.85	316.02	282.67	68.21	68.21
585	155.68	142.56	321.37	294.29	77.51	77.51
515	137.19	128.03	331.62	309.48	88.64	88.64
451	122.54	116.14	350.08	331.80	102.70	102.70
394	110.51	106.02	376.53	361.24	120.27	120.27
340	99.21	96.15	414.81	402.03	144.14	144.14
290	90.30	88.26	476.43	465.67	179.35	179.35

RUN 6 T_l= 95.4(C) V_l=0.589(m/s) Fr= 2.791 Re= 24914.3

T_w(C)	q_t(kW/m^2)	q_c	h_t (W/m^2/C)	h_c	Nu_t	Nu_c
753	211.06	183.80	323.81	281.99	61.84	61.84
674	188.72	169.06	329.39	295.07	70.36	70.36
602	168.64	154.42	336.46	308.10	79.62	79.62
537	151.35	141.05	347.13	323.51	90.18	90.18
477	136.82	129.38	363.83	344.04	103.15	103.15
422	121.74	116.37	378.89	362.17	116.26	116.26
371	115.96	112.12	428.78	414.60	142.35	142.35
323	105.87	103.20	477.48	465.44	171.09	171.09
278	95.99	94.17	542.95	532.66	208.84	208.84

RUN 7 T_l= 95.4(C) V_l=0.847(m/s) Fr= 5.761 Re= 35790.6

T_w(C)	q_t(kW/m^2)	q_c	h_t (W/m^2/C)	h_c	Nu_t	Nu_c
814	282.70	248.25	396.68	348.33	71.83	71.83
726	250.83	226.37	401.41	362.27	81.71	81.71
647	220.71	203.26	404.39	372.42	91.48	91.48
574	206.91	194.50	437.34	411.10	109.69	109.69
506	184.93	176.19	456.62	435.04	125.96	125.96
444	162.76	156.63	474.75	456.87	142.70	142.70
387	148.31	144.05	519.00	504.09	169.56	169.56
333	136.13	133.24	586.51	574.04	207.88	207.88
284	127.20	125.28	696.07	685.56	266.55	266.55

RUN 9 T_l= 95.3(C) V_l=1.047(m/s) Fr= 8.805 Re= 44226.1

T_w(C)	q_t(kW/m^2)	q_c	h_t (W/m^2/C)	h_c	Nu_t	Nu_c
884	338.29	293.83	431.89	375.14	72.22	72.22
791	314.38	282.79	455.79	409.98	86.51	86.51
705	274.78	252.35	455.03	417.90	96.41	96.41
627	248.56	232.63	472.75	442.44	111.15	111.15
553	227.47	216.27	502.90	478.15	130.72	130.72
485	205.25	197.48	534.70	514.43	152.80	152.80
422	186.18	180.81	579.60	562.90	180.72	180.72
363	170.22	166.59	648.27	634.45	220.18	220.18
308	160.42	158.04	773.80	762.34	286.22	286.22

RUN 10 T_l= 95.3(C) V_l=1.367(m/s) Fr= 15.021 Re= 57761.3

T_w(C)	q_t(kW/m^2)	q_c	h_t (W/m^2/C)	h_c	Nu_t	Nu_c
908	382.17	333.88	473.47	413.65	77.86	77.86
813	404.41	370.04	567.97	519.70	107.24	107.24
723	367.28	343.06	590.00	551.09	124.62	124.62
640	329.95	313.00	611.77	580.35	143.58	143.58
564	298.77	286.96	645.45	619.96	167.40	167.40
492	270.98	262.87	692.43	671.71	197.75	197.75
426	247.07	241.56	759.19	742.26	237.02	237.02
365	222.60	218.93	842.56	828.66	286.94	286.94
310	196.57	194.17	941.67	930.16	348.48	348.48

RUN 12 T_l= 95.3(C) V_l=1.748(m/s) Fr= 24.555 Re= 73844.5

T_w(C)	q_t(kW/m^2)	q_c	h_t (W/m^2/C)	h_c	Nu_t	Nu_c
766	466.33	437.58	700.93	657.72	142.25	142.25
683	426.55	406.11	732.87	697.75	164.77	164.77
605	395.36	380.98	785.04	756.49	194.95	194.95
532	352.44	342.39	817.37	794.08	222.64	222.64
466	316.15	309.16	866.11	846.97	257.37	257.37
405	281.56	276.74	925.05	909.22	298.41	298.41
350	254.30	251.01	1020.27	1007.05	355.98	355.98

RUN 12 T_l= 95.3(C) V_l=2.208(m/s) Fr= 39.158 Re= 93246.9

T_w(C)	q_t(kW/m^2)	q_c	h_t (W/m^2/C)	h_c	Nu_t	Nu_c
816	558.24	523.50	780.83	732.23	150.65	150.65
723	506.50	482.31	814.17	775.30	175.39	175.39
636	464.40	447.80	868.51	837.47	208.28	208.28
556	411.58	400.23	904.51	879.57	239.69	239.69
483	367.21	359.52	961.35	941.19	280.19	280.19
416	324.26	319.08	1027.49	1011.07	326.99	326.99
357	289.35	285.90	1131.40	1117.89	391.61	391.61

RUN 1 T_l= 90.1(C) V_l=0.011(m/s) Fr= 0.001 Re= 457.3

T_w(C)	q_t(kW/m^2)	q_c	h_t (W/m^2/C)	h_c	Nu_t	Nu_c
772	193.08	163.63	287.54	243.69	52.37	52.37
677	164.53	144.62	285.72	251.14	59.70	59.70
593	142.29	128.69	289.25	261.60	68.32	68.32
518	121.99	112.65	292.33	269.96	76.98	76.98
453	103.48	97.02	294.22	275.85	85.21	85.21
396	87.78	83.24	297.34	281.96	93.67	93.67
350	71.46	68.17	286.77	273.56	96.71	96.71
310	62.88	60.48	301.29	289.78	108.57	108.57
273	55.03	53.28	319.17	309.04	121.92	121.92

RUN 2 T_l= 90.0(C) V_l=0.124(m/s) Fr= 0.123 Re= 5075.8

T_w(C)	q_t(kW/m^2)	q_c	h_t (W/m^2/C)	h_c	Nu_t	Nu_c
875	240.36	197.30	310.49	254.87	49.50	49.50
755	194.35	166.86	297.19	255.16	55.83	55.83
653	161.43	143.46	292.26	259.74	63.34	63.34
565	139.29	127.42	300.13	274.54	74.03	74.03
487	122.19	114.32	316.52	296.12	87.73	87.73
417	107.89	102.70	341.68	325.25	105.17	105.17
353	95.84	92.47	379.87	366.51	129.01	129.01
295	84.19	82.06	432.89	421.94	161.40	161.40
242	79.36	78.08	562.19	553.13	228.35	228.35

RUN 3 T_l= 90.1(C) V_l=0.177(m/s) Fr= 0.253 Re= 7295.0

T_w(C)	q_t(kW/m^2)	q_c	h_t (W/m^2/C)	h_c	Nu_t	Nu_c
853	232.51	192.77	309.33	256.46	50.89	50.89
749	193.35	166.46	298.21	256.74	56.50	56.50
660	168.23	149.77	301.16	268.10	64.93	64.93
578	147.53	134.84	308.97	282.41	74.98	74.98
505	131.64	122.95	325.86	304.35	88.23	88.23
438	118.30	112.38	350.92	333.35	104.87	104.87
377	106.97	102.99	388.11	373.69	127.41	127.41
319	95.69	93.09	437.85	425.94	157.30	157.30
265	91.17	89.55	555.23	545.39	217.70	217.70

RUN 4 T_l= 90.1(C) V_l=0.255(m/s) Fr= 0.522 Re= 10483.5

T_w(C)	q_t(kW/m^2)	q_c	h_t (W/m^2/C)	h_c	Nu_t	Nu_c
794	215.09	183.14	310.54	264.42	55.64	55.64
714	188.13	164.78	306.63	268.58	61.32	61.32
643	170.58	153.44	314.87	283.24	69.89	69.89
577	156.73	144.16	329.49	303.06	80.63	80.63
515	142.96	133.79	345.31	323.15	92.53	92.53
457	132.36	125.72	371.58	352.94	108.42	108.42
402	123.43	118.71	409.76	394.09	129.88	129.88
350	118.19	114.90	474.72	461.52	163.21	163.21
300	112.06	109.85	564.21	553.10	210.37	210.37

RUN 5 T_l= 91.5(C) V_l=0.366(m/s) Fr= 1.077 Re= 15155.4

T_w(C)	q_t(kW/m^2)	q_c	h_t (W/m^2/C)	h_c	Nu_t	Nu_c
741	199.58	173.55	311.72	271.07	60.16	60.16
672	179.41	159.89	314.00	279.82	66.84	66.84
608	164.34	149.71	323.95	295.11	75.73	75.73
549	150.58	139.64	336.38	311.96	85.76	85.76
492	144.92	136.82	370.59	349.89	103.04	103.04
437	134.94	129.07	401.86	384.37	121.13	121.13
386	119.27	115.03	418.24	403.36	135.78	135.78
338	113.21	110.20	476.65	463.94	166.73	166.73
293	105.86	103.77	550.99	540.12	207.28	207.28

RUN 6 T_l= 91.3(C) V_l=0.526(m/s) Fr= 2.223 Re= 21762.8

T_w(C)	q_t(kW/m^2)	q_c	h_t (W/m^2/C)	h_c	Nu_t	Nu_c
876	279.57	236.32	360.56	304.79	59.12	59.12
787	247.09	215.98	360.34	314.96	66.73	66.73
706	222.57	199.99	367.57	330.28	76.06	76.06
634	198.01	181.54	371.50	340.60	84.87	84.87
567	186.80	174.82	400.96	375.24	100.97	100.97
503	170.73	162.14	424.82	403.44	117.27	117.27
440	165.54	159.54	487.96	470.28	147.55	147.55
382	144.56	140.43	514.41	499.72	169.15	169.15
328	136.80	134.02	602.49	590.23	215.30	215.30

RUN 7 T_l= 91.7(C) V_l=0.730(m/s) Fr= 4.287 Re= 30280.4

T_w(C)	q_t(kW/m^2)	q_c	h_t (W/m^2/C)	h_c	Nu_t	Nu_c
765	297.58	269.03	448.43	405.40	87.83	87.83
689	257.33	236.32	437.37	401.67	94.22	94.22
619	238.86	223.50	461.32	431.66	109.44	109.44
552	226.12	214.97	500.80	476.11	130.28	130.28
490	206.73	198.70	530.68	510.06	150.48	150.48
432	186.75	181.05	564.38	547.16	173.50	173.50
375	187.38	183.44	683.20	668.84	228.46	228.46
321	165.04	162.40	749.43	737.45	271.68	271.68

RUN 8 T_l= 91.9(C) V_l=0.954(m/s) Fr= 7.312 Re= 39592.3

T_w(C)	q_t(kW/m^2)	q_c	h_t (W/m^2/C)	h_c	Nu_t	Nu_c
747	345.85	319.17	535.03	493.76	108.88	108.88
674	309.99	290.34	541.23	506.94	120.91	120.91
605	281.19	266.79	557.90	529.33	136.35	136.35
540	263.36	252.87	599.27	575.41	159.73	159.73
479	244.43	236.89	646.05	626.12	187.21	187.21
422	222.52	217.15	692.64	675.94	217.01	217.01

RUN 9 T_l= 90.9(C) V_l=1.138(m/s) Fr= 10.407 Re= 46993.2

T_w(C)	q_t(kW/m^2)	q_c	h_t (W/m^2/C)	h_c	Nu_t	Nu_c
773	422.80	393.32	629.38	585.49	125.79	125.79
694	382.59	361.15	644.94	608.79	142.06	142.06
620	349.47	334.01	673.02	643.24	162.80	162.80
551	325.98	314.89	723.64	699.02	191.52	191.52
486	297.75	289.89	772.17	751.80	222.84	222.84
426	277.53	272.03	853.31	836.39	267.14	267.14

RUN 10 T_l= 91.0(C) V_l=1.441(m/s) Fr= 16.695 Re= 59524.2

T_w(C)	q_t(kW/m^2)	q_c	h_t (W/m^2/C)	h_c	Nu_t	Nu_c
838	500.41	462.74	679.12	628.01	126.43	126.43
750	497.97	471.01	767.29	725.75	159.61	159.61
667	443.65	424.58	783.88	750.18	180.24	180.24
590	399.79	386.39	817.96	790.55	207.21	207.21
518	367.60	358.25	880.37	857.98	244.58	244.58
452	338.13	331.69	962.87	944.53	291.95	291.95
389	318.00	313.69	1105.37	1090.37	365.82	365.82

RUN 11 T_l= 91.1(C) V_l=1.753(m/s) Fr= 24.698 Re= 72455.5

T_w(C)	q_t(kW/m^2)	q_c	h_t (W/m^2/C)	h_c	Nu_t	Nu_c
791	566.03	534.35	819.85	773.98	163.22	163.22
713	556.75	533.50	908.87	870.91	199.04	199.04
639	512.58	495.69	951.88	920.52	227.97	227.97
570	463.07	450.90	987.20	961.25	257.69	257.69
506	417.72	408.96	1030.76	1009.16	292.10	292.10
446	389.01	382.78	1125.84	1107.82	344.85	344.85
390	366.36	362.01	1269.12	1254.07	420.20	420.20

RUN 1 T_l= 79.6(C) V_l=0.011(m/s) Fr= 0.001 Re= 436.6

T_w(C)	q_t(kW/m^2)	q_c	h_t (W/m^2/C)	h_c	Nu_t	Nu_c
856	269.52	205.12	356.90	271.62	53.71	53.71
752	224.61	181.04	344.72	277.85	60.94	60.94
664	183.99	153.89	326.91	273.43	65.92	65.92
587	161.99	140.80	333.04	289.47	76.08	76.08
521	132.03	116.89	314.49	278.43	79.15	79.15
463	117.67	106.66	324.69	294.31	89.72	89.72
410	107.83	99.86	348.42	322.67	105.19	105.19
361	98.98	93.27	380.28	358.34	124.75	124.75

RUN 1 T_l= 79.6(C) V_l=0.054(m/s) Fr= 0.023 Re= 2090.4

T_w(C)	q_t(kW/m^2)	q_c	h_t (W/m^2/C)	h_c	Nu_t	Nu_c
800	251.83	199.52	360.42	285.56	59.73	59.73
714	214.07	176.80	349.21	288.42	65.88	65.88
640	181.90	154.84	337.55	287.33	71.13	71.13
574	161.50	141.62	341.20	299.19	79.81	79.81
516	145.40	130.66	350.53	314.99	90.10	90.10
463	132.91	121.93	367.28	336.95	102.78	102.78
414	113.52	105.37	362.87	336.84	109.33	109.33
368	105.30	99.31	394.22	371.78	128.23	128.23

RUN 2 T_l= 79.2(C) V_l=0.124(m/s) Fr= 0.124 Re= 4841.0

T_w(C)	q_t(kW/m^2)	q_c	h_t (W/m^2/C)	h_c	Nu_t	Nu_c
825	259.10	201.64	357.95	278.57	56.81	56.81
738	225.74	184.61	354.32	289.77	64.52	64.52
659	207.96	178.49	372.66	319.84	77.51	77.51
585	188.35	167.37	388.86	345.54	91.02	91.02
515	178.32	163.61	430.32	394.82	112.99	112.99
449	162.89	152.75	467.56	438.46	136.00	136.00
388	148.66	141.80	518.63	494.70	166.21	166.21
330	137.79	133.27	602.03	582.29	211.85	211.85

RUN 3 T_l= 79.2(C) V_l=0.179(m/s) Fr= 0.256 Re= 6955.4

T_w(C).	q_t(kW/m^2)	q_c	h_t (W/m^2/C)	h_c	Nu_t	Nu_c
918	305.28	225.48	373.80	276.09	51.49	51.49
827	275.45	217.43	379.15	299.28	60.87	60.87
745	244.68	202.42	379.98	314.34	69.49	69.49
669	226.96	196.21	399.79	345.62	82.88	82.88
596	215.34	193.27	435.14	390.54	101.66	101.66
524	198.77	183.33	469.33	432.88	122.50	122.50
457	190.44	179.83	534.96	505.16	155.22	155.22
392	178.08	171.02	612.21	587.95	196.43	196.43

RUN 4 T_l= 79.5(C) V_l=0.279(m/s) Fr= 0.626 Re= 10887.0

T_w(C)	q_t(kW/m^2)	q_c	h_t (W/m^2/C)	h_c	Nu_t	Nu_c
953	336.69	246.83	395.07	289.62	52.24	52.24
865	317.87	251.42	416.08	329.10	64.53	64.53
782	289.88	241.00	425.69	353.91	75.34	75.34
702	275.57	240.10	458.41	399.41	92.42	92.42
627	249.88	224.40	475.38	426.90	107.26	107.26
552	238.35	220.59	528.91	489.50	134.08	134.08
482	227.86	215.61	597.99	565.84	168.64	168.64
414	215.57	207.43	689.22	663.20	215.28	215.28
348	200.32	195.12	809.75	788.73	279.54	279.54

RUN 5 T_l= 79.5(C) V_l=0.369(m/s) Fr= 1.093 Re= 14378.3

T_w(C)	q_t(kW/m^2)	q_c	h_t (W/m^2/C)	h_c	Nu_t	Nu_c
820	313.84	257.45	436.63	358.18	73.41	73.41
746	291.73	249.27	452.23	386.41	85.33	85.33
676	273.44	241.68	475.39	420.16	99.95	99.95
608	263.66	240.32	520.33	474.27	121.78	121.78
542	244.95	228.02	555.17	516.81	143.16	143.16
480	235.76	223.67	622.57	590.65	176.53	176.53
419	222.89	214.49	701.43	674.99	217.68	217.68

RUN 6 T_l= 79.6(C) V_l=0.494(m/s) Fr= 1.961 Re= 19273.1

T_w(C)	q_t(kW/m^2)	q_c	h_t (W/m^2/C)	h_c	Nu_t	Nu_c
798	344.97	292.96	494.79	420.20	88.02	88.02
733	326.00	285.69	515.67	451.91	101.15	101.15
670	313.35	282.41	550.57	496.21	118.81	118.81
610	291.31	267.74	572.55	526.23	134.80	134.80
551	277.45	259.73	616.17	576.80	158.06	158.06
496	262.69	249.46	665.25	631.74	185.20	185.20
441	251.36	241.70	738.73	710.35	222.59	222.59

RUN 7 T_l= 81.7(C) V_l=0.595(m/s) Fr= 2.840 Re= 23431.6

T_w(C)	q_t(kW/m^2)	q_c	h_t (W/m^2/C)	h_c	Nu_t	Nu_c
835	387.68	328.01	528.07	446.78	90.18	90.18
762	355.96	310.64	538.06	469.55	101.94	101.94
692	336.47	302.47	569.22	511.70	119.67	119.67
624	314.00	288.84	600.45	552.32	139.20	139.20
560	292.88	274.40	638.62	598.31	162.36	162.36
498	269.07	255.68	677.74	644.02	188.33	188.33

RUN 8 T_l= 82.0(C) V_l=0.854(m/s) Fr= 5.862 Re= 33701.0

T_w(C)	q_t(kW/m^2)	q_c	h_t (W/m^2/C)	h_c	Nu_t	Nu_c
845	486.09	424.19	653.17	570.00	113.92	113.92
775	483.05	435.46	716.61	646.00	138.47	138.47
707	449.74	413.59	742.51	682.82	157.21	157.21
642	427.68	400.36	790.52	740.02	182.75	182.75
578	415.09	394.88	870.85	828.45	220.16	220.16
515	388.18	373.45	936.36	900.84	257.75	257.75

RUN 9 T_l= 81.9(C) V_l=1.074(m/s) Fr= 9.270 Re= 42367.6

T_w(C)	q_t(kW/m^2)	q_c	h_t (W/m^2/C)	h_c	Nu_t	Nu_c
940	647.30	561.39	771.86	669.42	122.30	122.30
852	599.80	536.24	798.12	713.55	141.61	141.61
770	546.75	500.05	817.04	747.25	160.97	160.97
692	515.83	481.76	871.95	814.36	190.36	190.36
616	493.97	469.67	958.44	911.28	231.67	231.67
544	459.13	442.081037.18	998.66	276.15	276.15	

RUN 10 T_l= 79.9(C) V_l=1.423(m/s) Fr= 16.280 Re= 55610.3

T_w(C)	q_t(kW/m^2)	q_c	h_t (W/m^2/C)	h_c	Nu_t	Nu_c
787	731.38	681.61	1066.67	994.08	210.62	210.62
709	704.09	667.51	1157.05	1096.94	251.79	251.79
635	664.54	638.06	1244.33	1194.75	297.36	297.36
563	628.42	609.59	1359.42	1318.69	356.32	356.32

RUN 11 T_l= 79.8(C) V_l=1.646(m/s) Fr= 21.779 Re= 64285.3

T_w(C)	q_t(kW/m^2)	q_c	h_t (W/m^2/C)	h_c	Nu$_t$	Nu$_c$
1014	964.34	855.19	1056.45	936.88	160.05	160.05
861	865.34	799.91	1139.12	1052.98	207.33	207.33
719	769.78	731.70	1245.14	1183.54	268.85	268.85
587	694.15	672.99	1428.03	1384.50	363.99	363.99

RUN 12 T_l= 79.8(C) V_l=2.035(m/s) Fr= 33.282 Re= 79443.9

T_w(C)	q_t(kW/m^2)	q_c	h_t (W/m^2/C)	h_c	Nu$_t$	Nu$_c$
737	912.38	871.45	1434.67	1370.31	305.49	305.49
620	849.42	824.73	1637.44	1589.85	402.62	402.62

RUN 1 T_l= 71.4(C) V_l=0.011(m/s) Fr= 0.001 Re= 418.3

T_w(C)	q_t(kW/m^2)	q_c	h_t (W/m^2/C)	h_c	Nu$_t$	Nu$_c$
890	341.66	269.15	433.15	341.23	65.36	65.36
768	265.49	219.08	397.69	328.17	70.81	70.81
671	218.21	187.19	383.02	328.58	78.63	78.63
586	184.61	163.60	380.92	337.56	88.89	88.89
511	161.76	147.41	394.69	359.67	103.51	103.51
444	144.14	134.35	420.66	392.08	122.49	122.49
383	127.73	121.09	453.32	429.77	145.33	145.33
328	114.35	109.90	503.59	483.97	176.53	176.53

RUN 1 T_l= 70.4(C) V_l=0.011(m/s) Fr= 0.001 Re= 416.3

T_w(C)	q_t(kW/m^2)	q_c	h_t (W/m^2/C)	h_c	Nu$_t$	Nu$_c$
875	332.81	263.91	429.87	340.87	66.19	66.19
757	261.68	217.37	399.02	331.46	72.39	72.39
658	219.12	189.71	393.00	340.24	82.50	82.50
573	187.81	168.04	397.77	355.90	95.07	95.07
497	162.16	148.84	409.34	375.70	109.98	109.98
429	147.99	139.03	451.27	423.97	134.95	134.95
368	126.04	120.06	472.72	450.32	155.42	155.42

RUN 2 T_l= 70.4(C) V_l=0.125(m/s) Fr= 0.126 Re= 4623.5

T_w(C)	q_t(kW/m^2)	q_c	h_t (W/m^2/C)	h_c	Nu_t	Nu_c
913	328.46	249.81	404.31	307.51	57.59	57.59
836	331.32	271.47	450.80	369.36	74.50	74.50
763	303.84	258.40	458.84	390.23	84.66	84.66
695	284.26	249.85	478.60	420.66	98.09	98.09
629	271.88	246.16	515.26	466.52	116.95	116.95
565	253.07	234.10	545.75	504.86	136.19	136.19
503	233.21	219.41	579.42	545.14	158.34	158.34
447	220.97	210.99	639.13	610.26	189.92	189.92

RUN 3 T_l= 70.5(C) V_l=0.180(m/s) Fr= 0.259 Re= 6645.2

T_w(C)	q_t(kW/m^2)	q_c	h_t (W/m^2/C)	h_c	Nu_t	Nu_c
830	345.66	287.17	474.38	394.12	79.99	79.99
760	318.39	273.46	482.91	414.77	90.25	90.25
694	300.40	266.09	506.38	448.55	104.67	104.67
629	290.97	265.18	550.80	501.98	125.75	125.75
567	272.70	253.56	585.67	544.55	146.57	146.57
507	252.11	238.07	621.35	586.75	169.73	169.73

RUN 4 T_l= 70.6(C) V_l=0.258(m/s) Fr= 0.535 Re= 9552.4

T_w(C)	q_t(kW/m^2)	q_c	h_t (W/m^2/C)	h_c	Nu_t	Nu_c
868	384.32	317.14	501.03	413.44	80.83	80.83
759	361.81	317.09	549.72	481.76	104.95	104.95
654	350.97	322.10	634.30	582.13	141.81	141.81
555	310.45	292.39	683.83	644.05	175.72	175.72

RUN 5 T_l= 70.6(C) V_l=0.371(m/s) Fr= 1.104 Re= 13730.1

T_w(C)	q_t(kW/m^2)	q_c	h_t (W/m^2/C)	h_c	Nu_t	Nu_c
841	435.18	374.18	587.95	505.54	101.44	101.44
777	408.80	360.83	604.64	533.69	114.17	114.17
716	386.63	349.04	628.60	567.49	129.35	129.35
656	363.95	334.92	656.19	603.84	146.88	146.88
598	351.66	329.31	706.77	661.84	171.77	171.77
542	333.46	316.55	756.06	717.71	198.85	198.85

RUN 6 T_l= 70.7(C) V_l=0.497(m/s) Fr= 1.983 Re= 18402.8

T_w(C)	q_t(kW/m^2)	q_c	h_t (W/m^2/C)	h_c	Nu_t	Nu_c
832	472.39	413.36	646.06	565.32	114.44	114.44
775	452.05	404.55	671.09	600.56	128.79	128.79
720	419.05	380.89	677.27	615.59	139.76	139.76
666	407.77	377.32	721.08	667.22	160.39	160.39
615	394.47	370.34	767.62	720.65	183.52	183.52
562	394.03	375.28	853.89	813.26	219.96	219.96
511	406.24	391.88	991.12	956.09	275.15	275.15

RUN 7 T_l= 70.7(C) V_l=0.599(m/s) Fr= 2.879 Re= 22177.6

T_w(C)	q_t(kW/m^2)	q_c	h_t (W/m^2/C)	h_c	Nu_t	Nu_c
884	537.90	466.79	686.80	596.00	114.75	114.75
818	515.57	459.53	718.98	640.84	131.56	131.56
755	495.07	451.08	757.02	689.76	150.92	150.92
693	475.81	441.61	803.13	745.41	174.09	174.09
634	448.42	422.07	841.23	791.78	197.28	197.28
577	412.91	392.75	867.14	824.79	219.31	219.31

RUN 8 T_l= 70.9(C) V_l=0.860(m/s) Fr= 5.941 Re= 31898.3

T_w(C)	q_t(kW/m^2)	q_c	h_t (W/m^2/C)	h_c	Nu_t	Nu_c
898	729.73	655.21	915.99	822.46	156.38	156.38
822	699.67	642.71	969.78	890.84	182.09	182.09

RUN 9 T_l= 71.0(C) V_l=1.063(m/s) Fr= 9.077 Re= 39444.2

T_w(C)	q_t(kW/m^2)	q_c	h_t (W/m^2/C)	h_c	Nu_t	Nu_c
848	829.97	767.49	1111.37	1027.70	204.89	204.89
777	808.00	759.96	1194.40	1123.38	240.22	240.22

RUN 10 T_l= 70.9(C) V_l=1.388(m/s) Fr= 15.488 Re= 51484.0

T_w(C)	q_t(kW/m^2)	q_c	h_t (W/m^2/C)	h_c	Nu_t	Nu_c
992	1050.83	948.90	1179.19	1064.81	185.42	185.42
888	1012.78	940.81	1287.48	1195.99	229.53	229.53
786	947.76	898.13	1383.68	1311.21	278.01	278.01
687	886.76	853.42	1511.95	1455.10	341.97	341.97

APPENDIX E

TYPICAL UPWARD TWO-PHASE EXPERIMENT DATA

APPENDIX E

TYPICAL UPWARD TWO-PHASE EXPERIMENT DATA

Test Sphere Diameter: 12.7 mm
Test Sphere Material: 316 Stainless Steel
No. 1 Tube needle Assembly

* * * * * * * * * * **TEST: TU1-1** * * * * * * * * * *

RUN 1 Water V =0.690(m/s) Steam V = 3.218(m/s)
Re = 29794.9 Void Fraction =0.436

T_w(C)	q_t(kW/m^2)	q_c	h_t (W/m^2/C)	h_c	Nu_t	Nu_c	$C_{D,two}$*
742	182.8	151.5	284.9	236.1	63.3	52.4	0.568
666	153.7	130.9	271.5	231.2	65.3	55.6	0.560
634	141.2	121.4	264.5	227.4	66.0	56.7	0.552
575	120.6	105.6	253.9	222.3	67.7	59.3	0.540
549	112.8	99.6	251.4	222.1	69.2	61.1	0.539
500	107.2	97.1	268.4	243.1	78.4	71.0	0.589
455	89.5	81.6	252.1	230.0	77.7	70.9	0.553
435	85.2	78.2	254.5	233.7	80.5	73.9	0.560
415	78.6	72.5	249.5	230.0	80.9	74.6	0.549
397	79.1	73.6	266.6	248.1	88.6	82.4	0.590
379	73.3	68.4	262.9	245.5	89.4	83.5	0.580
362	67.6	63.3	257.9	241.4	89.8	84.0	0.567
345	73.7	69.9	300.8	285.2	107.2	101.6	0.666

RUN 2 Water V =0.801(m/s) Steam V = 3.319(m/s)
Re = 34573.5 Void Fraction =0.422

T_w(C)	q_t(kW/m^2)	q_c	h_t (W/m^2/C)	h_c	Nu_t	Nu_c	$C_{D,two}$
738	193.2	162.3	302.8	254.4	67.5	56.7	0.568
698	168.5	142.3	281.6	237.8	65.5	55.3	0.534
632	140.1	120.5	263.5	226.7	65.9	56.7	0.511
604	134.8	117.6	267.5	233.4	69.1	60.2	0.527
576	128.6	113.6	270.3	238.7	72.1	63.6	0.538
524	107.2	95.6	252.5	225.3	71.5	63.8	0.507
437	88.4	81.3	262.1	241.1	82.6	76.0	0.537
418	81.8	75.5	257.2	237.5	83.1	76.7	0.527
400	77.6	72.0	258.7	240.1	85.6	79.4	0.530
383	77.8	72.8	275.1	257.5	93.1	87.1	0.566
366	75.1	70.7	282.8	266.1	98.0	92.2	0.581

*$C_{D,two}$ as in Eq. (7.15).

RUN 3 Water V =0.934(m/s) Steam V = 3.457(m/s)
Re = 40316.1 Void Fraction =0.406

T_w(C)	q_t(kW/m^2)	q_c	h_t (W/m^2/C)	h_c	Nu_t	Nu_c	$C_{D,two}$
736	204.1	173.5	321.0	272.9	71.7	60.9	0.565
696	186.9	160.9	313.6	270.1	73.1	63.0	0.561
662	158.2	135.8	281.6	241.7	68.1	58.5	0.503
631	147.2	127.7	277.2	240.4	69.3	60.2	0.501
603	140.5	123.4	279.5	245.5	72.3	63.5	0.513
575	122.3	107.3	257.3	225.7	68.6	60.2	0.471
525	104.9	93.3	246.9	219.6	69.9	62.2	0.458
481	92.4	83.3	242.9	218.9	72.6	65.4	0.455
460	95.7	87.6	265.9	243.4	81.5	74.6	0.504
421	84.7	78.3	263.6	243.6	84.8	78.4	0.501
386	77.9	72.8	272.1	254.2	91.6	85.6	0.518

RUN 4 Water V =1.106(m/s) Steam V = 3.666(m/s)
Re = 47737.7 Void Fraction =0.382

T_w(C)	q_t(kW/m^2)	q_c	h_t (W/m^2/C)	h_c	Nu_t	Nu_c	$C_{D,two}$
726	251.1	221.7	401.0	354.1	90.5	79.9	0.674
688	208.9	183.9	355.3	312.7	83.5	73.5	0.597
656	177.9	156.0	319.9	280.6	77.8	68.3	0.537
604	139.6	122.3	276.9	242.7	71.5	62.6	0.466
556	126.2	112.6	276.9	247.0	75.5	67.4	0.474
534	118.2	106.0	272.4	244.3	76.3	68.4	0.469
513	109.1	98.2	264.2	237.8	75.9	68.3	0.456
493	109.4	99.6	278.4	253.5	82.0	74.6	0.485
456	100.3	92.4	281.6	259.4	86.7	79.8	0.493
422	96.0	89.5	298.4	278.4	96.0	89.5	0.526
405	84.2	78.4	275.9	257.0	90.7	84.4	0.484

RUN 5 Water V =1.242(m/s) Steam V = 3.864(m/s)
Re = 53596.5 Void Fraction =0.363

T_w(C)	q_t(kW/m^2)	q_c	h_t (W/m^2/C)	h_c	Nu_t	Nu_c	$C_{D,two}$
739	242.9	211.9	379.9	331.4	84.5	73.7	0.594
700	214.4	188.0	357.2	313.2	82.9	72.7	0.564
667	175.2	152.4	309.3	269.0	74.4	64.7	0.486
638	155.2	135.2	288.9	251.5	71.7	62.5	0.455
611	147.4	129.6	288.5	253.6	73.8	64.9	0.459
562	120.2	106.1	260.1	229.7	70.4	62.2	0.416
518	118.6	107.4	283.9	257.1	81.1	73.4	0.465
497	114.3	104.3	287.9	262.7	84.4	77.0	0.475
459	101.6	93.6	283.5	261.1	87.0	80.1	0.469
441	98.1	90.9	288.1	266.9	90.4	83.8	0.478
407	92.4	86.6	301.6	282.6	98.9	92.7	0.502

RUN 6 Water V =1.453(m/s) Steam V = 4.251(m/s)
Re = 62688.1 Void Fraction =0.330

T_w(C)	q_t(kW/m^2)	q_c	h_t (W/m^2/C)	h_c	Nu_t	Nu_c	$C_{D,two}$
721	278.2	249.4	447.9	401.5	101.6	91.1	0.667
685	217.4	192.7	372.0	329.8	87.8	77.8	0.550
629	155.5	136.2	294.3	257.8	73.8	64.7	0.431
605	149.1	131.8	295.2	260.9	76.1	67.2	0.437
582	142.7	127.2	296.0	263.9	78.3	69.8	0.442
541	142.2	129.6	322.6	293.9	89.6	81.6	0.492
501	114.9	104.7	286.5	261.0	83.5	76.1	0.436
484	106.9	97.6	278.3	254.0	82.8	75.6	0.424
467	106.6	98.2	290.4	267.4	88.2	81.2	0.445
451	93.6	85.9	267.0	245.1	82.8	76.0	0.406

RUN 7 Water V =1.615(m/s) Steam V = 4.645(m/s)
Re = 69709.9 Void Fraction =0.302

T_w(C)	q_t(kW/m^2)	q_c	h_t (W/m^2/C)	h_c	Nu_t	Nu_c	$C_{D,two}$
788	310.6	273.1	451.4	396.9	95.6	84.0	0.621
743	257.8	226.4	401.2	352.4	89.0	78.2	0.554
706	211.2	184.2	348.6	303.9	80.4	70.1	0.480
648	166.5	145.5	304.1	265.7	74.7	65.2	0.421
597	147.7	131.1	297.5	264.1	77.4	68.7	0.420
573	142.0	127.1	300.1	268.7	80.2	71.8	0.427
529	121.6	109.7	283.1	255.5	79.7	71.9	0.405
510	114.1	103.4	278.6	252.4	80.3	72.8	0.400
491	108.8	99.2	278.7	254.0	82.3	75.0	0.402
472	107.6	98.9	289.2	265.8	87.3	80.3	0.420

RUN 8 Water V =1.912(m/s) Steam V = 5.739(m/s)
Re = 82536.3 Void Fraction =0.244

T_w(C)	q_t(kW/m^2)	q_c	h_t (W/m^2/C)	h_c	Nu_t	Nu_c	$C_{D,two}$
721	299.9	271.1	482.9	436.5	109.6	99.0	0.632
681	238.5	214.2	410.8	368.9	97.3	87.4	0.536
649	198.7	177.6	362.4	323.9	88.9	79.5	0.472
595	160.1	143.6	323.4	290.0	84.3	75.6	0.424
571	150.2	135.5	318.6	287.4	85.3	77.0	0.420
550	137.4	124.2	305.8	276.5	84.0	76.0	0.403
509	125.4	114.7	306.6	280.5	88.5	81.0	0.409
489	122.4	112.8	314.4	289.8	93.0	85.7	0.421
453	110.8	103.1	313.9	291.9	97.0	90.2	0.422
435	118.6	111.6	354.1	333.3	111.9	105.4	0.480

RUN 9 Water V =2.047(m/s) Steam V = 6.522(m/s)
Re = 88347.9 Void Fraction =0.215

T_w(C)	q_t(kW/m^2)	q_c	h_t (W/m^2/C)	h_c	Nu$_t$	Nu$_c$	$C_{D,two}$
883	355.1	301.9	453.4	385.4	87.4	74.3	0.529
833	284.3	239.9	388.0	327.3	78.5	66.3	0.452
790	255.0	217.3	369.9	315.1	78.2	66.6	0.438
717	196.3	168.1	318.5	272.6	72.6	62.2	0.382
652	181.0	159.6	327.9	289.1	80.1	70.7	0.407
595	159.2	142.8	322.0	288.7	84.0	75.3	0.408
543	141.5	128.8	319.6	290.9	88.6	80.6	0.410
519	129.3	118.1	308.6	281.8	88.0	80.3	0.397
497	120.6	110.6	304.0	278.8	89.1	81.7	0.392
475	120.6	111.7	321.6	298.0	96.7	89.6	0.418

* * * * * * * * * * **TEST: TU1-2** * * * * * * * * * *

RUN 1 Water V =0.854(m/s) Steam V = 3.887(m/s)
Re = 36869.8 Void Fraction =0.544

T_w(C)	q_t(kW/m^2)	q_c	h_t (W/m^2/C)	h_c	Nu$_t$	Nu$_c$	$C_{D,two}$
710	199.8	172.3	327.5	282.4	75.2	64.8	0.613
673	169.6	146.0	295.8	254.8	70.7	60.8	0.554
639	154.3	134.1	286.3	248.7	71.0	61.7	0.542
608	134.5	116.9	264.7	230.2	68.0	59.1	0.503
551	121.2	107.9	269.0	239.6	73.8	65.8	0.523
525	115.2	103.6	271.2	243.9	76.8	69.1	0.532
477	105.2	96.3	279.5	255.8	83.9	76.8	0.556
454	95.6	87.7	269.7	247.6	83.2	76.4	0.536
434	89.0	82.1	266.8	246.1	84.5	77.9	0.530
415	78.5	72.3	249.5	229.9	81.0	74.6	0.494
362	72.0	67.7	274.6	258.1	95.5	89.8	0.545
346	67.4	63.5	274.0	258.4	97.5	92.0	0.542

RUN 2 Water V =0.993(m/s) Steam V = 3.961(m/s)
Re = 42843.3 Void Fraction =0.534

T_w(C)	q_t(kW/m^2)	q_c	h_t (W/m^2/C)	h_c	Nu$_t$	Nu$_c$	$C_{D,two}$
700	194.5	168.1	324.2	280.2	75.2	65.0	0.565
663	168.6	146.1	299.5	259.5	72.3	62.7	0.524
630	151.3	131.9	285.6	248.9	71.5	62.4	0.504
599	138.8	122.1	278.5	244.9	72.3	63.6	0.496
493	107.8	98.0	274.7	249.8	80.9	73.6	0.505
469	102.4	93.9	277.8	254.6	84.2	77.2	0.512
447	86.1	78.6	248.1	226.5	77.2	70.5	0.454
427	90.1	83.4	275.7	255.4	88.1	81.6	0.510
388	78.3	73.1	271.6	253.7	91.3	85.3	0.502
370	77.2	72.6	285.7	268.8	98.3	92.5	0.528
353	74.5	70.5	294.6	278.6	103.8	98.2	0.544

RUN 3 Water V =1.376(m/s) Steam V = 4.199(m/s)
Re = 59386.5 Void Fraction =0.504

T_w(C)	q_t(kW/m^2)	q_c	h_t (W/m^2/C)	h_c	Nu_t	Nu_c	$C_{D,two}$
690	201.8	176.5	341.9	299.0	80.2	70.1	0.512
655	172.8	151.1	311.3	272.1	75.8	66.3	0.467
624	159.3	140.4	303.9	267.8	76.6	67.5	0.460
595	147.8	131.3	298.5	265.2	77.8	69.1	0.457
519	117.0	105.8	279.5	252.7	79.7	72.1	0.434
453	99.7	92.0	282.5	260.4	87.3	80.5	0.444
434	95.2	88.3	285.5	264.7	90.4	83.8	0.449
380	79.6	74.7	283.9	266.4	96.4	90.4	0.446
364	78.0	73.6	295.1	278.6	102.4	96.7	0.464

RUN 4 Water V =1.376(m/s) Steam V = 4.199(m/s)
Re = 59386.5 Void Fraction =0.504

T_w(C)	q_t(kW/m^2)	q_c	h_t (W/m^2/C)	h_c	Nu_t	Nu_c	$C_{D,two}$
706	244.0	216.9	402.7	358.0	92.9	82.6	0.612
668	196.3	173.4	345.9	305.5	83.1	73.4	0.524
635	173.5	153.6	324.2	287.0	80.7	71.5	0.493
579	138.6	123.4	289.7	257.8	76.9	68.5	0.444
553	138.1	124.6	304.9	275.3	83.5	75.3	0.473
528	127.6	115.8	298.0	270.4	84.0	76.2	0.465
505	120.4	110.0	297.5	271.7	86.3	78.9	0.467
483	110.3	101.1	288.2	264.1	85.9	78.7	0.452
442	101.1	93.8	296.0	274.7	92.8	86.1	0.467
423	94.6	88.1	293.2	273.1	94.1	87.7	0.463
371	83.0	78.4	306.8	289.9	105.6	99.8	0.484

RUN 5 Water V =1.548(m/s) Steam V = 4.327(m/s)
Re = 66790.6 Void Fraction =0.489

T_w(C)	q_t(kW/m^2)	q_c	h_t (W/m^2/C)	h_c	Nu_t	Nu_c	$C_{D,two}$
734	263.9	233.6	416.5	368.7	93.2	82.5	0.593
690	241.2	215.8	408.5	365.6	95.8	85.7	0.590
654	195.6	173.9	352.9	313.9	86.0	76.5	0.508
595	154.2	137.7	311.5	278.2	81.2	72.5	0.452
570	139.7	125.1	297.6	266.5	79.9	71.6	0.432
522	128.4	117.0	304.7	277.6	86.6	78.9	0.450
499	123.2	113.1	308.6	283.3	90.2	82.8	0.459
458	111.2	103.2	310.6	288.3	95.4	88.5	0.464
439	104.7	97.6	309.4	288.4	97.4	90.8	0.462
402	92.2	86.5	304.8	286.0	100.5	94.3	0.455
386	89.5	84.4	313.4	295.6	105.7	99.7	0.468

RUN 6 Water V =1.815(m/s) Steam V = 4.560(m/s)
Re = 78331.1 Void Fraction =0.464

T_w(C)	q_t(kW/m^2)	q_c	h_t (W/m^2/C)	h_c	Nu_t	Nu_c	$C_{D,two}$
702	270.3	243.8	449.3	405.1	104.1	93.8	0.604
666	212.9	190.1	376.4	336.1	90.6	80.9	0.502
609	169.5	151.8	333.0	298.3	85.4	76.6	0.447
584	163.1	147.5	337.2	304.9	89.1	80.5	0.457
539	137.6	125.2	313.9	285.5	87.4	79.5	0.427
497	127.4	117.4	320.9	295.8	94.0	86.6	0.442
459	115.4	107.4	321.5	299.1	98.6	91.7	0.444
425	101.8	95.2	313.5	293.4	100.4	94.0	0.433
408	98.6	92.7	320.1	300.9	104.7	98.5	0.443

RUN 7 Water V =2.023(m/s) Steam V = 4.779(m/s)
Re = 87287.0 Void Fraction =0.442

T_w(C)	q_t(kW/m^2)	q_c	h_t (W/m^2/C)	h_c	Nu_t	Nu_c	$C_{D,two}$
726	288.1	258.8	460.4	413.5	103.9	93.3	0.582
687	257.0	232.1	438.0	395.4	103.1	93.1	0.559
626	185.4	166.3	352.6	316.3	88.7	79.6	0.449
578	153.9	138.7	322.2	290.5	85.7	77.3	0.412
535	140.2	128.0	322.4	294.2	90.1	82.3	0.417
497	126.6	116.7	319.2	294.1	93.6	86.2	0.416
479	121.5	112.5	321.0	297.2	96.1	89.0	0.420
444	109.6	102.2	318.3	296.9	99.4	92.7	0.417
412	98.8	92.7	316.8	297.4	103.2	96.9	0.415

RUN 8 Water V =2.339(m/s) Steam V = 5.198(m/s)
Re = 100922.4 Void Fraction =0.407

T_w(C)	q_t(kW/m^2)	q_c	h_t (W/m^2/C)	h_c	Nu_t	Nu_c	$C_{D,two}$
716	306.4	278.2	497.4	451.7	113.5	103.0	0.592
680	247.8	223.6	427.0	385.2	101.2	91.3	0.506
625	188.0	169.0	358.2	322.0	90.2	81.1	0.425
579	162.1	146.8	338.4	306.5	89.8	81.4	0.405
538	142.9	130.5	326.6	298.2	91.0	83.1	0.393
500	129.2	119.0	322.7	297.3	94.2	86.8	0.392
466	119.3	110.9	326.1	303.2	99.2	92.2	0.397
449	118.7	111.1	339.8	318.1	105.5	98.7	0.416
418	111.6	105.4	351.6	331.9	113.7	107.3	0.431

RUN 9 Water V =2.578(m/s) Steam V = 5.616(m/s)
Re = 111241.4 Void Fraction =0.377

T_w(C)	q_t(kW/m^2)	q_c	h_t (W/m^2/C)	h_c	Nu_t	Nu_c	$C_{D,two}$
729	298.1	268.4	473.8	426.4	106.5	95.9	0.532
693	273.8	248.2	461.7	418.5	107.9	97.8	0.524
636	203.6	183.7	380.2	343.0	94.6	85.4	0.431
590	172.4	156.3	351.7	318.8	92.2	83.6	0.401
570	166.6	152.0	354.9	323.9	95.3	86.9	0.407
531	144.9	132.9	336.1	308.2	94.4	86.6	0.387
514	136.7	125.8	330.7	304.2	94.9	87.3	0.382
480	131.2	122.1	345.5	321.6	103.4	96.2	0.402
432	127.3	120.5	383.6	362.9	121.7	115.2	0.450

* * * * * * * * * * **TEST: TU1-3** * * * * * * * * * *

RUN 1 Water V =1.214(m/s) Steam V = 3.965(m/s)
Re = 52390.1 Void Fraction =0.679

T_w(C)	q_t(kW/m^2)	q_c	h_t (W/m^2/C)	h_c	Nu_t	Nu_c	$C_{D,two}$
727	207.7	178.2	331.4	284.3	74.7	64.1	0.517
686	185.1	160.3	316.1	273.8	74.5	64.5	0.499
617	153.4	135.2	297.0	261.6	75.5	66.5	0.479
558	127.3	113.5	278.1	248.1	75.7	67.5	0.454
504	114.4	104.0	282.9	257.1	82.1	74.7	0.470
457	104.4	96.4	292.8	270.5	90.1	83.2	0.491
414	86.5	80.3	275.2	255.6	89.3	83.0	0.460
376	79.0	74.3	286.0	268.7	97.6	91.7	0.479
343	69.0	65.2	284.1	268.7	101.6	96.1	0.472

RUN 2 Water V =1.359(m/s) Steam V = 4.083(m/s)
Re = 58630.9 Void Fraction =0.659

T_w(C)	q_t(kW/m^2)	q_c	h_t (W/m^2/C)	h_c	Nu_t	Nu_c	$C_{D,two}$
729	213.2	183.5	339.1	291.9	76.3	65.7	0.501
688	196.8	171.8	335.0	292.4	78.8	68.8	0.504
620	152.1	133.6	292.7	257.0	74.2	65.1	0.445
562	134.5	120.5	291.5	261.1	79.0	70.8	0.452
535	121.3	109.1	279.0	250.9	78.0	70.2	0.434
487	111.1	101.6	287.3	262.9	85.2	78.0	0.454
423	92.9	86.4	287.9	267.8	92.4	86.0	0.457
385	82.5	77.4	289.2	271.5	97.6	91.6	0.458
368	73.9	69.4	275.8	259.0	95.2	89.4	0.435

* * * * * * * * * * **TEST: TU1-3** * * * * * * * * * *

RUN 3 Water V =1.519(m/s) Steam V = 4.243(m/s)
Re = 65567.5 Void Fraction =0.635

T_w(C)	q_t(kW/m^2)	q_c	h_t (W/m^2/C)	h_c	Nu_t	Nu_c	$C_{D,two}$
717	238.2	209.9	386.0	340.0	87.9	77.5	0.553
678	203.9	179.9	352.9	311.3	83.8	74.0	0.508
615	156.6	138.5	304.4	269.2	77.6	68.6	0.441
560	138.2	124.3	300.6	270.4	81.6	73.4	0.443
535	127.7	115.5	293.8	265.6	82.2	74.3	0.435
489	114.9	105.4	295.6	271.0	87.4	80.2	0.442
448	105.5	98.0	303.4	281.8	94.4	87.7	0.457
410	90.5	84.6	292.2	273.0	95.4	89.2	0.439
376	85.9	81.1	310.8	293.5	106.1	100.2	0.467
345	74.8	70.9	305.1	289.6	108.7	103.2	0.456

RUN 4 Water V =1.708(m/s) Steam V = 4.486(m/s)
Re = 73732.5 Void Fraction =0.600

T_w(C)	q_t(kW/m^2)	q_c	h_t (W/m^2/C)	h_c	Nu_t	Nu_c	$C_{D,two}$
691	230.6	205.2	390.2	347.2	91.4	81.4	0.534
652	189.6	168.2	343.7	304.9	84.0	74.6	0.470
587	153.3	137.5	315.0	282.4	82.9	74.3	0.436
531	136.9	124.9	317.6	289.7	89.2	81.4	0.447
481	117.0	107.9	306.9	282.9	91.6	84.4	0.435
437	105.0	97.9	311.3	290.3	98.1	91.5	0.443
398	90.2	84.7	302.9	284.4	100.5	94.4	0.430
362	82.6	78.3	315.2	298.8	109.7	104.0	0.446
345	82.5	78.7	336.7	321.2	120.0	114.5	0.477

RUN 5 Water V =1.845(m/s) Steam V = 4.715(m/s)
Re = 79620.2 Void Fraction =0.571

T_w(C)	q_t(kW/m^2)	q_c	h_t (W/m^2/C)	h_c	Nu_t	Nu_c	$C_{D,two}$
721	270.7	242.0	436.3	390.0	99.0	88.5	0.575
681	232.3	208.0	400.0	358.2	94.8	84.9	0.530
617	172.4	154.1	333.3	297.9	84.7	75.7	0.442
566	150.1	135.8	322.2	291.5	86.9	78.6	0.433
519	132.3	121.1	315.9	289.1	90.1	82.4	0.429
477	118.1	109.2	313.3	289.6	94.0	86.9	0.428
439	108.6	101.5	320.4	299.3	100.7	94.1	0.439
404	95.6	89.8	314.3	295.4	103.4	97.2	0.430
372	84.0	79.3	308.4	291.3	105.8	100.0	0.420
357	86.4	82.3	335.8	319.6	117.6	112.0	0.459

RUN 6 Water V =2.037(m/s) Steam V = 5.157(m/s)
Re = 87915.9 Void Fraction =0.522

T_w(C)	q_t(kW/m^2)	q_c	h_t (W/m^2/C)	h_c	Nu_t	Nu_c	$C_{D,two}$
733	276.6	246.4	437.1	389.4	97.9	87.2	0.546
692	255.7	230.3	432.4	389.4	101.3	91.2	0.548
627	190.4	171.3	361.6	325.3	90.9	81.8	0.460
574	157.0	142.0	331.0	299.5	88.4	80.0	0.424
528	139.9	128.1	326.8	299.2	92.1	84.4	0.423
487	123.4	113.9	318.9	294.4	94.5	87.3	0.415
450	112.1	104.5	320.9	299.1	99.6	92.8	0.419
415	102.6	96.4	325.9	306.4	105.8	99.4	0.426
383	94.0	89.0	332.6	315.0	112.6	106.6	0.434
367	91.7	87.3	343.1	326.3	118.5	112.7	0.447

RUN 7 Water V =2.172(m/s) Steam V = 5.602(m/s)
Re = 93714.1 Void Fraction =0.481

T_w(C)	q_t(kW/m^2)	q_c	h_t (W/m^2/C)	h_c	Nu_t	Nu_c	$C_{D,two}$
700	286.5	260.2	477.7	433.8	110.9	100.7	0.591
661	229.3	207.0	408.6	368.7	98.8	89.2	0.504
602	170.6	153.5	340.1	306.2	88.0	79.3	0.420
552	149.3	135.9	330.1	300.6	90.4	82.3	0.412
508	132.2	121.6	324.1	298.1	93.7	86.2	0.408
467	121.7	113.2	331.4	308.3	100.6	93.6	0.419
431	112.9	106.1	340.9	320.3	108.3	101.7	0.433
398	101.8	96.3	342.3	323.8	113.6	107.5	0.434
381	98.6	93.6	350.4	332.8	118.8	112.9	0.444

RUN 8 Water V =2.380(m/s) Steam V = 6.732(m/s)
Re = 102711.6 Void Fraction =0.400

T_w(C)	q_t(kW/m^2)	q_c	h_t (W/m^2/C)	h_c	Nu_t	Nu_c	$C_{D,two}$
670	259.3	236.1	454.8	414.1	109.0	99.2	0.540
639	215.8	195.5	400.1	362.6	99.2	89.9	0.474
613	188.6	170.6	367.5	332.5	93.9	84.9	0.435
567	159.7	145.3	341.9	311.0	92.0	83.7	0.407
546	152.6	139.6	342.0	313.0	94.4	86.3	0.409
506	143.5	133.0	353.3	327.5	102.4	94.9	0.428
488	132.4	122.9	341.6	317.1	101.2	93.9	0.413
453	123.2	115.4	349.4	327.4	108.0	101.2	0.424
436	116.9	109.9	348.3	327.4	110.0	103.4	0.423
420	114.5	108.1	358.2	338.4	115.5	109.1	0.436

RUN 9 Water V =2.479(m/s) Steam V = 7.653(m/s)
Re = 107005.4 Void Fraction =0.352

T_w(C)	q_t(kW/m^2)	q_c	h_t (W/m^2/C)	h_c	Nu_t	Nu_c	$C_{D,two}$
636	206.6	186.7	385.7	348.5	96.0	86.7	0.446
612	188.2	170.3	367.7	332.8	94.0	85.1	0.427
589	179.7	163.6	367.2	334.4	96.4	87.8	0.429
568	167.8	153.4	358.7	327.8	96.5	88.2	0.420
548	158.9	145.9	355.1	325.9	97.8	89.8	0.418
529	145.2	133.4	338.8	311.2	95.5	87.7	0.399
511	135.8	125.0	330.6	304.3	95.2	87.7	0.390
494	134.4	124.6	341.5	316.6	100.5	93.1	0.405
477	129.3	120.4	343.0	319.3	102.9	95.8	0.407
461	124.3	116.1	344.4	321.8	105.4	98.5	0.409
445	120.4	113.0	348.7	327.2	108.8	102.1	0.415
430	119.5	112.7	362.3	341.8	115.3	108.8	0.432

* * * * * * * * * * **TEST: TU1-4** * * * * * * * * * *

RUN 1 Water V =1.103(m/s) Steam V = 5.040(m/s)
Re = 47610.6 Void Fraction =0.647

T_w(C)	q_t(kW/m^2)	q_c	h_t (W/m^2/C)	h_c	Nu_t	Nu_c	$C_{D,two}$
686	199.2	174.4	340.0	297.5	80.1	70.1	0.569
647	176.9	156.0	323.5	285.2	79.5	70.1	0.547
612	152.4	134.5	297.6	262.7	76.1	67.2	0.505
581	143.6	128.2	298.9	266.9	79.2	70.7	0.513
522	122.9	111.4	291.1	264.0	82.7	75.0	0.507
470	106.9	98.3	288.6	265.4	87.3	80.3	0.507
447	97.8	90.3	281.9	260.3	87.8	81.0	0.495
404	88.2	82.5	290.4	271.5	95.6	89.4	0.512
366	76.9	72.5	289.7	273.1	100.4	94.6	0.508
332	70.5	67.1	304.4	289.6	110.6	105.2	0.532
316	66.7	63.7	309.1	295.1	114.9	109.7	0.538

RUN 2 Water V =1.264(m/s) Steam V = 5.141(m/s)
Re = 54567.0 Void Fraction =0.634

T_w(C)	q_t(kW/m^2)	q_c	h_t (W/m^2/C)	h_c	Nu_t	Nu_c	$C_{D,two}$
701	225.1	198.6	374.8	330.7	86.9	76.7	0.591
660	187.7	165.5	335.4	295.8	81.3	71.7	0.529
593	149.2	132.9	302.8	269.6	79.1	70.5	0.484
564	136.9	122.7	295.3	264.7	79.8	71.6	0.475
510	119.8	109.1	292.4	266.2	84.3	76.8	0.477
462	105.7	97.5	291.9	269.3	89.2	82.3	0.479
419	91.9	85.5	287.9	268.1	92.9	86.5	0.473
400	87.3	81.7	291.3	272.7	96.4	90.3	0.479
363	77.0	72.7	292.5	275.9	101.6	95.9	0.479
316	63.1	60.1	292.2	278.1	108.5	103.3	0.473

RUN 3 Water V =1.453(m/s) Steam V = 5.276(m/s)
Re = 62703.6 Void Fraction =0.618

T_w(C)	q_t(kW/m^2)	q_c	h_t (W/m^2/C)	h_c	Nu_t	Nu_c	$C_{D,two}$
725	220.9	191.7	353.8	307.0	80.0	69.4	0.510
680	219.1	194.9	377.9	336.1	89.6	79.7	0.561
609	163.2	145.6	320.7	286.1	82.3	73.4	0.479
551	135.4	122.1	300.4	271.0	82.5	74.4	0.454
525	129.9	118.3	305.9	278.6	86.6	78.9	0.466
476	111.7	102.8	296.8	273.1	89.1	82.0	0.455
413	95.3	89.2	304.1	284.6	98.8	92.5	0.468
376	84.0	79.3	304.8	287.6	104.1	98.2	0.468
343	75.8	72.0	311.8	296.4	111.5	105.9	0.476
328	71.3	68.0	313.5	298.9	114.5	109.2	0.477

RUN 4 Water V =1.689(m/s) Steam V = 5.474(m/s)
Re = 72874.6 Void Fraction =0.595

T_w(C)	q_t(kW/m^2)	q_c	h_t (W/m^2/C)	h_c	Nu_t	Nu_c	$C_{D,two}$
734	277.1	246.7	436.8	388.9	97.7	87.0	0.599
691	235.1	209.8	398.1	355.2	93.3	83.2	0.549
623	172.7	153.9	330.1	294.1	83.3	74.2	0.456
568	152.8	138.3	326.3	295.4	87.7	79.4	0.459
519	133.0	121.7	317.3	290.5	90.5	82.8	0.451
475	117.6	108.8	314.0	290.5	94.5	87.4	0.449
454	110.9	103.1	313.3	291.2	96.7	89.9	0.448
416	98.4	92.2	311.5	291.9	100.9	94.5	0.446
398	94.5	89.0	317.0	298.4	105.1	99.0	0.454
365	83.3	78.9	314.1	297.4	108.8	103.1	0.447
336	77.3	73.7	328.0	313.0	118.5	113.1	0.465

RUN 5 Water V =1.869(m/s) Steam V = 5.654(m/s)
Re = 80642.3 Void Fraction =0.577

T_w(C)	q_t(kW/m^2)	q_c	h_t (W/m^2/C)	h_c	Nu_t	Nu_c	$C_{D,two}$
684	255.6	231.0	437.9	395.7	103.4	93.4	0.582
647	206.5	185.5	377.2	338.8	92.7	83.2	0.499
589	161.1	145.1	329.6	296.9	86.6	78.0	0.439
563	151.6	137.5	327.3	296.8	88.5	80.3	0.438
516	132.7	121.6	318.8	292.2	91.2	83.6	0.431
474	120.5	111.8	322.4	298.9	97.1	90.0	0.439
435	108.2	101.2	322.9	302.0	102.0	95.5	0.440
400	93.8	88.2	312.5	293.8	103.3	97.2	0.425
369	86.1	81.6	320.7	303.9	110.6	104.8	0.435
339	82.0	78.4	343.0	327.8	123.3	117.8	0.464

RUN 6 Water V =2.138(m/s) Steam V = 5.985(m/s)
Re = 92263.3 Void Fraction =0.545

T_w(C)	q_t(kW/m^2)	q_c	h_t (W/m^2/C)	h_c	Nu_t	Nu_c	$C_{D,two}$
704	289.2	262.4	479.1	434.7	110.7	100.5	0.597
663	232.9	210.4	414.0	374.1	100.0	90.4	0.515
599	171.7	154.9	344.4	310.7	89.4	80.7	0.429
546	148.7	135.8	333.7	304.7	92.1	84.1	0.420
499	128.3	118.2	321.7	296.3	94.0	86.6	0.408
457	119.3	111.3	334.2	311.9	102.8	95.9	0.427
419	106.1	99.8	333.0	313.2	107.5	101.1	0.425
384	93.7	88.7	330.3	312.6	111.6	105.6	0.421
353	86.7	82.7	343.6	327.7	121.2	115.6	0.436

RUN 7 Water V =2.338(m/s) Steam V = 6.297(m/s)
Re = 100897.4 Void Fraction =0.518

T_w(C)	q_t(kW/m^2)	q_c	h_t (W/m^2/C)	h_c	Nu_t	Nu_c	$C_{D,two}$
732	304.8	274.7	482.7	435.1	108.3	97.6	0.569
687	269.2	244.2	458.3	415.7	107.8	97.8	0.546
620	191.2	172.6	367.5	331.7	93.1	84.0	0.438
567	162.9	148.5	349.0	318.2	94.0	85.7	0.420
519	142.3	131.0	339.3	312.5	96.7	89.1	0.412
477	128.8	119.9	342.2	318.5	102.7	95.6	0.418
457	121.5	113.5	340.6	318.3	104.8	97.9	0.416
420	108.4	102.1	339.3	319.4	109.4	103.0	0.415
386	100.4	95.3	351.2	333.4	118.4	112.4	0.429
370	93.8	89.2	347.4	330.5	119.6	113.8	0.423

RUN 8 Water V =2.629(m/s) Steam V = 6.903(m/s)
Re = 113442.2 Void Fraction =0.472

T_w(C)	q_t(kW/m^2)	q_c	h_t (W/m^2/C)	h_c	Nu_t	Nu_c	$C_{D,two}$
706	342.1	315.0	564.6	519.9	130.2	119.9	0.644
666	276.5	253.7	488.4	448.1	117.5	107.8	0.556
606	198.6	181.3	392.7	358.3	101.1	92.3	0.446
557	167.3	153.6	365.9	335.9	99.6	91.5	0.418
515	146.7	135.7	353.4	326.9	101.3	93.7	0.406
496	139.6	129.7	352.9	327.9	103.6	96.2	0.407
459	127.6	119.6	355.9	333.5	109.2	102.3	0.412
425	117.3	110.7	361.0	340.8	115.6	109.1	0.418
394	106.5	101.1	362.7	344.5	121.0	114.9	0.419

RUN 9 Water V =2.838(m/s) Steam V = 7.515(m/s)
Re = 122485.3 Void Fraction =0.434

T_w(C)	q_t(kW/m^2)	q_c	h_t (W/m^2/C)	h_c	Nu_t	Nu_c	$C_{D,two}$
667	279.7	256.9	493.8	453.4	118.8	109.1	0.541
636	234.8	214.8	437.9	400.7	109.0	99.7	0.479
609	208.5	190.9	409.5	374.8	105.0	96.1	0.449
563	173.6	159.5	375.0	344.5	101.4	93.2	0.413
542	164.5	151.8	372.2	343.5	103.2	95.2	0.411
522	153.6	142.1	363.8	336.7	103.3	95.6	0.403
485	135.7	126.3	352.1	327.8	104.6	97.4	0.391
468	133.2	124.7	361.7	338.6	109.7	102.7	0.403
436	122.7	115.7	365.4	344.5	115.4	108.8	0.407
405	113.6	107.9	372.3	353.3	122.3	116.1	0.415

* * * * * * * * * * **TEST: TU1-5** * * * * * * * * * *

RUN 1 Water V =1.182(m/s) Steam V = 6.813(m/s)
Re = 51012.9 Void Fraction =0.670

T_w(C)	q_t(kW/m^2)	q_c	h_t (W/m^2/C)	h_c	Nu_t	Nu_c	$C_{D,two}$
885	302.8	249.4	385.9	317.8	74.3	61.2	0.574
828	267.6	224.1	367.9	308.0	74.9	62.7	0.560
734	209.3	179.0	330.2	282.4	73.9	63.2	0.520
654	177.4	155.8	320.5	281.5	78.2	68.7	0.521
584	149.9	134.3	309.8	277.4	81.8	73.2	0.515
523	131.1	119.6	309.9	282.8	87.9	80.2	0.524
495	120.4	110.5	304.5	279.5	89.4	82.0	0.518
469	114.2	105.7	309.5	286.4	93.8	86.8	0.528
422	101.1	94.7	314.3	294.4	101.1	94.7	0.538
378	92.5	87.7	333.0	315.6	113.4	107.5	0.570

RUN 2 Water V =1.357(m/s) Steam V = 6.931(m/s)
Re = 58555.1 Void Fraction =0.659

T_w(C)	q_t(kW/m^2)	q_c	h_t (W/m^2/C)	h_c	Nu_t	Nu_c	$C_{D,two}$
915	317.7	258.5	390.0	317.3	73.0	59.4	0.532
801	247.9	208.4	353.7	297.4	73.9	62.2	0.507
753	221.2	188.5	338.7	288.5	74.3	63.3	0.494
669	186.4	163.3	327.4	286.7	78.5	68.8	0.495
596	161.3	144.7	325.0	291.6	84.6	75.9	0.506
563	148.0	133.9	319.6	289.0	86.4	78.2	0.501
503	125.5	115.1	311.0	285.4	90.4	83.0	0.494
451	108.6	100.9	309.1	287.2	95.7	88.9	0.493
428	103.9	97.2	317.2	296.9	101.2	94.7	0.507
383	95.0	90.0	335.1	317.5	113.3	107.4	0.536
362	88.1	83.8	335.9	319.4	116.9	111.1	0.535

RUN 3 Water V =1.562(m/s) Steam V = 7.087(m/s)
Re = 67406.0 Void Fraction =0.644

T_w(C)	q_t(kW/m^2)	q_c	h_t (W/m^2/C)	h_c	Nu_t	Nu_c	$C_{D,two}$
911	356.3	297.7	439.3	367.1	82.5	68.9	0.574
850	290.4	243.2	387.2	324.2	77.1	64.5	0.512
799	249.5	210.3	356.9	300.9	74.7	63.0	0.478
711	204.5	176.8	334.6	289.4	76.7	66.4	0.464
672	188.7	165.3	329.9	288.9	78.9	69.1	0.465
602	164.2	147.2	327.4	293.5	84.8	76.0	0.474
570	149.8	135.2	319.0	288.0	85.6	77.3	0.465
512	129.3	118.5	314.1	287.8	90.4	82.8	0.464
485	124.0	114.6	321.8	297.4	95.6	88.4	0.478
437	107.2	100.1	318.1	297.1	100.3	93.7	0.474
415	102.2	96.1	325.2	305.6	105.5	99.2	0.485
371	98.8	94.2	365.3	348.4	125.7	119.9	0.546

RUN 4 Water V =1.819(m/s) Steam V = 7.313(m/s)
Re = 78514.3 Void Fraction =0.625

T_w(C)	q_t(kW/m^2)	q_c	h_t (W/m^2/C)	h_c	Nu_t	Nu_c	$C_{D,two}$
917	378.8	319.0	463.4	390.3	86.5	72.9	0.565
859	317.6	268.8	418.7	354.4	82.6	70.0	0.517
808	272.2	231.7	384.3	327.0	79.7	67.8	0.481
724	221.9	192.8	355.9	309.3	80.5	70.0	0.459
651	189.4	168.1	344.0	305.3	84.2	74.7	0.456
618	175.7	157.4	339.6	304.1	86.3	77.3	0.455
557	154.7	141.0	338.8	308.9	92.4	84.2	0.462
503	132.8	122.4	329.3	303.6	95.8	88.3	0.454
456	117.5	109.6	330.3	308.1	101.7	94.9	0.457
412	111.7	105.7	358.0	338.7	116.6	110.3	0.498
391	109.6	104.3	377.2	359.1	126.3	120.3	0.525

RUN 5 Water V =2.017(m/s) Steam V = 7.517(m/s)
Re = 87031.1 Void Fraction =0.608

T_w(C)	q_t(kW/m^2)	q_c	h_t (W/m^2/C)	h_c	Nu_t	Nu_c	$C_{D,two}$
899	375.3	319.0	469.5	399.1	89.2	75.8	0.551
843	321.3	275.2	432.3	370.3	86.6	74.2	0.515
753	242.6	209.9	371.5	321.4	81.5	70.5	0.452
715	222.1	194.1	361.4	315.8	82.6	72.1	0.446
645	191.3	170.4	350.8	312.6	86.4	77.0	0.443
584	168.3	152.7	348.1	315.8	91.9	83.4	0.449
555	155.9	142.3	342.5	312.7	93.5	85.4	0.444
529	147.0	135.2	343.0	315.4	96.7	88.9	0.448
480	127.4	118.3	335.3	311.3	100.2	93.1	0.440
458	121.5	113.5	339.8	317.5	104.4	97.6	0.447
415	114.0	107.8	362.2	342.7	117.5	111.2	0.479
394	115.8	110.5	394.6	376.4	131.7	125.6	0.523

RUN 6 Water V =2.313(m/s) Steam V = 7.886(m/s)
Re = 99827.3 Void Fraction =0.579

T_w(C)	q_t(kW/m^2)	q_c	h_t (W/m^2/C)	h_c	Nu_t	Nu_c	$C_{D,two}$
921	401.4	340.9	489.2	415.5	91.1	77.3	0.533
866	361.7	311.7	472.5	407.2	92.6	79.8	0.527
818	305.8	263.7	425.7	367.1	87.4	75.4	0.478
778	266.9	230.9	394.0	340.8	84.3	72.9	0.446
706	227.6	200.6	375.8	331.2	86.7	76.4	0.437
642	198.2	177.7	365.6	327.7	90.3	81.0	0.434
613	189.0	171.1	368.6	333.6	94.1	85.2	0.443
559	164.3	150.5	358.0	327.9	97.3	89.1	0.435
535	153.5	141.3	353.3	325.2	98.9	91.0	0.431
489	138.2	128.6	355.3	330.7	105.1	97.8	0.437
468	131.6	123.1	358.1	335.0	108.7	101.7	0.442
427	127.9	121.3	391.7	371.4	125.2	118.7	0.486

RUN 7 Water V =2.534(m/s) Steam V = 8.229(m/s)
Re = 109376.9 Void Fraction =0.555

T_w(C)	q_t(kW/m^2)	q_c	h_t (W/m^2/C)	h_c	Nu_t	Nu_c	$C_{D,two}$
817	329.7	287.9	460.2	401.8	94.7	82.7	0.500
776	282.6	246.8	418.3	365.4	89.7	78.3	0.457
739	256.5	225.5	401.4	353.0	89.4	78.6	0.443
705	237.7	210.7	392.7	348.2	90.6	80.3	0.439
644	203.3	182.6	373.9	335.9	92.2	82.8	0.425
616	192.4	174.2	372.9	337.6	94.9	85.9	0.428
564	171.7	157.5	370.0	339.4	100.0	91.7	0.430
540	161.3	148.8	366.7	338.1	101.9	94.0	0.428
496	145.6	135.7	368.1	343.0	108.0	100.7	0.434
455	134.1	126.2	377.9	355.8	116.5	109.7	0.447

APPENDIX F

TYPICAL DOWNWARD TWO-PHASE EXPERIMENT DATA

APPENDIX F

TYPICAL DOWNWARD TWO-PHASE EXPERIMENT DATA

Test Sphere Diameter: 12.7 mm
Test Sphere Material: 316 Stainless Steel

TD1 — No. 1 Tube needle Assembly
TD2 — No. 2 Tube needle Assembly
TD3 — No. 3 Tube needle Assembly

* * * * * * * * * * **TEST: TD1-2A** * * * * * * * * * *

RUN 1 Water V =2.003(m/s) Steam V = 1.129(m/s)
Re = 86437.4 Void Fraction =0.964

T_w(C)	q_t(kW/m^2)	q_c	h_t (W/m^2/C)	h_c	Nu_t	Nu_c	$C_{sat,F}$
679	91.8	71.7	158.6	123.9	37.7	29.4	0.405
642	87.5	70.4	161.4	129.8	39.9	32.1	0.425
576	75.2	62.6	157.9	131.5	42.0	35.0	0.431
547	70.0	59.2	156.8	132.6	43.3	36.6	0.435
493	59.8	51.7	152.4	131.7	44.9	38.8	0.431
468	55.9	48.8	151.9	132.6	46.1	40.2	0.432
424	48.3	42.9	149.3	132.5	47.9	42.5	0.428
404	45.2	40.5	149.0	133.3	49.1	43.9	0.429
367	40.0	36.3	149.9	136.0	51.8	47.0	0.432
350	36.9	33.6	147.6	134.5	52.2	47.6	0.425
319	32.5	29.9	148.2	136.4	54.8	50.4	0.425
292	28.9	26.9	151.0	140.2	58.1	54.0	0.430

RUN 2 Water V =2.128(m/s) Steam V = 1.144(m/s)
Re = 91852.5 Void Fraction =0.952

T_w(C)	q_t(kW/m^2)	q_c	h_t (W/m^2/C)	h_c	Nu_t	Nu_c	$C_{sat,F}$
671	102.4	83.0	179.5	145.6	43.0	34.9	0.428
638	96.2	79.4	178.9	147.7	44.4	36.7	0.436
577	83.8	71.2	175.7	149.3	46.8	39.7	0.441
524	73.1	63.5	172.6	149.9	48.9	42.5	0.442
476	64.2	56.8	170.9	151.2	51.3	45.4	0.444
434	56.6	50.8	169.5	152.2	53.7	48.2	0.444
396	49.4	44.9	167.1	151.7	55.6	50.5	0.439
362	44.3	40.7	169.2	155.5	58.9	54.1	0.444
347	41.1	37.9	166.7	153.7	59.3	54.7	0.436
318	37.4	34.9	171.8	160.0	63.7	59.3	0.449
304	36.1	33.8	176.4	165.2	66.7	62.4	0.460

*$C_{sat,F}$ as in Eq. (7.7).

RUN 3 Water V =2.362(m/s) Steam V = 1.161(m/s)
Re = 101942.0 Void Fraction =0.938

T_w(C)	q_t(kW/m^2)	q_c	h_t (W/m^2/C)	h_c	Nu_t	Nu_c	$C_{sat,F}$
720	121.9	98.0	196.7	158.1	44.7	35.9	0.413
682	116.3	96.0	199.9	165.0	47.3	39.0	0.432
646	108.2	90.8	198.1	166.3	48.7	40.9	0.437
581	92.9	80.0	193.2	166.5	51.2	44.1	0.438
524	80.6	71.0	190.3	167.6	54.0	47.5	0.441
473	70.2	62.9	188.1	168.5	56.7	50.8	0.441
429	61.1	55.5	186.0	169.0	59.3	53.9	0.438
389	53.5	49.1	185.1	170.1	62.1	57.1	0.437
354	47.6	44.2	187.6	174.3	66.1	61.4	0.442
322	42.6	39.9	191.8	179.9	70.7	66.3	0.450
307	40.7	38.4	196.5	185.1	74.0	69.7	0.460

RUN 4 Water V =2.774(m/s) Steam V = 1.178(m/s)
Re = 119733.2 Void Fraction =0.924

T_w(C)	q_t(kW/m^2)	q_c	h_t (W/m^2/C)	h_c	Nu_t	Nu_c	$C_{sat,F}$
668	127.2	108.1	224.2	190.5	53.9	45.8	0.439
635	119.7	103.2	223.7	192.8	55.7	48.0	0.445
576	105.1	92.5	220.7	194.3	58.8	51.8	0.449
524	91.6	82.0	216.4	193.7	61.4	54.9	0.447
477	80.5	73.0	213.7	194.0	64.2	58.2	0.446
455	76.2	69.6	214.6	196.2	66.2	60.5	0.449
415	67.2	62.1	213.2	196.8	69.1	63.8	0.447
380	59.3	55.2	211.9	197.4	72.0	67.1	0.444
348	52.9	49.7	213.8	200.7	75.9	71.3	0.446
318	49.3	46.7	225.7	213.9	83.6	79.2	0.469

RUN 5 Water V =3.135(m/s) Steam V = 1.186(m/s)
Re = 135302.9 Void Fraction =0.918

T_w(C)	q_t(kW/m^2)	q_c	h_t (W/m^2/C)	h_c	Nu_t	Nu_c	$C_{sat,F}$
676	136.2	116.4	236.5	202.0	56.3	48.1	0.428
644	129.0	111.8	237.1	205.4	58.5	50.6	0.436
585	113.7	100.6	234.3	207.3	61.8	54.6	0.441
533	100.4	90.3	232.0	208.7	65.0	58.5	0.444
486	87.8	80.0	227.7	207.4	67.6	61.6	0.439
444	77.0	70.9	224.0	206.2	70.0	64.5	0.434
406	69.3	64.5	226.6	210.8	74.4	69.2	0.440
372	61.4	57.5	225.8	211.7	77.6	72.7	0.437
341	55.5	52.4	230.2	217.4	82.5	77.9	0.444
327	54.2	51.4	239.1	227.0	87.5	83.0	0.460

RUN 6 Water V =3.460(m/s) Steam V = 1.192(m/s)
Re = 149322.5 Void Fraction =0.913

T_w(C)	q_t(kW/m^2)	q_c	h_t (W/m^2/C)	h_c	Nu$_t$	Nu$_c$	$C_{sat,F}$
687	148.7	128.0	253.5	218.1	59.7	51.3	0.434
655	141.4	123.3	254.9	222.2	62.1	54.2	0.443
596	124.2	110.4	250.5	222.7	65.3	58.0	0.446
543	110.0	99.4	248.4	224.4	68.8	62.2	0.449
496	96.8	88.5	244.7	223.8	71.8	65.7	0.447
453	85.7	79.2	242.6	224.2	74.9	69.3	0.444
415	76.9	71.8	244.1	227.8	79.2	73.9	0.448
381	67.7	63.6	241.1	226.5	81.8	76.9	0.441
350	60.6	57.4	243.1	230.0	86.1	81.4	0.443

RUN 7 Water V =4.199(m/s) Steam V = 1.200(m/s)
Re = 181222.4 Void Fraction =0.907

T_w(C)	q_t(kW/m^2)	q_c	h_t (W/m^2/C)	h_c	Nu$_t$	Nu$_c$	$C_{sat,F}$
697	171.8	150.1	287.7	251.3	67.0	58.5	0.446
668	169.3	150.1	298.0	264.2	71.6	63.4	0.470
613	150.8	135.8	293.8	264.6	75.0	67.5	0.472
564	135.3	123.5	291.8	266.3	78.9	72.0	0.475
519	119.9	110.5	286.4	264.1	81.7	75.3	0.471
478	108.2	100.8	286.5	266.7	85.9	80.0	0.474
441	97.0	91.0	284.9	267.2	89.4	83.9	0.471
407	88.4	83.6	288.3	272.4	94.5	89.3	0.477
376	80.2	76.3	290.9	276.5	99.4	94.5	0.480
361	76.2	72.6	291.7	278.1	101.7	96.9	0.480

RUN 8 Water V =5.321(m/s) Steam V = 1.206(m/s)
Re = 229636.8 Void Fraction =0.903

T_w(C)	q_t(kW/m^2)	q_c	h_t (W/m^2/C)	h_c	Nu$_t$	Nu$_c$	$C_{sat,F}$
702	205.3	183.1	340.9	304.0	78.9	70.4	0.474
676	204.8	185.0	355.9	321.4	84.8	76.6	0.502
650	195.5	177.8	355.8	323.6	87.2	79.3	0.506
600	176.4	162.3	352.5	324.3	91.4	84.0	0.508
556	160.1	148.8	351.5	326.7	95.9	89.1	0.512
514	143.5	134.3	346.2	324.1	99.3	93.0	0.507
477	130.9	123.4	347.4	327.6	104.3	98.3	0.511
442	118.9	112.8	347.3	329.5	108.8	103.2	0.510
410	108.9	103.9	350.9	334.8	114.5	109.3	0.515

RUN 9 Water V =6.249(m/s) Steam V = 1.209(m/s)
Re = 269669.7 Void Fraction =0.901

T_w(C)	q_t(kW/m^2)	q_c	h_t (W/m^2/C)	h_c	Nu_t	Nu_c	$C_{sat,F}$
674	228.3	208.6	397.7	363.4	94.9	86.7	0.521
652	221.7	203.9	402.0	369.6	98.3	90.4	0.530
609	203.2	188.6	399.6	370.8	102.6	95.2	0.533
569	186.0	173.9	396.8	371.0	106.6	99.7	0.533
532	169.4	159.4	392.2	369.0	110.1	103.5	0.530
498	156.0	147.6	392.0	370.9	114.7	108.6	0.532
466	143.5	136.5	391.7	372.5	119.1	113.2	0.532
437	144.0	138.1	427.6	410.1	134.8	129.3	0.582

* * * * * * * * * * **TEST: TD1-2C** * * * * * * * * * *

RUN 1 Water V =2.034(m/s) Steam V = 2.407(m/s)
Re = 87777.0 Void Fraction =0.965

T_w(C)	q_t(kW/m^2)	q_c	h_t (W/m^2/C)	h_c	Nu_t	Nu_c	$C_{sat,F}$
798	130.8	98.2	187.3	140.7	39.2	29.5	0.452
748	122.1	95.4	188.5	147.3	41.6	32.5	0.476
659	99.1	80.7	177.4	144.5	43.1	35.1	0.471
583	83.3	70.4	172.5	145.6	45.6	38.5	0.476
519	69.0	59.6	164.8	142.4	47.0	40.6	0.465
490	63.9	55.9	164.0	143.5	48.5	42.4	0.467
438	54.9	49.0	162.6	145.1	51.2	45.7	0.468
393	47.2	42.8	161.4	146.2	53.9	48.8	0.467
353	41.0	37.7	162.2	148.9	57.2	52.5	0.469
318	36.1	33.5	165.3	153.5	61.2	56.8	0.476
303	33.2	30.9	164.0	152.8	62.2	57.9	0.470

RUN 2 Water V =2.154(m/s) Steam V = 2.438(m/s)
Re = 92956.1 Void Fraction =0.952

T_w(C)	q_t(kW/m^2)	q_c	h_t (W/m^2/C)	h_c	Nu_t	Nu_c	$C_{sat,F}$
732	119.7	94.6	189.3	149.6	42.5	33.5	0.437
691	114.7	93.5	193.9	158.1	45.4	37.0	0.463
618	96.7	81.4	186.9	157.4	47.5	40.0	0.463
554	83.2	72.0	183.5	158.8	50.2	43.4	0.468
498	71.0	62.7	178.6	157.6	52.3	46.1	0.463
449	61.2	54.9	175.6	157.4	54.5	48.9	0.459
406	53.7	48.9	176.0	160.1	57.8	52.6	0.463
367	47.0	43.3	175.9	161.9	60.8	56.0	0.462
334	41.5	38.6	177.9	165.4	64.4	59.9	0.466
303	37.7	35.4	185.6	174.4	70.3	66.1	0.484

RUN 3 Water V =2.387(m/s) Steam V = 2.474(m/s)
Re = 103004.4 Void Fraction =0.939

T_w(C)	q_t(kW/m^2)	q_c	h_t (W/m^2/C)	h_c	Nu_t	Nu_c	$C_{sat,F}$
716	129.9	106.4	211.0	172.9	48.2	39.5	0.451
677	119.4	99.4	206.8	172.3	49.2	41.0	0.450
608	103.1	88.6	203.2	174.5	52.2	44.8	0.458
576	95.3	82.8	200.2	173.9	53.3	46.3	0.456
519	82.2	72.8	196.2	173.8	55.9	49.6	0.456
493	78.2	70.0	198.9	178.1	58.5	52.4	0.466
446	66.8	60.5	193.0	175.0	60.1	54.5	0.454
404	59.3	54.5	194.8	179.0	64.1	58.9	0.461
367	51.1	47.4	191.3	177.3	66.1	61.3	0.451
350	47.4	44.1	189.2	176.0	66.9	62.3	0.445
319	43.6	41.0	198.9	187.1	73.6	69.2	0.466

RUN 4 Water V =2.813(m/s) Steam V = 2.509(m/s)
Re = 121387.1 Void Fraction =0.926

T_w(C)	q_t(kW/m^2)	q_c	h_t (W/m^2/C)	h_c	Nu_t	Nu_c	$C_{sat,F}$
698	135.6	113.8	226.7	190.2	52.7	44.2	0.436
663	127.7	109.0	226.9	193.6	54.8	46.8	0.445
598	110.0	96.1	221.0	192.9	57.4	50.1	0.445
541	95.8	85.3	217.3	193.4	60.3	53.7	0.445
515	88.8	79.6	214.1	192.0	61.4	55.0	0.442
467	78.7	71.6	214.3	195.2	65.1	59.3	0.446
425	68.9	63.5	212.3	195.5	68.0	62.6	0.444
387	61.7	57.4	215.1	200.2	72.4	67.4	0.450
370	57.5	53.8	213.5	199.5	73.6	68.7	0.446
337	51.2	48.2	215.8	203.2	77.7	73.2	0.448
322	49.5	46.8	222.5	210.6	81.9	77.5	0.461

RUN 5 Water V =3.187(m/s) Steam V = 2.527(m/s)
Re = 137551.9 Void Fraction =0.919

T_w(C)	q_t(kW/m^2)	q_c	h_t (W/m^2/C)	h_c	Nu_t	Nu_c	$C_{sat,F}$
727	154.3	129.7	246.1	206.9	55.5	46.6	0.435
690	145.9	124.8	247.3	211.5	58.0	49.6	0.446
655	135.1	117.0	243.4	210.8	59.3	51.4	0.445
591	118.5	105.0	241.2	213.8	63.2	56.0	0.453
562	109.6	97.9	237.4	212.1	64.3	57.4	0.449
509	95.6	86.7	233.9	212.2	67.5	61.3	0.449
485	89.2	81.4	232.0	211.8	69.0	63.0	0.447
440	78.0	72.0	229.4	211.7	72.0	66.5	0.443
400	69.3	64.7	230.9	215.3	76.3	71.2	0.447
365	59.9	56.2	225.7	211.9	78.2	73.4	0.435
334	54.2	51.3	231.8	219.3	83.9	79.4	0.444

RUN 6 Water V =3.522(m/s) Steam V = 2.538(m/s)
Re = 151984.6 Void Fraction =0.915

T_w(C)	q_t(kW/m^2)	q_c	h_t (W/m^2/C)	h_c	Nu_t	Nu_c	$C_{sat,F}$
718	162.0	138.3	262.1	223.8	59.7	50.9	0.442
683	150.7	130.3	258.8	223.7	61.2	52.9	0.444
649	141.1	123.5	257.1	225.0	63.1	55.2	0.447
588	122.9	109.6	252.0	224.8	66.3	59.1	0.448
533	107.0	96.8	246.9	223.6	69.2	62.7	0.445
485	93.5	85.7	242.9	222.7	72.2	66.2	0.442
442	82.6	76.5	241.6	223.9	75.7	70.2	0.441
403	73.7	69.0	243.3	227.6	80.2	75.0	0.444
368	65.3	61.5	243.5	229.5	84.0	79.2	0.443
352	62.2	58.9	246.9	233.6	87.1	82.5	0.448

RUN 7 Water V =4.276(m/s) Steam V = 2.554(m/s)
Re = 184551.6 Void Fraction =0.909

T_w(C)	q_t(kW/m^2)	q_c	h_t (W/m^2/C)	h_c	Nu_t	Nu_c	$C_{sat,F}$
714	185.2	161.9	301.5	263.5	68.9	60.2	0.465
684	178.6	158.1	306.1	271.0	72.3	64.0	0.480
626	160.2	144.3	304.6	274.4	76.7	69.1	0.487
574	142.3	129.9	300.5	274.4	80.3	73.3	0.488
526	126.4	116.7	296.5	273.6	83.8	77.3	0.486
484	112.7	105.0	293.7	273.6	87.4	81.4	0.484
445	101.4	95.2	293.8	275.9	91.7	86.1	0.485
410	91.0	86.0	293.6	277.5	95.8	90.6	0.484
378	82.9	78.9	298.4	284.0	101.7	96.8	0.491

RUN 8 Water V =5.412(m/s) Steam V = 2.568(m/s)
Re = 233578.1 Void Fraction =0.904

T_w(C)	q_t(kW/m^2)	q_c	h_t (W/m^2/C)	h_c	Nu_t	Nu_c	$C_{sat,F}$
702	216.4	194.2	359.7	322.9	83.3	74.8	0.501
676	212.0	192.2	368.2	333.7	87.7	79.5	0.519
651	204.7	186.9	371.6	339.3	90.9	83.0	0.528
604	185.2	170.9	367.8	339.4	95.0	87.6	0.530
582	176.7	163.8	366.9	340.2	97.1	90.1	0.531
540	160.5	150.0	364.9	341.1	101.4	94.8	0.532
502	145.7	137.2	362.8	341.6	105.7	99.5	0.532
484	138.7	131.0	361.6	341.4	107.6	101.6	0.530
467	132.2	125.2	360.7	341.6	109.6	103.8	0.529
434	122.5	116.7	366.7	349.4	116.1	110.6	0.538
419	115.2	110.0	361.8	345.3	116.8	111.5	0.530

RUN 9 Water V =6.347(m/s) Steam V = 2.574(m/s)
Re = 273932.2 Void Fraction =0.902

T_w(C)	q_t(kW/m^2)	q_c	h_t (W/m^2/C)	h_c	Nu_t	Nu_c	$C_{sat,F}$
683	236.4	216.0	405.7	370.6	95.9	87.6	0.529
660	229.4	210.9	409.9	376.9	99.3	91.3	0.538
615	210.2	195.1	408.0	378.7	103.9	96.5	0.542
574	193.3	180.9	407.8	381.6	108.9	101.9	0.547
555	184.8	173.5	406.4	381.6	111.0	104.2	0.546
518	168.9	159.5	404.0	381.7	115.4	109.0	0.546
484	155.3	147.6	404.6	384.4	120.4	114.4	0.548
452	154.7	148.3	439.3	421.0	135.9	130.2	0.597

* * * * * * * * * * **TEST: TD1-2E** * * * * * * * * * *

RUN 1 Water V =2.326(m/s) Steam V = 5.264(m/s)
Re = 100370.5 Void Fraction =0.969

T_w(C)	q_t(kW/m^2)	q_c	h_t (W/m^2/C)	h_c	Nu_t	Nu_c	$C_{sat,F}$
694	111.7	90.3	188.2	152.2	44.0	35.6	0.479
657	108.2	89.9	194.3	161.5	47.2	39.3	0.509
622	100.8	85.2	193.2	163.3	48.8	41.3	0.515
559	86.3	74.7	187.8	162.7	51.0	44.2	0.514
531	81.1	71.1	188.2	165.0	52.9	46.4	0.521
480	69.4	61.8	182.7	162.8	54.7	48.7	0.512
456	63.8	57.2	179.3	160.7	55.2	49.5	0.503
414	55.7	50.6	177.8	161.5	57.8	52.5	0.502
394	53.1	48.6	180.6	165.3	60.2	55.1	0.511
376	49.7	45.8	180.4	166.1	61.6	56.7	0.510
326	40.7	37.9	179.8	167.6	65.8	61.3	0.505
298	36.7	34.5	185.5	174.5	70.8	66.6	0.518

RUN 2 Water V =2.415(m/s) Steam V = 5.328(m/s)
Re = 104202.7 Void Fraction =0.958

T_w(C)	q_t(kW/m^2)	q_c	h_t (W/m^2/C)	h_c	Nu_t	Nu_c	$C_{sat,F}$
674	119.3	99.6	207.7	173.4	49.5	41.3	0.494
639	109.6	92.8	203.4	172.1	50.4	42.7	0.492
606	101.9	87.5	201.6	173.0	51.9	44.6	0.495
575	94.5	82.0	199.1	172.8	53.1	46.1	0.495
545	87.2	76.5	195.9	171.7	54.1	47.4	0.491
518	81.1	71.7	194.0	171.7	55.4	49.0	0.491
446	66.9	60.7	193.7	175.8	60.4	54.8	0.498
404	58.3	53.6	192.0	176.3	63.2	58.0	0.495
367	51.6	47.8	193.3	179.3	66.8	62.0	0.497
350	48.3	45.0	193.1	179.9	68.3	63.7	0.496
305	40.4	38.1	197.3	186.1	74.6	70.3	0.502

RUN 3 Water V =2.595(m/s) Steam V = 5.407(m/s)
Re = 111973.3 Void Fraction =0.944

T_w(C)	q_t(kW/m^2)	q_c	h_t (W/m^2/C)	h_c	Nu$_t$	Nu$_c$	$C_{sat,F}$
702	126.7	104.5	210.3	173.4	48.7	40.1	0.443
668	122.4	103.2	215.6	181.9	51.8	43.7	0.466
634	114.6	98.1	214.5	183.6	53.5	45.8	0.471
603	106.8	92.5	212.3	183.9	54.8	47.5	0.473
546	93.2	82.4	209.1	184.9	57.7	51.1	0.475
495	81.1	72.9	205.4	184.6	60.3	54.2	0.473
450	71.2	64.9	203.6	185.4	63.2	57.5	0.472
410	63.1	58.1	203.8	187.8	66.6	61.3	0.474
374	55.6	51.7	203.3	189.1	69.7	64.8	0.472
342	49.3	46.2	204.2	191.4	73.1	68.6	0.472
313	44.2	41.8	208.1	196.5	77.7	73.4	0.478

RUN 4 Water V =2.946(m/s) Steam V = 5.493(m/s)
Re = 127133.2 Void Fraction =0.929

T_w(C)	q_t(kW/m^2)	q_c	h_t (W/m^2/C)	h_c	Nu$_t$	Nu$_c$	$C_{sat,F}$
697	138.4	116.7	232.0	195.7	54.0	45.6	0.443
663	132.4	113.6	235.2	202.0	56.8	48.8	0.458
630	124.5	108.3	234.8	204.2	58.8	51.1	0.464
571	109.0	96.7	231.3	205.4	62.0	55.0	0.468
518	94.7	85.3	226.3	203.9	64.6	58.2	0.464
472	83.5	76.3	224.7	205.3	67.9	62.0	0.465
430	73.7	68.1	223.5	206.4	71.1	65.7	0.463
393	65.0	60.6	222.3	207.1	74.3	69.2	0.461
359	58.7	55.2	226.8	213.3	79.3	74.6	0.469
328	53.3	50.5	233.7	221.5	85.3	80.9	0.481

RUN 5 Water V =3.278(m/s) Steam V = 5.538(m/s)
Re = 141449.1 Void Fraction =0.921

T_w(C)	q_t(kW/m^2)	q_c	h_t (W/m^2/C)	h_c	Nu$_t$	Nu$_c$	$C_{sat,F}$
694	147.1	125.6	247.5	211.4	57.8	49.4	0.443
660	138.4	119.9	247.2	214.2	59.9	51.9	0.449
597	120.5	106.6	242.2	214.3	63.0	55.7	0.451
542	105.0	94.4	237.7	213.8	65.9	59.3	0.450
492	91.8	83.7	234.0	213.3	68.9	62.9	0.448
448	81.8	75.5	235.0	216.9	73.1	67.4	0.452
409	73.1	68.1	236.8	220.8	77.4	72.2	0.456
373	63.6	59.7	232.6	218.4	79.7	74.9	0.446
341	57.5	54.4	238.2	225.4	85.3	80.8	0.455

RUN 6 Water V =3.590(m/s) Steam V = 5.567(m/s)
Re = 154921.6 Void Fraction =0.917

T_w(C)	q_t(kW/m^2)	q_c	h_t (W/m^2/C)	h_c	Nu_t	Nu_c	$C_{sat,F}$
700	152.4 130.4	254.1	217.5	59.0	50.5	0.429	
667	147.2	128.1	259.7	226.1	62.5	54.4	0.447
606	128.8	114.4	254.7	226.1	65.6	58.2	0.448
551	112.5	101.4	249.4	224.8	68.4	61.7	0.445
526	105.9	96.2	248.5	225.7	70.2	63.8	0.447
480	94.0	86.4	247.2	227.3	73.9	67.9	0.448
439	83.3	77.3	245.8	228.3	77.3	71.8	0.447
402	74.0	69.3	245.3	229.7	81.0	75.8	0.446
338	58.6	55.6	246.8	234.1	88.9	84.3	0.444

RUN 7 Water V =4.332(m/s) Steam V = 5.605(m/s)
Re = 186943.5 Void Fraction =0.910

T_w(C)	q_t(kW/m^2)	q_c	h_t (W/m^2/C)	h_c	Nu_t	Nu_c	$C_{sat,F}$
691	175.3	154.2	296.6	260.7	69.5	61.1	0.460
661	166.6	148.1	297.2	264.1	72.0	63.9	0.467
604	147.7	133.4	293.3	264.9	75.7	68.4	0.469
553	129.5	118.3	286.2	261.5	78.4	71.6	0.463
507	114.9	106.2	282.7	261.1	81.9	75.6	0.462
465	103.7	96.8	284.2	265.2	86.5	80.7	0.466
427	92.6	87.0	282.8	265.9	90.3	84.9	0.464
393	83.1	78.7	283.7	268.5	94.7	89.6	0.465
377	79.8	75.8	288.1	273.7	98.3	93.3	0.472

RUN 8 Water V =5.506(m/s) Steam V = 5.631(m/s)
Re = 237601.6 Void Fraction =0.906

T_w(C)	q_t(kW/m^2)	q_c	h_t (W/m^2/C)	h_c	Nu_t	Nu_c	$C_{sat,F}$
679	199.2	179.0	344.0	309.2	81.6	73.4	0.478
654	191.6	173.6	346.0	313.5	84.4	76.5	0.486
606	176.0	161.6	348.2	319.7	89.7	82.4	0.497
561	158.4	146.8	343.6	318.4	93.2	86.3	0.495
520	144.2	134.8	343.2	320.7	97.7	91.3	0.498
483	130.5	122.8	340.8	320.6	101.5	95.5	0.496
449	118.8	112.5	340.9	322.8	105.9	100.3	0.496
417	109.0	103.8	343.9	327.5	111.3	106.0	0.500

RUN 9 Water V =6.475(m/s) Steam V = 5.643(m/s)
Re = 279443.8 Void Fraction =0.904

T_w(C)	q_t(kW/m^2)	q_c	h_t (W/m^2/C)	h_c	Nu_t	Nu_c	$C_{sat,F}$
684	222.0	201.4	379.8	344.6	89.6	81.3	0.489
662	218.4	199.7	388.3	355.1	93.8	85.8	0.504
641	210.6	193.6	389.3	357.9	96.3	88.6	0.509
600	194.7	180.6	389.5	361.3	101.0	93.7	0.515
562	178.2	166.5	386.0	360.7	104.6	97.7	0.514
526	164.3	154.6	385.7	362.9	109.0	102.6	0.517
493	151.3	143.2	385.0	364.3	113.3	107.2	0.518
462	138.3	131.4	381.8	362.9	116.6	110.9	0.513

* * * * * * * * * * **TEST: TD2-1A** * * * * * * * * * *

RUN 1 Water V =1.966(m/s) Steam V = 1.218(m/s)
Re = 84842.0 Void Fraction =0.947

T_w(C)	q_t(kW/m^2)	q_c	h_t (W/m^2/C)	h_c	Nu_t	Nu_c	$C_{sat,F}$
732	111.5	86.4	176.4	136.6	39.5	30.6	0.406
691	105.1	83.9	177.7	141.9	41.6	33.2	0.424
553	76.0	64.8	167.7	143.0	45.9	39.2	0.429
497	65.5	57.1	164.8	143.8	48.3	42.1	0.431
449	56.8	50.5	163.0	144.9	50.7	45.0	0.430
406	49.1	44.3	160.7	144.9	52.8	47.6	0.426
368	42.1	38.4	157.3	143.3	54.3	49.5	0.417
334	37.9	35.0	161.9	149.4	58.6	54.1	0.429
304	33.2	30.9	162.6	151.4	61.5	57.2	0.428

RUN 2 Water V =2.055(m/s) Steam V = 1.244(m/s)
Re = 88685.9 Void Fraction =0.927

T_w(C)	q_t(kW/m^2)	q_c	h_t (W/m^2/C)	h_c	Nu_t	Nu_c	$C_{sat,F}$
718	108.6	85.0	175.9	137.5	40.0	31.3	0.370
679	107.9	87.7	186.2	151.5	44.2	35.9	0.409
609	92.5	77.8	181.8	152.9	46.6	39.2	0.415
548	79.4	68.5	177.3	153.0	48.8	42.1	0.415
520	73.3	63.9	174.5	152.1	49.7	43.3	0.412
470	62.9	55.7	170.0	150.7	51.5	45.6	0.406
447	58.8	52.6	169.5	151.5	52.8	47.2	0.407
406	50.4	45.5	164.9	149.0	54.1	49.0	0.397
369	45.5	41.7	169.5	155.5	58.5	53.7	0.409
336	40.4	37.4	171.4	158.9	61.9	57.4	0.413
320	37.6	35.0	170.7	158.8	63.0	58.6	0.409

RUN 3 Water V =2.226(m/s) Steam V = 1.276(m/s)
Re = 96056.8 Void Fraction =0.904

T_w(C)	q_t(kW/m^2)	q_c	h_t (W/m^2/C)	h_c	Nu_t	Nu_c	$C_{sat,F}$
700	120.0	98.0	200.0	163.3	46.4	37.9	0.395
629	103.8	87.8	196.5	166.1	49.3	41.7	0.403
566	89.8	77.9	193.0	167.4	52.1	45.1	0.407
510	77.0	68.1	187.8	166.0	54.1	47.8	0.403
485	72.3	64.5	187.8	167.5	55.8	49.8	0.406
440	62.6	56.6	184.3	166.7	57.9	52.4	0.401
399	54.9	50.2	183.5	168.0	60.8	55.6	0.400
363	48.0	44.4	182.5	168.8	63.4	58.7	0.397
331	42.7	39.9	184.9	172.5	67.2	62.7	0.401
316	40.4	37.9	186.9	175.1	69.4	65.1	0.404

RUN 4 Water V =2.386(m/s) Steam V = 1.296(m/s)
Re = 102965.2 Void Fraction =0.890

T_w(C)	q_t(kW/m^2)	q_c	h_t (W/m^2/C)	h_c	Nu_t	Nu_c	$C_{sat,F}$
689	128.2	107.2	217.6	181.9	51.1	42.7	0.411
655	118.8	100.7	214.1	181.5	52.2	44.2	0.411
592	103.1	89.6	209.6	182.1	54.8	47.6	0.413
537	90.5	80.2	207.3	183.8	57.9	51.3	0.417
511	83.4	74.4	202.9	181.0	58.4	52.1	0.410
465	73.9	67.0	202.5	183.5	61.7	55.9	0.413
424	64.6	59.2	199.5	182.8	64.0	58.6	0.408
387	57.4	53.1	200.2	185.3	67.4	62.4	0.410
354	50.7	47.4	200.1	186.7	70.5	65.8	0.408
324	45.9	43.2	205.2	193.2	75.4	71.0	0.417

RUN 5 Water V =2.537(m/s) Steam V = 1.311(m/s)
Re = 109472.0 Void Fraction =0.880

T_w(C)	q_t(kW/m^2)	q_c	h_t (W/m^2/C)	h_c	Nu_t	Nu_c	$C_{sat,F}$
704	136.0	113.7	225.3	188.3	52.1	43.5	0.403
669	128.2	109.0	225.6	191.8	54.1	46.0	0.411
635	118.3	101.7	221.0	190.0	55.0	47.3	0.408
575	102.8	90.3	216.6	190.3	57.8	50.8	0.410
521	90.4	81.0	214.9	192.4	61.2	54.7	0.414
473	79.1	71.9	212.2	192.6	64.0	58.1	0.412
431	69.2	63.6	209.4	192.3	66.6	61.1	0.408
393	60.9	56.4	208.1	192.9	69.5	64.4	0.406
359	53.9	50.3	208.2	194.6	72.8	68.0	0.405
343	51.8	48.6	213.0	200.2	76.1	71.5	0.414

RUN 6 Water V =2.898(m/s) Steam V = 1.336(m/s)
Re = 125045.7 Void Fraction =0.863

T_w(C)	q_t(kW/m^2)	q_c	h_t (W/m^2/C)	h_c	Nu_t	Nu_c	$C_{sat,F}$
695	153.0	131.4	257.0	220.8	60.0	51.5	0.429
664	146.9	128.1	260.6	227.2	62.9	54.8	0.442
634	138.2	121.7	258.9	228.1	64.6	56.9	0.444
578	121.7	109.0	254.5	228.0	67.6	60.6	0.445
529	107.9	98.1	251.8	228.8	71.0	64.5	0.446
484	95.3	87.6	248.4	228.2	73.9	67.9	0.443
444	84.6	78.5	246.2	228.4	77.0	71.4	0.440
408	75.7	70.8	246.0	230.1	80.6	75.4	0.440
375	68.2	64.2	248.1	233.8	84.9	80.0	0.443
360	64.9	61.4	250.3	236.7	87.4	82.7	0.446

RUN 7 Water V =3.477(m/s) Steam V = 1.359(m/s)
Re = 150067.0 Void Fraction =0.849

T_w(C)	q_t(kW/m^2)	q_c	h_t (W/m^2/C)	h_c	Nu_t	Nu_c	$C_{sat,F}$
702	179.9	157.8	299.1	262.4	69.3	60.8	0.453
670	173.7	154.4	304.9	271.0	73.1	64.9	0.468
611	153.3	138.5	300.1	271.1	76.9	69.4	0.470
584	143.4	130.4	296.6	269.7	78.4	71.3	0.468
533	127.8	117.7	295.2	271.9	82.7	76.2	0.471
510	119.0	110.1	290.5	268.8	83.8	77.5	0.466
467	107.2	100.2	292.4	273.3	88.8	83.0	0.471
447	100.8	94.5	290.7	272.7	90.5	84.9	0.468
410	90.2	85.2	291.2	275.2	95.1	89.9	0.469
376	81.2	77.2	293.7	279.4	100.3	95.4	0.471

RUN 8 Water V =3.975(m/s) Steam V = 1.371(m/s)
Re = 171548.3 Void Fraction =0.841

T_w(C)	q_t(kW/m^2)	q_c	h_t (W/m^2/C)	h_c	Nu_t	Nu_c	$C_{sat,F}$
676	195.1	175.3	338.8	304.3	80.7	72.5	0.486
647	186.2	168.7	340.2	308.2	83.6	75.7	0.493
594	166.4	152.7	337.0	309.4	88.0	80.8	0.496
545	149.3	138.6	335.5	311.3	92.7	86.0	0.499
523	139.9	130.3	331.0	308.4	94.0	87.5	0.494
481	125.7	118.1	330.0	310.0	98.5	92.6	0.495
443	112.4	106.3	327.6	309.9	102.5	97.0	0.491
408	102.7	97.7	333.0	317.0	109.0	103.7	0.499
392	97.5	93.1	333.9	318.8	111.6	106.6	0.499

RUN 9 Water V =4.691(m/s) Steam V = 1.383(m/s)
Re = 202455.2 Void Fraction =0.834

T_w(C)	q_t(kW/m^2)	q_c	h_t (W/m^2/C)	h_c	Nu_t	Nu_c	$C_{sat,F}$
700	228.1	206.1	380.1	343.4	88.2	79.7	0.499
673	222.6	203.0	388.3	354.1	92.7	84.6	0.515
622	203.1	187.6	389.3	359.4	98.4	90.9	0.525
598	191.5	177.5	384.6	356.6	100.0	92.7	0.521
553	173.2	162.0	382.4	357.7	104.6	97.9	0.522
512	156.1	147.1	378.8	356.8	108.9	102.6	0.520
475	142.1	134.8	379.5	359.9	114.2	108.3	0.523
440	128.9	122.9	379.1	361.4	119.0	113.5	0.522
424	123.0	117.6	379.7	363.0	121.8	116.4	0.522

RUN 10 Water V =5.314(m/s) Steam V = 1.389(m/s)
Re = 229326.1 Void Fraction =0.830

T_w(C)	q_t(kW/m^2)	q_c	h_t (W/m^2/C)	h_c	Nu_t	Nu_c	$C_{sat,F}$
710	247.0	224.1	404.9	367.4	93.0	84.3	0.498
683	242.7	222.2	416.1	381.0	98.3	90.0	0.518
632	223.9	207.6	421.0	390.3	105.2	97.6	0.532
585	200.8	187.7	414.4	387.5	109.4	102.2	0.529
541	182.6	172.1	414.0	390.1	114.9	108.3	0.532
502	163.3	154.8	406.9	385.6	118.6	112.4	0.525
465	150.0	143.1	411.0	391.9	125.1	119.3	0.531
448	140.2	133.9	402.9	384.8	125.3	119.7	0.520

* * * * * * * * * * **TEST: TD2-1E** * * * * * * * * * *

RUN 1 Water V =2.276(m/s) Steam V = 5.662(m/s)
Re = 98237.7 Void Fraction =0.954

T_w(C)	q_t(kW/m^2)	q_c	h_t (W/m^2/C)	h_c	Nu_t	Nu_c	$C_{sat,F}$
664	120.4	101.6	213.5	180.1	51.5	43.4	0.519
629	111.9	95.8	211.5	181.0	53.0	45.4	0.523
597	102.8	88.9	207.0	179.1	53.9	46.6	0.518
566	96.2	84.2	206.3	180.7	55.6	48.7	0.523
537	89.4	79.1	204.5	180.9	57.0	50.4	0.523
485	77.2	69.4	200.6	180.3	59.6	53.6	0.519
461	71.8	65.0	198.8	180.0	60.8	55.1	0.516
418	63.5	58.3	200.1	183.7	64.7	59.4	0.522
398	59.6	55.0	200.3	184.9	66.5	61.4	0.523
345	48.6	45.5	198.8	185.8	70.9	66.3	0.516
300	41.8	39.6	209.2	198.1	79.6	75.4	0.539

RUN 1 Water V =2.276(m/s) Steam V = 5.662(m/s)
Re = 98237.7 Void Fraction =0.954

T_w(C)	q_t(kW/m^2)	q_c	h_t (W/m^2/C)	h_c	Nu_t	Nu_c	$C_{sat,F}$
713	132.0	108.8	215.4	177.5	49.3	40.6	0.510
675	127.3	107.5	221.3	186.9	52.7	44.5	0.539
640	116.8	99.8	216.4	185.0	53.6	45.8	0.534
607	108.0	93.5	213.3	184.6	54.9	47.5	0.534
576	102.1	89.6	214.8	188.5	57.3	50.3	0.545
519	88.3	78.9	210.8	188.4	60.1	53.7	0.544
469	76.5	69.4	207.4	188.1	62.8	57.0	0.540
425	67.4	61.9	207.7	190.9	66.5	61.1	0.544
385	58.9	54.7	206.5	191.7	69.7	64.7	0.541
350	51.0	47.7	203.6	190.4	72.0	67.4	0.530
319	45.7	43.1	208.4	196.5	77.1	72.7	0.540
305	43.1	40.8	210.2	198.9	79.4	75.1	0.542

RUN 2 Water V =2.340(m/s) Steam V = 5.770(m/s)
Re = 100975.6 Void Fraction =0.936

T_w(C)	q_t(kW/m^2)	q_c	h_t (W/m^2/C)	h_c	Nu_t	Nu_c	$C_{sat,F}$
682	124.7	104.4	214.5	179.5	50.8	42.5	0.469
645	116.1	98.8	213.0	181.1	52.4	44.6	0.475
611	107.9	93.0	211.0	181.9	54.0	46.6	0.478
550	93.0	82.0	206.8	182.3	56.8	50.1	0.479
496	80.0	71.7	202.3	181.4	59.4	53.2	0.475
448	69.9	63.6	201.1	183.0	62.6	56.9	0.476
406	61.4	56.6	201.1	185.3	66.0	60.9	0.477
368	53.6	49.8	199.8	185.8	69.0	64.1	0.473
335	47.4	44.5	201.9	189.4	73.0	68.5	0.476
305	43.5	41.2	212.4	201.1	80.2	76.0	0.498

RUN 2 Water V =2.340(m/s) Steam V = 5.770(m/s)
Re = 100975.6 Void Fraction =0.936

T_w(C)	q_t(kW/m^2)	q_c	h_t (W/m^2/C)	h_c	Nu_t	Nu_c	$C_{sat,F}$
723	142.4	118.2	228.7	190.0	51.8	43.0	0.495
681	133.8	113.4	230.1	195.1	54.5	46.2	0.510
643	123.5	106.3	227.5	195.9	56.2	48.4	0.513
607	113.6	99.1	224.1	195.4	57.6	50.3	0.513
542	97.3	86.7	219.9	196.0	61.0	54.3	0.514
486	82.6	74.8	214.0	193.7	63.5	57.5	0.507
437	71.2	65.4	211.5	194.0	66.7	61.2	0.503
394	62.7	58.3	213.7	198.5	71.3	66.2	0.510
355	54.4	51.0	213.1	199.7	74.9	70.2	0.506
322	47.8	45.2	215.9	203.9	79.6	75.2	0.509
306	45.2	42.8	219.3	208.0	82.7	78.4	0.515

RUN 3 Water V =2.469(m/s) Steam V = 5.913(m/s)
Re = 106546.9 Void Fraction =0.914

T_w(C)	q_t(kW/m^2)	q_c	h_t (W/m^2/C)	h_c	Nu_t	Nu_c	$C_{sat,F}$
676	131.4	111.5	227.9	193.4	54.2	46.0	0.457
642	122.3	105.2	225.7	194.1	55.8	48.0	0.459
579	106.5	93.7	222.3	195.7	59.0	52.0	0.464
523	93.7	84.1	221.3	198.7	62.8	56.3	0.470
474	82.3	75.0	220.2	200.7	66.4	60.5	0.473
430	71.8	66.2	218.0	200.9	69.4	63.9	0.469
390	63.6	59.2	219.1	204.1	73.4	68.4	0.472
372	59.3	55.4	217.8	203.6	74.7	69.9	0.468
339	52.3	49.3	218.8	206.1	78.7	74.1	0.468
309	47.2	44.8	225.5	214.1	84.6	80.3	0.479

RUN 4 Water V =2.597(m/s) Steam V = 6.011(m/s)
Re = 112096.2 Void Fraction =0.899

T_w(C)	q_t(kW/m^2)	q_c	h_t (W/m^2/C)	h_c	Nu_t	Nu_c	$C_{sat,F}$
683	139.7	119.3	239.8	204.7	56.7	48.4	0.453
649	131.2	113.6	239.0	206.9	58.6	50.7	0.458
617	121.4	106.1	234.8	205.3	59.7	52.2	0.456
587	114.1	100.8	234.3	207.1	61.6	54.5	0.460
532	100.5	90.5	232.8	209.6	65.4	58.8	0.465
482	88.2	80.5	230.7	210.6	68.8	62.8	0.465
438	78.0	72.0	230.4	212.8	72.5	67.0	0.467
399	69.3	64.7	231.9	216.4	76.8	71.7	0.471
364	61.1	57.4	231.6	217.8	80.4	75.6	0.468
332	53.4	50.5	229.8	217.4	83.4	78.9	0.461
318	50.6	48.0	232.2	220.4	86.1	81.7	0.465

RUN 5 Water V =2.724(m/s) Steam V = 6.084(m/s)
Re = 117557.3 Void Fraction =0.888

T_w(C)	q_t(kW/m^2)	q_c	h_t (W/m^2/C)	h_c	Nu_t	Nu_c	$C_{sat,F}$
705	148.5	126.1	245.7	208.6	56.7	48.2	0.439
669	140.6	121.4	247.4	213.6	59.4	51.3	0.450
602	122.3	108.1	243.5	215.2	63.0	55.6	0.455
544	105.7	95.0	238.2	214.2	65.9	59.3	0.453
492	92.3	84.2	235.4	214.7	69.4	63.3	0.453
446	80.7	74.4	233.0	215.0	72.6	67.0	0.450
405	71.3	66.5	233.5	217.7	76.7	71.5	0.452
369	62.6	58.8	232.7	218.6	80.2	75.4	0.448
336	56.0	53.1	237.2	224.6	85.6	81.0	0.455
321	53.4	50.7	241.2	229.3	89.0	84.6	0.461

RUN 6 Water V =3.325(m/s) Steam V = 6.283(m/s)
Re = 143476.7 Void Fraction =0.860

T_w(C)	q_t(kW/m^2)	q_c	h_t (W/m^2/C)	h_c	Nu$_t$	Nu$_c$	$C_{sat,F}$
721	181.0	157.0	291.7	253.1	66.2	57.5	0.454
687	178.8	158.0	304.9	269.5	71.8	63.4	0.485
622	158.8	143.2	304.3	274.4	76.9	69.4	0.496
565	138.9	127.0	298.9	273.4	80.7	73.8	0.495
514	121.1	112.0	293.0	270.9	84.1	77.8	0.490
468	106.6	99.6	290.0	270.8	88.0	82.2	0.487
427	95.7	90.1	292.7	275.7	93.5	88.1	0.492
390	84.3	79.9	290.6	275.6	97.4	92.4	0.487
357	75.7	72.2	294.5	281.0	103.2	98.5	0.491

RUN 7 Water V =3.590(m/s) Steam V = 6.332(m/s)
Re = 154925.8 Void Fraction =0.853

T_w(C)	q_t(kW/m^2)	q_c	h_t (W/m^2/C)	h_c	Nu$_t$	Nu$_c$	$C_{sat,F}$
714	192.6	169.3	313.8	275.8	71.7	63.0	0.471
682	188.4	168.1	323.9	288.9	76.6	68.4	0.495
621	167.5	152.0	321.5	291.7	81.4	73.8	0.502
566	148.0	136.0	317.4	291.7	85.5	78.6	0.502
518	129.9	120.6	311.1	288.9	88.9	82.5	0.497
474	116.0	108.7	310.5	291.0	93.6	87.7	0.498
434	103.0	97.3	308.6	291.3	97.7	92.2	0.495
398	92.6	88.0	310.9	295.4	103.1	98.0	0.498
366	83.8	80.1	315.5	301.6	109.3	104.5	0.503

RUN 8 Water V =4.080(m/s) Steam V = 6.393(m/s)
Re = 176094.1 Void Fraction =0.845

T_w(C)	q_t(kW/m^2)	q_c	h_t (W/m^2/C)	h_c	Nu$_t$	Nu$_c$	$C_{sat,F}$
696	210.4	188.8	353.2	316.9	82.3	73.9	0.502
665	201.0	182.1	355.8	322.3	85.7	77.7	0.512
636	190.4	173.8	355.5	324.5	88.5	80.8	0.516
608	179.6	165.0	353.8	325.1	90.9	83.6	0.518
556	158.4	147.0	347.5	322.6	94.8	88.0	0.514
509	141.3	132.4	345.4	323.6	99.7	93.4	0.515
467	124.7	117.6	339.7	320.5	103.2	97.3	0.507
429	113.0	107.3	343.2	326.2	109.3	103.9	0.512
395	101.1	96.6	343.3	328.0	114.4	109.3	0.511

RUN 9 Water V =4.807(m/s) Steam V = 6.445(m/s)
Re = 207463.6 Void Fraction =0.838

T_w(C)	q_t(kW/m^2)	q_c	h_t (W/m^2/C)	h_c	Nu_t	Nu_c	$C_{sat,F}$
702	227.2	205.0	377.5	340.6	87.4	78.9	0.492
675	224.8	205.1	391.2	356.9	93.3	85.1	0.516
623	205.8	190.2	393.7	363.7	99.4	91.9	0.528
599	195.7	181.8	392.7	364.7	102.0	94.7	0.530
553	175.9	164.8	388.7	364.0	106.4	99.7	0.528
511	158.9	149.9	386.6	364.8	111.3	105.0	0.529
492	151.4	143.3	386.8	366.2	114.1	108.0	0.530
455	136.9	130.3	385.7	367.2	118.9	113.2	0.528
422	123.1	117.7	382.8	366.2	123.1	117.8	0.523

RUN 10 Water V =5.452(m/s) Steam V = 6.472(m/s)
Re = 235303.7 Void Fraction =0.835

T_w(C)	q_t(kW/m^2)	q_c	h_t (W/m^2/C)	h_c	Nu_t	Nu_c	$C_{sat,F}$
691	253.3	232.2	428.7	392.9	100.4	92.1	0.530
666	244.0	225.0	430.9	397.3	103.7	95.6	0.537
619	223.2	207.8	430.0	400.3	109.0	101.5	0.542
576	203.5	191.0	427.8	401.5	114.0	107.0	0.544
536	186.3	176.1	427.8	404.4	119.6	113.0	0.548
498	169.2	160.8	424.7	403.6	124.2	118.1	0.546
464	153.4	146.5	421.3	402.3	128.4	122.6	0.541
448	145.8	139.5	418.8	400.7	130.2	124.6	0.538

* * * * * * * * * * **TEST: TD3-3A** * * * * * * * * * *

RUN 1 Water V =1.948(m/s) Steam V = 1.439(m/s)
Re = 84055.1 Void Fraction =0.923

T_w(C)	q_t(kW/m^2)	q_c	h_t (W/m^2/C)	h_c	Nu_t	Nu_c	$C_{sat,F}$
640	95.7	78.8	177.3	145.9	43.9	36.1	0.400
608	89.7	75.1	176.6	147.8	45.4	38.0	0.406
550	78.3	67.3	174.2	149.7	47.9	41.1	0.411
498	68.3	60.0	171.8	150.7	50.3	44.1	0.413
452	59.5	53.1	169.4	151.1	52.4	46.8	0.411
411	52.3	47.3	168.3	152.2	54.9	49.7	0.411
375	46.4	42.4	168.9	154.6	57.8	52.9	0.413
342	40.7	37.6	168.3	155.4	60.2	55.6	0.410
313	36.0	33.5	169.1	157.5	63.1	58.8	0.410
300	34.7	32.5	173.7	162.6	66.1	61.9	0.420

RUN 1 Water V =1.948(m/s) Steam V = 1.439(m/s)
Re = 84055.1 Void Fraction =0.923

T_w(C)	q_t(kW/m^2)	q_c	h_t (W/m^2/C)	h_c	Nu_t	Nu_c	$C_{sat,F}$
658	93.6	75.2	167.8	134.9	40.7	32.8	0.370
625	87.2	71.4	166.2	136.1	41.9	34.3	0.374
594	81.3	67.7	164.7	137.0	43.0	35.8	0.377
538	70.2	59.8	160.4	136.7	44.7	38.1	0.375
488	62.4	54.5	160.9	140.5	47.6	41.6	0.385
444	53.6	47.5	155.9	138.0	48.7	43.1	0.375
405	47.6	42.8	156.2	140.4	51.3	46.2	0.378
370	42.0	38.2	155.9	141.9	53.7	48.9	0.378
338	37.1	34.1	155.8	143.1	56.1	51.5	0.377
310	33.0	30.6	157.4	145.9	59.0	54.7	0.379

RUN 2 Water V =2.017(m/s) Steam V = 1.487(m/s)
Re = 87026.0 Void Fraction =0.894

T_w(C)	q_t(kW/m^2)	q_c	h_t (W/m^2/C)	h_c	Nu_t	Nu_c	$C_{sat,F}$
674	105.2	85.5	183.4	149.1	43.8	35.6	0.370
639	100.4	83.5	186.1	154.8	46.1	38.4	0.385
576	87.2	74.7	183.1	156.8	48.8	41.8	0.391
520	75.6	66.1	179.7	157.2	51.2	44.8	0.391
471	65.9	58.7	177.5	158.0	53.6	47.8	0.391
428	59.1	53.5	180.3	163.4	57.5	52.1	0.401
408	54.7	49.8	177.8	161.9	58.2	53.0	0.396
371	47.1	43.2	173.6	159.4	59.7	54.8	0.385
339	42.6	39.6	178.8	166.2	64.3	59.8	0.397
309	38.2	35.8	182.7	171.2	68.6	64.3	0.403

RUN 3 Water V =2.151(m/s) Steam V = 1.549(m/s)
Re = 92826.0 Void Fraction =0.858

T_w(C)	q_t(kW/m^2)	q_c	h_t (W/m^2/C)	h_c	Nu_t	Nu_c	$C_{sat,F}$
681	120.5	100.2	207.5	172.7	49.2	40.9	0.385
646	112.5	95.1	206.1	174.2	50.7	42.9	0.390
613	104.0	89.0	202.7	173.5	51.8	44.3	0.389
582	96.8	83.9	200.8	174.0	53.1	46.0	0.390
526	85.1	75.4	199.9	177.0	56.5	50.0	0.396
476	75.1	67.7	199.7	180.0	60.0	54.0	0.401
432	64.8	59.0	195.0	177.8	61.9	56.4	0.393
393	57.1	52.6	194.9	179.7	65.1	60.0	0.394
358	50.0	46.6	194.3	180.8	68.1	63.3	0.391
326	44.7	42.0	198.0	185.9	72.5	68.1	0.397
311	42.4	40.0	200.8	189.2	75.1	70.8	0.401

RUN 4 Water V =2.417(m/s) Steam V = 1.629(m/s)
Re = 104327.7 Void Fraction =0.816

T_w(C)	q_t(kW/m^2)	q_c	h_t (W/m^2/C)	h_c	Nu_t	Nu_c	$C_{sat,F}$
672	137.7	118.2	240.8	206.6	57.6	49.4	0.408
639	129.6	112.8	240.7	209.5	59.7	52.0	0.415
607	121.2	106.6	239.1	210.4	61.5	54.1	0.417
577	112.3	99.7	235.4	209.0	62.7	55.6	0.414
522	100.0	90.5	236.9	214.3	67.3	60.8	0.424
497	93.0	84.7	234.2	213.2	68.6	62.5	0.422
451	80.3	73.9	228.6	210.3	70.8	65.1	0.413
410	72.0	67.0	232.1	216.0	75.7	70.5	0.420
374	63.4	59.5	231.7	217.5	79.4	74.5	0.419
357	60.2	56.7	234.4	220.9	82.2	77.5	0.423
326	54.8	52.0	242.9	230.8	89.0	84.6	0.436

RUN 5 Water V =2.605(m/s) Steam V = 1.667(m/s)
Re = 112415.7 Void Fraction =0.797

T_w(C)	q_t(kW/m^2)	q_c	h_t (W/m^2/C)	h_c	Nu_t	Nu_c	$C_{sat,F}$
684	154.0	133.4	263.7	228.5	62.2	53.9	0.424
653	145.3	127.4	262.9	230.5	64.2	56.3	0.428
623	137.0	121.3	262.0	232.0	66.2	58.6	0.432
568	120.8	108.8	258.4	232.7	69.5	62.6	0.434
542	114.3	103.7	258.5	234.6	71.7	65.0	0.437
495	100.9	92.7	255.3	234.4	75.0	68.8	0.436
453	89.6	83.1	253.8	235.4	78.4	72.7	0.435
434	83.7	78.0	251.1	233.8	79.5	74.0	0.430
397	75.4	70.8	253.6	238.2	84.2	79.1	0.434
365	67.0	63.4	253.2	239.4	87.8	83.0	0.432
335	61.3	58.3	260.8	248.2	94.3	89.7	0.443

RUN 6 Water V =2.864(m/s) Steam V = 1.707(m/s)
Re = 123585.9 Void Fraction =0.779

T_w(C)	q_t(kW/m^2)	q_c	h_t (W/m^2/C)	h_c	Nu_t	Nu_c	$C_{sat,F}$
668	162.0	142.8	285.1	251.4	68.5	60.4	0.436
640	153.3	136.5	284.3	253.0	70.5	62.7	0.439
612	144.7	129.8	282.4	253.3	72.2	64.8	0.440
562	130.8	119.1	283.5	258.2	76.8	69.9	0.449
516	116.2	107.0	279.8	257.7	80.1	73.8	0.447
474	104.3	97.0	279.1	259.5	84.1	78.2	0.449
436	93.5	87.6	278.1	260.7	87.8	82.3	0.448
402	83.7	79.0	277.4	261.8	91.6	86.4	0.446
370	76.0	72.2	281.1	267.0	96.7	91.9	0.450
342	69.4	66.3	287.3	274.5	102.9	98.3	0.458

RUN 7 Water V =3.251(m/s) Steam V = 1.748(m/s)
Re = 140287.5 Void Fraction =0.760

T_w(C)	q_t(kW/m^2)	q_c	h_t (W/m^2/C)	h_c	Nu_t	Nu_c	$C_{sat,F}$
674	181.3	161.6	316.0	281.8	75.4	67.3	0.449
645	172.5	155.2	316.4	284.6	77.9	70.1	0.454
592	155.5	142.0	315.9	288.4	82.6	75.4	0.462
544	137.5	126.8	309.6	285.5	85.6	79.0	0.456
501	125.0	116.5	312.2	291.0	91.1	84.9	0.465
461	111.6	104.8	309.3	290.5	94.7	88.9	0.461
425	100.9	95.4	310.7	293.8	99.5	94.1	0.463
392	91.5	87.1	313.8	298.7	105.0	99.9	0.467
362	82.9	79.3	317.1	303.4	110.5	105.7	0.469

RUN 8 Water V =3.597(m/s) Steam V = 1.775(m/s)
Re = 155245.6 Void Fraction =0.749

T_w(C)	q_t(kW/m^2)	q_c	h_t (W/m^2/C)	h_c	Nu_t	Nu_c	$C_{sat,F}$
674	196.9	177.2	343.0	308.7	81.8	73.7	0.462
645	188.3	170.9	345.4	313.6	85.1	77.2	0.470
618	176.2	160.9	340.4	310.9	86.5	79.0	0.467
591	167.1	153.6	340.1	312.6	89.0	81.8	0.470
543	149.9	139.3	338.7	314.7	93.9	87.2	0.473
498	134.0	125.6	336.6	315.6	98.5	92.4	0.473
458	120.1	113.4	335.7	317.1	103.1	97.4	0.472
421	108.3	103.0	337.3	320.6	108.5	103.2	0.474
388	96.9	92.6	336.6	321.7	113.1	108.1	0.472
372	92.3	88.5	339.0	324.8	116.3	111.5	0.474

RUN 9 Water V =4.208(m/s) Steam V = 1.806(m/s)
Re = 181588.2 Void Fraction =0.736

T_w(C)	q_t(kW/m^2)	q_c	h_t (W/m^2/C)	h_c	Nu_t	Nu_c	$C_{sat,F}$
685	217.0	196.3	370.8	335.5	87.4	79.1	0.458
657	213.4	195.1	383.0	350.2	93.1	85.1	0.479
604	192.5	178.1	382.0	353.6	98.6	91.3	0.485
579	180.8	168.0	377.3	350.7	100.2	93.1	0.481
533	162.6	152.5	375.5	352.2	105.3	98.7	0.483
491	145.9	137.8	373.1	352.5	110.1	104.0	0.482
453	131.8	125.3	373.5	355.2	115.5	109.8	0.483
418	118.6	113.4	372.9	356.4	120.5	115.1	0.481
402	113.5	108.8	376.2	360.6	124.2	119.0	0.485

RUN 10 Water V =4.742(m/s) Steam V = 1.824(m/s)
Re = 204649.2 Void Fraction =0.728

T_w(C)	q_t(kW/m^2)	q_c	h_t (W/m^2/C)	h_c	Nu_t	Nu_c	$C_{sat,F}$
681	240.5	220.2	413.7	378.8	97.9	89.7	0.484
653	229.1	211.1	414.2	381.7	101.1	93.2	0.489
600	206.0	191.9	411.8	383.7	106.8	99.5	0.493
552	187.3	176.2	414.8	390.2	113.7	107.0	0.501
508	166.7	157.8	408.8	387.2	118.2	111.9	0.496
468	150.3	143.2	408.9	389.7	124.1	118.3	0.497
431	136.1	130.5	411.5	394.4	130.8	125.3	0.499
414	128.6	123.5	410.1	393.9	133.3	128.0	0.497

RUN 11 Water V =5.665(m/s) Steam V = 1.845(m/s)
Re = 244490.4 Void Fraction =0.720

T_w(C)	q_t(kW/m^2)	q_c	h_t (W/m^2/C)	h_c	Nu_t	Nu_c	$C_{sat,F}$
690	278.6	257.6	472.6	437.0	110.9	102.6	0.507
667	275.6	256.5	485.9	452.2	116.8	108.7	0.526
646	266.9	249.6	489.3	457.5	120.4	112.6	0.532
585	235.3	222.2	485.6	458.6	128.1	121.0	0.535
548	216.7	205.9	484.3	460.0	133.4	126.7	0.536
513	199.2	190.1	482.2	460.2	138.5	132.2	0.536
481	185.1	177.5	486.3	466.3	145.3	139.3	0.541
465	175.8	168.8	481.1	462.0	146.4	140.6	0.535

* * * * * * * * * * **TEST: TD3-3E** * * * * * * * * * *

RUN 1 Water V =2.289(m/s) Steam V = 6.550(m/s)
Re = 98801.1 Void Fraction =0.935

T_w(C)	q_t(kW/m^2)	q_c	h_t (W/m^2/C)	h_c	Nu_t	Nu_c	$C_{sat,F}$
655	116.4	98.4	210.0	177.4	51.2	43.2	0.467
621	109.7	94.2	210.4	180.6	53.2	45.7	0.476
591	101.6	88.2	207.2	179.8	54.3	47.1	0.475
534	87.4	77.3	201.4	178.0	56.4	49.8	0.469
509	82.2	73.4	201.3	179.6	58.2	51.9	0.473
461	72.1	65.3	199.7	180.8	61.1	55.3	0.473
419	62.6	57.4	196.3	179.8	63.3	58.0	0.467
400	60.3	55.6	201.0	185.5	66.5	61.4	0.480
364	53.0	49.4	200.9	187.1	69.7	64.9	0.478
332	47.1	44.2	202.9	190.5	73.6	69.1	0.480
304	41.7	39.4	205.0	193.8	77.6	73.3	0.482

RUN 2 Water V =2.338(m/s) Steam V = 6.739(m/s)
Re = 100887.8 Void Fraction =0.909

T_w(C)	q_t(kW/m^2)	q_c	h_t (W/m^2/C)	h_c	Nu_t	Nu_c	$C_{sat,F}$
675	121.6	101.9	211.6	177.3	50.4	42.3	0.424
641	117.1	100.1	216.6	185.1	53.6	45.8	0.444
609	109.4	94.7	215.1	186.3	55.2	47.8	0.447
550	95.4	84.4	212.1	187.6	58.3	51.5	0.450
498	83.6	75.2	210.0	188.9	61.4	55.3	0.453
474	78.1	70.7	208.7	189.1	62.8	56.9	0.451
411	63.1	58.1	203.1	187.0	66.2	61.0	0.441
374	56.7	52.8	207.0	192.7	70.9	66.0	0.449
326	47.4	44.7	209.8	197.7	76.8	72.4	0.452
298	43.7	41.5	220.9	209.9	84.3	80.1	0.473

RUN 3 Water V =2.436(m/s) Steam V = 7.001(m/s)
Re = 105145.1 Void Fraction =0.874

T_w(C)	q_t(kW/m^2)	q_c	h_t (W/m^2/C)	h_c	Nu_t	Nu_c	$C_{sat,F}$
662	130.3	111.7	232.0	198.7	56.1	48.0	0.430
629	121.5	105.4	229.7	199.2	57.6	50.0	0.432
598	114.6	100.7	230.2	202.2	59.8	52.5	0.439
569	105.8	93.7	225.8	199.9	60.7	53.7	0.434
515	92.3	83.1	222.3	200.2	63.7	57.3	0.434
468	80.9	73.8	219.9	200.7	66.7	60.9	0.433
426	72.1	66.6	221.4	204.6	70.9	65.5	0.438
354	55.9	52.5	219.9	206.6	77.4	72.7	0.433
339	52.6	49.6	220.5	207.8	79.3	74.7	0.433
310	48.1	45.7	229.2	217.7	86.0	81.6	0.447

RUN 4 Water V =2.646(m/s) Steam V = 7.360(m/s)
Re = 114189.5 Void Fraction =0.832

T_w(C)	q_t(kW/m^2)	q_c	h_t (W/m^2/C)	h_c	Nu_t	Nu_c	$C_{sat,F}$
667	153.2	134.1	270.3	236.6	65.0	56.9	0.457
636	144.2	127.6	269.4	238.4	67.0	59.3	0.461
606	136.0	121.6	269.0	240.4	69.3	61.9	0.466
501	104.9	96.4	261.5	240.3	76.2	70.0	0.465
479	99.1	91.6	261.9	242.1	78.5	72.5	0.467
417	83.2	78.0	262.0	245.6	84.7	79.4	0.468
382	73.4	69.2	260.4	245.8	88.3	83.3	0.464
350	65.5	62.2	262.3	249.2	92.9	88.2	0.465
321	58.7	56.1	266.2	254.3	98.2	93.9	0.468

RUN 5 Water V =2.802(m/s) Steam V = 7.545(m/s)
Re = 120943.1 Void Fraction =0.811

T_w(C)	q_t(kW/m^2)	q_c	h_t (W/m^2/C)	h_c	Nu_t	Nu_c	$C_{sat,F}$
679	166.7	146.5	287.8	253.0	68.3	60.0	0.461
647	158.0	140.5	289.0	257.1	71.1	63.2	0.469
586	138.6	125.5	285.1	258.0	75.1	67.9	0.472
533	120.7	110.6	279.1	255.8	78.3	71.7	0.468
485	108.3	100.5	281.6	261.4	83.7	77.7	0.476
442	94.6	88.5	276.7	259.0	86.7	81.2	0.468
403	84.5	79.7	278.7	263.0	91.8	86.6	0.472
368	75.9	72.2	283.0	269.0	97.7	92.8	0.477
337	68.6	65.6	289.5	276.9	104.4	99.8	0.485

RUN 6 Water V =3.028(m/s) Steam V = 7.744(m/s)
Re = 130677.9 Void Fraction =0.791

T_w(C)	q_t(kW/m^2)	q_c	h_t (W/m^2/C)	h_c	Nu_t	Nu_c	$C_{sat,F}$
655	172.3	154.2	310.7	278.2	75.7	67.8	0.476
626	164.3	148.4	312.5	282.4	78.7	71.1	0.484
572	146.6	134.3	310.7	284.7	83.2	76.2	0.488
524	129.5	119.9	305.9	283.2	86.7	80.3	0.485
480	114.8	107.2	302.2	282.2	90.4	84.4	0.482
441	102.8	96.8	301.9	284.2	94.8	89.2	0.482
405	92.2	87.4	302.8	287.1	99.6	94.4	0.483
372	83.3	79.5	306.4	292.2	105.2	100.4	0.486
342	75.7	72.6	312.6	299.8	111.8	107.2	0.493

RUN 7 Water V =3.381(m/s) Steam V = 7.959(m/s)
Re = 145899.0 Void Fraction =0.769

T_w(C)	q_t(kW/m^2)	q_c	h_t (W/m^2/C)	h_c	Nu_t	Nu_c	$C_{sat,F}$
686	194.5	173.8	332.2	296.9	78.3	70.0	0.468
655	183.8	165.7	331.3	298.6	80.7	72.8	0.472
625	181.1	165.2	344.7	314.6	86.8	79.2	0.498
570	160.2	148.0	340.8	314.9	91.4	84.5	0.499
520	140.5	131.1	334.6	312.2	95.3	88.9	0.494
497	133.5	125.1	336.1	315.1	98.5	92.3	0.498
475	126.4	119.0	336.9	317.3	101.3	95.4	0.500
454	119.0	112.5	335.9	317.4	103.6	97.9	0.498
435	112.2	106.4	335.4	318.0	106.1	100.6	0.497
416	105.2	100.1	333.2	316.8	107.9	102.6	0.493
398	100.2	95.6	336.1	320.7	111.5	106.4	0.497
381	94.6	90.5	336.5	321.9	114.1	109.2	0.497
365	89.8	86.2	339.2	325.3	117.6	112.8	0.499

RUN 8 Water V =3.708(m/s) Steam V = 8.095(m/s)
Re = 160028.7 Void Fraction =0.756

T_w(C)	q_t(kW/m^2)	q_c	h_t (W/m^2/C)	h_c	Nu_t	Nu_c	$C_{sat,F}$
681	213.7	193.4	367.7	332.8	87.1	78.8	0.494
648	201.0	183.5	366.8	334.8	90.0	82.2	0.498
617	188.6	173.4	365.2	335.7	92.9	85.4	0.501
587	177.4	164.2	364.6	337.4	95.9	88.8	0.504
559	166.7	155.2	363.6	338.5	98.9	92.1	0.505
507	146.9	138.1	361.2	339.6	104.6	98.3	0.506
460	128.8	122.0	357.6	338.9	109.5	103.8	0.501
419	115.2	110.0	361.8	345.3	116.8	111.5	0.507
381	101.9	97.8	362.9	348.3	123.1	118.2	0.506

RUN 9 Water V =4.303(m/s) Steam V = 8.255(m/s)
Re = 185700.7 Void Fraction =0.742

T_w(C)	q_t(kW/m^2)	q_c	h_t (W/m^2/C)	h_c	Nu_t	Nu_c	$C_{sat,F}$
657	220.5	202.3	395.9	363.0	96.2	88.2	0.494
631	211.0	194.7	397.2	366.6	99.4	91.7	0.500
606	201.1	186.6	397.4	368.8	102.3	94.9	0.503
582	190.7	177.8	395.6	368.8	104.7	97.6	0.504
537	173.1	162.7	395.9	372.3	110.4	103.8	0.508
516	158.9	149.6	381.6	359.4	109.2	102.8	0.490
478	149.2	141.7	395.2	375.5	118.5	112.6	0.510
442	134.4	128.4	393.7	376.0	123.4	117.9	0.507
409	122.5	117.6	397.3	381.3	130.0	124.7	0.511
393	116.0	111.5	395.8	380.6	132.2	127.1	0.508

RUN 10 Water V =4.837(m/s) Steam V = 8.343(m/s)
Re = 208741.3 Void Fraction =0.734

T_w(C)	q_t(kW/m^2)	q_c	h_t (W/m^2/C)	h_c	Nu_t	Nu_c	$C_{sat,F}$
674	242.0	222.3	421.6	387.3	100.6	92.4	0.493
646	233.4	216.0	427.9	396.0	105.3	97.5	0.505
592	206.8	193.2	420.3	392.7	110.0	102.8	0.502
567	197.6	185.6	423.0	397.3	113.9	107.0	0.508
521	177.8	168.3	422.8	400.3	120.3	113.9	0.511
499	169.5	161.1	425.2	404.1	124.3	118.2	0.515
458	150.8	144.1	421.1	402.5	129.3	123.6	0.510
421	136.5	131.2	425.0	408.4	136.7	131.4	0.514

RUN 11 Water V =5.778(m/s) Steam V = 8.435(m/s)
Re = 249336.8 Void Fraction =0.726

T_w(C)	q_t(kW/m^2)	q_c	h_t (W/m^2/C)	h_c	Nu$_t$	Nu$_c$	$C_{sat,F}$
677	266.5	246.6	461.8	427.2	109.8	101.6	0.494
651	262.2	244.4	476.2	443.9	116.6	108.7	0.514
600	237.5	223.5	475.1	447.0	123.2	115.9	0.519
554	215.0	203.8	474.1	449.3	129.6	122.9	0.521
532	204.7	194.7	474.0	450.8	133.1	126.5	0.523
511	194.4	185.4	473.0	451.1	136.2	129.9	0.523
491	185.3	177.2	473.8	453.1	139.8	133.7	0.524
472	175.8	168.6	472.7	453.2	142.7	136.8	0.523
454	168.6	162.1	476.5	458.1	147.1	141.4	0.527